Fall 1991

Local heat transfer to surfaces immersed in the freeboard region of a fluidized bed

Kun-Yung Tsai
University of New Hampshire, Durham

INFORMATION TO USERS

This manuscript has been reproduced from the microfilm master. UMI films the text directly from the original or copy submitted. Thus, some thesis and dissertation copies are in typewriter face, while others may be from any type of computer printer.

The quality of this reproduction is dependent upon the quality of the copy submitted. Broken or indistinct print, colored or poor quality illustrations and photographs, print bleedthrough, substandard margins, and improper alignment can adversely affect reproduction.

In the unlikely event that the author did not send UMI a complete manuscript and there are missing pages, these will be noted. Also, if unauthorized copyright material had to be removed, a note will indicate the deletion.

Oversize materials (e.g., maps, drawings, charts) are reproduced by sectioning the original, beginning at the upper left-hand corner and continuing from left to right in equal sections with small overlaps. Each original is also photographed in one exposure and is included in reduced form at the back of the book.

Photographs included in the original manuscript have been reproduced xerographically in this copy. Higher quality 6" x 9" black and white photographic prints are available for any photographs or illustrations appearing in this copy for an additional charge. Contact UMI directly to order.

UMI

University Microfilms International
A Bell & Howell Information Company
300 North Zeeb Road, Ann Arbor, MI 48106-1346 USA
313/761-4700 800/521-0600

Order Number 9200573

Local heat transfer to surfaces immersed in the freeboard region of a fluidized bed

Tsai, Kun-Yung, Ph.D.

University of New Hampshire, 1991

U·M·I
300 N. Zeeb Rd.
Ann Arbor, MI 48106

-

LOCAL HEAT TRANSFER TO SURFACES IMMERSED IN THE FREEBOARD REGION OF A FLUIDIZED BED

BY

KUN-YUNG TSAI

Diploma of Chemical Engineering,
Taipei Institute of Technology, Taiwan, 1956
MS of Chemistry,
University of Missouri - St. Louis, 1980
MS of Chemical Engineering,
University of New Hampshire, 1982

DISSERTATION

Submitted to the University of New Hampshire
in Partial Fulfillment of
the Requirements for the Degree of

Doctor of Philosophy

in

Engineering

September, 1991

This dissertation has been examined and approved.

Ihab Farag

Dissertation director, Ihab H. Farag
Associate Professor
Department of Chemical Engineering

Stephen S. T. Fan

Stephen S. T. Fan, Professor
Department of Chemical Engineering

Gael H. Ulrich

Gael D. Ulrich, Professor
Department of Chemical Engineering

William Mosberg

William Mosberg, Associate Professor
Department of Mechanical Engineering

Shan S. Kuo

Shan S. Kuo, Professor
Department of Computer Science

July 11, 1991

Date

ACKNOWLEDGEMENTS

This dissertation could never have been finished if it hadn't been for the support of many individuals. It is my pleasure to acknowledge their kind help. First, I would like to thank my advisor, Dr. Ihab H. Farag, for his patience and guidance throughout this work. I also wish to express my profound gratitude to him for allowing me to finish up this dissertation in Taiwan, which is far away from UNH. Many good ideas and results were generated under stimulating discussions with him through this immense distance.

I wish to thank all my committee members for their teaching and advice. They helped me to understand what research is really about and how to conduct research. I am also grateful to Dr. Stephen S. T. Fan and the Department of Chemical Engineering of UNH for accepting me as a graduate student. After working for more than twenty years, it is a real pleasure to be able to go back to school to accept the challenge of studying for Ph. D. degree.

I also owe thanks to the Chairman of the Board, Mr. Y. S. Chen, and the President, Mr. Y. S. Kuan, of Chinese Petroleum Corporation for their constant encouragement and support. Thanks also go to many colleagues of the Refining & Manufacturing Research Center for their assistance in overcoming some

of the difficulties encountered in experiments. Special thanks go to Dr. M. S. Chou for his help.

Most of all, I would like to thank my beloved wife Ann. Without her encouragement, love, and support, it would have been impossible to finish this dissertation. I also thank my sons Ming & Mingo for sharing my sorrow and joy while I was in the United States. I'll always remember those hard and happy days at Durham.

TABLE OF CONTENTS

LIST OF TABLES

LIST OF FIGURES

LIST OF SYMBOLS

A	exposed surface area of the heating plate (m^2)
Ar	Archimedes number (-)
a	decay constant (1/m)
C	solids concentration (kg/m^3)
C_1	constant, Equation (1.1)
C_2	constant, Equation (1.1)
C_3	constant, Equation (2.9)
C^*	solids concentration at Z>TDH (kg/m^3)
C_d	fluid-particle drag coefficient (-)
C_f	heat capacity of the fluidizing gas (J/kg·K)
C_L	effective heat capacity of lean phase, Equation (2.6) (J/kg·K)
C_0	solids concentration at bed surface (kg/m^3)
C_s	heat capacity of the solid material (J/kg·K)
C_{Z_t}	solids concentration at the column exit (kg/m^3)
D	inner diameter of the bed column (cm)
D_t	outside tube diameter (m)
d_p	particle size (μm)
$\overline{d}_p$	surface-mean particle size (μm)
d_p^*	entrained solid particle size (μm)
$\overline{d}_p^*$	surface-mean entrained solid particle size (μm)
E	solids elutriation rate, Equation (2.12) ($kg/m^2 \cdot s$)
f	output frequency of the AC inverter (1/s)
f_b	volume fraction of bed particles with velocity V_p^* (-)

f_e volume fraction of entrained particles (-)

G net upward solids flux ($kg/m^2 \cdot s$)

G^* solids flux at Z>TDH ($kg/m^2 \cdot s$)

G_d downward solids flux ($kg/m^2 \cdot s$)

G_u upward solids flux ($kg/m^2.s$)

G_{u0} upward solids flux at bed surface ($kg/m^2 \cdot s$)

g gravitational acceleration (m/s^2)

H column height measured from perforated plate (m)

H_f H corresponding to freeboard exit (m)

H_b dynamic bed height (m)

H_0 static bed height (m)

h total heat transfer coefficient ($W/m^2 \cdot K$)

h_c fluid-particle heat transfer coefficient ($W/m^2 \cdot K$)

h_D dense phase-tube heat transfer coefficient, Equation (2.5) ($W/m^2 \cdot K$)

h_f fluid convective heat transfer coefficient ($W/m^2 \cdot K$)

h_L lean phase-tube heat transfer coefficient, Equation (2.5) ($W/m2 \cdot K$)

h_r radiative heat transfer coefficient ($W/m^2 \cdot K$)

h_s particle convective heat transfer coefficient ($W/m^2 \cdot K$)

I DC current applied to the wire segment in the plate (A)

K Defined in Equation (2.11) for turbulent fluctuation; or $K = k(\pi/6)/(3^{1/2}/2)$, Equation (8.18) (-)

K_s $(k_d/k_s)(\pi/6)$

K^* elutriation constant, Equation (1.7) ($kg/m^2 \cdot s$)

k number of layers of particles which are surrounded by the fluid at $T=T_w$, Equation (8.7) (-)

k_1 thermal conductivity of the epoxy resin (W/m·K)

k_2 thermal conductivity of the steel plate (W/m·K)

k_a cluster-surface attachment rate constant (1/s)

k_d cluster-surface detachment rate constant ($1/s.m^3$)

k_f thermal conductivity of the fluidizing gas (W/m·K)

k_L effective thermal conductivity of lean phase, Equation (2.6) (W/m·K)

k_s thermal conductivity of the solid material (W/m·K)

L characterizing length of the heating plate, Equation 3.10 or Equation (8.21) and Figure (8.1) (m)

$N_{p,max}$ maximum allowable number of particles on the heat transfer surface per unit surface area (m^{-2})

Nu Nusselt number = $h_s \cdot L/k_f$ (-)

Nu_L Nusselt number for lean-phase heat transfer, Equation (2.6) or as defined in Table 7.1 (-)

Nu_p Nueeslt number for gas-solid heat transfer, $Nu_p = h_c \cdot d_p/k_f$ (Figure 2.1); or for bed-surface heat transfer, $Nu_p = h \cdot d_p/k_f$ (Figures 2.5, 2.6) (-)

n number of total particles per unit freeboard volume ($1/m^3$); or exponent in Equation (2.8)

n_s number of attached particles per unit volume ($1/m^3$)

Pr Prandtl number, $Pr = C_f \cdot \mu/k_f$ (-)

Pr_L Prandtl number for lean-phase gas-solids suspension, Equation (2.6) (-)

Q heat generation or power dissipation (W)

q specific heat generation rate (W/m^3)

Q_i heat loss from insulated plate surface (W)

Q_r radiative heat dissipation (W)

R inner radius of the bed column (cm)

Re Reynolds number, $Re = U_0 \cdot \rho \cdot L/\mu$, Equation (3.10) (-)

Re_L Reynolds number for lean-phase gas-solids suspension, Equation (2.6) or as defined in Table 7.1 (-)

Re_{mf} minimum fluidization Reynolds number, Equation (1.2)

Re_p particle Reynold number, $Re_p = d_p \cdot \rho \cdot U_0 / \mu$ (-)

r radial position (cm)

(S/V) surface area for heat transfer per unit freeboard volume (1/m)

T temperature (°C)

TDH transport disengagement height (m)

T_j temperature of the thermal couple junction point (°C)

T_0 ambient fluid or suspension temperature (°C)

T_w surface temperature of the heating plate (°C)

t time (s)

U_e suction air velocity at the sampler mouth (m/s)

U_{mf} minimum superficial gas velocity (m/s)

U_0 superficial gas velocity (m/s)

U_t terminal velocity (m/s)

V voltage drop across the wire segment in the plate (volt)

V_p particle velocity (m/s)

V_p^* particle velocity at Z>TDH (m/s)

V_{pa} average particle speed (m/s)

V_{pd} downward particle velocity (m/s)

V_{pu} upward particle velocity (m/s)

W width of the heating plate, Figure (8.1) and Equation (8.22) (m)

X coordinate (mm); or variable defined in Equations (2.8), (2.9), (3.3)-(3.5); or variable defined in Equation 8.20 (m^6/kg)

X_1 thickness of the epoxy resin layer of the probe (m)

X_2-X_1 thickness of the steel plate of the probe (m)

x	entrainable solids fraction at specified U_0 (-)
Y	Defined in Equation (8.20) (-)
y	dimensionless freeboard height, $y = (H-H_0)/D$ (-)
Z	column height measured from dynamic bed surface (m)
Z_f	freeboard height (m)
α	exponent of C, Equation (8.23) (-)
β	exponent of C_s/θ, Equation (8.23) (-)
δ	constant in Equation (2.12) (s/m)
ϵ	effective emissivity of plate surface-suspension system, Equation (3.2) (-)
ϵ_w	emissivity of the wall surface (-)
ϵ	bed effective emissivity of the bed particles (-)
θ	cluster- or particle-surface residence time (s)
κ	constant in Equation (2.12) ($kg/m^2 \cdot s$)
μ	viscosity of fluidizing gas ($kg/m \cdot s$)
μ_L	effective viscosity of lean phase, Equation (2.6) ($kg/m \cdot s$)
ν	constant, Equation (6.7) (-)
ξ	turbulent decay constant, Equation (2.11) (1/m)
ρ	density of fluidizing gas (kg/m^3)
ρ_L	density of lean phase, Equation (2.6) (kg/m^3)
ρ_s	density of particle material (kg/m^3)
σ	Stefan-Boltzmann constant, 5.67×10^{-8} $M/m^2 \cdot K^4$; or fraction of allowable sites occupied Equation 8.8 (-)
τ	velocity relaxation time of motion for a particle, Equation (6.7) (s)
bar	averaged values

ABSTRACT

LOCAL HEAT TRANSFER TO SURFACES IMMERSED IN THE FREEBOARD REGION OF A FLUIDIZED BED

by

Kun-Yung Tsai
University of New Hampshire, September, 1991

This work describes the local heat transfer in the freeboard region of a fluidized bed. Plate surface to particle suspension heat transfer coefficients in the freeboard of a fluidized bed (30 cm i.d.) have been measured by a newly designed miniature heating plate. Four types of plate orientations have been employed to investigate the directional effect of gas-solids flow to plate surface on the heat transfer rate. Local solids concentrations in the freeboard were also obtained by a nozzle-type sampling probe.

Results indicate that the heat transfer coefficient varies with axial and radial plate location, plate orientation, and gas velocities. Variations of heat transfer coefficients with radial position are more significant at lower freeboard heights than at higher ones for all the gas velocities (0.28-0.64 m/s) examined. For plates parallel to both the axial and radial directions of the column, the heat transfer coefficient (h) is higher at the center than at wall. The plate with exposed surface parallel to the axial and perpendicular to the radial directions gives nearly the same

value of h at the center and the wall. At lower freeboard levels, the center-facing surface exhibits higher heat transfer rate than the wall-facing one, which can be explained from the higher solids concentration and center to wall movement of particles. Plate with downward exposed surface exhibits the highest heat transfer rate at high gas flow rates because of direct bombardment of solid particles splashed from the bed. Variations of heat transfer coefficients with elevation in the freeboard are as much as an order of magnitude. However, these variations with elevation are relatively insensitive to plate orientations investigated.

A surface-to-suspension heat transfer model has also been developed to elucidate the surface to particle heat transfer mechanism in this lean phase system. The proposed model can explain reasonably well the inter-dependence of the measured heat transfer coefficient, solids concentration, heat capacity, particle size, and solids velocity in the freeboard.

CHAPTER 1

INTRODUCTION

The focus of the present work is the local heat transfer in the freeboard of a fluidized bed. Several terms and phenomena needed for the following discussions are defined and described in this chapter. The motivation, objectives, and approach of this study are also discussed.

1.1 Background

Fluidization is an operation by which fine solids are transformed into a fluid-like state through contact with a gas or liquid or both. The smooth, liquid-like flow of particles in a fluidized bed provides several advantages over the fixed beds (Kunii and Levenspiel, 1969). Consequently, the applications in chemical engineering are numerous.

A fluidized bed usually consists of three distinct zones (Figure 1.1). At the bottom of the bed is the grid zone where gas is forced to flow through the distributor in the form of jets or small bubbles. Above this zone is the dense or bubbling zone. In the bubbling zone, bubbles grow by coalescence as they rise to the surface of the bed. As bubbles break at the surface of the bed, particles are thrown up above the bed surface and are entrained by the flowing gas stream.

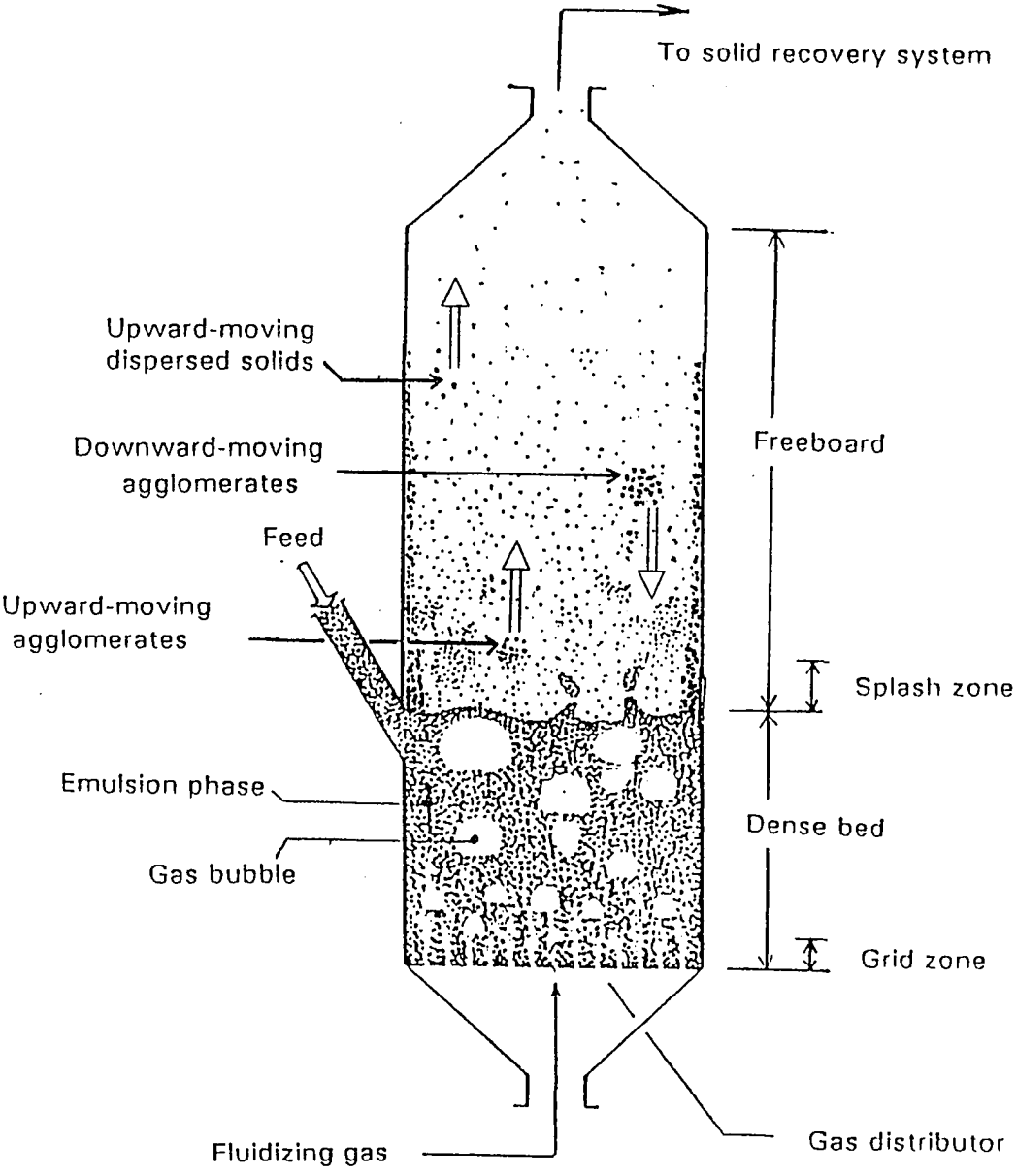

Figure 1.1: Fluid bed definitions.

The third zone of the vessel, between the surface of the dense bed and the top of bed where the gas stream exits, is called the freeboard.

The freeboard region provides space for reaction of ejected particles and the gas, for the disengagement of entrained or elutriated solids, and for the possible placement of heat transfer surfaces. Solids concentration in the freeboard is much smaller than that in the dense phase. The material in this zone can be called a lean or dispersed phase. Some particles in this region are carried far above the bed surface and are elutriated while others fall back to the bed. A very important design parameter in a fluidized bed combustion system is the height of the freeboard region. The accurate heat transfer coefficients in the freeboard region are also essential for the design and operation of a fluidized bed system.

1.2 Minimum Fluidization

When gas or liquid passes upward through a bed of solid particles at a very low flow rate, the particles are stationary and form a packed bed. If the flow rate is increased, a point is reached where the solid particles are supported or very nearly supported by the drag exerted by the fluid. At this point, the particles become mobile. This is said to be the point of minimum fluidization (Fig.1.2). The superficial

fluid velocity in the column at which minimum fluidization is achieved is called the minimum fluidization velocity, U_{mf}.

The preferred method for determining U_{mf} is to make a plot of pressure drop across the bed of solids versus superficial fluid velocity (Figure 1.3). The minimum fluidization velocity is defined as the superficial velocity at which the extrapolated linear portions of the fixed bed and the fully fluidized lines intersect with each other.

U_{mf} can also be calculated from a number of correlations published in the literature. One of the best correlations is the one derived by equating the pressure drop calculated from Ergun's equation (Ergun, 1952) with the pressure drop required to support the bed weight. Wen and Yu (1966a,b) simplified the equation and obtained:

$$Re_{mf} = [C_1^2+C_2 \cdot Ar]^{1/2}-C_1 \qquad (1.1)$$

where Re_{mf} is the minimum fluidization Reynolds number, and Ar is the Archimedes number:

$$Re_{mf} = \frac{\bar{d}_p \cdot U_{mf} \cdot \rho}{\mu} \qquad (1.2)$$

$$Ar = \frac{\rho \cdot (\rho_s-\rho) \cdot g \cdot \bar{d}_p^3}{\mu^2} \qquad (1.3)$$

As suggested by Grace (1982), the parameters C_1 and C_2 are 27.2 and 0.048 respectively. Substituting these values into Equation 1.1 and combining Equations 1.1 to 1.3, two limiting

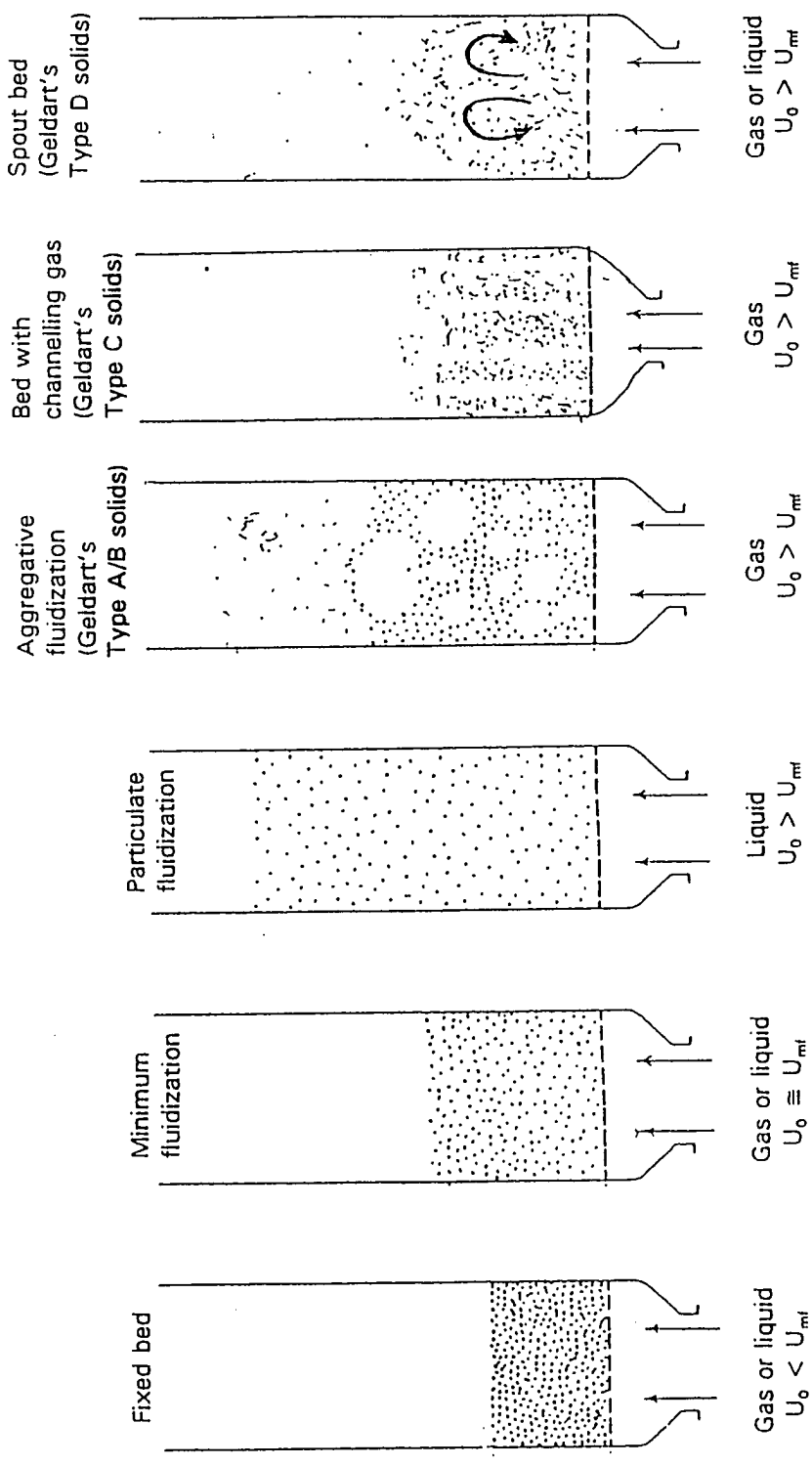

Figure 1.2: Various kinds of fluid-solids contact conditions.

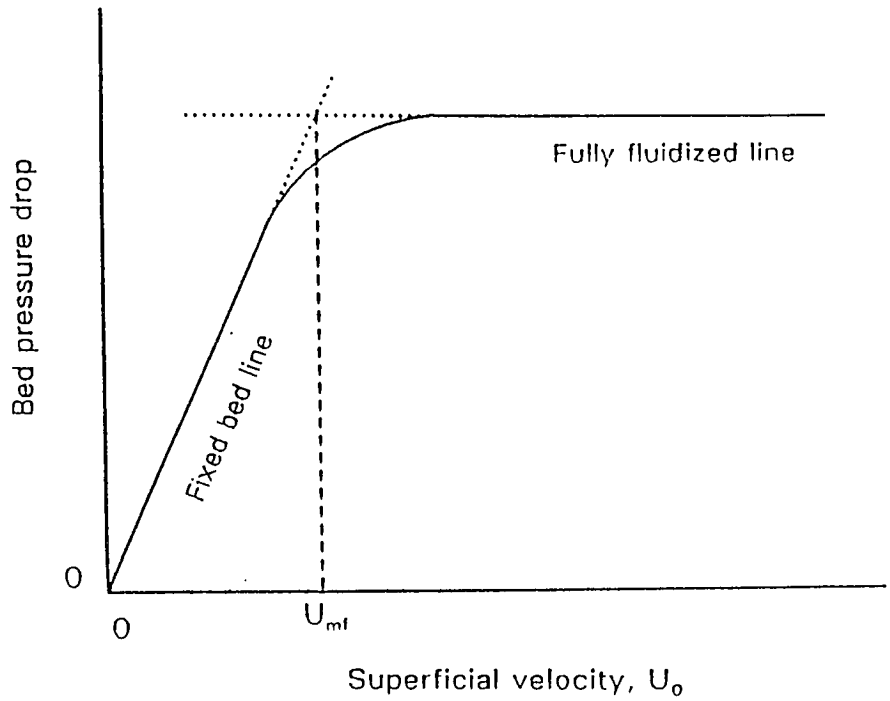

Figure 1.3: Illustration of bed pressure drop versus superficial velocity curve used to determine minimum fluidization velocity.

equations can be obtained for small and large particles:

$$\text{For } Ar < 10^3 \; ; \quad U_{mf} = 0.00075 \frac{(\rho_s - \rho) \cdot g \cdot \bar{d}_p^2}{\mu} \qquad (1.4)$$

$$\text{For } Ar > 10^7 \; ; \quad U_{mf} = 0.202 [(\rho_s - \rho) \cdot g \cdot \frac{\bar{d}_p}{\rho}]^{1/2} \qquad (1.5)$$

1.3 Powder Properties

Geldart (1973) introduced a categorization of particles with respect to how they fluidize. His chart is reproduced in Figure 1.4.

Type A particles are smaller and lighter on the axes of Figure 1.4 and they are designated as aeratable. Most cracking catalysts are in this category with particle sizes of about 20 to 100 microns.

Type B particles are in the group called bubbly. Dense materials like glass, sand, ore, and light particles over 150 microns are likely to be Type B. The particles do not display any cohesive properties and therefore once the minimum fluidization velocity is exceeded, the excess gas appears in the form of bubbles (Figure 1.2).

Very fine particles are difficult to fluidize and belong to the cohesive type, Type C. They are especially prone to electrostatic effects and interparticle forces. Gas usually

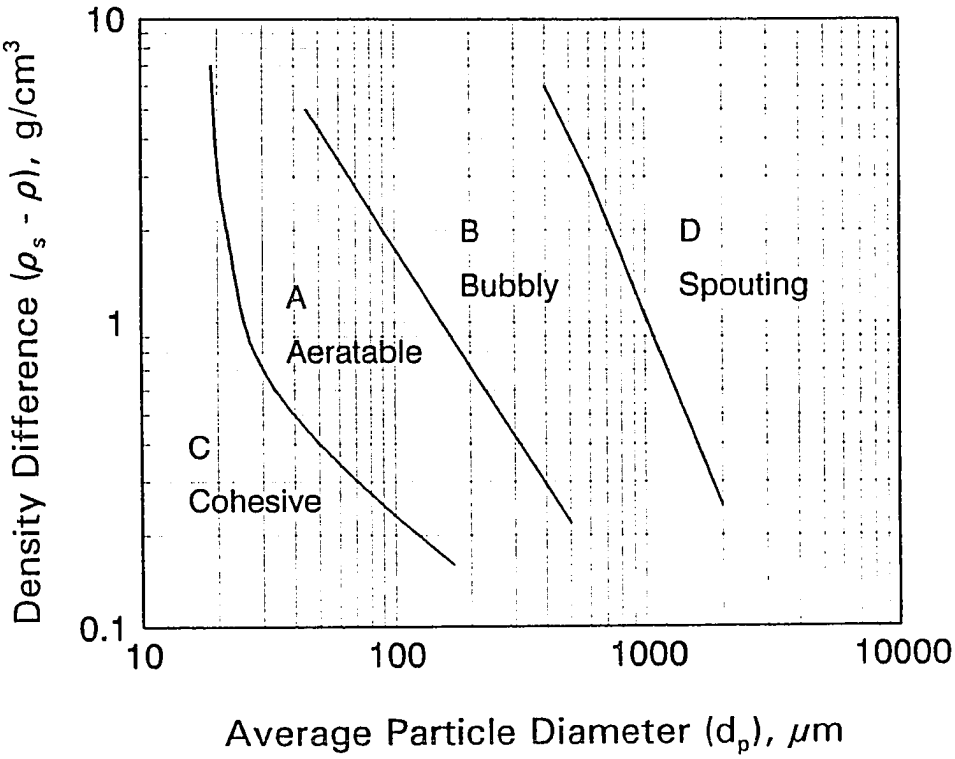

Figure 1.4: Geldart's particle classification scheme.

flows through the bed in channels which result in lower pressure drop over the bed (Figure 1.2).

Type D particles are large, on the order of 1 or more millimeters. They differ from Type B particles in that as velocity increases, a jet can be formed in the bed and bed material is then blown out with the jet in a spouting motion. There is considerable bed motion since particles move down and into the jet to replace the entrained material (Figure 1.2).

Among these four types, Types A and B powders are encountered most commonly in practice. The particles employed in this study belong to Type A powder.

1.4 Dense Bed

With an increase in gas flow, a fluidized bed may expand smoothly or it may develop gas pockets of very little solids concentration known as bubbles. These two regimes are referred to as particulate and aggregative fluidization, respectively (Figure 1.2).

The particulate fluidization is common for liquid-fluidized beds but not commonly found for gas-fluidized ones.

For aggregative fluidization, Toomey and Johnstone (1952) proposed a concept of "two-phase model of fluidization" as

shown in Figure 1.1. They assumed that the gas in excess of minimum fluidization requirement flowed through the bed in the form of bubbles. Thus, the bed is composed of an emulsion phase and a bubble phase. The emulsion phase acts as if the bed were at minimum fluidization condition.

1.5 Entraiment and Origin of Ejected Particles

During operation of a fluidized bed, a large amount of fine particles can be elutriated continuously. It may therefore become necessary to keep a proper freeboard height to minimize the entrained rate or to use a cyclone separator to recycle the entrained fines back into the dense bed.

To be entrained, particles must be thrown up from the dense bed, dispersed and suspended in the dispersed phase, and carried through it without disengagement. Of these processes, the ejection and dispersal of solids from the dense phase exerts the most powerful influence. The gas bubbles rising through the dense bed are responsible for ejecting solids from its surface.

The ejected particles are reported to be primarily from the following three sources:

1. Individual particles, falling or raining through the gas pockets at the moment they leave the dense bed, remain with the gas surrounding them.

2. Some of the solids that are lifted by the bubble wake are thrown upwards when the bubble bursts at the bed surface (Leva and Wen, 1971; Yates and Rowe, 1977).
3. Solids contained in the leading bulge of the bubble are detached at the surface when the bubble breaks (Do et al.,1972).

The mechanisms of solids ejection at the bubbling bed surface are still not well understood. From the experimental evidence, however, it appears that all the above mechanisms may contribute to solids ejection.

1.6 Transport Disengagement Height

The transport disengagement height (TDH) is defined as a height of the freeboard above which the elutriation becomes approximately constant. In practical terms, this is the height above which an appreciable decrease in upward solids flux occurs due to gravity alone. It is often used in establishing the total freeboard height in a piece of equipment.

Zenz and Weil (1958) and Zenz and Othmer (1960) gave a simple graphic correlation of the TDH that has been widely used (Figure 1.5). The correlation is based primarily on fluid cracking catalyst particles. According to the authors, this correlation can be applied to particles with sizes up to 400 microns in diameter.

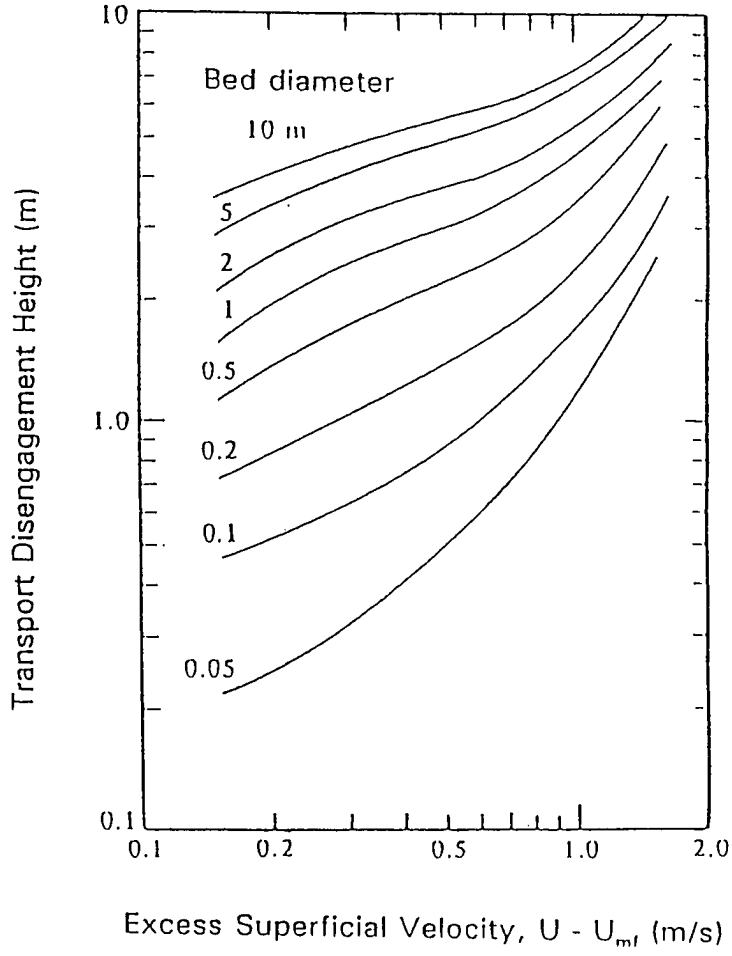

Figure 1.5: Simple graphic correlation based on Zenz & Weil (1958) for predicting transport disengagement heights with fine solids.

Fournol et al. (1973) studied fluid cracking catalyst and obtained

$$TDH = 1000\frac{U^2}{g} \qquad (1.6)$$

for a 0.61-m-diameter column with superficial gas velocity (U) ranging between 0.11 to 0.22 m/s.

Entrainment above the TDH is generally correlated in terms of a specific rate constant or elutriation constant $K^*(d_p)$ which refers to the upward solid flux per unit cross-sectional area of the column and has the unit of $kg/m^2 \cdot s$. Correlations for $K^*(d_p)$ differ widely. Wen and Hashinger (1960) covers their own data and earlier data over the range of variables $40 < d_p < 150$ μm, $0.16 < \rho < 1.2$ kg/m^3, $1300 < \rho_s < 5000$ kg/m^3, and $0.22 < U_0 < 1.32$ m/s:

$$\frac{K^*(d_p)}{\rho(U_0-U_t)} = 1.7\times10^{-5}\cdot\left[\frac{(U_0-U_t)^2}{(g\cdot d_p)}\right]^{1/2}\cdot\left(\frac{U_t\cdot d_p\cdot\rho}{\mu}\right)^{0.725}\cdot\left[\frac{(\rho_s-\rho)}{\rho}\right]^{1.15}\cdot\left[\frac{(U_0-U_t)}{U_t}\right]^{0.10} \qquad (1.7)$$

Equation 1.7 can be used to estimate the flux of each size fraction of solids above the TDH, within the given constraints.

1.7 Particles and Gas Behavior in the Freeboard

Lewis et al. (1962) in describing the particle elutriation and entrainment phenomena in the freeboard of a fluidized bed observed that three distinct phases are present in the freeboard, i.e., upward-moving dispersed solids, upward-moving

agglomerates projected from bed surface, and downward-moving agglomerates (Figure 1.1). The dispersed solids are formed from dissipation of both ascending and descending agglomerates. Upward-moving agglomerates occasionally reverse direction and move downward.

Horio et al.(1980) divided the freeboard into two distinct zones, a particle ascending zone and a particle descending zone. They concluded that:

1. Particle flow is distributed between an ascending zone at the center and a descending zone near the wall.
2. The particle concentration in the wall descending zone is greater than in the ascending zone. The thickness of the wall zone decreased with freeboard height, and increased with fluidizing velocity at a given height (Morooka et al., 1980).
3. Particle velocities in the ascending zone are greater than the superficial gas velocity. This was attributed to induced gas circulation in the freeboard.

The motion of particles in the freeboard is also influenced by the gas velocity field (Zenz and Weil, 1958; Do et al., 1972). The intermittent high velocity gas bursts originated from bubbles at the bubbling bed surface impose a fluctuating and highly irregular time-dependent velocity profile over the cross section of the freeboard (Zenz and

Weil, 1958). They suggested that the gas velocity profile becomes more and more stable with freeboard height. From the bed surface to the TDH, the effective gas velocity dissipates from the surface value of the bubble to the operating superficial velocity. Above TDH, the velocity profile remains constant.

Horio et al.(1980) also suggested that particle transport through the freeboard is controlled mainly by the gas velocity fluctuation induced by the bubble eruption at the bed surface. They observed that the decay of the erupting bubble is similar to that of a steady free jet.

Pemberton and Davidson (1984) introduced the concept of "ghost bubbles" in the freeboard flow. They suggested that the gas from a bursting bubble at the bed surface behaves as a discrete entity while in the freeboard. As the ghost bubble moves in the freeboard, it dispersed into the bulk gas flow.

1.8 Applications of Fluidization

The traditional applications of fluidized beds have been in coal gasification, catalytic cracking or hydrogenation of heavy oil fractions, roasting of ores, production of chemicals, and pneumatical transportation of materials.

Fluid beds allow greater interaction between various

phases present and increase kinetic growth rate. Fluid catalytic cracking of medium to heavy oil fractions is a good example of this kind. In this process, vaporized hydrocarbons crack into lower molecular weight compounds by contacting with a suitable catalyst. This process is endothermic with rapid carbon deposition and deactivation of the catalyst. The catalyst can be returned to its original activity by burning off the carbon in air. The key to a successful cracking process is the ability to supply the necessary large amount of heat and to rapidly regenerate many tons of catalyst per hour. The process accomplishes this efficiently and rapidly by burning the deposited carbon in the regenerator and supplying the heat for the reaction when the suspended and flowing catalyst solids are continuously circulated back to the reactor.

Another example is the H-coal process. In the process coal is continuously fluidized by hydrogen in the presence of catalyst particles where the pulverized coal is hydrogenated into liquid fuels (Griswald et al., 1966; Hellwig et al., 1966).

One of the special features of the fluidized bed is its remarkable temperature uniformity. This uniformity has recommended the fluidized bed as a vehicle for effecting catalytic reaction, especially the highly exothermic and temperature-sensitive reactions, such as the production of

phthalic anhydride by the catalytic oxidation of naphthalene and the Sohio process for producing acrylonitrile.

Fluidized bed technology will continue to be selected in many applications such as catalytic refining of various petroleum intermediates (Farag and Tsai, 1987). Coal-fired power plants will also continue to play a major role in the coming decade. Fluidized bed combustion has the potential to become the method of choice for burning coal (Farag et al., 1987, 1989) and other low-grade fuels, i.e., garbage, wood, and refinery wastes in industrial and utility boilers with acceptable performance.

1.9 Importance of Heat Transfer

One of the most attractive features of a fluidized bed is the favorable rate of heat transfer to or from immersed heat transfer surfaces. This high rate of heat transfer is due to the bubble-induced circulation of solids. Since conversion and selectivity of catalytic reaction as well as deactivation rate of the catalyst itself are very temperature-sensitive, this ability of a fluidized bed to maintain close to isothermal conditions makes it attractive for a variety of reactions, especially exothermic reactions with high rates of heat release.

To maintain a given temperature level in the bed, we need

to remove or add a definite amount of heat by contact with an appropriate heat exchange surface. Consequently, one of the most important considerations in the fluidized bed reactors is heat transfer. Poor design of the heat transfer surface leads to a loss in selectivity for a catalytic reaction.

In fluidized bed combustion, the fuel combustion heat is transferred to the heat transfer surface in the bed which controls the temperature of the bed. The volume of the fluidized bed is strongly affected by the space requirement of the heat transfer tubes in the bed. Clearly, a proper design of bed volume requires an accurate prediction of the heat transfer coefficient.

The heat transfer coefficient between a gas-fluidized bed and an immersed tube or containing wall is generally of order 300-600 $W/m^2 \cdot K$. This value is nearly an order of magnitude larger than the heat transfer coefficient for packed beds under corresponding conditions, and nearly two orders of magnitude larger than the heat transfer coefficient for a corresponding flow of the same gas through an empty vessel.

In the freeboard of a fluidized bed coal combustor, it has been estimated that 1/2 to 1/3 of in-bed heat transfer rate may be obtained (Adibhatla and Boggs, 1985). The total heat transfer in the freeboard is determined by energy balance and the desired bed temperature. The tube surface temperature

is set by the operating requirements for process heating. The temperature of the gas/solid mixture is set by the unit operating conditions. Clearly, accurate design of the freeboard heat transfer surface and freeboard volume requires accurate prediction of the heat transfer coefficient.

1.10 Motivation

Measurements of heat transfer between dense beds and immersed tubes have been carried out by many investigators. Many experimental data and correlations were reported in the literature (Vreedenberg, 1958; Zabrodsky, 1966; Lewis et al., 1962; Andeen and Glicksman, 1976; Berg and Baskakov, 1974; Gel'perin et al., 1968; Saxena et al., 1978; and Chadran et al., 1980, Bak et al., 1987; Krell et al., 1990).

Recently, attention has been focused on the solid-to-surface heat transfer study in circulating fluidized beds, in which large amounts of entrained solids are circulated back into the dense bed, (e.g., Fraley et al., 1983; Grace, 1986; Basu et al., 1987; Wu et al., 1987; Glicksman, 1988; Wu et al., 1989; Tremblay et al., 1990). Circulating fluidized beds (CFB's) are becoming common in applications involving gas-solid reactions, such as calcination and combustion of solid fuels and wastes. Compared with dense bed reactors, CFB reactors operate at lower solids concentration and higher solids velocity.

In the freeboard region of a fluidized bed, the solids concentration is much lower than that in the dense bed or in CFB's. Nonetheless, heat transfer surfaces in the freeboard region can be used to extract significant heat from the gas/solid mixture. Information on heat transfer study in the freeboard region of fluidized beds is scarce before 1980. In the past decade, a few experimental studies have been published, e.g., Biyikli et al. (1982, 1983, 1987a, 1987b), Bak et al. (1989), Hashimoto et al. (1990), Xavier and Davidson (1981), George and Grace (1982), Byam et al. (1981), Wood et al. (1980), Tabatabaie-Farashahi et al. (1981), Kortleven et al. (1986), Chakoraborty and Vickers (1984), Adibhatla and Boggs (1985), and Grewal et al. (1987).

All the former heat transfer studies in the freeboard region are concentrated on the measurement of heat transfer coefficients for immersed tubes located horizontally across or vertically along the freeboard. The tubes employed in the former studies usually encompass a relatively large distance in the freeboard region. Therefore, the heat transfer coefficients obtained are average values of a relatively large region. These results are practical enough for the freeboard heat transfer design. However, for some applications (e.g., fluidized bed catalytic reactors), an understanding of the local heat generation and dissipation are essential to achieve better temperature control and obtain high performance on yield and selectivity. The local heat transfer coefficients

are both of academic and practical significance in the application of fluidized bed technology. As far as we know, no local surface-to-suspension heat transfer coefficients in the freeboard region have been published.

Moreover, since the heat transfer in the freeboard is closely related to the movement of particles, the directional movement of the particles might cause directional variation in local heat transfer coefficients. It would be interesting to measure the heat transfer coefficients on plates facing various directions and compare the results with those obtained from horizontal or vertical tubes.

Although a number of correlations and models have been reported to describe the variables affecting the surface-suspension heat transfer rate in dense fluidized beds and CFB's (e.g., Mickley and Fairbanks, 1955; Fraley et al., 1983; Subbarao and Basu, 1986; Martin, 1981; Zabrodsky, 1966; Botterill, 1975; Ziegler et al., 1964b), the correlations are rather limited for dilute phases such as those in the freeboard (Hashimoto et al., 1990; Biyikli et al., 1983 and 1987b) and in solids-gas transfer lines (Wen and Miller, 1961). To our knowledge, in freeboard region, no mechanistic suspension-surface heat transfer model based on gas-solids dynamics has been published. Such a model is essential for the explanation of the observed heat transfer phenomena and the prediction of the heat transfer rate from the gas-solids hydrodynamics in

the freeboard.

1.11 Objectives

The goal of the investigation is to study and characterize the local heat transfer to surfaces immersed in the freeboard of a fluidized bed. In the present study, four major objectives were set and accomplished:

Objective	Explanation
1	To measure the local suspension-to-surface heat transfer coefficients in the freeboard region of a fluidized bed
2	To measure the concentration of solid particles and calculate the solid flux and velocity in the freeboard
3	To compare the measured heat transfer and solid concentration data in the freeboard with published ones
4	To present a mechanistic model to explain the observed dependence of the heat transfer rate on solid properties, concentration, and velocity in the freeboard.

1.12 Project Scope

To accomplish the above goals and objectives, this study has been divided into several phases:

Phase	Scope
1	Design, construction, and testing of a new miniature heat transfer probe to measure the heat transfer coefficient in gas-solid suspension
2	Design, construction, and testing of the gas-solid concurrent flow fluidized bed

3 Design and implementation of the solid concentration monitoring hardware

4 Testing of the complete unit

5 Characterization of the heat transfer to surfaces immersed in the freeboard of the bed

6 Development of dimensional and dimensionless correlations for the resulting heat transfer data

7 Study of the solids hydrodynamics in the freeboard of a fluidized bed

8 Comparison of data with published work

9 Proposal and development of a theoretical model to analyze the heat transfer data and compare the model results with the data from pilot plant runs.

1.13 Approach

1.13.1 Heat Transfer Probe Construction and Testing

Accurate measurement of the heat transfer coefficient in the freeboard is essential as this is the main parameters to be correlated in the present work. In the first phase of the investigation an electrically heated heat transfer probe was designed and constructed. Details of the unit are given in Section 3.2. The accuracy of the probe for heat transfer measurements was tested and verified by comparison of the measured and theoretically calculated heat transfer coefficients for the probe placed in an free-air stream of varying velocity.

Further details are discussed in Chapter 3.

1.13.2 Experimental Setup Installation

In the second phase of this investigation the fluidized bed was built and all the necessary heat transfer rate and solids concentration measuring hardware was installed. The column was loaded with fluidized cracking catalyst (FCC) particles and the system was tested for leaks, non-uniform fluidization, and other undesirable characteristics. The solids sampling system was tested and verified for accuracy assurance in solids concentration measurements.

Further details of the experimental setup, hardware for data-acquisition, and the procedure for testing the set up are given in Chapter 4.

1.13.3 Data Acquisition

The operation of the gas-solid fluidized bed was started by loading a fixed amount of the FCC solids into the column and introducing air into the column at a specified rate. After steady-state conditions had been achieved, temperature readings of heat transfer probes and the solids-air suspension, and other related physical operating conditions of heat transfer measurement hardware were recorded for calculation of suspension-to-surface heat transfer coefficient. The solids sampling system was also operated at the steady-state conditions. By varying the probe and sampler locations in the

radial and axial directions of the freeboard of the bed, a series of heat transfer and solids concentration data was obtained at each gas flow rate.

Further details are described in Chapter 5.

1.13.4 Freeboard Solids Dynamics & Results and Discussion of Solids Concentration Measurements

Solids dynamics is concerned with interactions between solids concentration, solids (or cluster of solids) velocity, and solids flux in the column. Attempts were made in this objective to estimate solids velocity and flux from the solids concentration data along the freeboard height of the bed. Some dynamic models were introduced and discussed. Results were used for heat transfer model correlations.

Further details are shown in Chapter 6.

1.13.5 Results and Discussions of Heat Transfer Coefficients Measurements

Experimental results for heat transfer measurements are presented. Variations of suspension-to-surface heat transfer coefficient with radial and axial positions in the freeboard are discussed for various plate orientations. Published data from similar systems are also presented for comparison. Dimensional and dimensionless correlations between the

resulting heat transfer data and the operating superficial gas velocity are also presented and discussed.

Further details are presented in Chapter 7.

1.13.6 Theoretical Modeling and Data Comparison

Experimental studies with fluidized beds tend to be difficult, expensive, and time consuming. Therefore, mathematical models and simulation studies are particularly attractive to investigate the heat transfer phenomena in the gas-solid fluidized bed system. A suspension-to-surface heat transfer model was developed to elucidate the surface to particle heat transfer mechanism in this lean phase system. The model is based on the transient gas-convective heating of single particles when sliding over the heated plate and the assumption of instantaneous attachment-detachment equilibrium between particles and the plate surface. The data obtained from the experiments were then compared with the data from the theoretical model developed.

Further details on the model and its assumptions are given in Chapter 8.

1.14 Sequence of Presentation

The sequence of presentation of material in this dissertation includes a review of related work (Chapter 2); discussion of the heat probe basis, design, and applicability (Chapter 3); presentation of the experimental setup (Chapter 4); discussion of experimental techniques for measuring the heat transfer coefficient and solids concentration (Chapter 5); explanation of solid dynamics in the freeboard (Chapter 6); presentation of experimental results and related discussions (Chapter 7); development of the heat transfer model (Chapter 8); conclusion (Chapter 9); and recommendations (Chapter 10).

CHAPTER 2

LITERATURE REVIEW

The subject of the present investigation is to study the suspension-to-surface heat transfer phenomena in the freeboard of a bubbling fluidized bed. This work covers the general areas of fluidization, solid-gas measurement, suspension-to-surface heat transfer rate measurement, and heat transfer data modeling in fluidized beds. This chapter reviews the literature relevant to this work, and presents a summary of published investigations.

2.1 Introduction of Fluidized-Bed Heat Transfer

One of the reasons fluidized beds have such wide applications is their excellent heat transfer characteristics, as described in Chapter 1. Heat transfer phenomena in fluidized beds are generally categorized into three different modes: particle-to-particle, gas-to-particle, and particle-to-surface (or suspension-to-surface) heat transfer.

Heat transfer between particles is important when blending particles of different temperatures. For example, it may be important to estimate the time required for temperature equalization in feeding particles at one temperature to a bed at a different temperature, or in case where some particles

are undergoing reaction while others are not (as in coal combustion). Wen and Chang (1967) have shown that particle-to-particle heat transfer through points of contact is negligible.

Heat transfer between gas and particles is so rapid that a fine particle in a fluidized bed can be considered to have a uniform internal temperature. An exception may occur if an extremely exothermic process, such as burning coal, is taking place. Some experimental data of gas-to-particle heat transfer coefficient are shown in Figure 2.1.

In view of heat recovery and reaction temperature control, suspension-to-surface heat transfer is the most important one of the three heat transfer modes described above. The heat transfer coefficient (h) between an immersed surface and a gas-solid fluidized bed can be taken approximately as the sum of three components (Baskakov et al., 1973):

$$h = h_s + h_f + h_r \qquad (2.1)$$

The particle convective component (h_s) is due to the heat transfer via unsteady-state conduction between the heat transfer surface and the solid particles directly adjacent to it and then the convection of the heated particles to the bulk of the bed. For particle sizes between 40 to 800 μm (Geldart's Type A and B particles), the contribution by the particle convection is predominant for non-pressurized systems

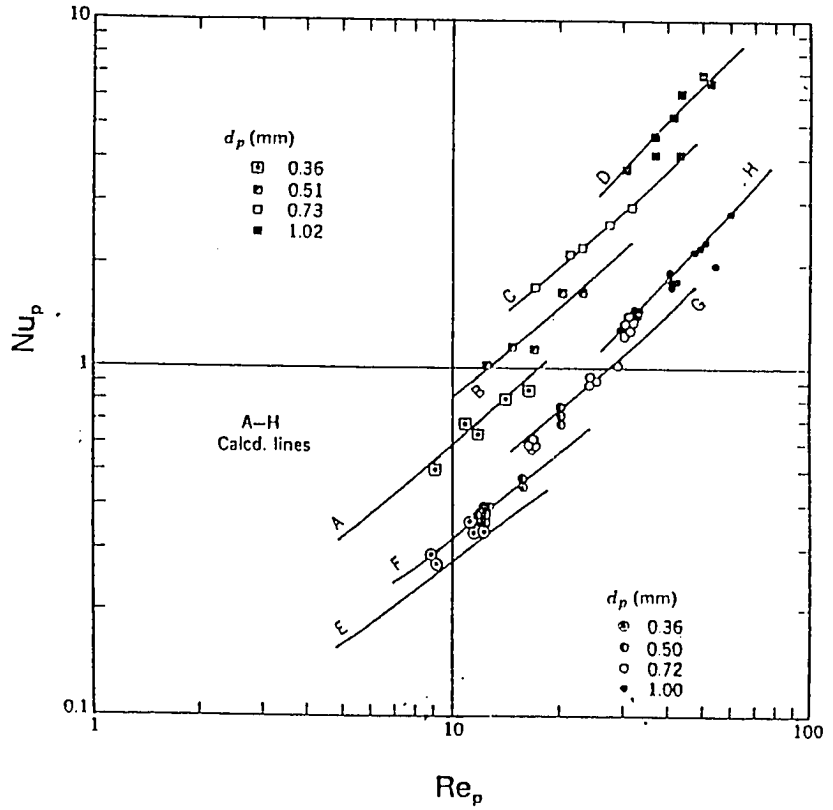

Figure 2.1: Experimental and calculated data for gas-solid heat transfer in fluidized beds.

at temperatures < 900 °K where the radiation heat transfer can be neglected (Botterill,1975). The favorable heat transfer coefficients between fixed surfaces and fluidized beds of fine particles result from high values of h_s.

The gas-convective term (h_f) occurs through mixing of gas percolating along the surface in the interstitial voids between the particles. Its contribution becomes increasingly important for denser and larger particles and at high operating pressures. Baskakov et al. (1974) correlated this term with some measurable parameters:

$$\frac{h_f \cdot \bar{d}_p}{k} = 0.009\ Ar^{0.5}\ Pr^{0.33} \qquad (2.2)$$

Whereas, Denloye and Botterill (1977) obtained a dimensional correlation:

$$\frac{h_f \cdot \bar{d}_p^{0.5}}{k} = 0.86\ Ar^{0.39}\ , \qquad (10^3 < Ar < 2\times10^6) \qquad (2.3)$$

Both equations show that the gas-convective component increases with particle size.

Radiative transfer term (h_r) for fluidized bed of large particles can be estimated approximately from the following well-known equation:

$$h_r = \frac{\sigma (T_w^4 - T_0^4)}{\left[\frac{1}{\epsilon_w} + \frac{1}{\epsilon_{bed}} - 1\right](T_w - T_0)} \qquad (2.4)$$

where T_w and T_0 are the wall (or surface) and bed temperature

respectively. For smaller particles, the radiative heat transfer phenomenon is more complex because the particle temperature changes appreciably during contacting with the surface. Experimental results of Baskakov et al. (1973) have shown that the fraction of radiative heat transfer increases with increasing wall temperature and particle size (Figure 2.2). Much lower fraction of radiative heat transfer were found by Yoshida et al.(1974), using catalyst particles of mean size 180 μm.

Since the present work is mainly concerned about the suspension-to-surface heat transfer, the following literature review concerning fluidized bed heat transfer will be restricted to this mode.

2.2 Mechanism of Suspension-to-Surface Heat Transfer

The mechanism of heat transport between particles and heat exchange surfaces is generally believed to involve heat absorption or release of particles. The gas in the system serves as a heat transfer medium and a stirring agent for the solids. Mechanisms based on these ideas have been suggested by various investigators (Mickley and Fairbanks, 1955; van Heerden et al., 1953; Wicke and Fitting, 1954), and experimentally examined by Ziegler and Brazelton (1964a).

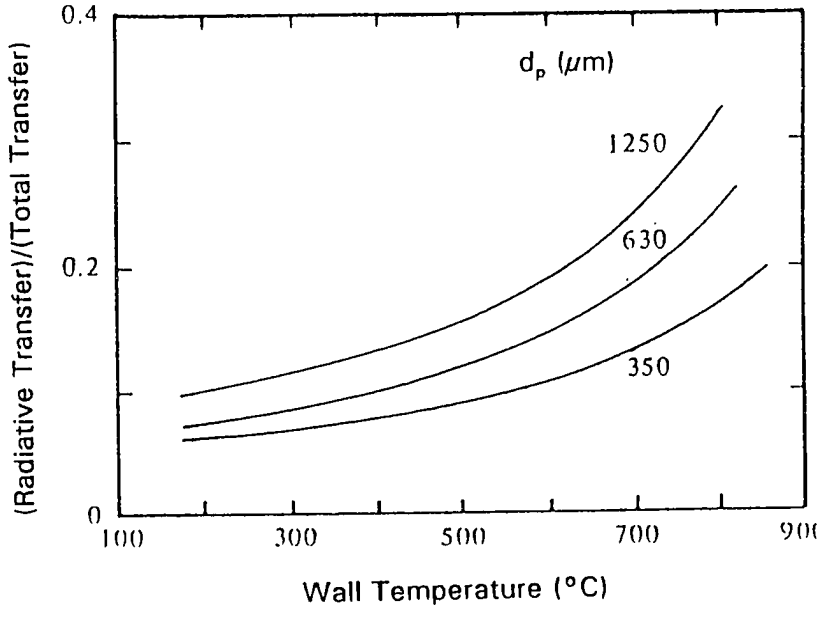

Figure 2.2: Fraction of total heat transfer resulting from radiation for three different sizes of chamotte particles as a function of wall temperature. Bed temperature was 850° C. Results are from Baskakov et al. (1973).

A number of theoretical models based on unsteady-state conduction to moving solid particles have been proposed for the suspension-surface heat transfer. Most of these models are proposed for suspension-surface heat transfer in dense fluidized beds. Some typical examples are briefly examined in the following sections.

2.2.1 Film Theory

In this approach, the principle resistance to heat transfer from a heating surface to a fluidized bed is assumed to be due to a fluid film. The decrease in film resistance is due to a reduction in film thickness caused by scouring action of moving solid particles (Leva,1959; Levenspiel and Walton, 1954; Dow and Jacob, 1951; Wasan and Ahluwalia, 1969). However, experimental results showed that the absorption of heat by solid particles rather than the reduction of the film resistance was the main mechanism for heat removal from the surface in a fluidized bed of small particles (Van Heerden et al.,1953; Ziegler and Brazelton, 1964a, 1964b).

2.2.2 Packet Theory

Mickley and Fairbanks (1955) proposed that when a cluster of particles rests on or close to a heated surface, the heat is absorbed by the "packet" or "cluster" of particles. The heated packet is then convected into the core of the bed and

is replaced by a fresh packet of particles. The composition and effective properties of the packet are assumed to be same as that of a bed at minimum fluidizing conditions. Unsteady - state diffusion of heat into a packet will commence upon contact of the packet with the heating surface. The instantaneous rate of heat flow into the packet is proportional to the root square of the product of heat capacity and thermal conductivity of the packet, and inversely proportional to the root square of the packet-surface contact time.

Gelperin and Einshtein (1971) correlated various data based on the packet theory. However, the use of these correlations requires knowledge of parameters for each particular fluidized bed system. Experimental data obtained by Harakas and Beatty (1963), Botterill et al. (1967), and Gabor (1972) are much lower than the instantaneous heat transfer coefficients predicted from the model for short residence times.

2.2.3 Particle Theories

The heat transfer is modeled by unsteady state conduction from the heater surface to a single particle (Zabrodsky, 1966; Botterill, 1975; Ziegler et al., 1964), or to depths of two particles (Botterill et al., 1967), or to a particle chain of essentially unlimited length (Gabor, 1970). In this type of

model, analysis is based on the heat transfer to distinct particles, rather than on treating the bulk of the bed as a homogeneous medium using average bed properties and an effective thermal conductivity. For this model, the primary resistance to heat flow is the gas phase.

In all the above-mentioned models (Sections 2.2.1-2.2.3), a knowledge of particle residence time and its distribution is necessary to predict the heat transfer rates in fluidized beds.

2.2.4 Kinetic Theory

Martin (1981) proposed a model that makes use of some basic ideas adopted from the kinetic theory of gases. The effect of various parameters (particle diameter, temperature, pressure, physical properties of the fluidizing gas, particles velocity, and gas velocity) on the heat transfer coefficient can be predicted quite well by using this model.

2.2.5 Models for Lean Phases

Biyikli et al. (1989) recently developed a phenomenological model for predicting heat transfer to tubes located in the freeboard region of gas fluidized beds. The model considers that the tube surface experiences alternating contact with a dense emulsion phase and a lean void phase.

The basic idea is originated from the Ismail and Chen's study (1984), which concluded that solids particles were carried from the dense bed into the freeboard in periodic bursts, rather than in a continuous stream.

According to this model, the total convective heat transfer coefficient is expressed as the sum of the average dense phase and lean phase heat transfer coefficients weighted by the fraction of contact by each phase:

$$\begin{aligned} h &= h_f + h_s \\ &= h_L \cdot f_L + h_D \cdot (1 - f_L) \end{aligned} \qquad \textbf{(2.5)}$$

where f_L is the fraction of total time for lean phase contact. The dense phase heat transfer coefficient (h_D) is based on the packet theory for bubbling beds. The lean phase (with void fractions greater than 0.8) heat transfer coefficient (h_L) for this model is based on a form suggested by Knudsen and Katz (1985):

$$Nu_L = a \cdot Re_L^b \cdot Pr_L^{1/3} \qquad \textbf{(2.6)}$$

where $Nu_L = h_L \cdot D_t / k_L$, $Re_L = \rho_L \cdot U_0 \cdot D_t / \mu_L$, $Pr_L = C_L \cdot \mu_L / k_L$, and D_t is the outside tube diameter; all physical and thermal properties are based on the lean phase.

The model could accurately correlates heat transfer data for tubes located in the freeboard of gas fluidized beds of 275 and 850 μm glass beads and 465 μm sand. However, the model needs tedious estimations of physical and thermal

properties of the gas-solids system and the particle-surface contact parameters of each specific fluidization condition. Moreover, Equation 2.6 was originally obtained for single phase convection. There is no theoretical background for the extension of the application to two-phase (i.e., solid/gas) mixture.

Xavier and Davidson (1981) also suggested a similar model for describing suspension-(tube)surface heat transfer in the splash zone of spouted beds of 885 and 1340 μm sand particles. They suggested that the heat transfer coefficient was a function of the fraction of time during which the surface is immersed in the bed. The dense phase coefficient is also based on the packet theory, while the lean phase coefficient is based on the interaction between the free-gas stream and the transfer surface. The model correlated the observed dependence of tube-suspension heat transfer coefficients with superficial gas velocity rather well. However, its application is limited to the splash zone of spouted beds.

Subbarao and Basu (1986) proposed a model for wall-to-bed heat transfer in circulating beds, using the packet theory in which clusters of solids and voids reach the heat transfer surface alternatively. Comparison was made with the data of Fraley et al. (1983). Basu and Nag (1987) later refined the model by taking into account the heat transfer to voids/bubbles and the effect that solids tend to aggregate

near the wall of the column to form a coreannulus structure. Agreement with experimental data was only fair.

Sekthira et al. (1988) proposed a model based on heat transfer to single particles. Solid particles are assumed to move down the heat transfer surface at their terminal velocity and receive thermal energy by convection from the fluid surrounding the particle. This model showed reasonable agreement with their own data. However, no comparisons with other data were reported.

The model proposed recently by Basu (1990) is similar to the Basu and Nag (1987) model. The only differences are that the fraction of wall coverage by clusters is derived from the particle population density expression of Sekthira et al. (1988); and the cluster residence time is based on simple experiments and concepts presented by Glicksman (1988).

Due to the lean phase nature and non-random motion of particles in the freeboard of a fluidized bed, the above models for dense beds and lean phases (mostly in circulating fluidized beds) can not be directly applied to predict or describe the heat transfer phenomena in the freeboard region. A mechanistic model is essential to predict and explain the dependence of suspension-to-surface heat transfer coefficient on solids physical properties, solids concentration, and solids dynamics in the freeboard. The development of such a

model is one of the objectives of this investigation.

The review of the theories for suspension-to-surface heat transfer mechanism is summerized in Table 2.1.

Table 2.1: Theories of Suspension-to-Surface Heat Transfer

Theory	Heat Transfer Mechanism	Reference
1. Film theory	Surface resistance is reduced by scoring action of particles	Leva (1959) Levenspiel & Walton (1954) Dow & Jacob (1951) Wasan & Ahluwalia (1969)
2. Packet theory	Heat transfer is enhanced by unsteady-state conduction between surface and packets of particles	Mickley & Fairbanks (1955) Gelperin and Einshtein (1971)
3. Particle theory	Heat transfer is enhanced by unsteady-state conduction between surface and distinct particles	Ziegler et al. (1964) Zabrodsky (1966) Botterill et al. (1967) Gabor (1970) Botterill (1975)
4. Kinetic theory	Heat transfer is enhanced by collision energy transfer between surface and particles	Martin (1981)
5. Theories for lean phases	Heat transfer surface experiences alternating contact with a dense emulsion phase and a lean void phase	Xavier & Davidson (1981) Subbarao and Basu (1986) Bibikli et al. (1989)
	Heat transfer surfaces experiences continuous streams of gas-particles suspension. Heat transfer is enhanced by distinct particles	Sekthira et al. (1988) Basu (1990)

2.3 Suspension-to-Surface Heat Transfer in Dense Beds

As described by Kunii and Levenspiel (1969), bed-surface heat transfer coefficients in gas fluidized beds have been found to be 20 to 40 times those for gases alone. Since the bed represents a complex interaction of gas and solid, many factors will affect this heat transfer behavior. Some possible factors usually considered by investigators are listed below:

(1). Properties of gas:
density, viscosity, specific heat, thermal conductivity

(2). Properties of solids:
size, shape, density, specific heat, thermal conductivity

(3). Minimum fluidization conditions:
minimum fluidization gas velocity, voidage

(4). Fluidization conditions:
superficial gas velocity, voidage

(5). Geometric dimensions:
bed size (diameter), dimension of heat exchange surface, location of heat exchange surface, orientation of heat exchange surface, static bed height, gas distributor.

A large number of experimental studies that deal with the effect of various variables on suspension-surface heat transfer in dense beds have been reported in the literature. Some pertinent results are discussed in the following sections.

2.3.1 Effect of Superficial Gas Velocity

Zabrodsky et al. (1978) studied the dependence of bed-to-surface heat transfer on superficial gas flow rate and particle size in air-fluidized beds of quartz sand. Results indicate that as U_0 increases h tends to increase, passes through a maximum, and then falls (Figure 2.3). These results could be explained by the packet model described in Section 2.2.2. At low flow rates, the primary effect of increasing U_0 is to improve the stirring action of bubbles so that the renewal frequency of fresh particles at the wall increases and heat transfer is improved. However, the fraction of time the heat transfer surface is covered by bubbles also increases, and this eventually outweighs the renewal effect and leads to the decrease in h. With the increase in particle size, the contribution due to the unsteady-state heat conduction to moving particles becomes less important, the maximum for larger particles becomes less pronounced (Figure 2.3).

2.3.2 Effect of Particle Size

Baskakov et al. (1973) and Zabrodsky et al. (1978) studied the effect of particle size on maximum bed-to-surface heat transfer coefficient for corundumand catalyst particles fluidized by air. Their results are shown in Figure 2.4. Over a broad range of particle sizes where particle convective transfer is dominant, h_{max} decreases with increasing d_p. The

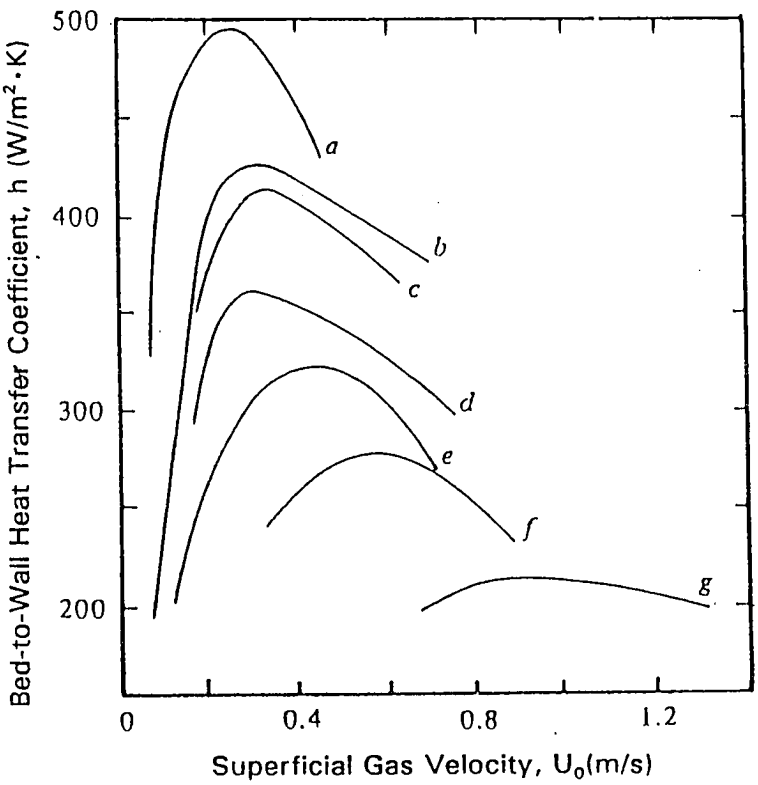

Figure 2.3: Bed-to-wall heat transfer coefficient plotted against superficial velocity for quartz sand particles of different mean size: (a) 140 μm, (b) 198 μm, (c) 216 μm, (d) 428 μm, (e) 515 μm, (f) 650 μm, (g) 1100 μm. Results are from Zabrodsky et al. (1978).

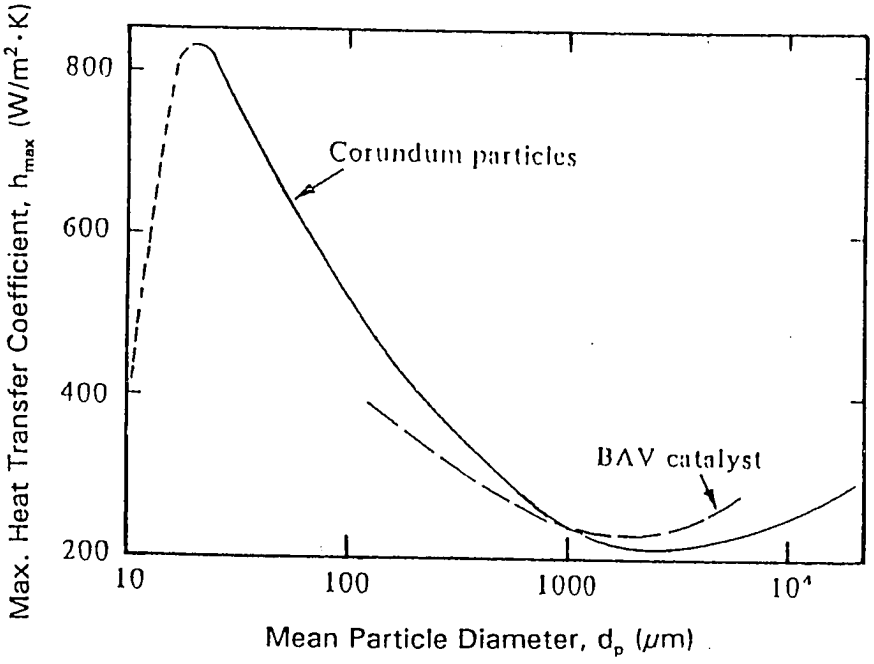

Figure 2.4: Effect of particle size on maximum bed-to-wall heat transfer coefficient for corundum and catalyst particles fluidized by air. Results are from Baskakov et al. (1973) and Zabrodsky et al. (1978).

qualitative interpretation of this result is that beds of smaller particles circulate fresh solid to contacting walls more rapidly at a given gas velocity. When d_p exceeds a certain value, typically in the range 1-3 mm, however, h_{max} begins to increase again because the gas-convective heat transfer become dominant.

2.3.3 Effect of Gas and Solid Thermal Properties

Mickley and Fairbanks (1955) investigated the effect of gas thermal conductivity on the maximum bed-to-wall heat transfer coefficients in fluidized beds of fine (d_p = 70 and 80 μm) particles. Results of using Freon, ammonia, methane, helium, and air as fluidizing gases indicated that h_{max} is proportional to the gas thermal conductivity to a power of 0.33.

Ziegler et al (1964) studied the effects of solid thermal properties on heat transfer to gas fluidized beds. Heat transfer coefficients were measured from an immersed sphere and cylinder to a bed of solids fluidized in an air stream. Three solid materials (i.e., copper, nickel, and solder) of same density but with varying thermal properties (heat capacity and thermal conductivity) have been used as testing solids. The heat transfer coefficient was found to increase with solid heat capacity and was independent of solid thermal conductivity. They concluded that h is proportional to $C_s^{0.5}$

both from theoretical analysis and experimental data. Effects of gas thermal conductivity on bed-to-surface heat transfer coefficient were also found to be $h \propto k^{0.5}$ from theoretical analysis. The exponent is in reasonable agreement with the value of 0.6 suggested in the literature (Wen and Leva, 1954).

2.3.4 Effect of Heater Length

Mickley and Fairbanks (1955) by analyzing the slug flow of a solid past the immersed surface in a fluidized bed concluded that the average heat transfer coefficient varies with heater length (L) as $h \propto L^{-0.5}$. The result is similar to that reported by Dow and Jakob (1951), i.e., the heat transfer coefficients between bed walls and fluidized beds operated at low gas rates (where an unbroken downward flow of solid occurred at the wall) varied as the -0.65 power of the heater length. Van Heerden et al. (1953) also observed similar behavior. The reason for decreasing heat transfer rate with increasing heater length is that thermal equilibrium between particles adjacent to heated surface may have been achieved with longer heater length.

2.3.5 Effect of Surface Geometry and Location

Surface geometry also plays an important role in suspension-to-surface heat transfer. Most frequently encountered surfaces are container wall, horizontal tubes, and vertical

tubes.

Zenz (1983) correlated a number of data and presented heat transfer as a function of particle Reynolds number and voidage over a wide range. The correlation shown in Figure 2.5 can be used to give a conservative heat transfer coefficient for vertical tubes and walls in commercial reactors. Similarly, Figure 2.6 applies to horizontal heat transfer tubes. Although the details of particle renewal at the surface of horizontal tubes differ from those for vertical tubes (Selzer and Thomson, 1977), the overall heat transfer coefficients usually do not differ greatly. Typically, the heat transfer coefficients for horizontal tubes are slightly lower than those for vertical tubes.

Vreedenberg (1960) found different heat transfer results for a vertical tube located in different radial positions of a bed (Figure 2.7). This may arise from nonuniform radial distributions of bubbles in the bed.

Noack (1970), Gelperin and Einstein (1971), and Berg and Baskakov (1974) investigated local heat transfer coefficient versus angular position for horizontal tubes in fluidized beds. At low gas velocities, the traces of heat transfer coefficients show maxima near the equator, where bubbles tend to sweep past frequently. Minima occur on the underside, where a film of gas covers the surface; and at the top, where

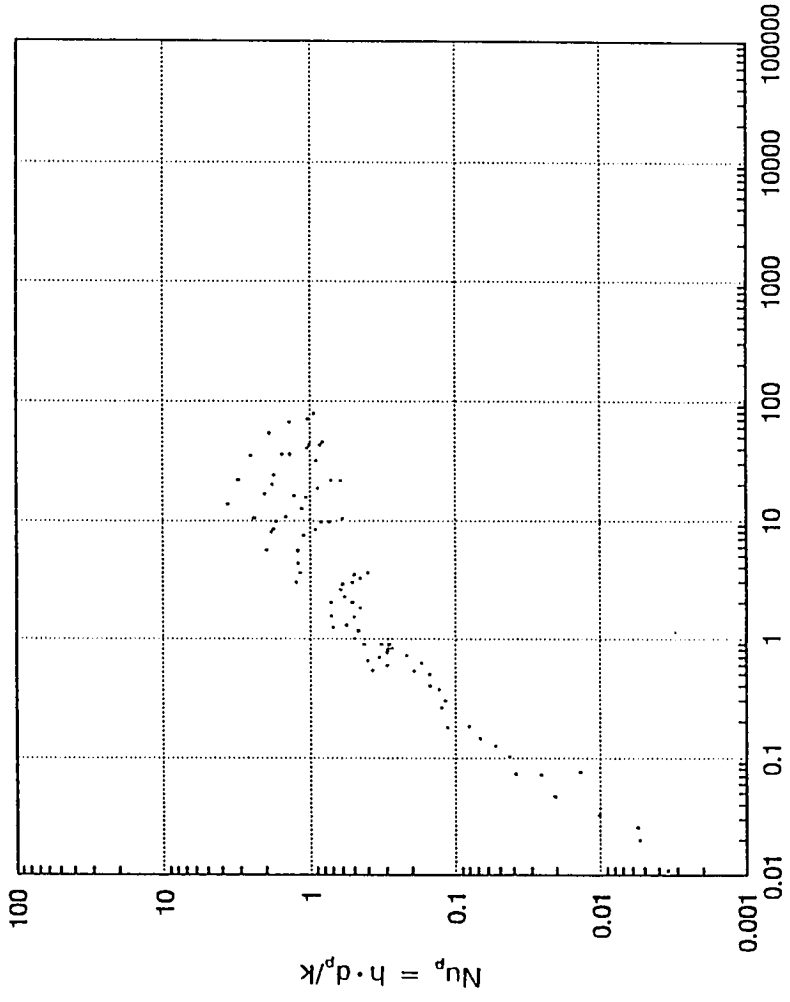

Figure 2.5: Zenz correlation for vertical heat transfer surface in fluidized beds.

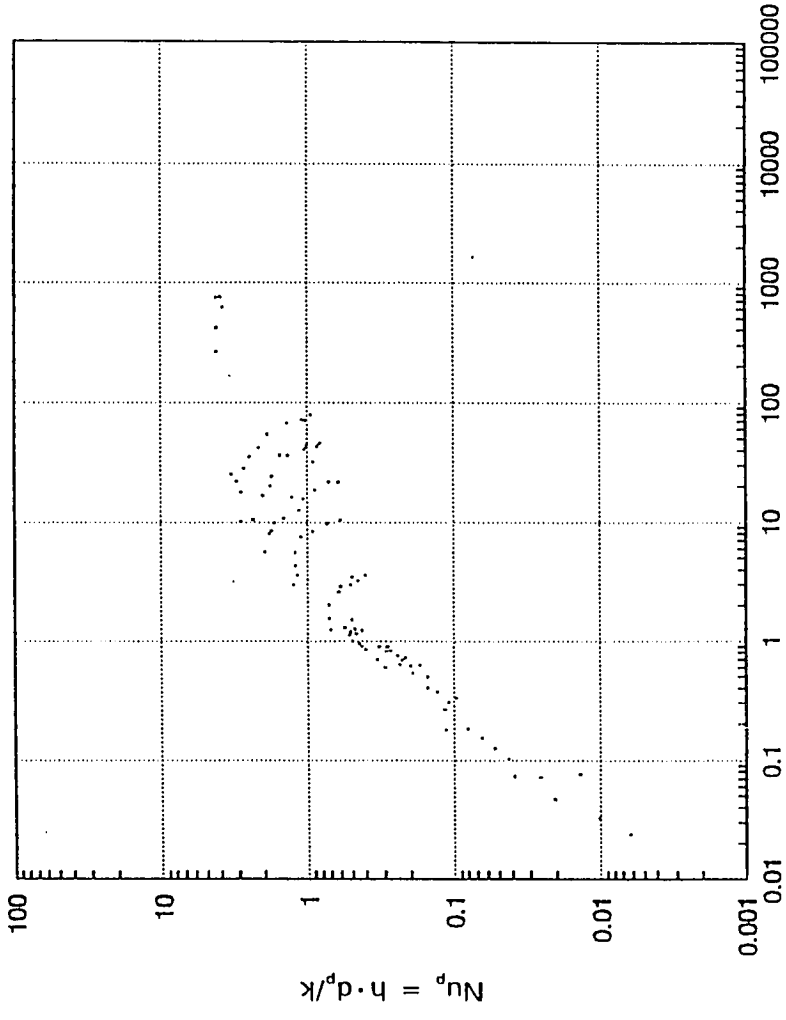

Figure 2.6: Zenz correlation for horizontal heat transfer surface in fluidized beds.

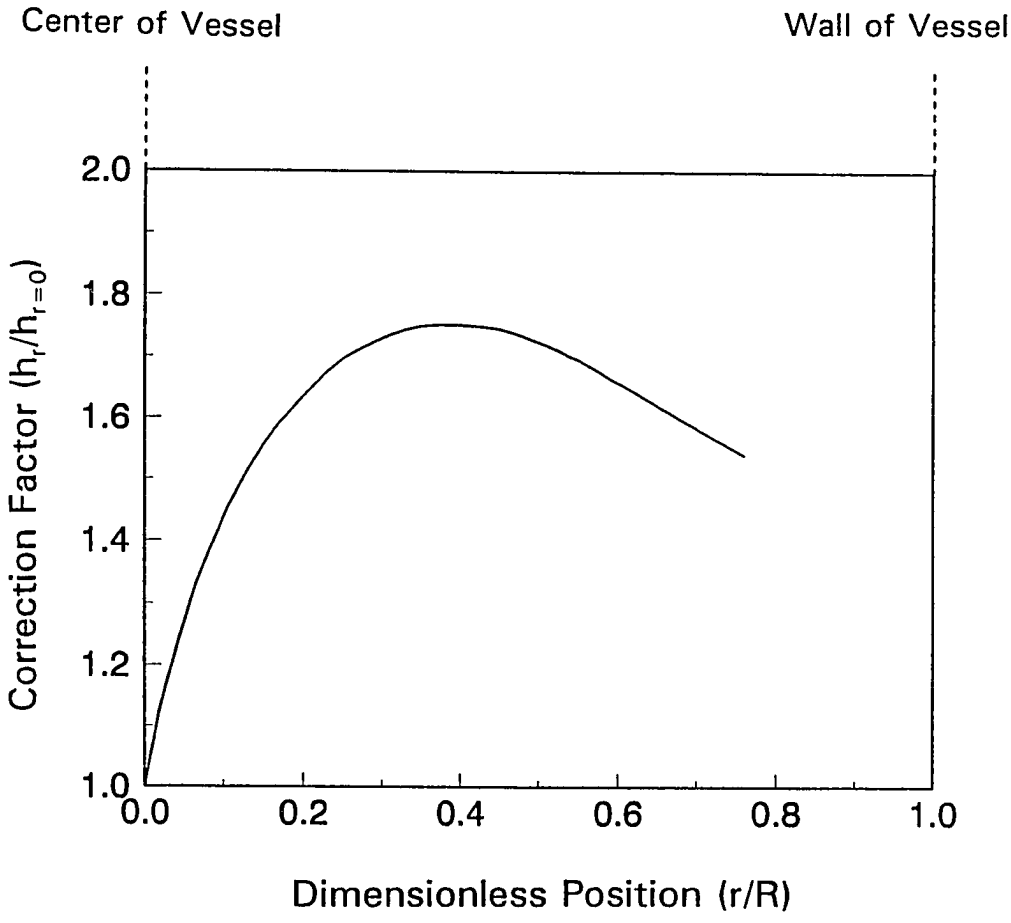

Figure 2.7: Bed-to-tube heat transfer correction factor for nonaxial location of immersed vertical tubes (originally given by Vreedenberg, 1960).

top, where particles are seldom replaced and the tube supports a stagnant cap of particles. With increasing gas velocities, the position of the maximum moves around to the top of the cylinder (Baskakov, et al., 1974), because of the regular dislodgement of particles there and the greater proportion of time the top surface is in contact with particles relative to the sides and the bottom.

For vertical tubes, the local heat transfer coefficient tends to fall with increasing height (Selzer and Thomson, 1977), but less rapidly than predicted from the packet theory under the assumption that particle movement is purely parallel to the surface. This implies that part of the solids motion is normal to the surface.

The effects of various factors on the suspension-to-surface heat transfer in dense bed are summerized in Table 2.2.

2.4 Suspension-to-Surface Heat Transfer in Lean Phase

Many factors affect the suspension-to-surface heat transfer rate in lean phases. Most frequently encountered direct variables are superficial gas velocity (U_0), particle size (d_p), solids flux (G) or concentration (C), and geometry, dimension and spatial location of heat transfer surfaces. Some of the these variables are inter-dependent. For example,

Table 2.2 Summary of Factors Affecting Suspension-to-Surface Heat Transfer in Dense Beds

Factor	Effects on Heat Transfer	Reference
1. Increasing superficial gas velocity (U_0)	h tends to increase first (due to higher surface renewal frequency by particles), passes through a maximum, and then falls (due to higher surface renewal frequency by bubbles)	Zabrodsky et al. (1978)
2. Increasing particle size (d_p)	(1). d_p<40 μm : h increases due to decreasing channeling effect	Baskakov et al. (1973) Zabrodsky et al. (1978)
	(2). 40 μm<d_p<1 mm : h decreases due to decreasing renewal frequency of particles	
	(3). d_p>1~3 mm : h increases due to increasing gas convective component	
3. Increasing thermal conductivity of gas (k), or solid (k_s)	h tends to increase with increasing k but independent of k_s	Mickley & Fairbanks (1955)
4. Increasing heat capacity of solid (C_s)	h increases with $C_s^{0.5}$	Ziegler et al (1964)
5. Increasing heater length (L)	h decreases with $L^{-0.5\sim-0.65}$	Dow & Jakob (1951) Heerden et al. (1953) Mickley & Fairbanks (1955)
6. Surface geometry & location	(1). h is slightly lower for horizontal tube compared with vertical tube	Zenz (1983)
	(2). for horizontal tubes, h is higher at sides with lower U_0, or at top with higher U_0	Noack (1970) Gelperin & Einstein (1971) Berg & Baskakov (1974)
	(3). h decreases with increasing surface elevation	Selzer & Thomson (1977)

solids flux and concentration in the freeboard of a fluidized bed may be affected by the superficial gas velocity and physical properties of the bed material and may be varied with freeboard height and radial position. Effects of some influential variables on the surface-suspension heat transfer in lean phases are reviewed.

2.4.1 Effects of Solids Flux or Concentration

Kiang et al. (1976) studied the wall-to-bed heat transfer in a fast-fluidized bed (4" diameter x 12' length) of 60-70 μm cracking catalysts. Several miniature heaters (3/4" o.d. x 2 1/4") were used for measurement of heat transfer coefficients. These heaters were located 21", 51", 93", and 123" above the distributor plate. Results indicated that heat transfer coefficients as high as those of a classical dense fluidized bed could be obtained. The study also shows: (1) the heat transfer coefficient increases with increasing solids recirculation rate, and (2) the heat transfer coefficient is very uniform in the bed.

Several investigators (Kobro and Brereton, 1986; Andersson et al., 1987; Basu et al., 1987; Feugier et al., 1987; Grace et al., 1987; Wu et al., 1987; Chen et al., 1988; Furchi et al., 1988; Skethira et al. 1988) showed that the suspension to surface heat transfer coefficient increases with suspension density.

Basu et al. (1987) reported that the particle heat transfer coefficient is proportional to the square root of suspension density. They explained that since the fraction of the wall area covered by the cluster is proportional to the square root of the cross-section average of the bed or suspension, the overall heat transfer coefficient will be proportional to the square root of suspension density.

However, the experiments of Chen et al. (1988) indicated that heat transfer coefficient was a linear function of the suspension density. The higher the suspension density, the higher the particle convective heat transfer coefficient. This indicates that particle exchange between the wall and the bulk increases with suspension density.

The reason for different degree of dependence of the heat transfer coefficient on the suspension density may be attributed to different systems used by Basu and Chen. Table 2.3 summarized some results of the effect of suspension density on the heat transfer coefficient. These results indicate that the heat transfer coefficient varied with suspension density to a power ranging from 0.18-1.68, mostly in the range of 0.4-0.8. Particles of smaller size gave higher value of C exponent.

Table 2.3 Summary of some results of the effect of suspension density on heat transfer coefficient.

Reference	d_p (μm)	Bed	Probe Size	C (kg/m^3)	α	h (W/m^{2}K)
Basu et al. (1987)	87 227 (silica)	D: 102mm H: 5.5m T: RT	2.5 cm	15-90	0.74 0.5	120-350 130-300
Subbarao & Basu (1986)	130 260 (sand)	(ibid)	(ibid)	10-100 10-80	0.37 0.18	110-250 110-150
Anderson et al. (1987)	240 (sand)	D: 70x70 cm H: 8.5 m T: 1000-1200 K	1 cm ϕ		0.39	
Sekthira et al. (1988)	300	T: 230°C	0.7 m	10-45	0.57	30-70
Furchi et al. (1988)	269	T: 30°C	6x1 m	10-45	0.41	35-70
Feugier et al. (1987)	95 215 625	D: 15 cm H: 7.0 m	15 cm ϕ, wall 95 cm L	4-40 10-60 20-50	1.05 1.03 1.68	20-200 20-100 5-30
Wu et al. (1987)	188 356	D: 152 mm sq. H: 7.0 m	1.5 m 2pcs	10-50 15-150	0.37 0.82	35-70 25-200
Grace et al. (1987)	303	(ibid) T: 750-850°C	(ibid)	8-35	0.34	70-110
Kobro & Brereton (1986)	170 250	T: 25°C	10 cm	20-80 20-80	0.62 0.46	90-210 55-150
Kobro & Brereton (1986)	170 250	T: 850°C	10 cm	9-60 20-75	0.46 0.53	130-310 130-250

1. α is the exponent in $h \propto C^{\alpha}$
2. Probe size in length or diameter
3. D: the bed diameter
4. H: the column height
5. h: total heat transfer coefficient
6. T: temperature

2.4.2 Effects of Surface Location

Byam et al. (1981) measured heat transfer coefficients in a fluidized bed combustor operating at 6 atm and 1630 °F. The combustor used for the study was 3 ft x 2 ft in plan area. The maximum bed depth was 9 ft and contained within this volume was 178 ft^2 of 1 1/4 inch diameter tubing arranged horizontally on a 3.5" horizontal and 3" vertical pitch. The cooling surface formed part of a tube bank of 6.7 ft deep. Water was used for cooling medium. Heat transfer in the splash zone and in the freeboard was investigated by varying the bed height between 4 and 9 ft. Results indicated that the overall heat transfer coefficient in the splash zone could be represented by an equation of the form

$$(h-h_{freeboard}) = \text{constant} \cdot e^{[-a(Z-Z_m)^2]} \qquad (2.7)$$

where $h_{freeboard}$ is the freeboard heat transfer coefficient, a is the constant, and z_m is the position relative to the surface of maximum immersed coefficient. The correlation seems unique in the study of freeboard heat transfer. Again, no mechanistic model or explanation was proposed or described in the report.

George and Grace (1982) measured overall heat transfer coefficients for a horizontal tube of diameter 25 mm in the freeboard region above fluidized beds of 102, 470, and 890 μm sand in a 0.25 m x 0.43 m x 3.0 m pilot column. The heat

transfer probe was a horizontal internally-finned tube with 25.4 mm outside diameter. The surface temperature was measured by eight thermocouples embedded in its surface. Internal cooling was provided by silicone oil whose temperature rise was measured by a differential thermocouple. A correlation between heat transfer coefficients and freeboard height was introduced:

$$\frac{h-h_f}{h_{bed}-h_f} = \frac{1}{1+\text{constant} \cdot X^n} \qquad (2.8)$$

where X equals z/z', z' represents the value of z at which $(h-h_f)/(h_{bed}-h_f)$ reaches 0.025, and n is a constant. This correlation is similar to that proposed by Biyikli et al. (1983) for horizontal tubes in freeboard. Again, no theoretical explanation was proposed.

Biyikli et al. (1983) investigated heat transfer around a horizontal tube (31.75-mm diameter) in freeboard region of fluidized beds (0.2 x 0.3 x 3 m) of glass beads (d_p = 275 and 850 μm) and silica sand (d_p = 285 and 456 μm). The horizontal tube for heat transfer coefficient measurement was embedded 8 Inconell foil strips to generate the required heat flux. Thermocouples, located in grooves under the strips, were used to determine rod surface temperature. Local heat transfer coefficients in the freeboard were found to be nonuniform around the tube. At gas velocity of 40 times minimum fluidization velocity, the coefficients at the top and bottom segments of the tube were found to be as much as three times

greater than the coefficients at the sides of the tube. The authors assumed that the trend is due to particle motion that results in more particle contact at bottom and top of the tube, and less contact at sides of the tube. Averaged heat transfer coefficients around the tube were found to drop more sharply at lower gas velocities than at higher ones. Data of George and Grace (1979) show similar trend.

Biyikli et al. (1987) measured suspension-to-horizontal-tubes heat transfer coefficients in the freeboard of high-temperature fluidized beds (300, 500, and 750 °C bed temperatures) of silica sand (d_p = 465 and 1200 μm) and limestone (d_p = 1400 μm). The circular bed had an inside diameter of 46 cm. An instrumented test tube of 3.8 cm o.d. and 24 cm length was placed horizontally into the bed for heat transfer measurement. Four thermoucouples were embedded into semi-circular grooves on the tube surface for measuring surface temperatures. Water was used for cooling medium. Heat transfer coefficients were measured at freeboard elevations of 19, 58, and 147 cm above a static bed height of 36 cm. Results indicated that, in general, for a given type of particle and at a given operating temperature, the heat transfer coefficient for a horizontal tube crossing the freeboard increases with increasing gas velocity and decreasesing tube elevation.

A functional relationship was proposed:

$$\frac{h-(h_r+h_f)}{h_{bed}-(h_r+h_f)} = \frac{1}{1+C_3\left[\frac{X}{U_n}\right]^{C_4}} \qquad (2.9)$$

where C_3 and C_4 are system parameters, X (=Z/TDH) is the dimensionless freeboard height, and U_n (= $[U_0-U_{mf}]/[U_t-U_{mf}]$) is the dimensionless superficial gas velocity. No theoretical background for the correlation was discussed.

Bi et al. (1989) measured heat transfer coefficients at different radial positions in a fast fluidized bed. They showed that the heat transfer coefficient was generally lower at the core than at the wall. The difference decreases with height. This expected result was due to the lower bed density in the core, especially in the top of the furnace (Tung et al., 1988).

Kunii and Levenspiel (1991) stated that in freeboard region, fast fluidization, and circulating solid systems, a thin layer of fine particles flows down along the containing walls. Also, when horizontal tubes are present in the freeboard, clusters of particles hit these tubes now and then. Variation of heat transfer coefficient with freeboard height was shown to be approximately:

$$\frac{h-(h_f+h_r)}{h_{bed}-(h_f+h_r)} \approx e^{-(a/2)\,Z} \qquad (2.10)$$

Data from Guigon et al. (1988) for h on horizontal tube banks

(50 mm dia.) immersed in a 1.19 x 0.79 m fast circulating fluidized bed of d_p = 260 μm were correlated with Equation 2.9. Only fair agreement was obtained. No detailed mechanistic explanation was described in the paper.

2.4.3 Effects of Gas Velocity

Hashimoto et al. (1990) measured heat transfer coefficients to the surface of vertical tubes (2.7 m x 48mm dia.) in the freeboard of a turbulent fluidized bed (0.45 m i.d. x 7 m) of particles with d_p = 48 μm. The heat transfer probe had a dimension of 48 mm o.d. x 0.5 m length with a cartridge heater 0.016 m in outside diameter and 0.5 m long inserted in the probe. The surface temperature was measured using thermocouples let into the surface at four positions, the arithmetic mean of the four temperatures being taken as the surface temperature. Experimental data indicated that heat transfer coefficient by particle convection (h_s) varied with $U_0^{1.9}$ for U_0 = 0.1-1.0 m/s. No solids concentration or velocity was measured in this study.

2.4.4 Effects of Particle Size

Wu et al. (1989) and Bi et al. (1990) indicated that the effect of particle size on the particle convective heat transfer is significant. Use of finer particles gives a higher heat transfer coefficient. This is due to the increas-

es in the contact surface area between particles and the surface. A typical example showing this effect was given by Bak et al. (1989).

Bak et al. (1989) characterized heat transfer for a vertical tube in a fluidized-bed combustor (bed: 15 cm dia., 1-m high; freeboard: 25 cm dia.,0.5 m high; particle size: 0.33-0.78 mm; bed temperature: 800-950 °C). A stainless tube 1.3 cm in diameter and 30 cm long was positioned at the wall in the freeboard for measuring the heat transfer coefficient. Air was used for the cooling medium. Results indicated that for d_p = 0.33-0.78 mm, the heat transfer coefficient in the freeboard was inversely proportional to the particle size to a power of 0.78 and directly proportional to the air velocity to a power of 0.18. No solids concentration measurement was made in the study.

2.4.5 Effects of Contact Time and Area of Heat Transfer Surface

The earliest study concerning the effect of particle-surface contact time on the heat transfer coefficient is the work of Mickley and Fairbanks (1955). From their Packet Theory for bed-surface heat transfer, the heat transfer coefficient was proposed to be inversely proportional to the square root of the contact time. The contact time was related to the operating conditions of the bed. Martin (1981) proposed a single-particle model for bed-surface heat transfer based on

a theory analogous to the kinetic theory of randomly moving gases. He assumed that the solid-surface contact time is proportional to particle diameter and inversely proportional to the particle velocity. This assumption lead to the success of his model. Although their models were derived from heat transfer study in the dense beds, the results revealed that the particle-surface contact time is an important control factor.

For lean phases, Glicksman (1988) stated that the average contact time of particles at the wall is one of the two important hydrodynamic factors which affect the wall-to-bed heat transfer in a circulating fluidized bed. He also showed that small heat transfer probes give higher heat transfer than larger ones. The reason is that heat transfer is limited by the temperature change of particle clusters moving down the walls. Larger probes result in longer contact time which causes thermal equilibrium between particles and the surface.

The reviewed published works for suspension-to-surface heat transfer are summerized in Table 2.4.

2.5 Lean Phase Gas-Solid Dynamics and Measurements

Lean phase gas-solid dynamics is closely related to bed-to-surface heat transfer. In order to evaluate the effects of variables stated in Section 2.4 on the particle

Table 2.4 Summary of the Literature Review for Suspension-to-Surface Heat Transfer in Lean Phases

Investigators	Bed		Solid	Heat Transfer Probe & Location	Results and Comments
	Dia. (cm)	Height (cm)			
Kiang et al. (1976)	10.2	366	60-70 μm cracking catalysts	fast bed	(1). h increases with solids flux. (2). h is uniform in fast fluidized bed. (3). No correlation proposed.
Byam et al. (1981)				freeboard of FBC cooling tubes	(1). h decreases with z^2. (2). No model or correlation proposed.
George & Grace (1982)	25	300	102, 470, 890 μm sand	25 mm o.d. horizontal tube in freeboard	(1). h decreases with freeboard height. (2). No mechanistic explanation.
Biyikli et al. (1983)			275, 850 μm glass beads; 285, 465 μm sand	31.75 mm o.d. horizontal tube in freeboard	(1). Nonuniform local h around the tube. h at top and bottom may be 3 times those of sides at large U_0. (2). Correlations between h and z were given.
Biyikli et al. (1987)			465, 1200 μm sands; 1400 μm limestone	horizontal tube in free board	(1). Correlation between h, z, and U_0 was given. (2). No theoretical background for the correlation.

Table 2.4 Summary of the Literature Review for Suspension-to-Surface Heat Transfer in Lean Phases (cont'd)

Investigators	Bed		Solid	Heat Transfer Probe & Location	Results and Comments
	Dia. (cm)	Height (cm)			
Bak et al. (1989)	15	100	330-780 μm	vertical tube in freeboard	(1). $h \propto d_p^{0.78}$. (2). $h \propto U_0^{0.18}$. (3). No solids conc. data.
Hashimoto et al. (1990)			48 μm	0.5 m x 48 m o.d. vertical tube in freeboard	(1). $h_s \propto U_0^{1.9}$ (U_0 = 0.1-1.0 m/s). (2). No solids conc. or velocity data.
Basu (1990)	10.2		87, 130, 227, 250, μm sand		(1). $h \propto C^{0.5}$ (C=10-80 kg/m^3). (2). Small particles give higher transfer rates. (3). Compressive mechanisms were given and validated. (4). Model parameters are not easy to estimate.
Kunii & Levenspiel (1991)					Theoretical consideration gave h decreases exponentially with z. Decay constant for h is half of that for solids flux or solids concentration.

convective heat transfer coefficient, an understanding of the hydrodynamics of the freeboard of the fluidized is necessary. Some published gas-solid dynamics works pertinent to the present study are reviewed in the following.

2.5.1 Solids Concentration Measurements

Lewis et al. (1962) studied entrainment from fluidized beds. They measured the vertical pressure gradient in the freeboard, and they derived particle density distributions from the results. They found that the density decreases with distance from the bed surface.

Morooka et al. (1980) used a capacitance probe to measure the hold-up of solid particles (65-68 μm) in the freeboard of a 12 cm i.d. fluidized bed. Results indicated that in the region of the freeboard higher than 30 cm from the dense bed, cross-sectionally averaged solids holdup decreased exponentially with increasing height. A much greater decrease in solids hold-up was observed in the splash zone of the freeboard.

Geldart (1981) measured solids concentration in the freeboard by using valves which could isolate the freeboard into separate vertical sections while the air supply to the bed was simultaneously shut off. The measured solids concentration in the freeboard decreases approximately exponentially

with height. This method can only give cross-sectionally averaged solids hold-up in the axial direction.

Pemberton and Davidson (1986) proposed a "three-phase model" to describe particles motion in the freeboard of fluidized beds. They postulated that in the freeboard there existed three phases: upward moving particles in the bulk gas, downward moving particles in the bulk gas, and the downward moving particles near the wall. Turbulent fluctuation of gas caused by erupting bubbles and solids emerging from bed surface was found to be decayed exponentially with distance above the bed surface in the freeboard (Pemberton and Davidson, 1984). Based on this model, solids hold-up in the freeboard was calculated to be varied with distance above the bed, z, as:

$$\frac{C}{C_0} = \exp[-K(1-e^{-\xi z})] \qquad \textbf{(2.11)}$$

where K is a function of turbulent fluctuation of gas on the bed surface, turbulent decay constant, ξ, bed diameter, superficial gas velocity, terminal velocity of bed particle, particle density, and particle diameter. The model gives detailed mechanism of gas-particle hydrodynamics in the freeboard. The authors also concluded that the film of fine particles falling near the freeboard wall appeared to induce gas circulation in the freeboard. This circulation may induce gas velocities to two or more times the mean upward gas velocity. This might explain the published observation that

the addition of fine particles amplifies the carry-over of coarse particles.

Glicksman and Piper III (1987) measured spatial distribution of solids hold-up in the freeboard of a fluidized bed of particles of 210 μm mean diameter. A fast-acting trapper was employed for sampling solids in the axial direction of the freeboard. A bubble probe using a light beam between two fiber optic probes was used to determine the presence of bubbles from the bed, and a hot-wire anemometer was used to measure the gas jet velocity from the bed surface. Experimental results indicated that in the splash zone solids hold-up decreases exponentially with distance above the bed surface. The decay constant varied inversely with $(U_0/U_{mf} - 1)$. The variation of solids holdup with distance above the bed surface and with U_0/U_{mf} is identical to the results for the splash zone heat transfer coefficient. The mean particle size in the freeboard did not vary significantly with height within the splash zone (36 cm) of the bed surface. No radial distribution of solids holdup was observed in this report.

Rhodes et al. (1988), using a sampling probe, investigated radial and axial variations of solids flux in the 150 mm diameter riser of an experimental circulating fluidized bed (CFB) of particles of d_p = 64 μm. They demonstrated that a non-isokinetic solids sampling method might be used to build up profiles of net solids flux in the raiser of a CFB. Their

preliminary results indicated that these profiles were parabolic in form with an upward-moving, high velocity dilute core surrounded by a slowly-falling relatively dense annulus. They also observed that the upward solids flux in the core region and the downward solids flux in the wall region both decreased with height in the riser. This effect was explained in terms of a transfer of solids from the core to the wall. No mathematical analysis was included.

Baron et al. (1990) studied the effect of static bed height on particle entrainment for a 0.61 m dia. gas-fluidized bed of silica sand of 65 μm mean diameter. In their study, the static bed heights were varied from 0.45 to 0.9 m and superficial gas velocities from 0.15 to 0.30 m/s. Results indicated both fluxes of particles ejected from the bed surface and entrained above the TDH increased with bed height. The effect of bed height becomes stronger when the gas velocity is increased. This study indicates that the effect of static bed height on solids dynamics cannot be ignored in the related studies.

Recently, Kunii and Levenspiel (1990) proposed a "Freeboard-Entrainment Model" to describe solids entrainment and holdup in the freeboard of bubbling fluidized beds. They have assumed that the freeboard above a bubbling or turbulent fluidized bed is composed of three distinct phases: the upward-moving solids agglomerates, the downward-moving solids

agglomerates, and the upward-moving dispersed phases. By solving mass balance equations for these three phases, they derived equations that indicate the upward solids flux and solids holdup in the freeboard decrease exponentially with increasing freeboard height. This work gives a theoretical background for Morooka et al.'s (1980) experimental observations: the solids holdup decreases exponentially with freeboard height.

2.5.2 Gas and Solids Velocities

Fournol et al. (1973) employed a hot wire anemometer to measure gas velocities in the freeboard. They obtained flat velocity profiles across the freeboard cross-section at a freeboard level (3.8 m) higher than TDH for two superficial gas velocity values. This indicates that there is little effect of particles on the gas flow in the freeboard levels high than TDH.

Horio et al. (1980) used a fiber optic probe and a hot wire anemometer to measure the particle and gas velocities respectively in the freeboard of a gas fluidized bed. They measured the freeboard turbulence in a 0.24 m diameter column with zero entrainment. They reported that the turbulence intensity at a specified freeboard height increased with increasing superficial gas velocity, static bed height, and with decreasing particle size. Turbulence intensity values

between 5% to 40% in the freeboard have been reported. The results of particle velocities measurements indicated that the velocities of particles at the center of column are larger than the superficial gas velocity.

Kale and Eaton (1985) conducted an experimental investigation of gas-particle flows through diffusers in the freeboard region of a fluidized bed of 50-100 μm glass beads. Gas velocity was measured by using a single-component laser-Doppler anemometer. Results indicated that the turbulence intensities above the bed for the straight-channel case was fairly uniform and decreased slowly in the axial direction. They also measured solids elutriation rates by solids collection at the bed exit. They concluded that the elutriation rate increased exponentially with increasing air velocity:

$$E = \kappa \cdot e^{\delta U_0} \qquad (2.12)$$

the parameter δ is approximately constant for a given static bed height and is not a function of the diffuser angle. The parameter κ, on the other hand, decreases with the diffuser opening angle and accounts for the effect of decreasing elutriation rate by the diffuser-type freeboard. No solids velocity data in the freeboard were reported.

Hamdullahpur (1985) measured the axial and lateral velocity distributions of air and particles (60 μm wood and 300 μm sand) in the freeboard of a two- dimensional (319 mm x

176 mm) fluidized bed. A laser-Doppler velocimeter was used. The gas-phase measurements revealed a fast decay of gas, local mean and r.m.s. velocity profiles with freeboard height. The lateral gas velocity distribution showed a maximum at the column center when measurements were made at locations close to the bed surface. The location of the maximum gas velocity shifted towards the column wall at higher freeboard levels. Particle velocity measurements indicated a two-stage decay of the velocity profile with height. Lateral distributions of sand velocity indicated a rather uniform pattern except at the wall vicinity where a sharp drop was observed. The results also indicated that, at the bed surface of the column center, the upward sand velocity might be two times as high as the corresponding superficial gas velocity.

The review in lean phase gas-solid dynamics and measurements is summerized in Table 2.5.

Table 2.5 Summary of the Literature Review for Gas-Solids Dynamics & Measurements in Lean Phases

Investigators	Bed Dia. (cm)	Solid	Measuring Technique		Results and Comments
			Gas Velocity	Solids Velocity or Conc.	
Lewis et al. (1962)				pressure drop	Pressure distribution can not yield an accurate indication of solids concentration in the splash zone.
Fournal et al. (1976)	60	58 μm FCC	hot wire		(1). Flat gas velocity profiles across the freeboard. (2). The measuring location may be above TDH.
Horio et al. (1980)	24	164-1350 μm glass beads	hot wire	fiber optics	(1). Turbulent intensity of gas increases with U_0 and bed height; decreases with z. (2). Particle velocity may be higher than U_0 at the column center; the particles near the wall move in reverse direction.
Morooka et al. (1980)	12	65-68 μm		fiber optics; capacitance probe	(1). Solids concentration decreases exponentially with z. Much greater decrease was observed in the splash zone. (2). Lateral distribution of solids is almost flat ($r/R < 5/6$). (3). Interal circulation of solids occurs within $z < TDH$.

Table 2.5 Summary of the Literature Review for Gas-Solids Dynamics & Measurements in Lean Phases (cont'd)

Investigators	Bed Dia. (cm)	Solid	Measuring Technique		Results and Comments
			Gas Velocity	Solids Conc. or Velocity	
Geldart (1981)				shutter valves	(1). Solids concentration decreases exponentially with z. (2). No radial distribution data of solids concentration.
Kale & Eaton (1985)		50~100 μm glass beads	LDV	cyclone	Entrainment rate increases exponentially with U_0 and related with diffuser angle of the free board.
Hamdullahpur (1985)	32	60 μm wood; 300 μm sand	LDV	LDV	(1). A two-stage decay of solids velocity profile with height was observed. (2). At the bed surface of the column center, the upward sand velocity may be two times the corresponding superficial gas velocity.
Pemberton & Davidson (1986)					Solids concentration is related to z and properties of solids by theoretical consideration.

Table 2.5 Summary of the Literature Review for Gas-Solids Dynamics & Measurements in Lean Phases (cont'd)

Investigators	Bed Dia. (cm)	Solid	Measuring Technique		Results and Comments
			Gas Velocity	Solids Velocity or Conc.	
Glicksman & Piper III (1987)		210 μm	hot wire	trapper	(1). Solids concentration decreases exponentially with z; the de cay constant is proportional to U_0-U_{mf}. (2). h decreases with z in similar trend as solids concentration. (3). No solids concentration dis tribution data in radial di- rection.
Rhodes et a. (1990)	15 cm CFB	64 μm		sampler	(1). Non-isokinetic sampling can be used in the present study for solids flux measurement. (2). Solids flux in the raiser is parabolic in the radial direc- tion.
Baron et al. (1990)	61	65 μm sand			Effect of bed height should be con- sidered in the study of freeboard hydrodynamics
Kunii & Levenspiel (1990)					Solids conc. in the freeboard de- creases exponentially with z from theoretical consideration.

2.6 Summary

The above review clearly supports the motivation of the present work. No detail local suspension-to-surface heat transfer data in the freeboard region have been published. Also, no directional effects on the heat transfer coefficient in the freeboard region have been published. Furthermore, no mechanistic model for suspension-to-surface heat transfer in freeboard has been proposed in the literature. These topics constitute the major objectives of the present study.

CHAPTER 3

HEAT TRANSFER PROBE

One of the focuses of the present study is the measurement of local heat transfer coefficients in the freeboard of a fluidized bed. The investigation of directional effects of gas-solids flow on suspension-surface heat transfer is another major objective. These studies require a miniature heat transfer probe that can be placed in a specified location and direction in the freeboard region.

In this chapter, probes commonly used in previous heat transfer measurements are first listed. Detailed construction of the probes designed for this work are then described. Finally, the applicability of these newly designed probes for heat transfer measurements is discussed and tested.

3.1 List of Heat Transfer Probes

Some techniques and probes used for previous heat transfer measurements in fluidized beds are listed in Table 3.1. None of the probes listed in the table meets the requirements (i.e., small relative to freeboard volume and variable in orientation) for the present study.

Table 3.1: Techniques and probes employed in previous heat transfer measurements in fluidized beds.

Heating Method	Probe	Temperature Measurement	Probe Location[1]	Reference
electrical heating	metal sphere (19.4 mm dia.)	built-in thermocouple	DB, FR (immersed, local)	Shirai (1962)
	vertical cylinder (3/8" o.d. x 6")	skin thermocouple	CFB (immersed, local)	Fraley et al. (1983)
	vertical cylinder (32 mm o.d. x 284 mm)	skin thermocouple	DB (immersed)	Chandran et al. (1980)
	horizontal cylinder (32 mm o.d. x 150 mm)	skin thermocouple	FR (immersed, across)	Biyikli et al. (1983)
	horizontal bar (40 x 20 x 10 mm)	skin thermocouple	DB, FR (immersed, center)	Xavier & Davidson (1981)
	metal strip (0.5 x 0.072 x 0.0010"thick)	thermocouple at both end	DB (immersed, local)	Mickley & Fairbanks (1955)
water	vertical tubes (12.7 mm o.d.)	thermocouple	DB, FR (immersed, wall)	Tabatabaie-Farashahi et al. (1981)
	horizontal tube (38.1 mm o.d.)	thermocouple	DB, FR (immersed, across)	Grewal et al. (1987)
	end of a metal rod (25 mm dia. x 100 mm)	thermocouple[2]	CFB (flush with column wall)	Basu (1990)

(1). CFB: circulating fluidized bed; DB: dense bed; FR: freeboard.
(2). Measuring temperature gradient along the rod.

3.2 Flat-Plate Heat Transfer Probe

The newly designed probe is shown in Figure 3.1. The probe was fabricated by adhering a segment of electrical heating Ni-Cr wire and a thermocouple between two sheets of steel plate. Metal parts were electrically insulated by the epoxy resin adhesive. Lateral sides of the plate were thermally insulated by adhering sheets of corkboard. For certain measurements, one side of the plate was also thermally insulated.

Plate-fluid or plate-suspension heat transfer coefficients were measured by applying a heat flux (Q/A) to the plate at a specified value of air velocity. At steady state condition (when the ambient fluid temperature (T_0) and the thermocouple junction temperature (T_j) were both invariant with time) the plate surface to suspension and to gas heat transfer coefficient (h_s+h_f) can be calculated from the following equation (Baskakov et al., 1973):

$$h_s + h_f = h - h_r = \frac{Q - Q_r - Q_i}{A \cdot (T_w - T_0)} = \frac{(I \cdot V) - Q_r - Q_i}{A \cdot (T_w - T_0)} \qquad (3.1)$$

where Q_r is the radiative heat dissipation rate, Q_i is the insulation heat loss rate, and A is the exposed surface area of the plate. Due to the low solids concentration in the freeboard (Morooka et al., 1980), Q_r can be estimated from the

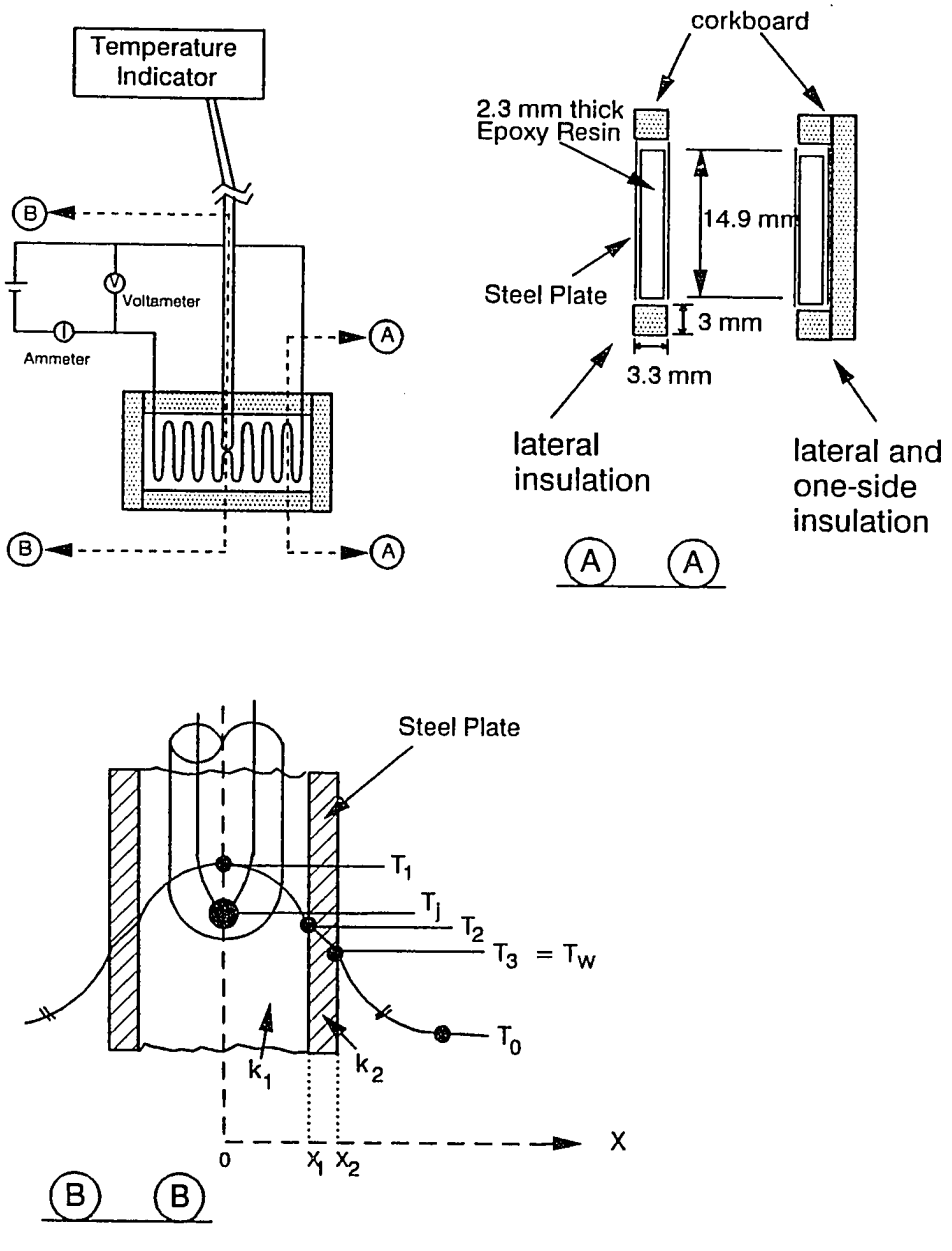

A-A : cross-sectional view
B-B : temperature profile in the vinicity of the thermocouple junction point

Figure 3.1: Schematic diagram of the heating plate.

equation:

$$Q_r = A \cdot \sigma \cdot \epsilon \cdot (T_w^4 - T_0^4) \qquad (3.2)$$

where σ is the Stefan-Boltzmann constant (5.67×10^{-8} $W/m^2 \cdot K^4$), and ϵ is the effective emissivity (0.60). Detailed explanation for the applicability of Equation 3.2 is discussed in Appendix 5. For lateral sides, Q_i may be neglected due to the relatively low temperature at the surface of the epoxy layer. For one-side insulated plate, Q_i can be calculated according to the method given in Appendix 4.

Before Equations 3.1 and 3.2 can be utilized to obtain the heat transfer coefficient, the plate surface temperature (T_w) needs to be estimated from the measurable thermocouple junction temperature T_j and physical properties of the plate.

3.3 Applicability of The Probe

3.3.1 Estimation of Plate Surface Temperature T_w

The mode of heat transfer inside the plate and in the gas film surrounding the plate is shown in Figure 3.1. By assuming a steady state constant specific heat generation rate (q) from the wire segment buried in the epoxy region and neglecting the heat dissipated from periphery of the plate, the governing differential equation in the epoxy region ($0 \leq X \leq X_1$) is given by:

$$\frac{d^2T}{dX^2} = -\frac{q}{k_1} \tag{3.3}$$

subjected to boundary conditions:

$$\frac{dT}{dX} = 0 \qquad \text{at} \quad X=0 \tag{3.4}$$

$$T = T_2 \qquad \text{at} \quad X=X_1 \tag{3.5}$$

where q is the specific heat generation rate (W/m^3) and k_1 is thermal conductivity of the epoxy resin ($W/m \cdot K$), and T is the temperature in the epoxy region.

Equations 3.3 to 3.5 can be solved to give the temperature change across the epoxy region, (T_1-T_2):

$$\begin{aligned} T_1-T_2 &= \frac{q}{2 \cdot k_1} X_1^2 \\ &= \frac{q \cdot X_1 \cdot A}{2 \cdot k_1 \cdot A} X_1 \\ &= \frac{Q/A}{2 \cdot k_1} X_1 \end{aligned} \tag{3.6}$$

where Q is the rate of energy generation. The temperature change across the steel plate ($X_1 \leq X \leq X_2$) is given by the one dimensional conductive equation:

$$T_2-T_3 = \frac{Q/A}{k_2}(X_2-X_1) \tag{3.7}$$

where k_2 is thermal conductivities of the steel plate. By assuming that T_j can be approximately given by:

$$T_j \approx \frac{(T_1+T_2)}{2}$$

T_j and T_w (i.e., T_3) can be related:

$$\begin{aligned} T_j - T_w &= T_j - T_3 \\ &\approx \frac{T_1+T_2}{2} - T_3 \\ &= \frac{(T_1-T_2)+2(T_2-T_3)}{2} \\ &= (Q/A)\cdot\left[\frac{X_1}{4k_1} + \frac{(X_2-X_1)}{k_2}\right] \end{aligned} \qquad (3.9)$$

The parameters in Equation 3.9 for calculating (T_j-T_w) are listed in Table 3.2. For example, (T_j-T_w) is equal to 1.33 °C for a heating rate (Q) of 2 W.

Table 3.2 Physical constants of the heating plate.

Dimensions	0.0149 m x 0.035 m x 0.0033 m	(Fig. 3.1)
Area, A	10.43×10^{-4} m^2 (two sides)	(Fig. 3.1)
Epoxy resin thickness, X_1	1.15×10^{-3} m	(Fig. 3.1)
Steel plate thickness, X_2-X_1	0.50×10^{-3} m	(Fig. 3.1)
Epoxy resin thermal conductivity, k_1	0.42 W/m·K	(Shah, 1984)
Steel plate thermal conductivity, k_2	45 W/m·K	(Perry, 1973)

3.3.2 Comparison of Calculated and Measured T_w

The validity of Equation 3.9 was tested by comparing the calculated surface temperature (T_{wc}) with the measured surface temperatures (T_{wm}) of the heating plate in an air current with a specified power dissipation, Q. The schematic diagram of the experimental apparatus is shown in Figure 3.2. The temperature measuring instrument and the surface temperature probe were calibrated according to the standard procedures in the manual to assure the accuracy of temperature measurements. The tip of the surface temperature probe was closely attached to the metal surface of the heating plate to measure the surface temperature.

The experimental and calculated surface temperatures are shown in Table 3.3. In all cases, the differences between T_{wc} and T_{wm} are small. The resulting error in heat transfer coefficient (h) calculation is within +2%~-5% It clearly indicates that Equation 3.9 can be utilized to estimate the surface temperature quite accurately.

The effect of the small difference of T_{wc} and T_{wm} on the result of the heat transfer coefficient measurement is small. In all cases, the relative differences in heat transfer coefficients calculated from T_{wc} and T_{wm} are smaller than 5%.

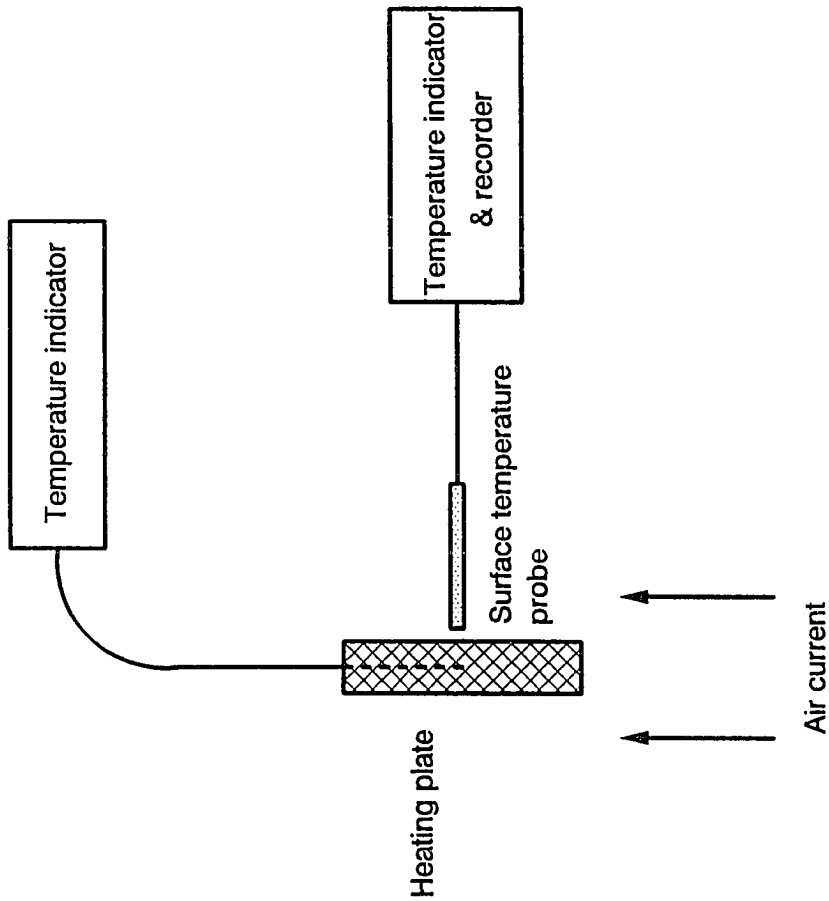

Figure 3.2: Surface temperature measurement system.

Table 3.3: Comparison between calculated and measured plate surface temperature, T_{wc} and T_{wm} and the resulting % error in heat transfer coefficient (h) calculation.*

Q (W)	T_j (°C)	T_{wc} (°C)	T_{wm} (°C)	$T_{wc}-T_{wm}$ (°C)	% Error** of h
3.825	104	101.4	101.8	-0.4	+0.52
"	102	99.4	99.7	-0.3	+0.40
"	98	95.4	96.4	-1.0	+1.42
"	85	82.4	80.7	+1.7	-2.96
1.132	53	52.2	51.5	+0.7	-2.57
"	51	50.2	49.0	+0.8	-4.76
"	49	48.2	47.5	+0.7	-3.02
"	47	46.2	45.3	+0.9	-4.24

* T_{wc} : Calculated outer surface wall temperature of the plate (Eq. 3.9)
T_{wm} : Measured outer surface wall temperature of the plate
T_j : Measured thermocouple temperature
h : Plate-air heat transfer coefficient

** The % error of h is calculated as follows:

$$\frac{h-h'}{h}\times 100\% = \frac{\left[\frac{(Q-Q_r)/A}{T_{wm}-T_0}-\frac{(Q-Q_r)/A}{T_{wc}-T_0}\right]}{\frac{[(Q-Q_r)/A]}{T_{wc}-T_c}}\times 100\% = \frac{(T_{wm}-T_{wc})}{(T_{wc}-T_0)}\times 100\%$$

where ambient temperature T_0 = 25 °C, and the heat loss is negleted.

3.3.3 Measurement of Plate-Air Heat Transfer Coefficient

Applicability of the heat transfer probe and Equations 3.1 to 3.3 was confirmed by comparing the coefficients measured in the free air stream and those calculated from literature.

Schematic diagram of the experimental apparatus is shown in Figure 3.3. The plate temperature (T_j) and the air temperature (T_0) were measured by temperature indicators (Yamatake-Honeywell, Japan). The air velocity was measured by a thermal anemometer (Model 8525, Alnor Co., USA). The air velocity was varied between the range of 0 ~ 6.3 m/s. The surface temperature T_w was estimated as described above. The heat transfer coefficient was then determined by Equations 3.1 and 3.2.

Values of h_f for comparison were calculated by substituting the experimental conditions into the equation:

$$\frac{h_f \cdot L}{k_f} = 0.906 \cdot Pr^{1/3} \cdot Re^{1/2} \qquad (3.10)$$

where L (0.0149 m) is the characteristic length of the heating plate. Equation 3.10 is given in Kays et al.(1980) for constant free-stream velocity along a semi-infinite plate with fixed surface heat flux.

Experimental and calculated results for plate-air heat transfer coefficients are shown in Table 3.4 and Figure 3.4. Experimental data for air flow parallel to the exposed plate

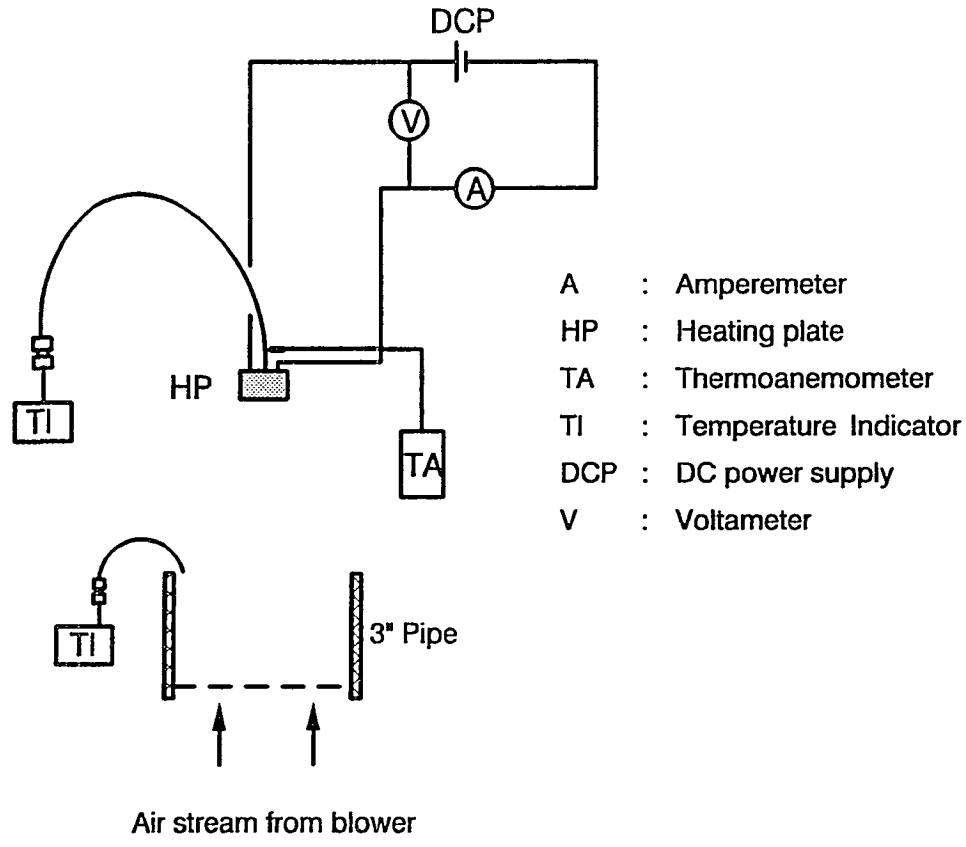

Figure 3.3: Experimental setup for measuring air-plate heat transfer coefficient.

surface are in good agreement with those calculated from Equation 3.10 for U_0 = 0.4~6.3 m/s. The results indicate that the plate is suitable for heat transfer measurements.

No h_f value for air flow normal to the plate surface has been published in the literature. From our measurements, the heat transfer coefficients for air flow normal to the plate surface are approximately equal to those parallel to the surface as shown in Table 3.4.

Table 3.4: Experimental Results for the Measurement of Air-Plate Heat Transfer Coefficients[1]

U_0 (m/s)	Q (W)	T_0 (°C)	T_j (°C)	T_w (°C)	Qr (W)	h_{fe} (W/m²·K)	Re	Pr	h_{fc} (W/m²·K)
0.00	1.071	17	68	67.3	0.224	16.1			
0.00	1.597	17	98	96.9	0.414	14.2			
0.40	1.071	27	65	64.3	0.167	23.3			
0.40[2]	1.071	27	64	63.3	0.163	22.8			
1.09	1.071	17	42	41.3	0.095	38.5	1028	0.706	44
1.09	2.617	17.5	85	83.3	0.320	33.5	917	0.703	44
3.24	1.071	17	30	29.3	0.048	79.9	3174	0.707	76
5.44	1.071	17	28	27.3	0.038	96.2	5330	0.707	98
6.24	1.071	17	27	26.3	0.034	106.9	6110	0.707	105
0.00	0.967	18	68	67.4	0.222	14.5			
1.09	1.000	18	40	39.3	0.083	41.3	1028	0.706	44
1.87	0.989	18	33	32.3	0.054	62.7	1760	0.707	57
3.24	0.978	18	30	29.3	0.042	79.4	3174	0.707	76
4.36	0.967	18	28	27.4	0.035	95.1	4270	0.707	89
5.44	0.956	18	27	26.4	0.031	105.6	5330	0.707	98

(1). All data were measured for air flow parallel to the plate surface, except specifically specified.
(2). Air flow normal to the plate surface.
(3). h_{fe}: heat transfer coefficient, experimental data.
h_{fc}: heat transfer coefficient, calculated from Eq.(3.10).

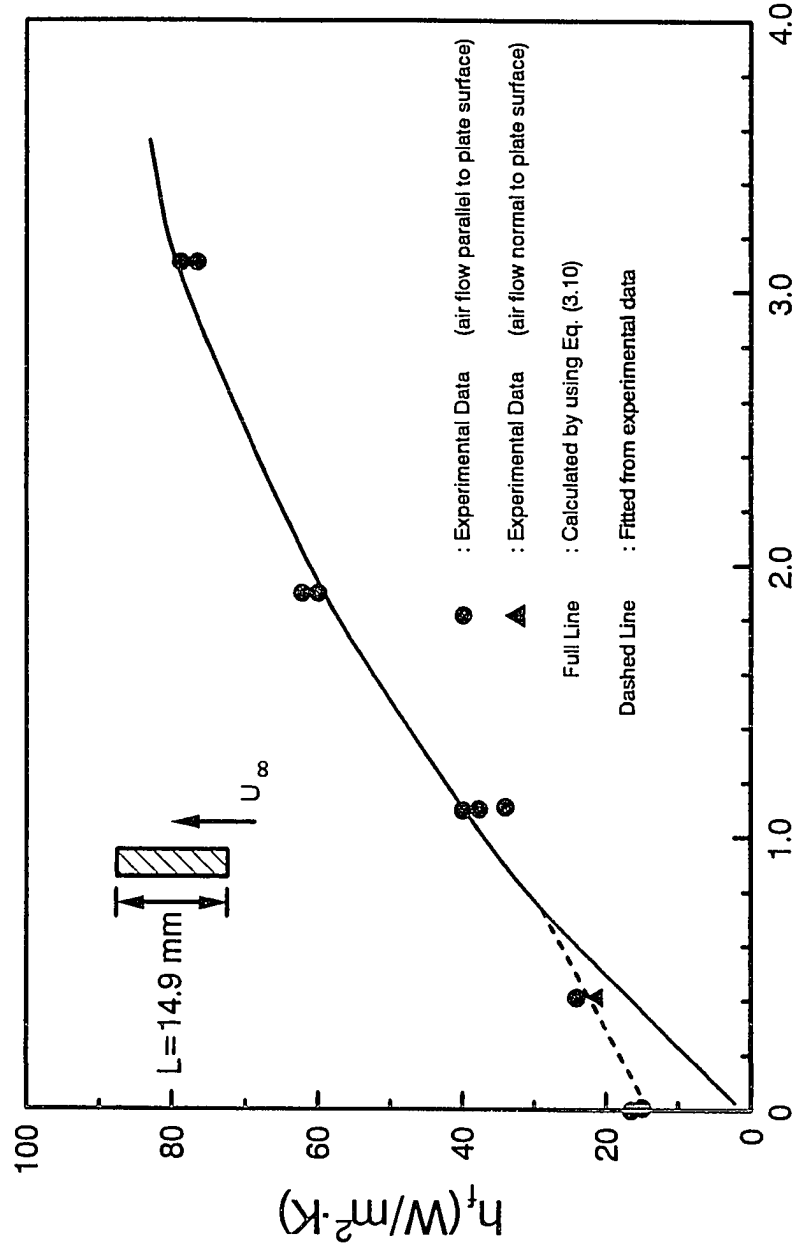

Figure 3.4: Experimental and calculated air-plate heat transfer coefficients for air flow. Deviation of the experimental data from those calculated by Eq. (3.10) at U_0 < 0.6 m/s might be caused by dominant heat transfer from natural convection at low gas velocities. Eq. (3.10) is applicable only for forced convection.

3.4 Summary of the Heat Transfer Probe

The structure and construction of a miniature heat transfer plate were discussed in this chapter. Applicability of the plate and Equations 3.1, 3.2, and 3.9 for heat transfer coefficient measurement has been confirmed by comparing the coefficients measured in the free air stream and those calculated from literature.

CHAPTER 4

EXPERIMENTAL SETUP

This study was conducted with the objective of analyzing the heat transfer in gas-solid suspension in the freeboard of a fluidized bed. The investigation included several phases of work, as described in Section 1.12. This chapter discusses the detail of experimental setups including the fluidized bed, bed particles, the setup for heat transfer coefficient measurement, and the apparatus for solids concentration measurement.

4.1 Experimental Fluidized Bed

A cold flow bubbling fluidized bed unit was designed, constructed, tested, and operated. Its schematic diagram is shown in Figure 4.1. The main body of the fluidized bed is a transparent acrylic column with an inner diameter of 0.3 m and a total column height of 2.0 m. This unit was designed to operate at atmospheric pressure and room temperature. The fluidizing gas (air) was introduced into the bed from a 15 HP Roots blower (air flow rate 8 m^3/min, maximum pressure 5000 mm water). that can provide a maximum superficial velocity of 1.9 m/s. The superficial air velocity in the column can be varied by an AC inverter. The gas distributor consists of a 10 mm thick acrylic perforated plate with 2.0 mm holes in an

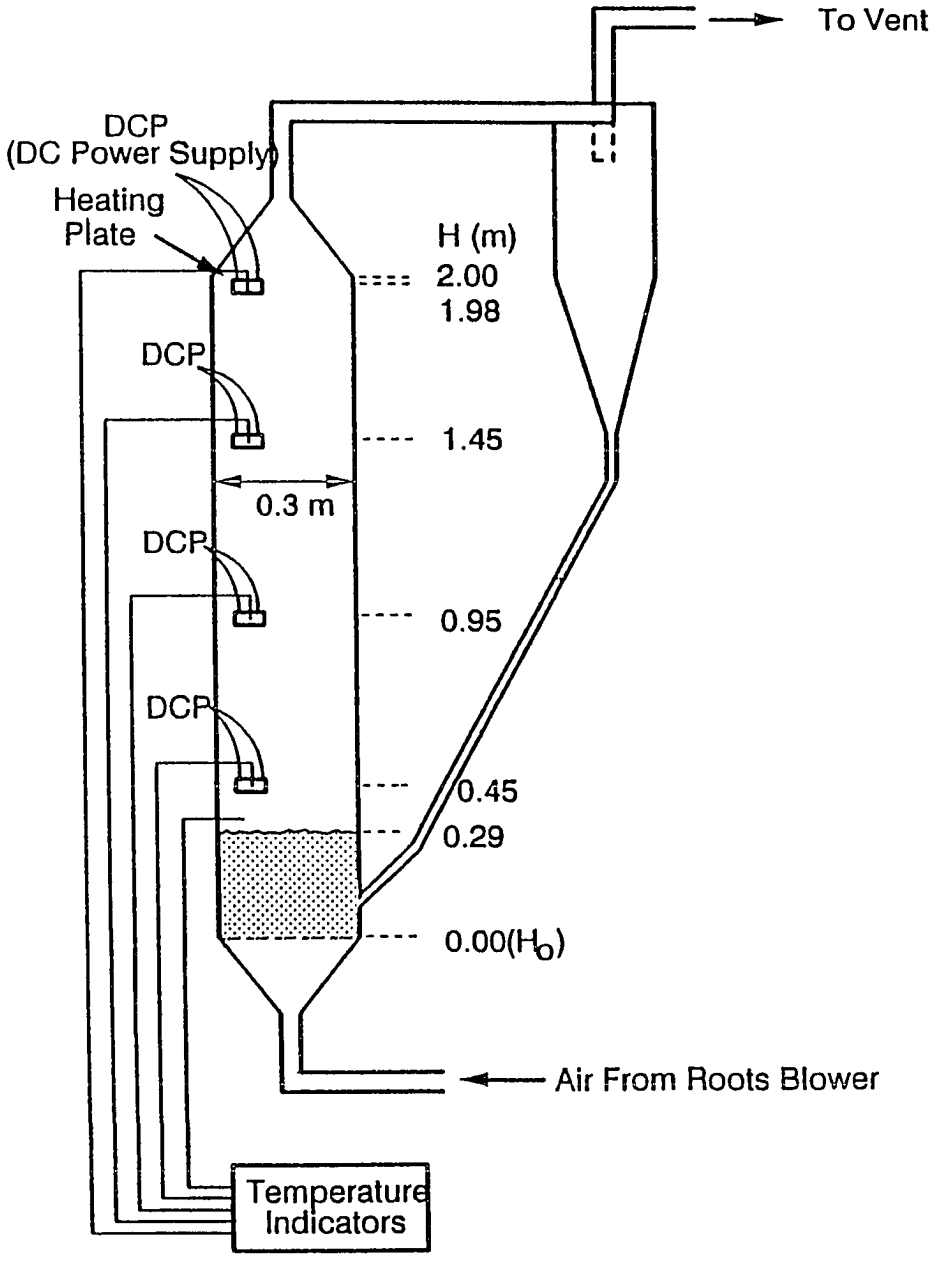

Figure 4.1: Schematic diagram of the fluidized bed.

equilateral square arrangement of 8.5 mm pitch. A filter cloth is placed under the perforated plate to retain the solid particles. The cyclone is used for collecting entrained solid particles that can be circulated back into the dense bed via the down-flow pipe.

4.2 Solid Particles

Equilibrium FCC solid particles (Focus-1, Fitrol Co., USA) were used as bed material. The volumetric-mean diameter of the bed particles is 90 μm, and its size distribution is shown in Figure 4.2. Physical properties of Focus-1 particles are shown in Table 4.1. For easy comparison, the physical properties of Focus-1 as well as other equilibrium FCC catalyst particles are given in Table 4.2.

Table 4.1: Physical properties of test solid particles

Item	Value	Note
Volumetric mean particle size (μm)	89.6	
Pore volume (cm^3/g)	0.22	
Inner particle porosity	0.342	(1)
Bulk density (g/cm^3)	0.796	(1)
True density (g/cm^3)	2.36	(1)
Apparent density (g/cm^3)	1.554	(1)
Inter-particle void volume fraction	0.487	(1)
Specific heat (J/g·K)	0.774	(2)
Apparent thermal conductivity (W/m·K)	0.69	(3)
Minimum gas fluidization velocity (m/s)	0.005	(4)

(1). Obtained by using water displacement method. Bulk density is the weight of solid particles per unit packed volume; true density is the density of solid material constituting the particle; apparent density is the density of a particle (or mean density of particles) including pores therein.
(2). Measured by using differential thermal analyzer (DTA).
(3). Estimated from data in Perry's Handbook.
(4). Calculated by using Eq. (1.4).

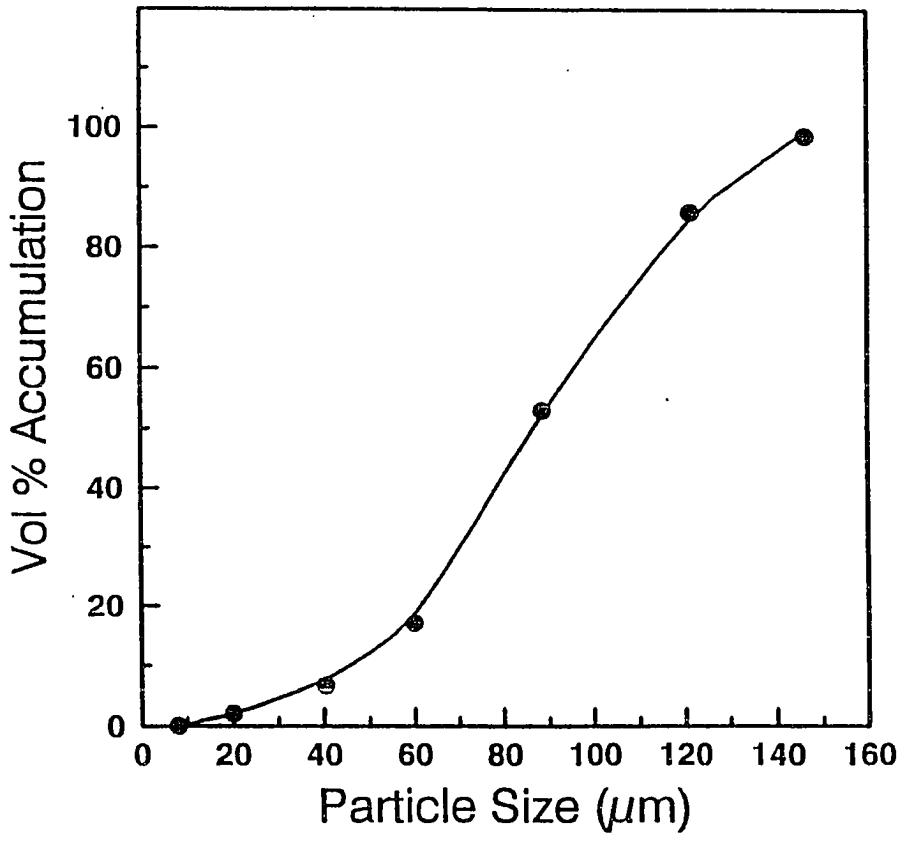

Figure 4.2: Particle size distribution of the FCC solids.

Table 4.2: Physical properties of equilibrium FCC catalysts.

Physical properties & composition	Focus 1*	Sigma +400*	Silica† /Alumina	Zeolite†
Surface area (m^2/g)	91	96	140	97
Pore volume (cc/g)	0.22	0.25	0.43	0.45
Bulk density (g/cc)	0.75	0.80	0.70	0.68
Av. particle size (μm)‡	89.6	89	63	62
< 20 μm (wt%)			0	0
< 40 μm (wt%)			8	6
< 80 μm (wt%)			69	75
SiO_2 (wt%)	47.0	60.9	n.a.	n.a.
Al_2O_3 (wt%)	51.7	38.3	21.5	25.4
C (wt%)	0.01	0.02	0.2	0.04
Na (wt%)	0.36	0.43	0.02	0.04
La (wt%)	0.47	0.48	n.a.	n.a.
Fe (wt%)	0.53	0.48	0.39	0.37
Sb (wt%)	0.11	0.07	n.a.	n.a.
Ni (wt%)	0.04	0.08	n.a.	n.a.
V (wt%)	0.07	0.15	n.a.	n.a.
V+Na+Cu (wt%)			0.016	0.026

n.a.: not available.
* : equilibrium (used) catalyst taken from cracker of Chinese Petroleum Corp.
† : Japan Chem. Eng. Soc., "Fluidized Bed Reaction and Equipment", p. 205, Chemical Industrial Publishing Co., Japan (1988).
‡ : measured by a laser-scattering type particle size analyzer (Leed and Northrup Microtrac Model 7991-01, USA)

4.3 Instruments for Heat Transfer Measurement

The setup for heat transfer coefficients measurement has been illustrated in Figure 3.2. The detail of the heating plate was also discussed in Chapter 3. The orientations of the plate will be discussed in Chapter 5. The location of the probes are shown in Figure 4.1.

4.4 Instruments for Solids Concentration Measurement

This section describes the instruments used for solids concentration measurement.

4.4.1 Techniques for Solids Concentration Measurement

Table 4.3 lists some common methods for solids concentration measurement in gas-solids two-phase systems. Most of these methods can be applied to low solids concentration systems such as the raiser of CFB beds or the freeboard regions of bubbling fluidized beds. In Table 4.3, the capacitance and optical fiber probes are ideal for low temperature applications. Light scattering or reflection methods (e.g., Laser-Doppler photometric systems) have disadvantages of high equipment cost and of limited applications in bright-fired environments, such as in the freeboard of a fluidized bed coal combustor. Trapping of solids by shutter plate is limited to bench-scale columns, and no local data can be obtained. For

the thermal response method (instantaneous heating of a particle followed by detection of particle temperature by an intrusion thermocouple probe, Morooka et al., 1980), the experimental data may be affected by the distance between the heater and the thermocouple. Sampling either by suction tube or trapper has merits of simple instrumentation and easier, although laborious, operation. Local data can also be obtained by varying the sampler location. This method was therefore selected for the present study.

Table 4.4 Methods for lean-phase solids concentration measurement

Method	Reference
Light scattering or reflection	Horio et al. (1985)
Capacitance	Patrose & Caram (1982) Bakker & Heertjes (1958) Ismail & Chen (1984) Chandran & Chen (1982) Morooka et al. (1980)
Pressure drop(1)	Kojima et al. (1989)
Shutter plate	Morooka et al. (1980) Pemberton & Davidson (1986)
Trapper	Glicksman & Piper III (1987)
Cyclone collection(2)	Choi et al. (1989)

(1). Applicable to CFB's and fast fluidized bed only.
(2). For entrained solids only.

4.4.2 Solids Sampling System

Schematic flow diagram of the solids sampling system and detail drawing of the sampler mouth are shown in Figure 4.3. The nozzle-type sampler mouth is similar to that used by Fournol et al. (1973) for cracking catalyst solids entrainment investigation in a large gas fluidized bed. As shown in Figure 4.3, solid particles in the freeboard are first sucked into the mouth and then accelerated in the reducing section to prevent particle settlement in the glass transfer tube. The sucked solids are settled down and gathered in the collector. The suction air flow rate, calibrated by the auxiliary rotameter and the soap-film gas flow meter, can be varied by the control valve.

Solids concentration can be calculated from the following equation:

$$C = \frac{\text{Weight of sampled solids (g)}}{\text{Sampling time (s)} \cdot \text{Suction air flowrate (L/s)}} \qquad (4.1)$$

Detailed calibration and operation procedures will be described in Chapter 5.

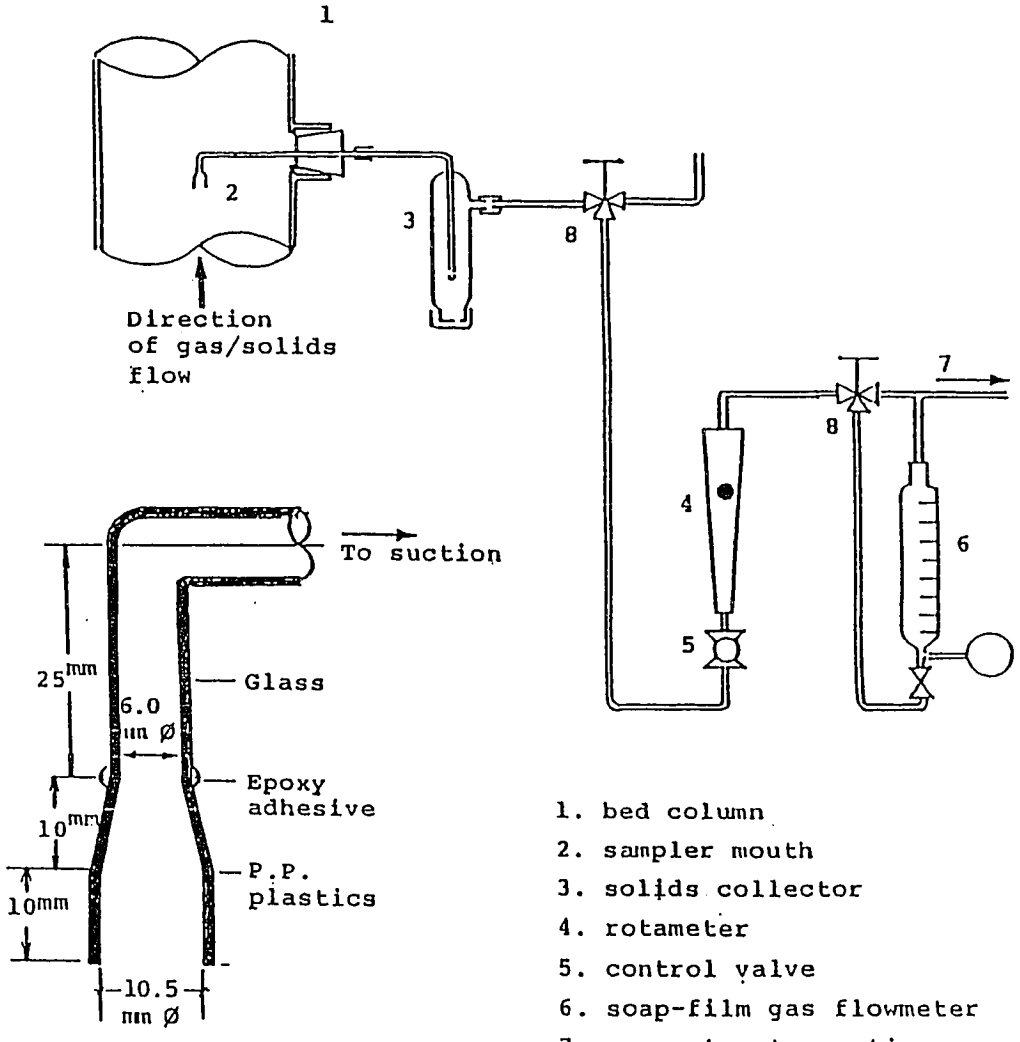

Figure 4.3: Schematic diagram of the solids sampling system.

4.5 Summary

In the present study, an air-fluidized bed (0.3 m i.d. x 2.0 m height) was constructed. The bed can be operated to a maximum superficial gas velocity of 1.9 m/s at ambient temperature. Equilibrium FCC catalyst particles (Focus-1) were used as bed material. The miniature heating plate described in Chapter 3 was immersed into the freeboard for heat transfer measurements. A solids sampling system has also been illustrated for measurement of local solids concentration in the freeboard region. Detail specifications of the experimental fluidized bed and its auxiliary equipments are described in Appendix 6. Procedures for testing and operating the bed will be described in Chapter 5.

CHAPTER 5

EXPERIMENTAL TECHNIQUES

This chapter discusses the experimental techniques for measuring the local heat transfer coefficients and solids concentration in the freeboard region. Experimental schedule is shown in the following table (Table 5.1).

Table 5.1 Experiment schedule

Task	Variable Adjusted	Data Measured	Result
1	f	air velocity at the gas exit of the cyclone	correlation between U_0 and f
2	U_0	dynamic bed height	dynamic bed height vs. U_0
3	U_0, r, H, and orientation of heat transfer plate	suspension-surface heat transfer coefficient in the freeboard	$h_s + h_f$ vs. U_0, r, and H for each plate orientation
4	U_0, r, and H of solid sampling probe	solids concentration in the freeboard	solids concentration vs. r and H

f : frequency output of the AC inverter attached to the blower.
U_0 : superficial gas velocity
r : radial position in the experimental column
H : axial position in the experimental column (measured from upper surface of the perforated plate)
h_s : particle convective heat transfer coefficient
h_f : gas convective heat transfer coefficient

5.1 Calibration of the Gas Flow Rate

The rate of gas flow from the Roots blower was calibrated by measuring the air velocity at the gas exit of the cyclone before the solids were loaded into the column (Figure 4.1). The air velocity was measured by a thermal anemometer (Model 8525, Alnor Co., USA) calibrated according to the procedure given in the operational manual. The flow rate of air can be varied by changing the frequency (f) output of an inverter attached to the blower. The superficial air velocity (U_0) in the column can be correlated with the inverter frequency (f) by the following equation:

$$U_0 = 0.03\ f \quad (m/s) \tag{5.1}$$

for f equal to 5.0~30 Hz.

5.2 Static Bed Height

After the gas flow rate was calibrated, the bed was loaded with FCC solids (Section 4.2). A static bed height of 29 cm was used in all experiments. However, the results from this work can be applied to other static bed heights by incorporating data of solids concentration and other related physical properties of the solid particles into the heat transfer model developed in Chapter 8.

5.3 Bed Temperature

The bed temperature was not controlled. It varied with ambient temperature in the range of 17-30 °C. The bed temperature was measured by a temperature indicator (Yamatake-Honeywell, Japan) with a thermocouple inserted in the free-board at the location where r = 14 cm and H = 1.5 m.

5.4 Measurement of Local Heat Transfer Coefficients and Dynamic Bed Height

Local heat transfer coefficients were measured by immersing the four electrical heating plates at specified locations and orientations (Figures.4.1 and 5.1). After the probes had been fixed in position, air was introduced into the bed at a specified rate. The column was then inspected to see if there was leakage of solids from the column wall. A heat transfer measurement system was actuated after confirming no leakage. When both temperature readings of the probe and the bed had become invariant with time (typically, 5 min after actuating the blower and the heater), readings of temperature indicators and voltage and current of DC power supply systems were recorded. Heat transfer coefficients contributed from solids and gas convection were then calculated by using Equation 3.1.

Seven different superficial gas velocities in the range of 0.28-0.64 m/s were employed in the experiments for each type of plate orientation at a specific spatial location.

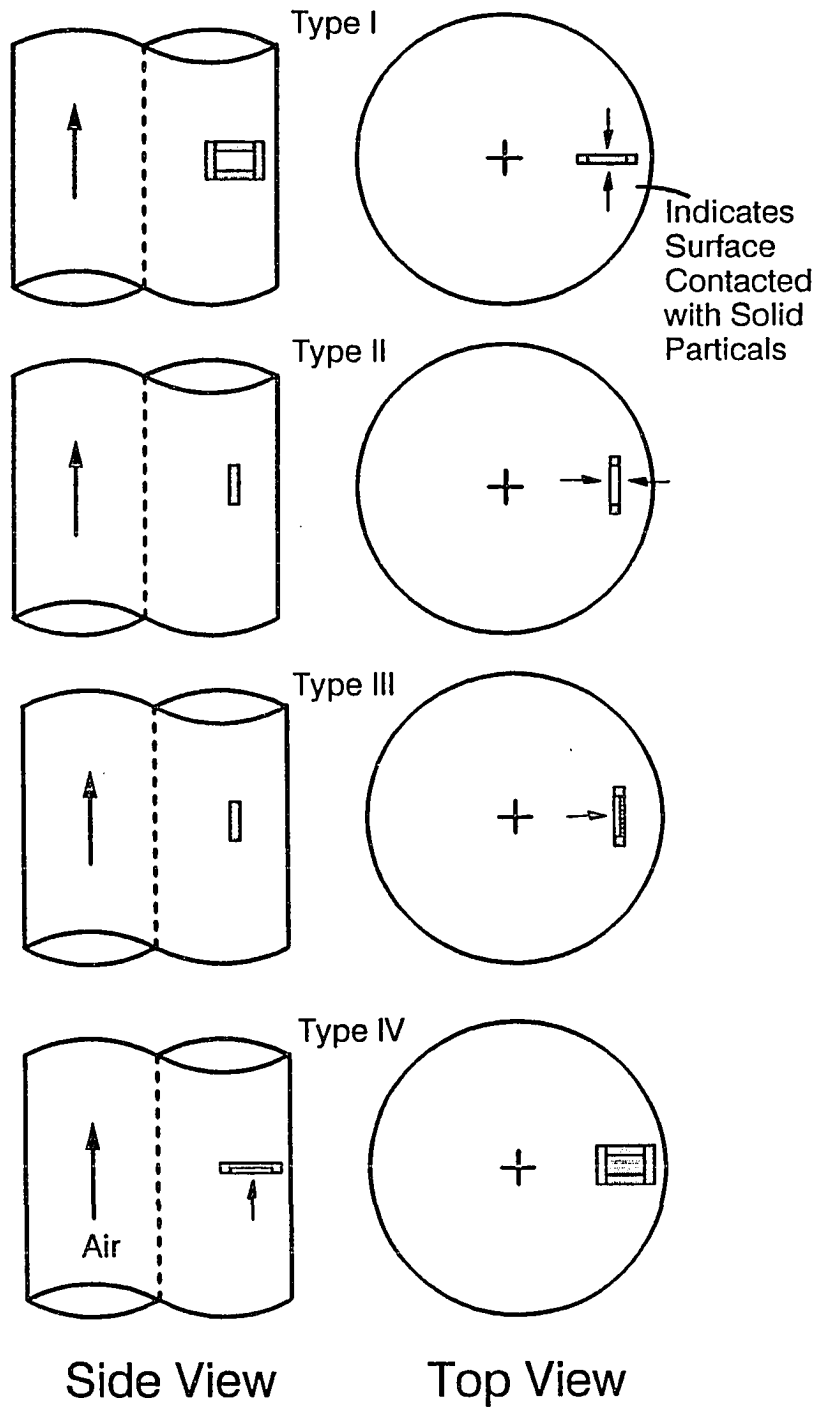

Figure 5.1: Types of plate orientation.

During operation, a maximum of 1300 c.c. of solids was accumulated in the downcomer pipe (1.94" i.d.) at U_0 = 0.64 m/s. At steady state, solids inventory in the column was 93.4% of that initially loaded. This measurement suggested that solids inventory in the column was > 93.4 % of total solids with U_0 <0.64 m/s. No appreciable change in solids inventory was observed after repeated operations.

Types of plate orientation are shown in Figure 5.1. and Table 5.2. Types I and II have their both sides exposed to the suspension. While one side of the plate of orientation Types III and IV was insulated. Locations of plates are shown in Table 5.3.

Consistency of the experimental data was checked by examining the heat transfer data for plate orientation Types I and II (Table 5.2) at r=0. At this location, heat transfer coefficients should be consistent if the data were reproducible.

Table 5.2: Plate orientations.

Orientation Type	Plate position relative to fluidized bed axis		Direction to which heating surface is facing	One side insulation
	Axial	Radial		
I	parallel	parallel		no
II	parallel	perpendicular	center line and wall	no
III	parallel	perpendicular	center line	yes
IV	perpendicular	parallel	down	yes

Table 5.3: Plate locations.

Orientation	Radial location		Axial location	
	$r(10^{-2}$ m)	r/R	$H-H_0(10^{-2}$ m)	$y=(H-H_0)/D$
Type I-III	0, 3, 6, 9, 12, 13.2	0, 0.2, 0.4, 0.6, 0.8, 0.88	16, 66, 116, 169	0.533, 2.2, 3.87, 5.63
Type IV	0, 3, 6, 9, 12, 13.5	0, 0.2, 0.4, 0.6, 0.8, 0.88	27, 72, 124, 175	0.9, 2.4, 4.13, 5.58

5.5 Measurements of Local Solids Concentration

Local solids concentrations in the freeboard were measured by immersing the sampler tube into the specified location of the freeboard with the enlarged mouth facing downward (Figure 4.3). After steady operation was achieved, which could be judged from the steady solid level in the down-flow pipe, solids suction pump was actuated to initiate the sampling. Collected solids were weighed, and solids concentration in the sampling location was then calculated according to Equation 4.1.

The required sampling time depended on the weight of sampled solids. Suction air flow rate was well known as a main control factor that affects the measured result (Stenhouse and Lloyd, 1974; Logan et al., 1974). The influence of this factor to the measured solids concentration was also tested in this study to determine proper suction air flow rates.

Locations of the sampling tube in the freeboard and the operating superficial gas velocities are listed in Table 5.4. For each U_0 at a specified sampling location, the sampling operation was repeated for two to four times to examine if there was any fluctuation in the measured solids concentration.

Table 5.4: Solids sampler location and operating superficial gas velocity.

U_0 (m/s)	: 0.34, 0.40, 0.46, 0.52, 0.58, 0.64
r (m)	: 0, 0.06, 0.09, 0.12, 0.135
$H-H_0$ (m)	: 0.23, 0.75, 1.23, 1.65

5.6 Determination of Particle Size Distribution

Particle size distributions for selected solids samples were analyzed by a laser-scattering type particle size analyzer (Leed & Northrup Microtrac Model 7991-01, USA).

5.7 Summary

The operation of the fluidized bed was first started by calibrating the gas flow rate. Then a fixed amount of FCC solids was loaded into the column. Finally, air was introduced into the column at a specified flow rate.

Measurements of heat transfer rate and solids concentration in the freeboard region were initiated when the system had reached a steady state condition. By varying locations or orientations of the heating plates and solids sampler in the freeboard, a series of local heat transfer coefficients and solids concentrations can be obtained at a specified gas flow rate.

CHAPTER 6

SOLIDS DYNAMICS IN FREEBOARD REGION

A solids dynamics model proposed by Kunii and Levenspiel (1990) is introduced in this chapter. By utilizing this model, the solids flux and velocity can be estimated from the measured solids concentrations. These estimated results will be useful for the development of heat transfer model described in Chapter 8.

For easy discussion of solids dynamics pertinent to the present study, the experimental results for solids concentration measurements and particle size distribution are also presented and discussed in this chapter.

6.1 Solid Dynamics Model

Kunii and Levenspiel (1990) have proposed a "freeboard-entrainment model" to account for the complex phenomena occurring in the freeboard of a fluidized bed. They have postulated that there are three distinct phases in the freeboard as shown in Figure 6.1: Phase 1 contains gas stream with completely dispersed solids. The fines are carried upward and out of the bed at velocity V_1; Phase 2 is composed of agglomerates coming from the bed and moving upward at velocity V_2; Phase 3 refers to agglomerates and thin wall layers of

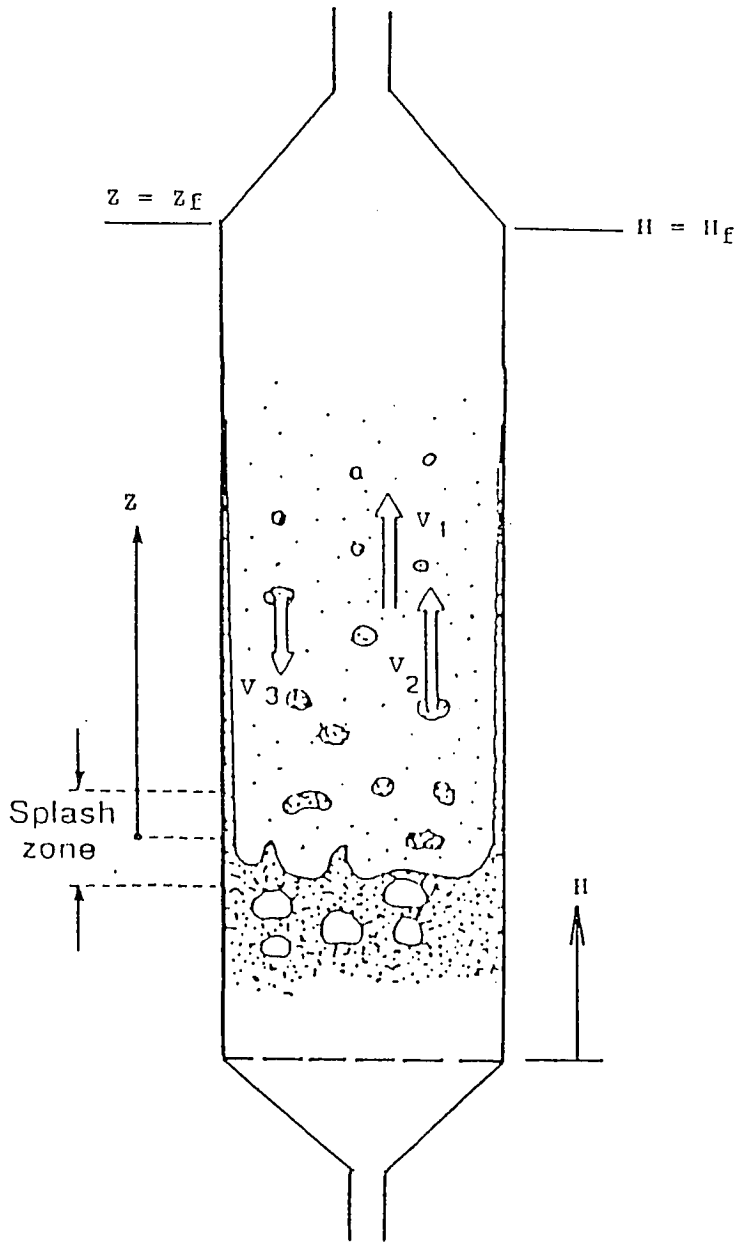

Figure 6.1: Fluidized bed with fine solids and agglomerates in the freeboard (Kunii and Levenspiel, 1990).

particles moving downward at velocity V_3.

The thickness of strands sliding down the wall has been measured as several millimeters by Rhodes and Geldart (1988), Boder et al. (1988), and Horio et al. (1988). Kunii and Levenspiel (1990) have further postulated that at any level in the freeboard, the rate of removal of fines from the agglomerates to form dispersed solid of Phase 1 is proportional to the fraction of agglomerates at that level and that the upward-moving agglomerates will eventually reverse direction and move downward. The frequency of change from Phase 2 to Phase 3 is proportional to the volume fraction of Phase 2 at that level.

By solving the mass balance equations for the three phases with proper boundary conditions, the net upward flux (G_u) of solids at any level in the freeboard was found to be

$$\frac{G_u - xG^*}{G_{uo}} = e^{-aZ} \qquad (6.1)$$

where G^* is the flux of solids at Z>TDH (transport disengaging height), G_{uo} is the upward flux at bed surface (i.e., Z=0), x is the fraction of bed solids for which U_t(terminal velocity) < U_0. The parameter a with unit of m^{-1} is the decay constant for the decrease of solids flux with respect to height in the freeboard.

In deriving Equation 6.1, it is assumed that the amount

of solids thrown into the freeboard is very much larger than those eventually removed from the bed, i.e., $xG^* << G_{uo}$. Hoggen et al. (1986) measured G_u in a large fluidized bed, and found that $G_u/G_{uo} \approx 10^{-2}$ for d_p = 150-212 μm at U_0 = 0.61 m/s and Z = 3 m. Since $xG^* < G_u$, the above result indicates that the assumption of $xG^* << G_{uo}$ in Kunii and Levenspiel's model (1990) is valid. The axial distribution of solids concentration in the freeboard can be given as (Kunii & Levenspiel, 1990):

$$\frac{\bar{C}-x\bar{C}^*}{C_0} = e^{-aZ} \qquad (6.2)$$

where $\bar{C}_0$ and $\bar{C}^*$ are radially averaged solids concentrations at Z=0 and Z>TDH respectively. The condition $\bar{C}_0 >> x\bar{C}^*$ was assumed in deriving Equation 6.2.

In the following, the experimental results of solids concentration measurements will be presented. With the measured solids concentrations, the decay constant (a) for the present system can be estimated from Equation 6.2. Solids flux along the axial direction of the freeboard can then be found from Equation 6.1. Finally, the solids velocity can be obtained by dividing the solids flux by the solids concentration at the corresponding axial location. Detail procedures will be presented in Section 6.3.

6.2 Results and Discussion of Solids Concentration Measurements

6.1.1 Effect of Suction Rate on Solids Concentration Results

Figure 6.2 shows an example of variation of measured solids concentration with suction gas velocity (U_e) at the sampler mouth entrance. The experimental data are given in Table 6.1. The results indicate that by controlling U_e to a value close to the superficial air velocity (U_0), the influence of U_e on the measured concentration (C) can be minimized. In this work, all solids concentrations were obtained by setting U_e close to U_0.

Table 6.1: Variation of measured solids concentration with suction gas velocity (U_e) at the sampler mouth entrance (H=1.04 m, U_0=0.411 m/s, r=0, T=29-31°C).

Suction air flow rate (L/min)	U_e (m/s)	Sampling time (min)	Wt. of collected sample (g)	Solids conc. (g/L)
1.13	0.218	32	2.541	0.0703
1.64	0.316	33	5.069	0.0937
1.91	0.368	34	7.399	0.114
2.50	0.481	27	8.008	0.119
2.78	0.535	27	8.539	0.114

6.2.2 Solids Concentration Data

Experimental data for solids concentration are tabulated

in Appendix 2. Radial distributions of solids concentration in the freeboard for H = 0.52, 1.04, 1.52, and 1.94 m are shown in Figures 6.3-6.6. Larger variation in the measured concentration C was observed for H = 0.52 m where solids were splashed from bed surface. At higher freeboard levels (e.g., H > 1.02 m), solids concentration is higher in the vicinity of bed wall. Variations of the measured solids concentration with radial positions are summarized as follows:

(1). In the splash zone ($H-H_0$ = 0.23 m, Figure 6.2), for U_0 < 0.52 m/s, C is higher at the column center than at the wall.

(2). In the middle freeboard ($H-H_0$ = 0.75, 1.23 m; Figures 6.4, 6.5), for all U_0's investigated, C is flat in the core region (r/R < 1/2) of the column; while there is a maximum C in the wall vicinity (r/R = 4/5). C is nearly the same at the wall and the center.

(3). In the freeboard near the column exit ($H-H_0$= 1.65 m, Figure 6.6), for all U_0's investigated, C increases with increasing radial position measured from column center. For U_0 = 0.64 m/s, C is more than two times larger at the wall than at the center.

Axial variation of solids concentrations will be discussed in Section 6.3.

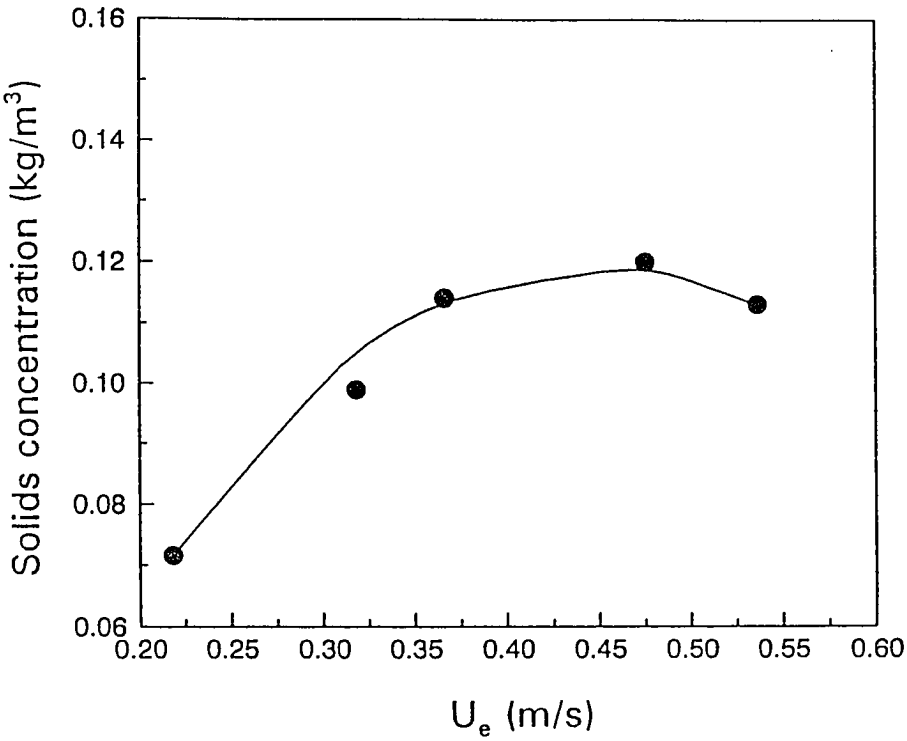

Figure 6.2: Variation of the measured solids concentration with suction gas velocity (U_e) at the entrance.

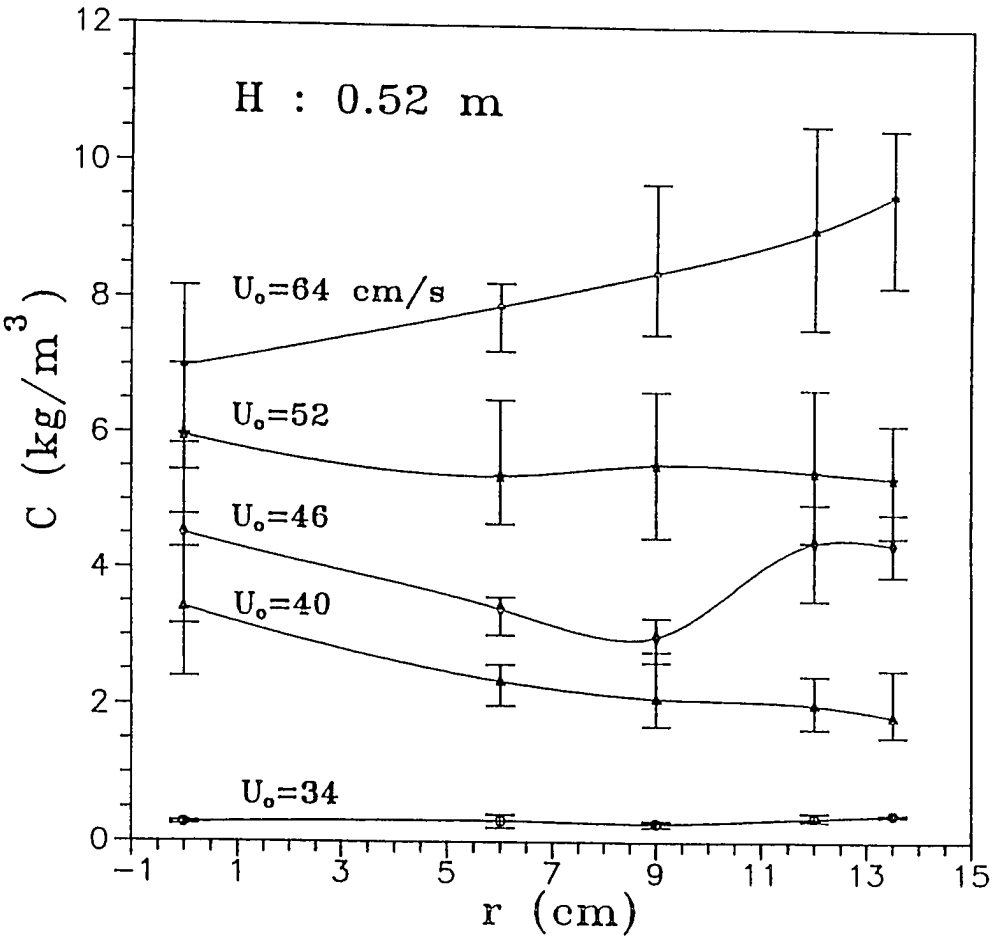

Figure 6.3: Radial distribution of solids concentration in the freeboard (H = 0.52 m).

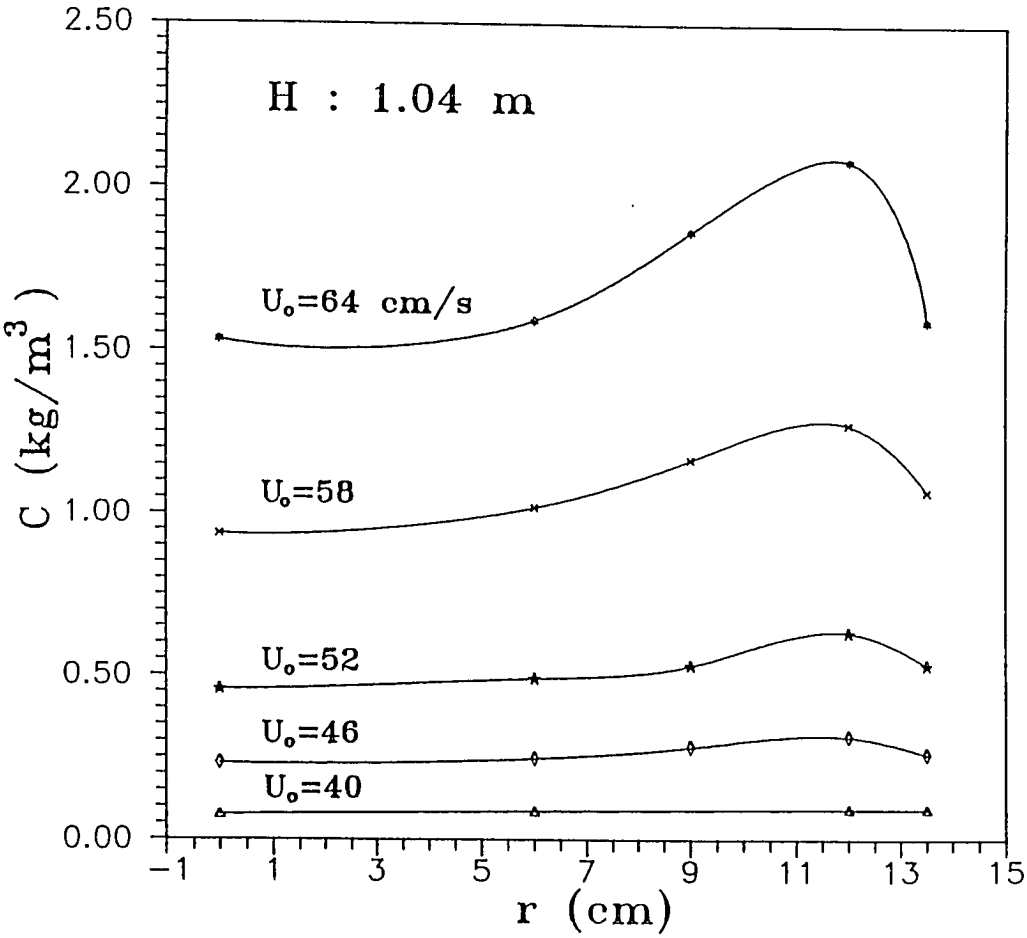

Figure 6.4: Radial distribution of solids concentration in the freeboard (H = 1.04 m).

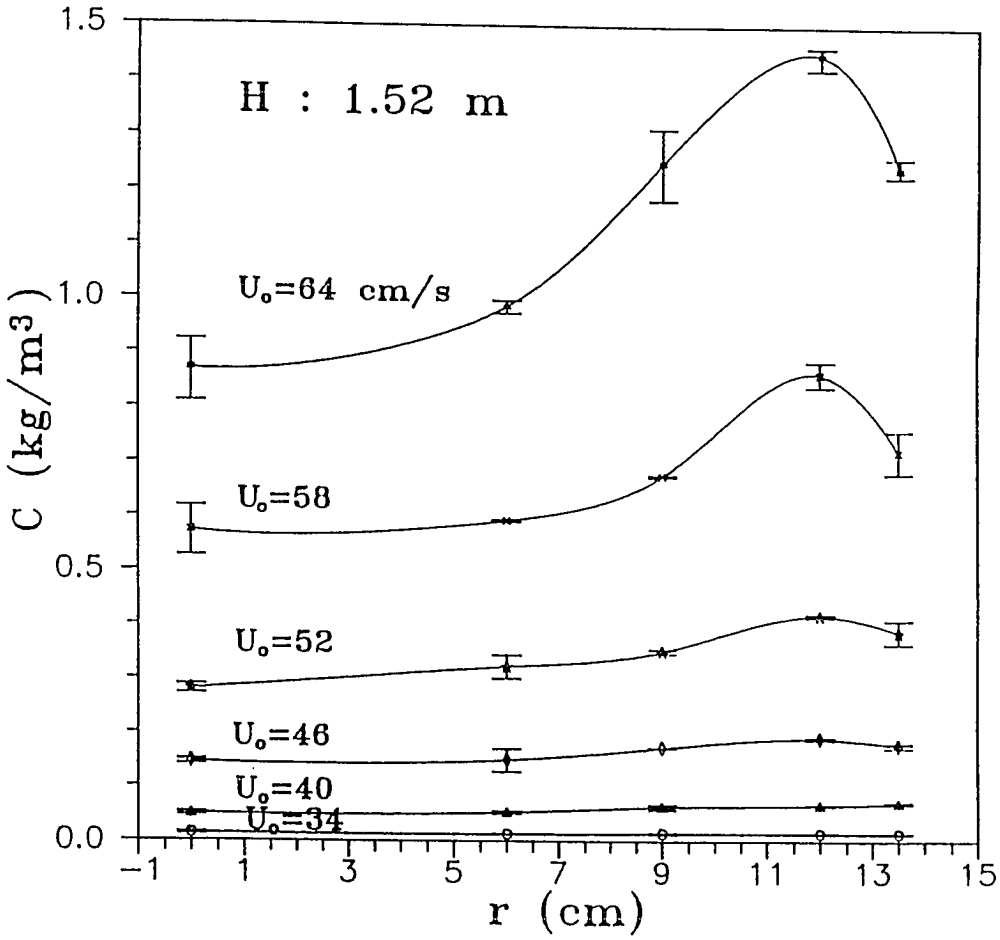

Figure 6.5: Radial distribution of solids concentration in the freeboard (H = 1.52 m).

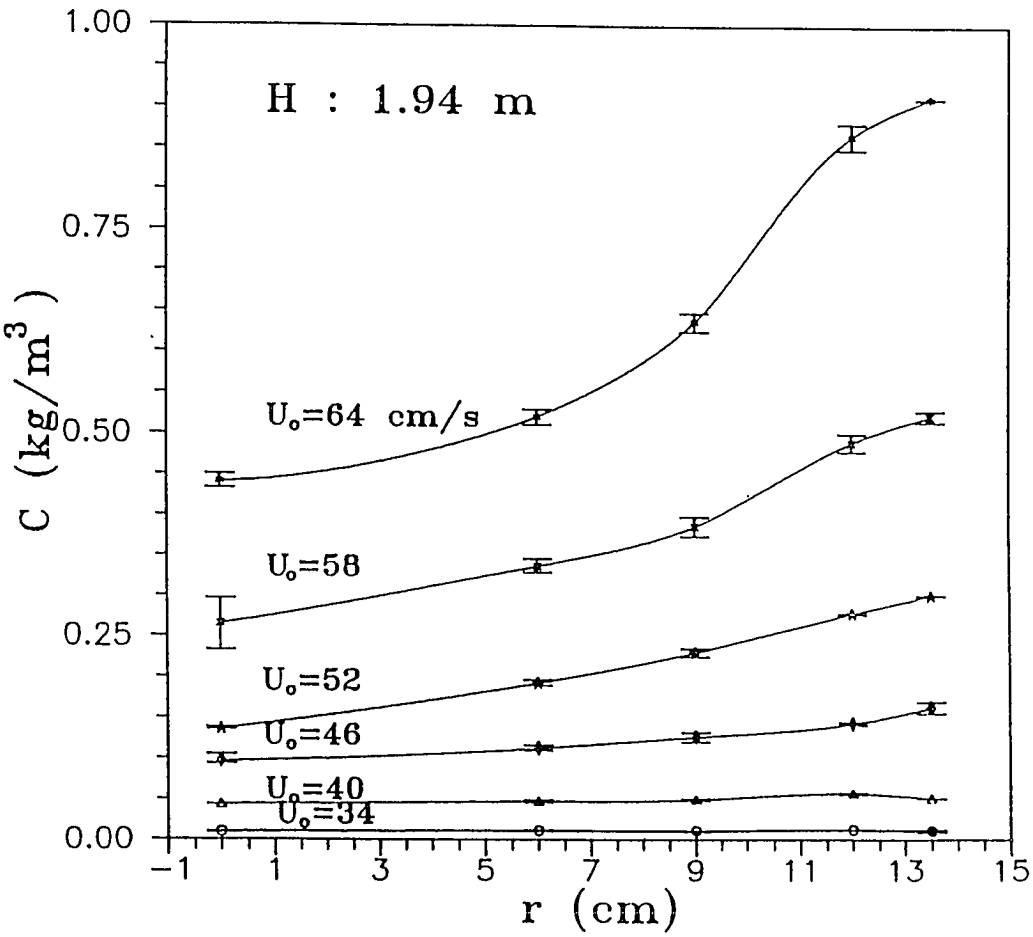

Figure 6.6: Radial distribution of solids concentration in the freeboard (H = 1.94 m).

6.2.3 Particle Size Distribution

Particle size distributions of sampled solids are shown in Appendix 2 (Table A.2.7).

Axial variations of cross-sectionally averaged particle size are shown in Figure 6.7. The results are similar to those reported by Morooka et al. (1980) for FCC particles (d_p: 65-68 μm, ρ_s: 0.96-1.11 g/cm^3) in the freeboard of a 12 cm i.d. fluidized bed.

Radial variations of particle size are not significant except for lower freeboard levels as shown in Figure 6.8 for H = 0.52 m where solids move violently. The average particle diameter $\bar{d}_p$ increases with U_0 for all freeboard levels as shown in Figure 6.9.

6.3 Estimation of Solids Flux and Velocity in Freeboard

Kunii and Levenspiel's model is utilized in this section to estimate solids flux and velocity in axial direction of the freeboard.

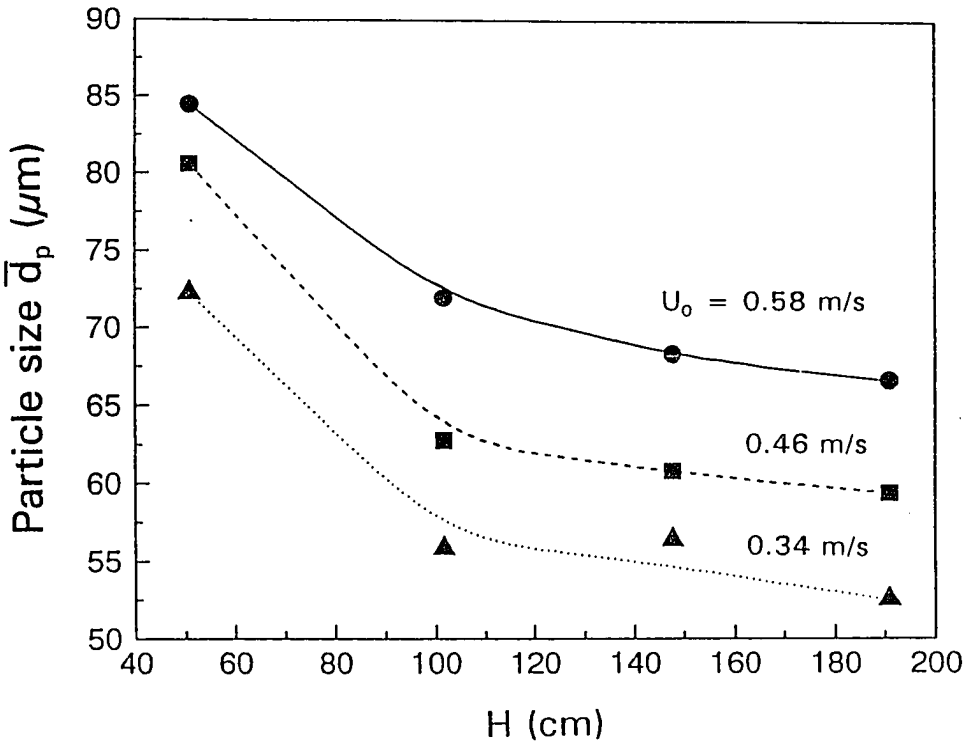

Figure 6.7: Axial variation of average particle size.

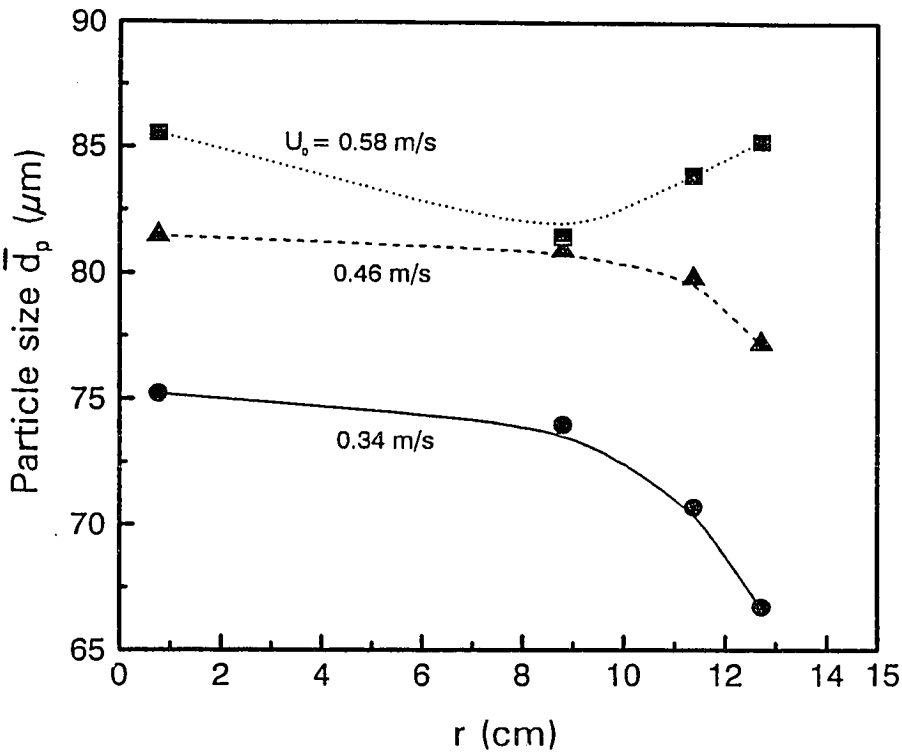

Figure 6.8: Radial variation of $\overline{d}_p$ in the freeboard (H = 0.52 m).

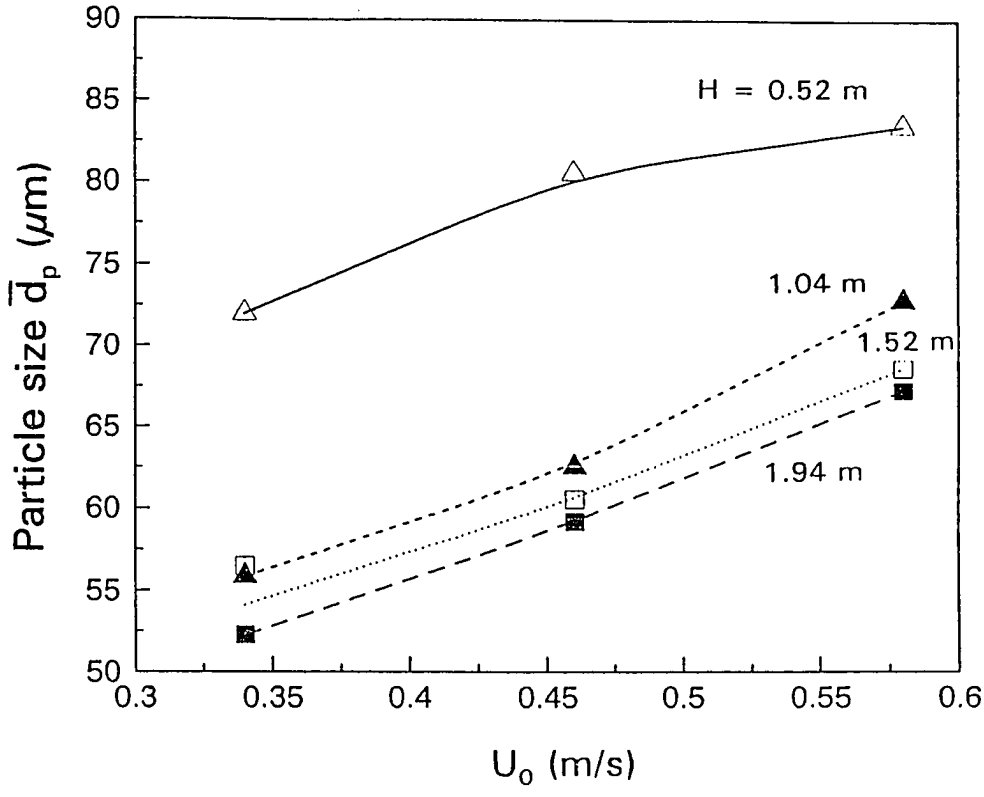

Figure 6.9: Variation of average particle size with superficial gas velocity in the freeboard.

6.3.1 Decay Constant

To estimate the decay constant (a), Equation 6.2 can be rewritten in logarithmic form:

$$\ln(\bar{C}-x\bar{C}^{*}) = \ln\bar{C}_0 - aZ \qquad (6.3)$$

The decay constant can be obtained from the slope of $\ln(\bar{C}-x\bar{C}^{*})$ vs. Z plot. A typical $\ln(\bar{C}-x\bar{C}^{*})$ vs. Z plot in this study is shown in Figure 6.10. The solids concentration $\bar{C}^{*}$ for each U_0 was obtained by extrapolating $\bar{C}$ to a freeboard height beyond TDH, as shown in Figure 6.11. The parameter x in Equation 6.3 and Figure 6.10 was obtained from the terminal velocity distribution pattern of the bed particles as shown in Figure 6.12 and Table 6.2. Table 6.3 lists all the data required for preparing Fig 6.10.

As can be seen in Figure 6.10, two distinct regions exist for Z < 0.5 m and Z > 0.6 m. The region for Z < 0.5 m is near the bed surface where the solids kinematics was observed to be quite different from that for Z > 0.6 m. The fluctuating nature of solids concentration at Z = 0.12~0.20 m (H = 0.53 m) shown in Figure 6.2 compared with those at Z > 0.6 m (Figures 6.4 to 6.6) also indicate the difference.

Table 6.4 lists two sets of decay constants estimated from slopes of straight lines shown in Figure 6.10.

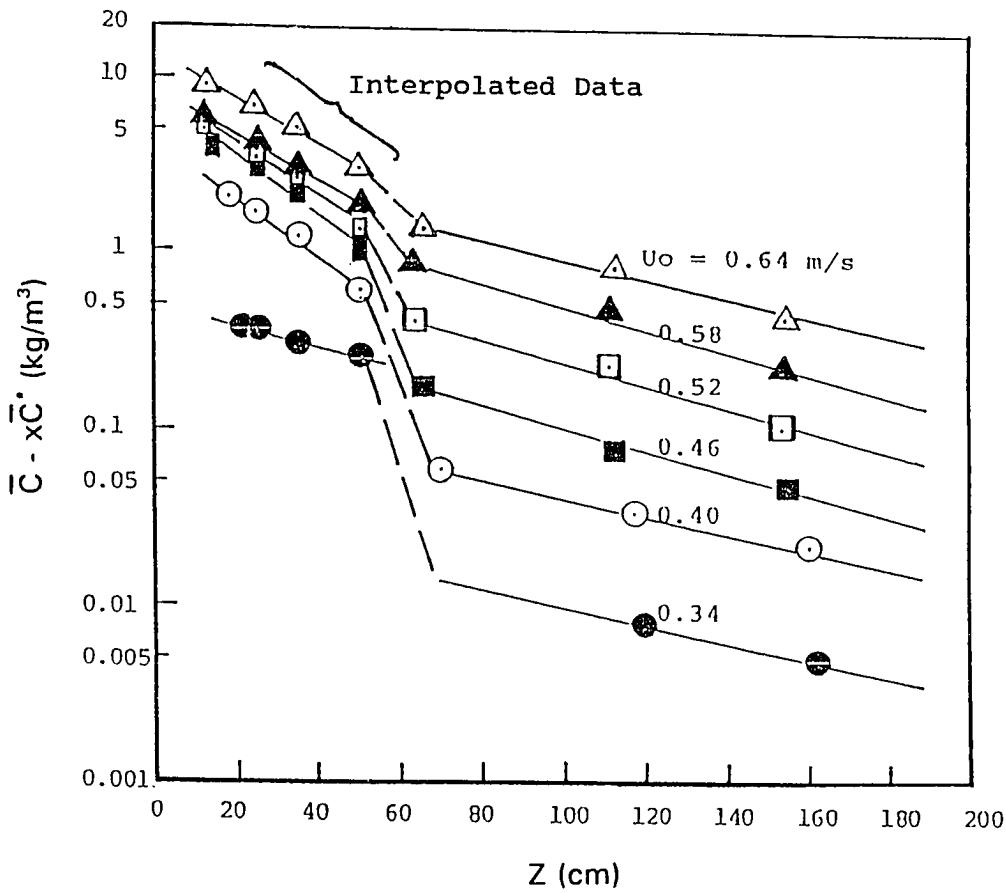

Figure 6.10: Axial variation of ($\bar{C}$-x$\bar{C}^*$) in the freeboard.

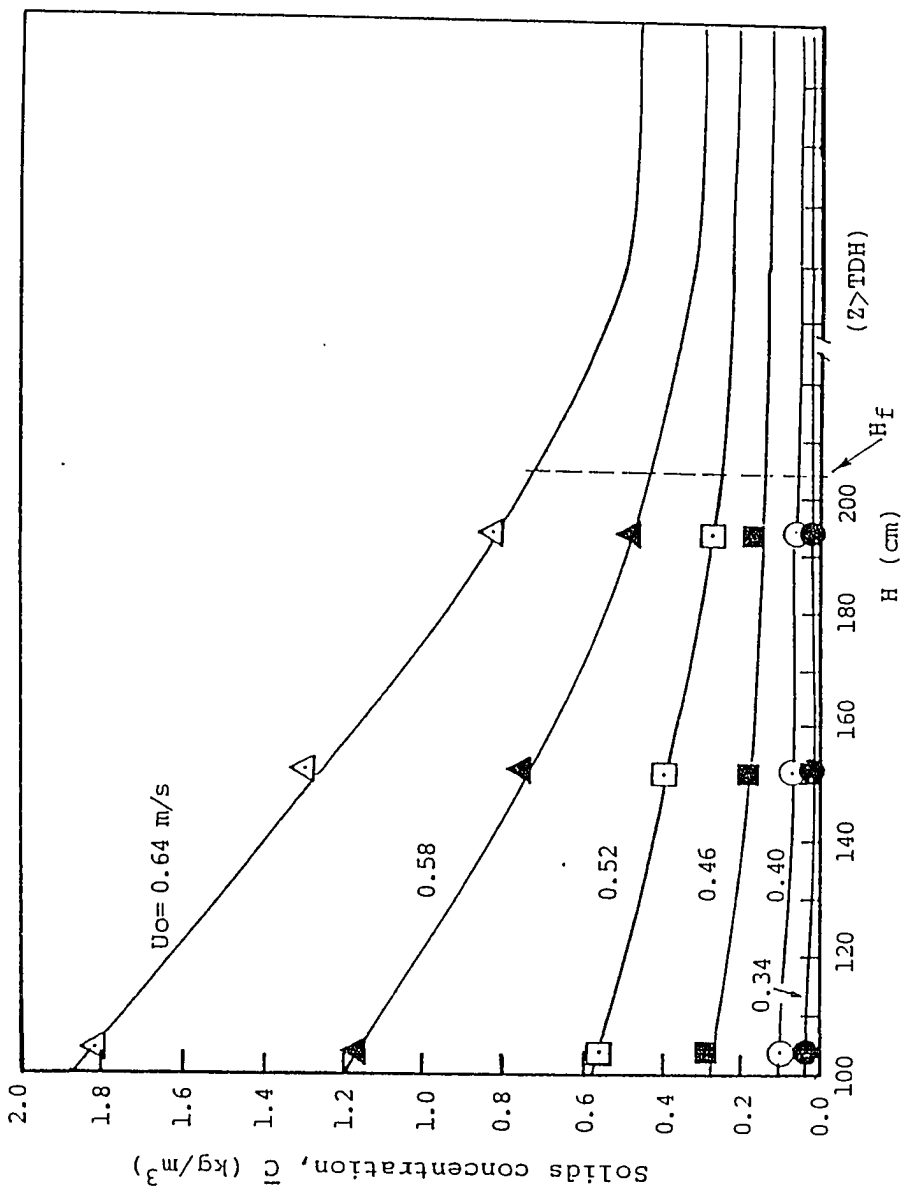

Figure 6.11: Solids concentration at higher levels of the freeboard (for lower freeboard, see Appendix 2).

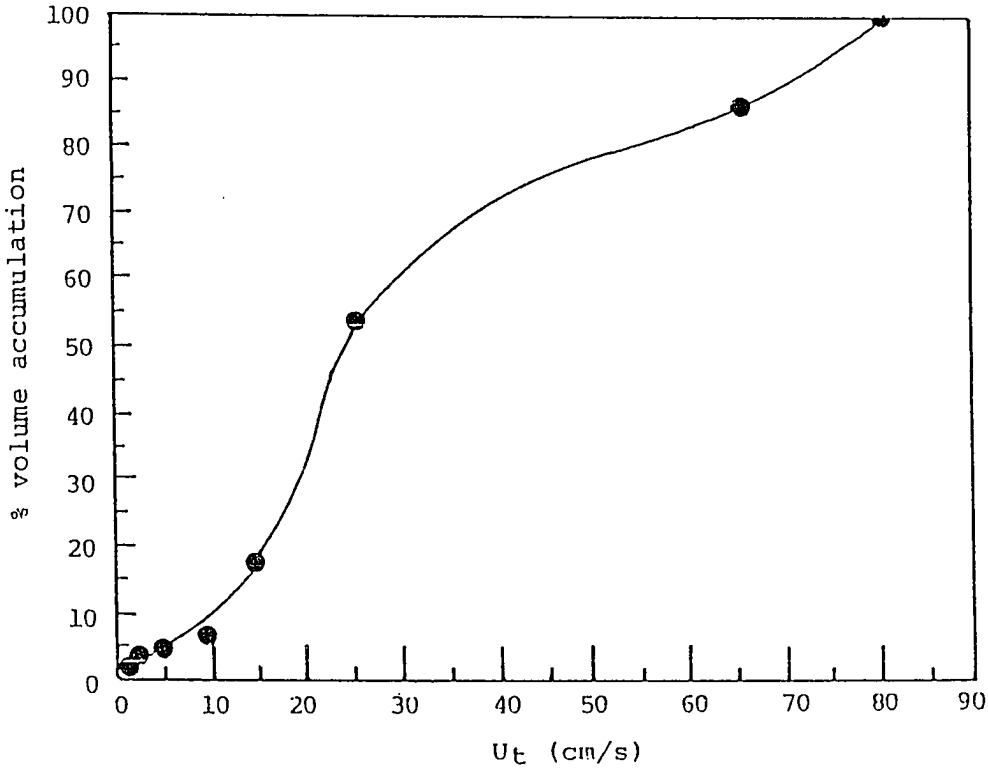

Figure 6.12: Distribution of terminal velocity (U_t) of particles.

Table 6.2: Particle size distribution and terminal velocity of the test solid particles.

d_p (μm)	%volume		$Cd \cdot Re^2$ (1)	Re (2)	U_t (cm/s) (3)
	Fraction (5)	Accumulation			
2.8	0.0	0.0	0.00165	0.000069	0.037
3.9	0.2	0.2	0.00446	0.000186	0.072
5.5	0.2	0.4	0.01251	0.000521	0.142
7.8	0.0	0.4	0.03569	0.00149	0.287
11	0.0	0.4	0.100	0.00417	0.569
16	1.1	1.6	0.308	0.0128	1.20
22	1.2	2.8	0.801	0.0333	2.27
31	1.4	4.3	2.24	0.0933	4.51
44	2.5	6.8	6.41	0.267	9.10
62	10.8	17.7	17.92	0.60	14.5
88	35.7	53.4	51.25	1.5	25.6
125	33.0	86.5	147	5.5	66.0
176	13.5	100.0	410	9.5	81.0
89.6 (4)			54.1 (4)	1.6 (4)	26.8 (4)

(1). $Cd \cdot Re^2 = 4 \cdot g \cdot d_p^3 \cdot \rho \cdot (\rho_s - \rho) / (3 \cdot \mu^2) = (4/3)\ Ar$, where Ar is the Archimedes number.
ρ = 0.0012 g/cm^3 for air at 25 °C
ρ_s = 1.554 g/cm^3 for the solid particles
μ = 0.00018 g/cm·s for air at 25 °C
g = 980 cm/s^2

(2). For Re < 0.4 (Stokes' region), $Re = Cd \cdot Re^2/24$; for Re > 0.4 , Re is obtained from a $Cd \cdot Re$ vs. Re plot given in Kunii and Levenspiel's work (1969).

(3). $U_t = Re \cdot \mu / (d_p \cdot \rho)$.

(4). Average values of respective columns.

(5). Calculated from % volume accumulation column, this results in the discontinuity of the solids distribution for d_p =7.8 and 11 μm.

Table 6.3: $(\bar{C}-x\bar{C}^*)$ calculated from experimental data.

U_0 (m/s)	x	$\bar{C}^*$ (kg/m³)	Port #1		Port #2		Port #3		Port #4		$\bar{C}-x\bar{C}^*$ (g/L)		
			Z (m)	$\bar{C}-x\bar{C}^*$ (kg/m³)	Z (m)	$\bar{C}-x\bar{C}^*$ (kg/m³)	Z (m)	$\bar{C}-x\bar{C}^*$ (kg/m³)	Z (m)	$\bar{C}-x\bar{C}^*$ (kg/m³)	0.25	Z(m)= 0.35	0.50
0.34	0.67	0.010	0.20	0.361	0.72	-	1.20	0.0077	1.62	0.0046	0.352	0.281	0.245
0.40	0.73	0.044	0.18	1.949	0.70	0.0589	1.18	0.0332	1.60	0.0199	1.623	1.194	0.595
0.46	0.76	0.130	0.14	3.941	0.66	0.180	1.14	0.078	1.56	0.0462	2.960	2.138	1.020
0.52	0.78	0.220	0.12	5.253	0.64	0.387	1.12	0.221	1.54	0.098	3.710	2.693	1.361
0.58	0.82	0.340	0.12	5.661	0.64	0.872	1.12	0.468	1.54	0.204	4.202	3.131	1.809
0.64	0.85	0.510	0.13	8.607	0.65	1.370	1.13	0.856	1.55	0.339	6.602	4.995	2.923

Table 6.4: Decay constants (a) of solids concentration.

U_0 (m/s)	Decay constant, a (1/m)	
	Z < 0.5 m	Z > 0.6 m
0.64	2.931	1.362
0.58	3.012	1.608
0.52	3.636	1.519
0.46	3.765	1.518
0.40	3.694	1.206
0.34	-	1.227

Table 6.5 lists decay constants reported in the literature and calculated in the present study. The average decay constant of 3.4 m^{-1} from the present study for the lower freeboard region (Z< 0.5 m) is comparable to those given by similar fluidized bed systems (e.g., Jolley and Stantan (1952), Nazemi et al.(1974), and Zenz and Weil (1958)).

The decay constants obtained will be utilized in Section 6.3.2 to estimate the solids flux in the freeboard.

6.3.2 Solids Flux in the Freeboard

The solids flux at Z>TDH (i.e., G^*) should be known before we can use Equation 6.1 to estimate solids flux (G_u) in the freeboard. G^* can be calculated from the following equation:

$$G^* = \overline{V}_p^* \cdot \overline{C}^* \qquad (6.4)$$

Table 6.5: Comparison of decay constants.

Investigator	$\bar{d}_p$ (μm)	ρ_s (kg/m^3)	D (m)	U_0 (m/s)	a (1/m)	$a \cdot U_0$ (1/s)	Z (m)
Jolley & Stantan (1952)	76	1330	0.0508	0.12-0.25	3.5	0.69	<1
Zenz & Weil (1958)	60	940	0.0508 x 0.61	0.30-0.71	4.2	2.17	<1
Tweddle et al. (1970)	163	1370	0.1652	0.76	6.1	4.6	<1
Nazemi et al. (1974)	59	840	0.61	0.09-0.34	3.6	0.78	<1
Large et al. (1976)	127	2650	0.61	0.20-0.30	6.4	1.78	<1
Bachovchin et al. (1979)	448	2630	0.1524	0.73-0.90	4.0	3.2	<1
This work (1991)	90	1554	0.30	0.34-0.64	3.4 1.4	1.74 0.70	>0.5 >0.6

where $\bar{V}_p^*$ is the average particle velocity for Z>TDH.

For a spherical particle moving vertically in an up-flow air current, the velocity (V_p) of the particle in laminar motion can be described as follows (Zenz and Weil, 1958):

$$V_p = (U_0 - \tau \cdot g)[1 - e^{-t/\tau}] + V_{p0} \cdot e^{-t/\tau} \quad (6.5)$$

$$U_t = \tau \cdot g \quad (6.6)$$

$$\tau = \frac{4 \cdot (\rho s - \rho) \cdot d_p^2}{3 \nu \mu} \quad (6.7)$$

where V_{p0} is the initial particle velocity from the bed surface, and τ is the velocity relaxation time of motion. For the particle motion in Stokes' region, ν is 24 for spherical particles, and 37.5 for irregular particles, as suggested by Zenz and Weil (1958). The parameter τ can be calculated from Equation 6.6 and U_t listed in Table 6.2. For the present study, τ equal 0.004~0.083 sec. At the freeboard exit ($Z=Z_f$), the average particle residence time is 0.5~1.0 sec. The values of $\exp(-t/\tau)$ in Equation 6.5 are very small (i.e., 2.4×10^{-3}~5.9×10^{-6}), as can be calculated by substituting τ of 0.083 sec and t of 0.5~1.0 sec into $\exp(-t/\tau)$. Assuming V_{p0} to be $2U_0$, the term $V_{p0}\, e^{-t/\tau}$ in Equation 6.5 is also negligible with a contribution less than 0.003 at U_0 equal to 0.64 m/s. Therefore, as Z > TDH, Equation 6.5 can be simplified as: $V_p = U_0 - \tau.g$. Substituting Equation 6.6 into the above simplified equation, the entrained particle velocity V_p^* (i.e., V_p

for Z > TDH) can be approximated as

$$V_p^* = U_0 - U_t \tag{6.8}$$

where U_t is the terminal velocity of the particle.

The average entrained particle velocity ($\overline{V}_p^*$) for Z > TDH is given by

$$\overline{V}_p^* = \frac{[\sum (V_p^* \cdot f_b)]}{\sum f_b} \tag{6.9}$$

where f_b is the volume fraction of bed particles with mean velocity V_p^*.

Data sheet for calculating V_p^*, $\overline{V}_p^*$, f_c, and $\overline{d}_p^*$ at U_0 = 0.28 ~ 0.64 m/s are shown in Table 6.6, where f_c is the volume fraction of entrained particles. Calculated results of $\overline{V}_p^*$, $\overline{d}_p^*$, and G^* are summarized in Table 6.7. Variations of G^* and $\overline{V}_p^*$ versus U_0 are shown in Figure 6.13.

Table 6.6: Calculation of elutriated particle size distribution and particle velocity.

d_p (μm)	U_t (cm/s)	f_b (%)	U_0 = 64 cm/s			U_0 = 58 cm/s			U_0 = 52 cm/s		
			V_p^* (cm/s)	$V_p^* \cdot f_b$ (%·cm/s)	f_c (%)	V_p^* (cm/s)	$V_p^* \cdot f_b$ (%·cm/s)	f_c (%)	V_p^* (cm/s)	$V_p^* \cdot f_b$ (%·cm/s)	f_c (%)
173	80	4									
152	75	4									
137	70	5									
125	65	4									
115	60	4	4	16	0.050						
109	55	3	9	27	0.848	3	9	0.36			
106	50	4	14	64	2.01	8	32	1.19	2	8	0.36
104	45	3	19	57	1.79	13	39	1.46	7	21	0.95
102	40	4	24	96	3.02	18	72	2.69	12	48	2.17
98	35	5	29	145	4.56	23	115	4.29	17	85	3.84
93	30	4.5	34	153	4.82	28	126	4.70	22	99	4.47
86	25	8	39	312	9.82	33	264	9.85	27	216	9.75
77	20	20	44	880	27.69	38	760	28.4	32	640	28.89
63	15	17.5	49	858	26.99	43	753	28.1	37	648	29.30
47	10	5	54	270	8.50	48	240	8.96	42	210	9.48
32	5	3	59	177	8.57	53	159	5.93	47	141	6.37
20	2.5	2	61.5	123	3.87	55.5	111	4.14	49.5	99	4.07
Sum (Σ)		83		3178			2680			2215	

Table 6.6: Calculation of elutriated particle size distribution and particle velocity (cont'd).

d_p (μm)	U_t (cm/s)	f_b (%)	U_0 = 46 cm/s			U_0 = 40 cm/s			U_0 = 34 cm/s		
			V_p^* (cm/s)	$V_p^* \cdot f_b$ (%·cm/s)	f_c (%)	V_p^* (cm/s)	$V_p^* \cdot f_b$ (%·cm/s)	f_c (%)	V_p^* (cm/s)	$V_p^* \cdot f_b$ (%·cm/s)	f_c (%)
173	80	4									
152	75	4									
137	70	5									
125	65	4									
115	60	4									
109	55	3									
106	50	4									
104	45	3	1	3	0.617						
102	40	4	6	24	1.35						
98	35	5	11	55	3.10	5	25	1.84			
93	30	4.5	16	72	4.06	10	45	3.31	4	18	1.85
86	25	8	21	168	9.46	15	120	8.84	9	72	7.40
77	20	20	26	520	29.30	20	400	29.5	14	280	28.78
63	15	17.5	31	543	30.59	25	438	32.2	19	333	34.22
47	10	5	36	180	10.14	30	150	11.0	24	120	12.33
32	5	3	41	123	6.93	35	105	7.73	29	87	8.94
20	2.5	2	43.5	87	4.90	37.5	75	5.52	31.5	63	6.47
Sum (Σ)		83		1775			1358			973	

Table 6.6: Calculation of elutriated particle size distribution and particle velocity. (cont'd)

d_p (μm)	U_t (cm/s)	f_b (%)	U_0 = 28 cm/s		
			V_p^* (cm/s)	$V_p^* \cdot f_b$ (%·cm/s)	f_c (%)
173	80	4			
152	75	4			
137	70	5			
125	65	4			
115	60	4			
109	55	3			
106	50	4			
104	45	3			
102	40	4			
98	35	5			
93	30	4.5			
86	25	8	3	24	3.86
77	20	20	8	160	25.72
63	15	17.5	13	228	36.66
47	10	5	18	90	14.46
32	5	3	23	69	11.90
20	2.5	2	25.5	51	11.09
Sum (Σ)		83		592	

Table 6.6 (cont'd): $\overline{V}_p^*$ & $\overline{d}_p^*$

U_0 (cm/s)	$\overline{V}_p^*$ (cm/s)	$\overline{d}_p^*$ (μm)
64	38.3	61.5
58	33.9	60.2
52	29.1	58.9
46	24.7	57.4
40	20.9	55.4
34	16.2	53.0
28	11.2	49.4

$$\overline{V}_p^* = \frac{\sum V_p^* \cdot f_b}{\sum f_b} \text{ (cm/s)}$$

$$\overline{d}_p^* = \frac{1}{\sum (f_c/d_p)} \times 100 \text{ } (\mu\text{m})$$

$$f_c = \frac{V_p^* \cdot f_b}{\sum V_p^* \cdot f_b}$$

Table 6.7: Calculated behavior of solids at Z > TDH.

U_0 (m/s)	H_b (m)	Z_f (m)	$\bar{C}_{Zf}$ (kg/m^3)	$\bar{C}^*$ (kg/m^3)	G^* (kg/m^2·s)	$\bar{V}_p^*$ (m/s)	$\bar{d}_p^*$ (μm)
0.34	0.32	1.72	0.0106	0.010	0.0016	0.162	53.0
0.40	0.34	1.70	0.0448	0.044	0.0092	0.209	55.4
0.46	0.38	1.66	0.137	0.130	0.032	0.247	57.4
0.52	0.40	1.64	0.241	0.220	0.064	0.291	58.9
0.58	0.40	1.64	0.420	0.340	0.115	0.339	60.2
0.64	0.39	1.65	0.723	0.510	0.195	0.383	61.5

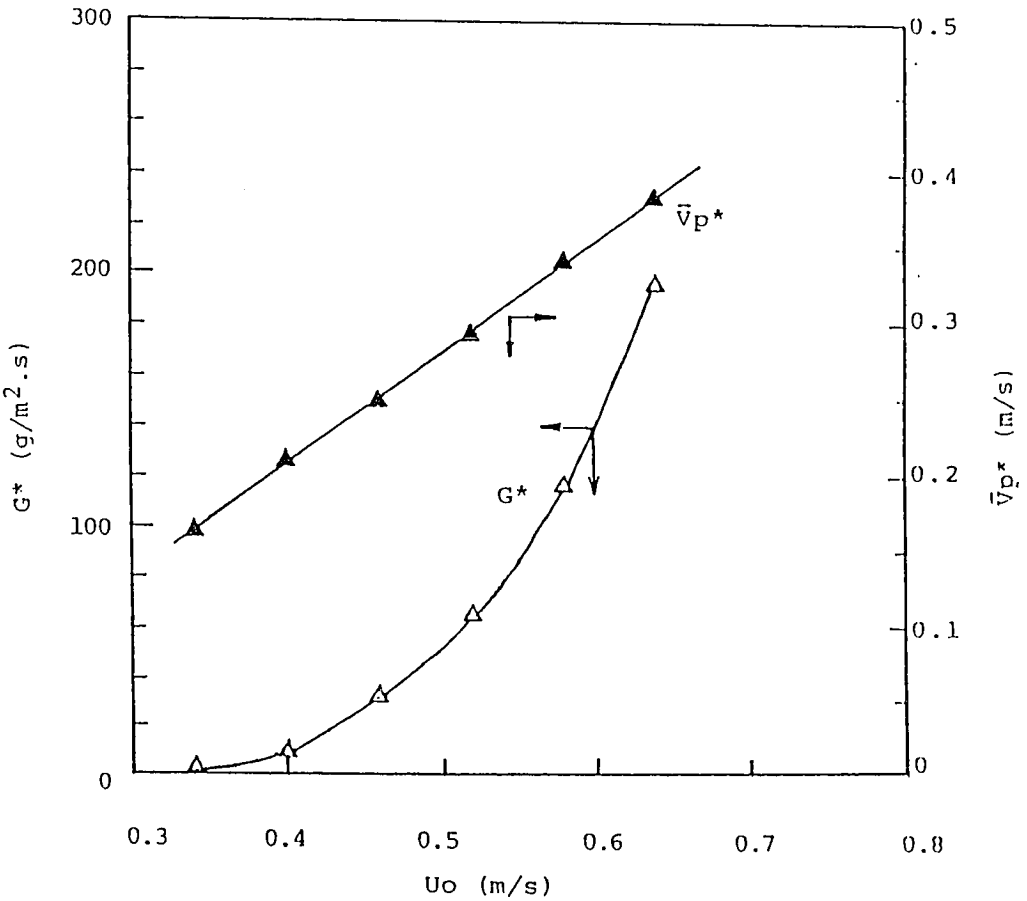

Figure 6.13: Dependence of G^* and $\bar{V}_p^*$ on U_0.

As explained earlier in this section, t is much larger than τ at $Z = Z_f$ for the superficial gas velocities and particles used in this study. It is reasonable to assume that

$$\overline{\overline{V}}_p = \overline{\overline{V}}_{pu} \approx \overline{\overline{V}}_p^* \qquad (6.10)$$

at $Z = Z_f$. Substitution of Equation 6.10 into Equation 6.1 yields

$$\frac{G_u - xG^*}{\overline{\overline{V}}_p^* \cdot \overline{C}_{Z_t} - xG^*} = e^{[a^* (Z_t - Z)]} \qquad (6.11)$$

where $\overline{C}_{Zf}$ is the cross-sectionally averaged solids concentration at the column exit. $\overline{C}_{Zf}$ for each U_0 was obtained from Figure 6.11 (at $H = H_f = 204$ cm) and listed in Table 6.7. From Equation 6.11, the upward solids flux (G_u), at any level in the freeboard can be estimated.

Figure 6.14 shows a comparison of particle size distribution between experimental data (solids sampled at H=1.94 m) and calculated d_p^* (solids at Z > TDH) for $U_0 = 0.46$ m/s. The agreement suggests that the column height of 1.94 m is near or larger than the TDH at the superficial gas velocity and that the above approach for calculating solids fluxes at Z>TDH is reasonable.

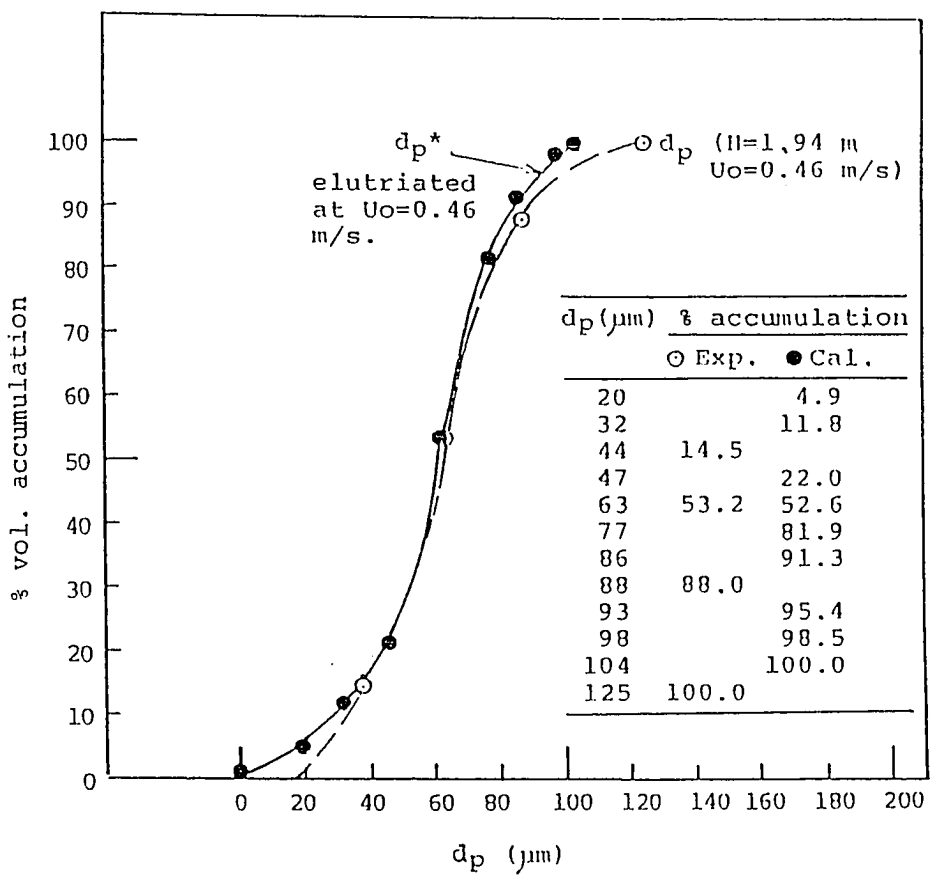

Figure 6.14: Comparison of particle size distribution between experimental data (○) and calculated results (●).

Downward solids flux (G_d) at any level can be calculated from the following mass balance equation (Kunii and Levenspiel, 1990):

$$G = G_u - G_d \approx \overline{V}_p^* \cdot \overline{C}_{Z_f} \tag{6.12}$$

where G is the net upward solids flux in the column.

6.3.3 Solid Particle Velocity in the Freeboard

Once the solids fluxes in the freeboard have been obtained, the averaged upward and downward velocities of solid particles can be determined:

$$\overline{V}_{pu} = \frac{G_u}{\overline{C}} \tag{6.13}$$

$$\overline{V}_{pd} = \frac{G_d}{\overline{C}} \tag{6.14}$$

Calculated data of $\overline{V}_{pu}$ and $\overline{V}_{pd}$ are shown in Table A.3.1 and A.3.2 for U_0 = 0.34~0.64 m/s at the four sampling freeboard levels and at the column exit. In Table A.3.1 and A.3.2, average solids speed ($\overline{V}_{pa}$) at any freeboard level is expressed as:

$$\overline{V}_{pa} = \left[\frac{G_u}{(G_u+G_d)}\right] \cdot \overline{V}_{pu} + \left[\frac{G_d}{(G_u+G_d)}\right] \cdot \overline{V}_{pd} \tag{6.15}$$

Variations of cross-sectionally averaged particle velocities $\overline{V}_{pa}$, $\overline{V}_{pu}$, and $\overline{V}_{pd}$ with freeboard height Z are shown in

Figures 6.15, 6.16, and 6.17 respectively. The plot of $\overline{V}_{ps}$ vs. Z (Figure 6.15) is similar to that reported by Hamdullaphur (1985) using a Laser Doppler Velocimeter for 300 μm sand particles in the freeboard of a two-dimensional fluidized bed (Figure 6.18). Hamdullaphur's results have indicated that there exhibits a two-stage decay of the r.m.s. particle velocity profile with the freeboard height. Similar results have been observed in this study. Also for this work, $[(V_{ps})_{z=0}]/U_0$ is equal to 1.0 for U_0= 0.34 m/s and 1.88 for U_0= 0.64 m/s (see Figure 6.15). These results are similar to those given by Hamdullaphur (2.2 for U_0 = 0.20 m/s and 1.8 for U_0 = 0.45 m/s, Figure 6.18).

The higher average particle speed (Figure 6.15) and upward velocity (Figure 6.16) at Z>1.3 m as compared with those at Z = 0.6-1.3 m may be attributed to low descending velocities (Figure 6.17) of the elutriated finer particles (Figure 6.6).

As shown in Figure 6.19, approximately linear variations of $\overline{V}_{pu}$ with U_0 were observed. This linear variation is similar to that reported by Morooka et al. (1980) for FCC particles (d_p = 65~68 μm, ρ = 0.96~1.11 g/cm^3), as shown in Figure 6.20.

Compared with the published results, the solids flux and velocity estimated by the method employed in the present study seem reasonable.

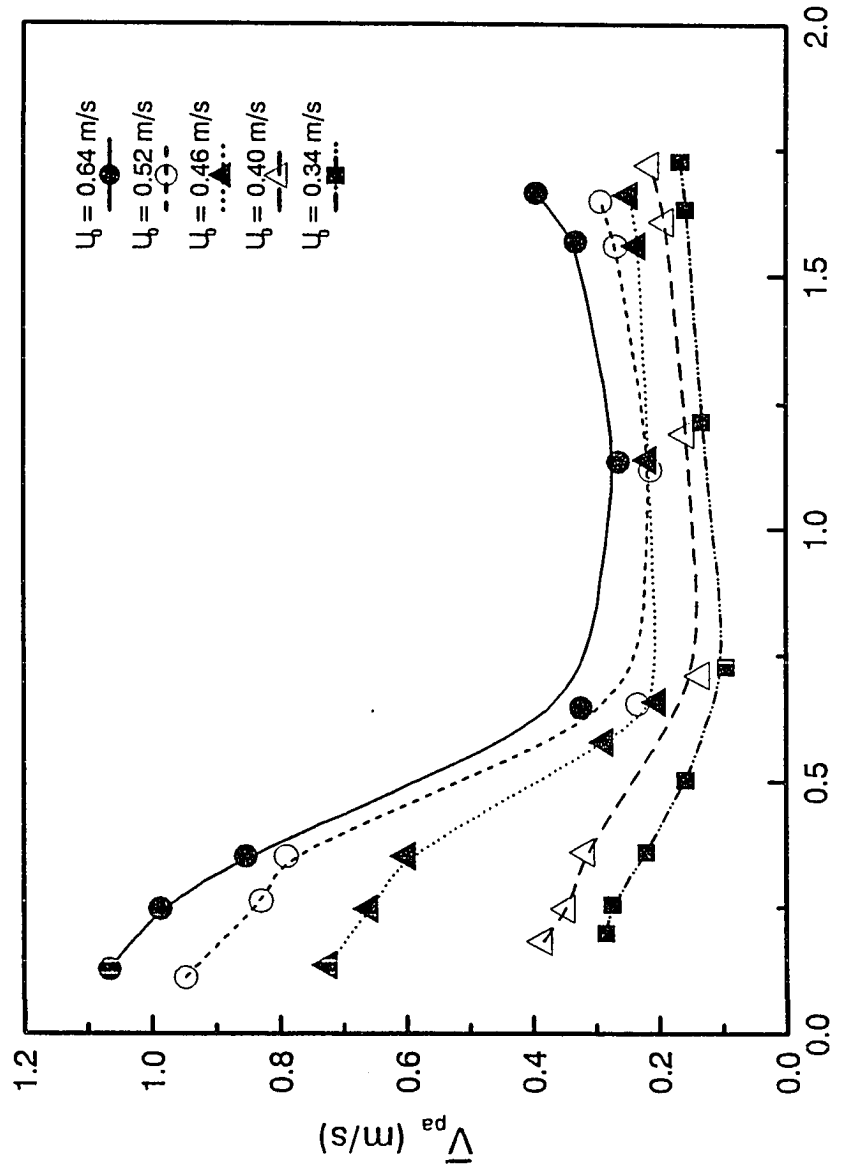

Figure 6.15: Axial variation of average particle speed ($\overline{V}_{pa}$).

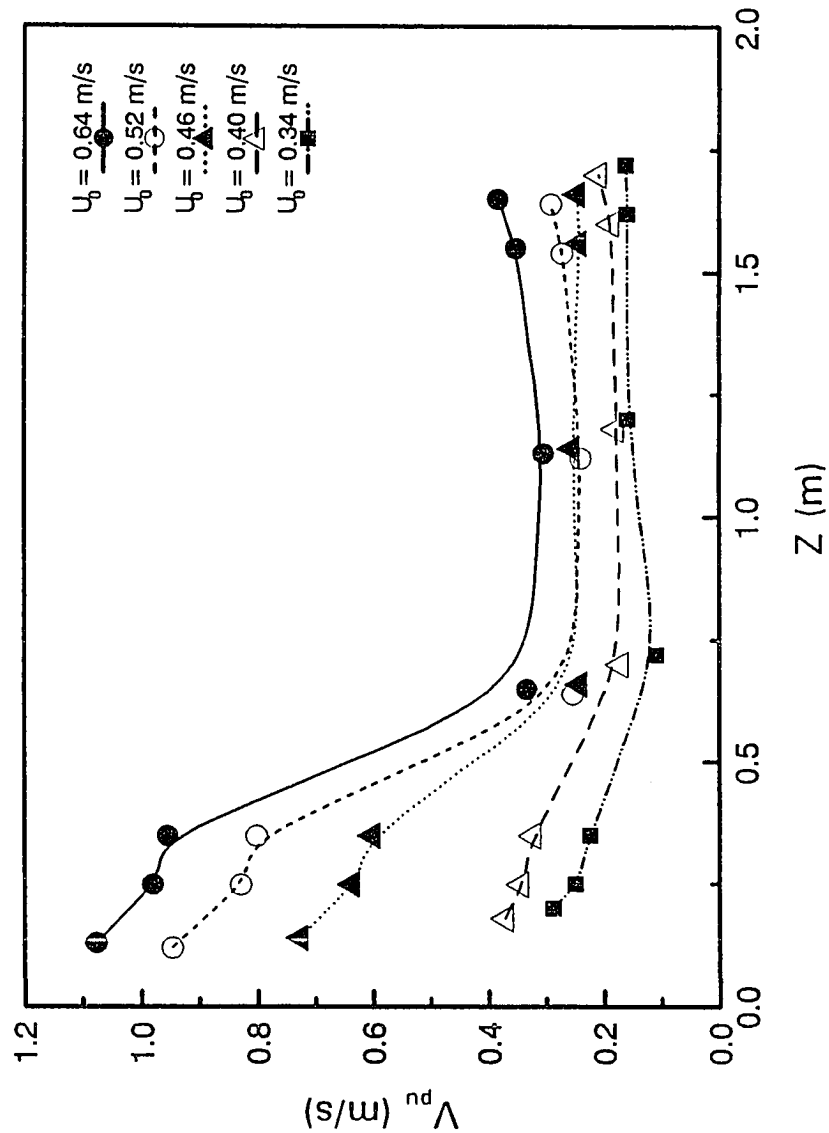

Figure 6.16: Axial variation of upward solids velocity ($\overline{V}_{pu}$).

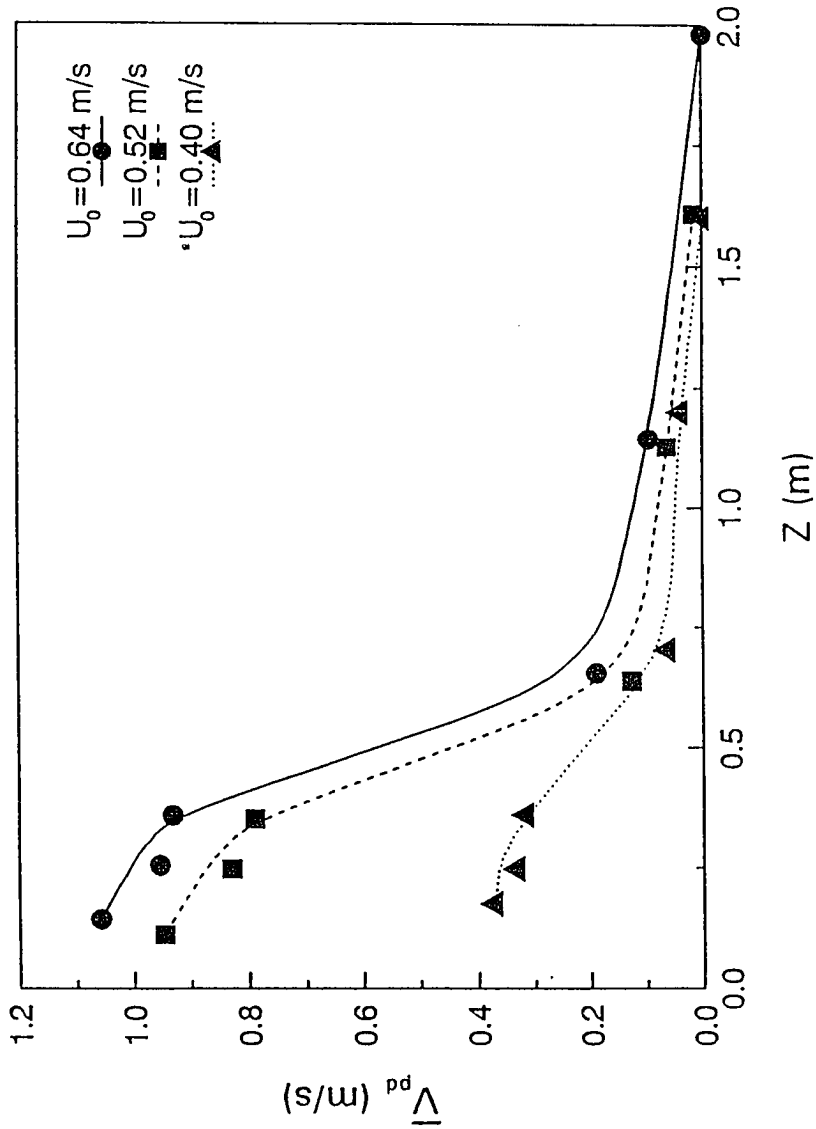

Figure 6.17: Axial variation of downward solids velocity ($\overline{V}_{pd}$).

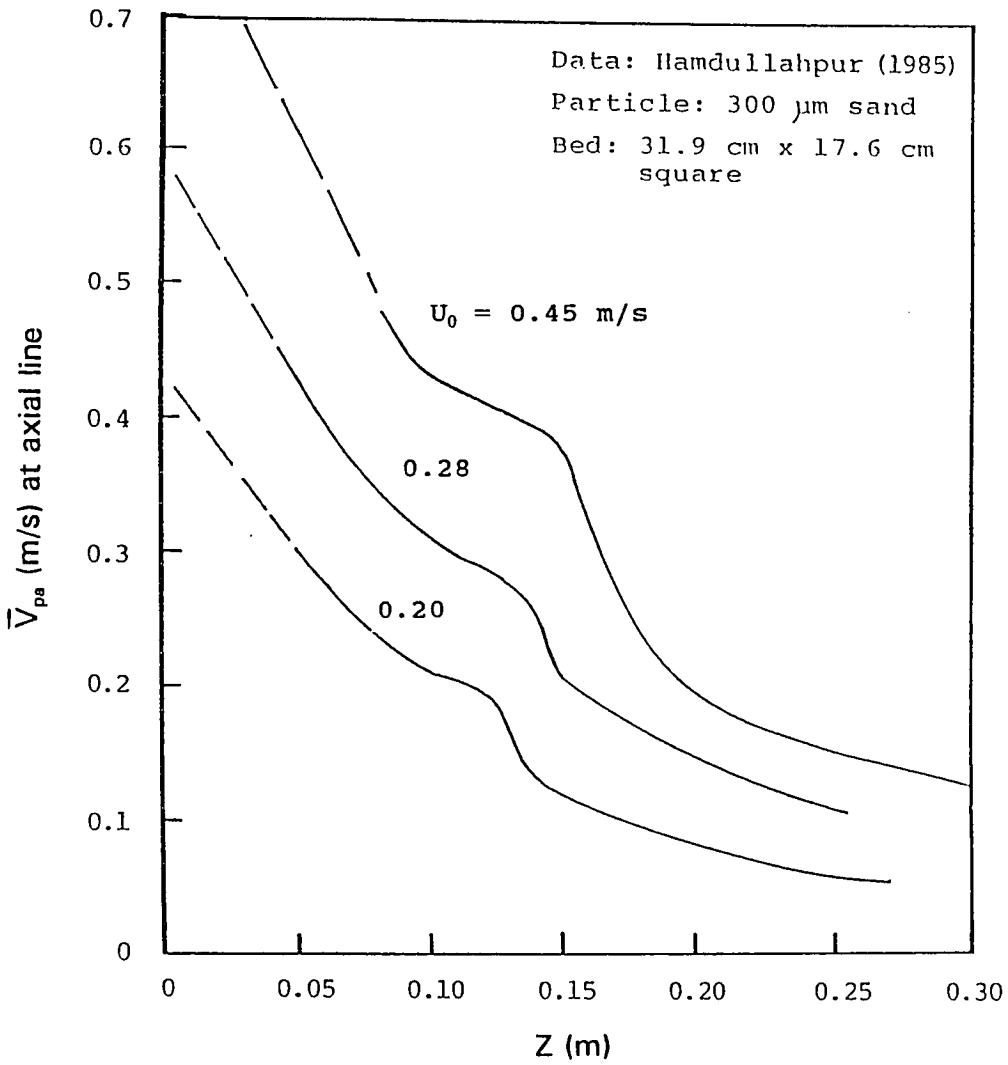

Figure 6.18: Axial variation of r.m.s. particle velocity in the freeboard of a gas fluidized bed of sand (Hamdullahpur, 1985).

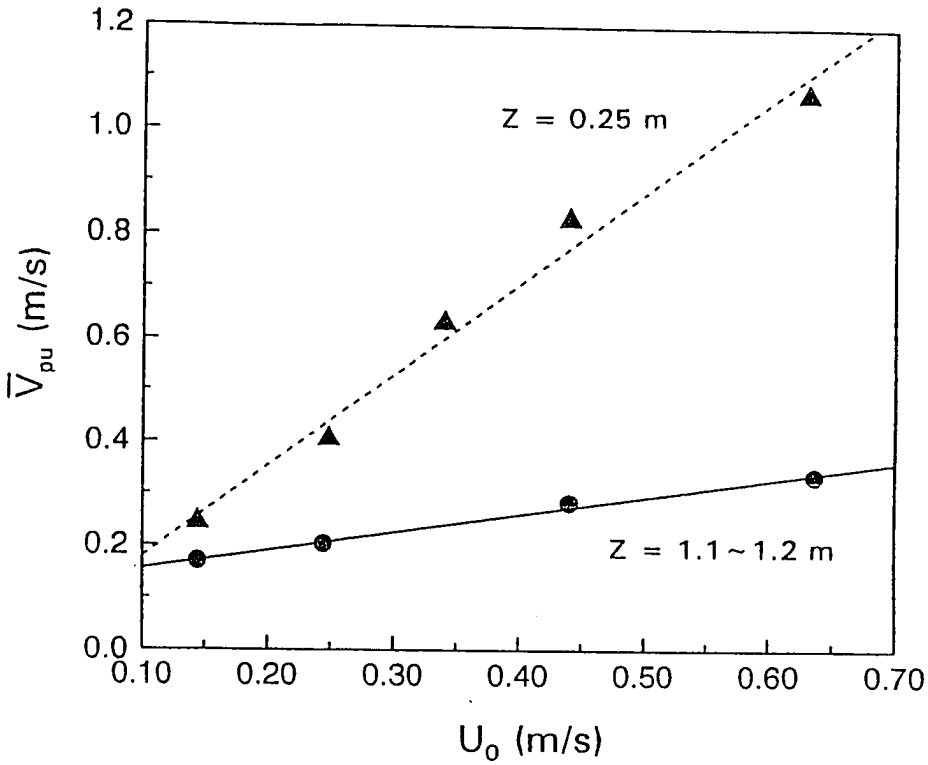

Figure 6.19: Variation of upward solids velocity ($\overline{V}_{pu}$) with U_0.

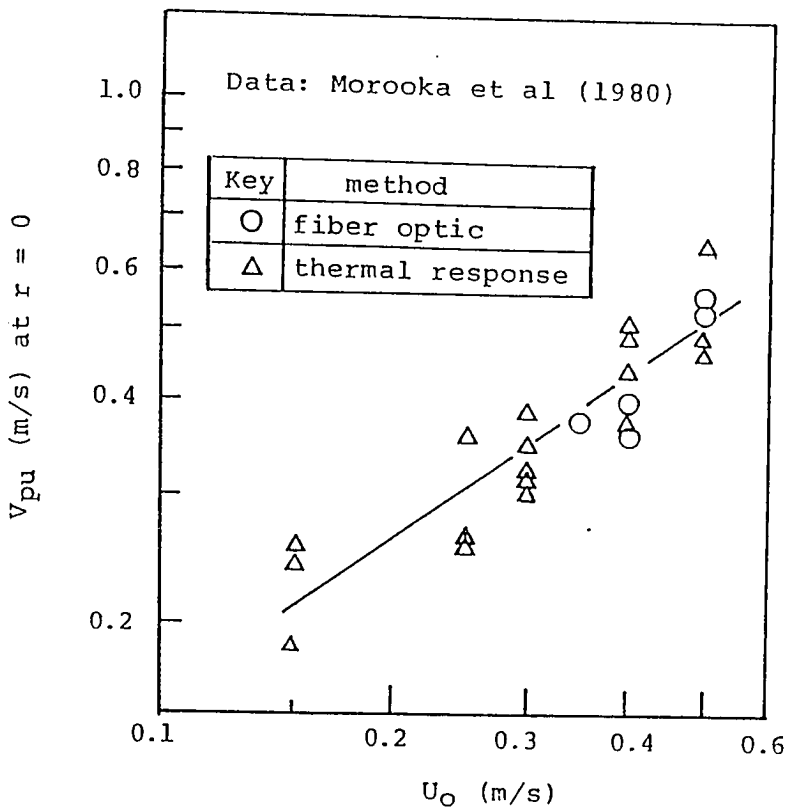

Figure 6.20: Effect of superficial gas velocity on ascending velocity of solid particles at r=0 (Morooka et al.,1980).

6.4 Summary of the Solids Dynamics

Results of solids concentration (C) measurements indicate that in the lower freeboard (splash zone), C is higher in the core than in the center for $U_0 < 0.5$ m/s. In higher freeboard levels, however, C increases with increasing radial position measured from column center.

Particle size distributions of sampled solids indicate that radial variations of particle size are not significant except for lower freeboard levels. Cross-sectionally averaged particle size generally decreases with freeboard height, and increases with U_0 for all freeboard levels.

Values of cross-sectionally averaged solids concentrations ($\bar{C}$) have been incorporated into a model proposed by Kunii and Levenspiel for solids dynamics analysis. The result indicates a two-stage decay of concentration profile with the freeboard height. Value of the average decay constant (a) in the splash zone ($Z < 0.5$-0.6 m) is comparable to the published data in the range of U_0 investigated.

Solids flux and particle velocity in the freeboard have also been estimated by incorporating Zenz and Weil's (1958) idea into Kunii and Levenspiel's model. Results indicate that the calculated average particle velocity ($\overline{V}_{ps}$) exhibits a two--stage decay pattern with respect to freeboard height, similar

to that found by Hamdullaphur (1985) using a Laser Doppler Velocimeter for 300 μm sand particles.

CHAPTER 7

RESULTS AND DISCUSSIONS

Results of heat transfer measurements in the freeboard are presented in this chapter. Radial and axial variations of the heat transfer coefficients for four types of plate orientations are discussed. Correlations between heat transfer coefficients and operating variables are also reported.

7.1 Experimental Data

Experimental data for heat transfer coefficient measurement are listed in Tables A.1.1 to A.1.30 of Appendix 1. Heat transfer coefficients listed in these tables refer to those contributed from solids and gas convection only (i.e., h_s+h_f) as shown in Equation 3.1. An example of calculation of heat transfer coefficients from the measured parameters is shown in Appendix 8.

7.2 Radial Variation of Heat Transfer Coefficients

7.2.1 Lower Freeboard (Splash Zone)

Figures 7.1(a) to 7.1(d) show radial variation of the measured solids concentration along with the surface-to-

suspension heat transfer coefficients for the four plate orientations at superficial velocities (U_0) of 0.4 m/s and 0.64 m/s in the lower freeboard (H = 0.45-0.52 m). There are larger radial variations in the heat transfer coefficient and the solids concentration at higher gas velocity (U_0= 0.64 m/s) than those at the lower one (U_0= 0.40 m/s).

At U_0 = 0.40 m/s (Figure 7.1b), there is large fluctuation (± 24%) in the solids concentration at this low freeboard. The average solids concentration is 86% higher at the center than in the wall vicinity. However, there is no apparent variation in the heat transfer coefficient along the radial direction for the four plate Types (Figure 7.1a). The solids concentration is not the sole control factor for heat transfer in this case. As can also be seen from Figure 7.1(a), heat transfer coefficients are lowest with the plate surface facing downward (Type IV) at H = 0.45 m ($H-H_0$ = 0.16 m or y = 0.533) and U_0 = 0.40 m/s. Similar results were reported in the study of heat transfer around a horizontal tube in the freeboard region of a glass beads fluidized bed at low gas flow rates (Biyikli et al., 1983).

At U_0 = 0.64 m/s (Figure 7.1 d), there is also large fluctuation (± 15%) in solids concentration at this low freeboard. The average solids concentration is 35% higher in the vicinity of the wall than at the center. The downward-facing plate (Type IV) gives the highest heat transfer rates

among the four Types of plate orientation. Direct and rapid bombardment of the plate by splashed particles from the bed accounts for this high rate. For a Type IV plate, higher transfer rates in the vicinity of the column wall (r/R > 1/2) are related to higher solids concentration in that region. The low transfer rate at r = 13.5 cm (Figure 7.1 b) is speculated to be caused by downward flowing solids clusters that approach the exposed heat transfer surface in the rear. Wall-side downward solids flux in the freeboard is a common phenomenon, as reported by Morooka et al. (1980) for fine particles such as FCC catalysts.

As also shown in Figure 7.1 (b), two Types of center--facing plates (Type II and III) exhibit nearly the same heat transfer rate in the core region of the freeboard (r < 7.5 cm or r/R < 0.5) at the plate elevation of H-Ho = 0.16 m. However, for the annular region (r > 0.5), Type III (one center-facing exposed surface only) plate gives a heat transfer rate of 31% (max. value at r=12 cm) higher than that of Type II (one center-facing and one wall-facing surface).

Consider the equation:

$$[h_s+h_f]_{\text{center-facing}} \cdot \left(\frac{A}{2}\right) + [h_s+h_f]_{\text{wall-facing}} \cdot \left(\frac{A}{2}\right) = [h_s+h_f]_{\text{average}} \cdot A \qquad (7.1)$$

the wall-facing surface gives a transfer coefficient ($[h_s+h_f]_{\text{wall-facing}}$) of 150 $W/m^2 \cdot K$, which is only 55% of that given by center-facing surface at r = 12 cm ($[h_s+h_f]_{\text{center-facing}}$ = 290 $W/m^2 \cdot K$). This

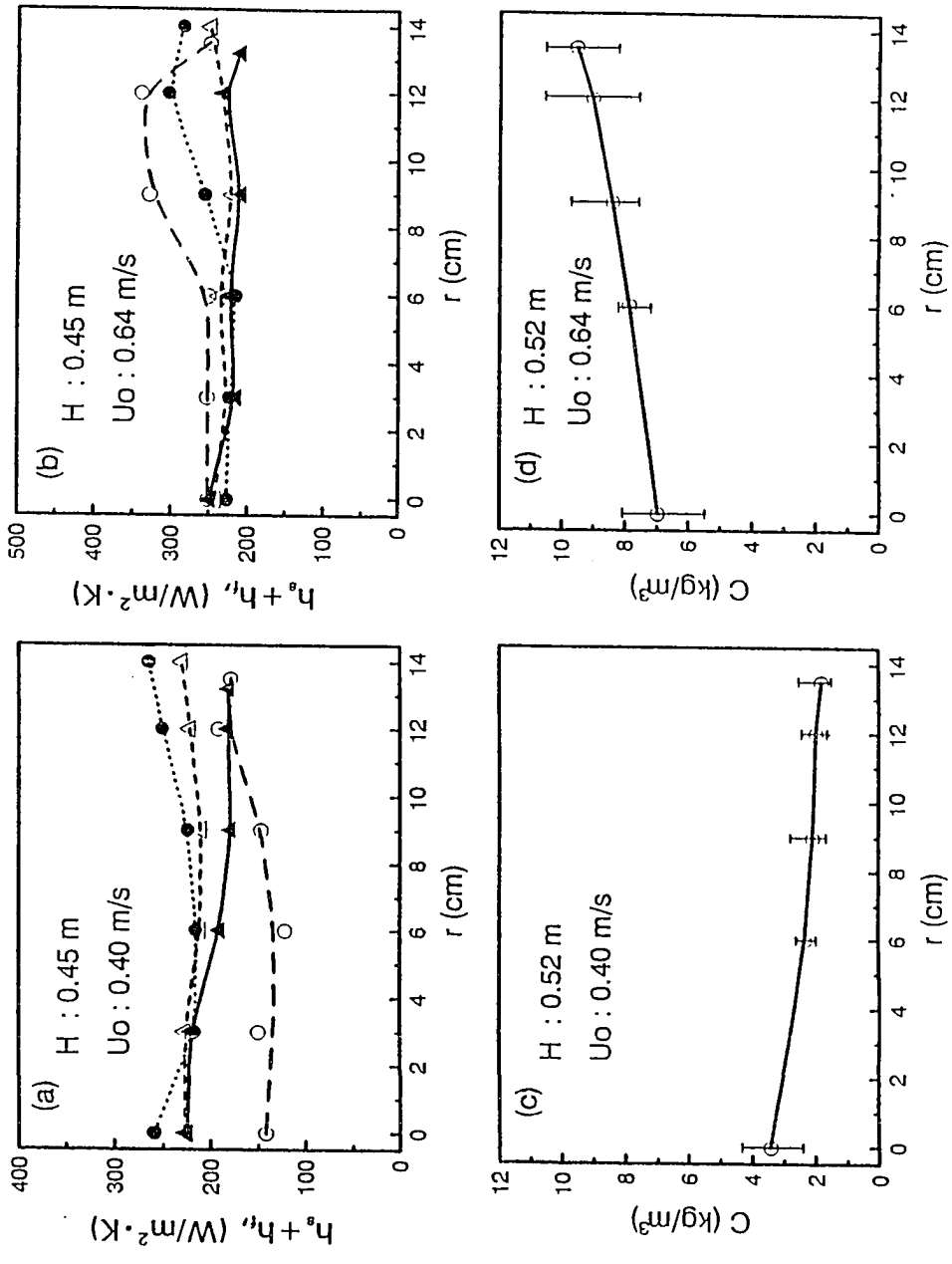

Figure 7.1 Radial variations of heat transfer coefficient (a and b: Plate Type: I [▲], II [△], III [●], IV [○]) and solids concentration (c; 6) at lower freeboard.

may arise from wallward moving particles in the splash zone of the bed as reported by Morooka et al. (1980) for bubbling bed, and Rhodes et al. (1988) in the riser of a circulating fluidized bed. At this elevation (H = 0.45 m), Type I and II plates show similar heat transfer characteristics. The heat transfer coefficients are relatively invariant with respect to the radial direction.

7.2.2 Freeboard above the Splash Zone

Radial variations of the heat transfer coefficient and the solids concentration at H= 0.95 m ($H-H_0$ = 0.66 m) are shown in Figure 7.2. At this freeboard elevation, the solids concentration increases gradually from center to the wall vicinity at U_0 = 0.64 m/s (Figure 7.2 d). This shows that there is a significant center-to-wall solids movement that causes a higher heat transfer rate as exhibited by plate Type III. The center- facing surface gives a transfer coefficient of 180 $W/m^2 \cdot K$, which is 50% higher than that of wall-facing surface at r = 12 cm (120 $W/m^2 \cdot K$). Similar to the heat transfer characteristics in the splash zone, plate Type IV gives the highest transfer rate due to direct bombardment of upward-moving particles. Radially averaged transfer rate (185 $W/m^2 \cdot K$) for Type IV is 50% higher than that (120 $W/m^2 \cdot K$) for Types I and II. Except for Type III, radial variations of heat transfer coefficient are relatively small at this gas flow rate.

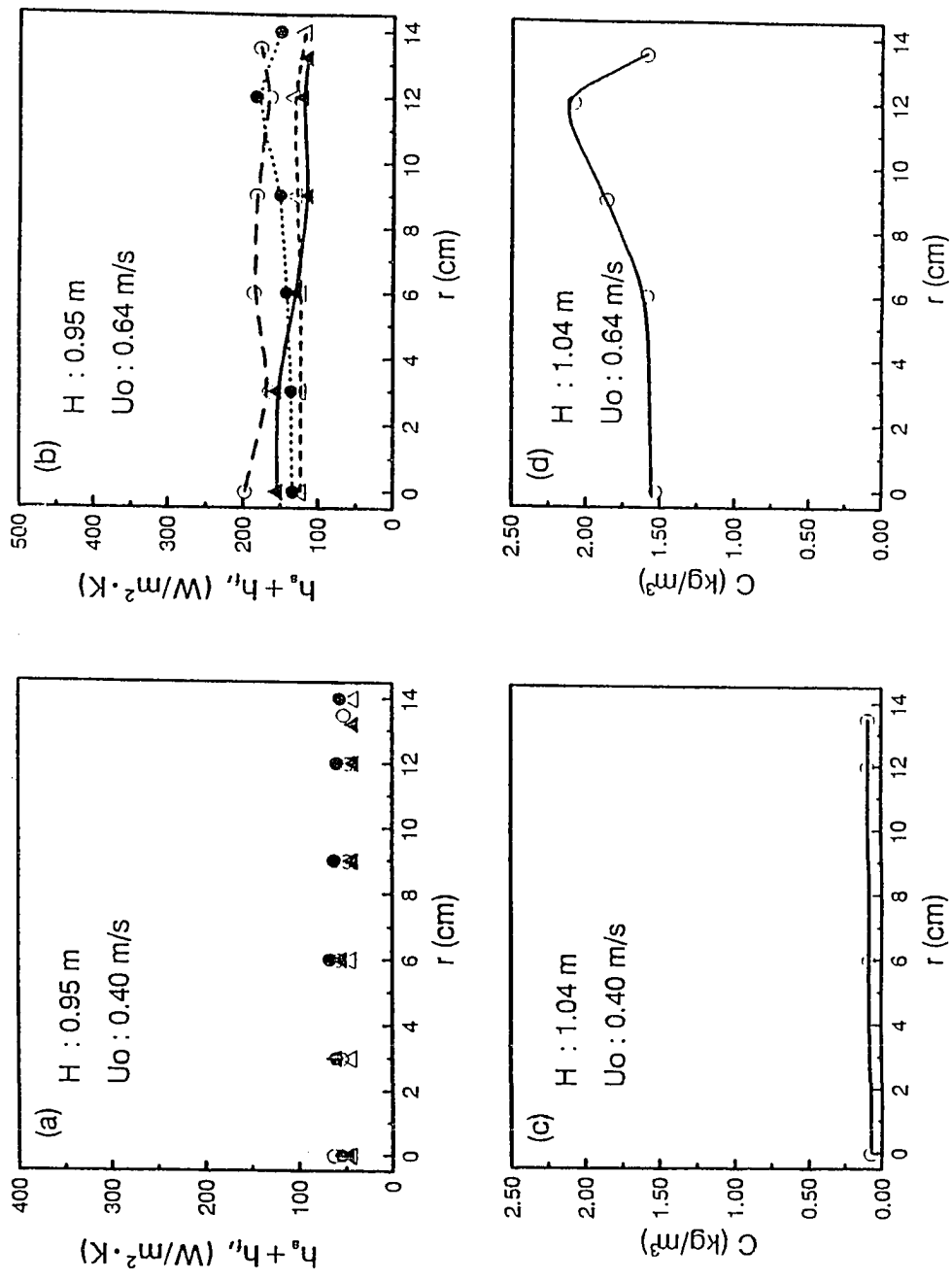

Figure 7.2 Radial variations of heat transfer coefficient (a and b: Plate Type: I [▲], II [△], III [●], IV [○]) and solids concentration (c; d) at higher freeboard.

For U_0 = 0.40 m/s at location of H= 0.95 m ($H-H_0$ = 0.66 m), Figures 7.2 (a) and 7.2 (c) indicate that radial variations of both solids concentration and heat transfer coefficients are insignificant. There is no significant difference in heat transfer rate among the four plate Types.

7.2.3 Comparison of Heat Transfer Coefficients Measured at Wall and Center of Column

Dependence of (h_s+h_f) on U_0 for plates located at column center and in the vicinity of column wall are shown in Figure 7.3.

For a Type I plate, (h_s+h_f) is greater at the center than in the wall vicinity. This can be attributed to the higher particle velocity parallel to the plate in the column core ($r/R < 0.85$), as shown by Morooka et al. (1980).

Figure 7.3 (b) shows that plate orientation Type II gives nearly the same value of (h_s+h_f) at the center and the wall. A Type III plate gives higher transfer coefficients in the vicinity of the column wall as shown in Figure 7.3 (c). Comparison of the two plate Types also indicates that the center-facing surface (Type III) exhibits higher heat transfer rate than the wall-facing one (Type II). This could be attributed to the center-to-wall movement of particles which bump into the surface directly (e.g., Morooka et al.,1980).

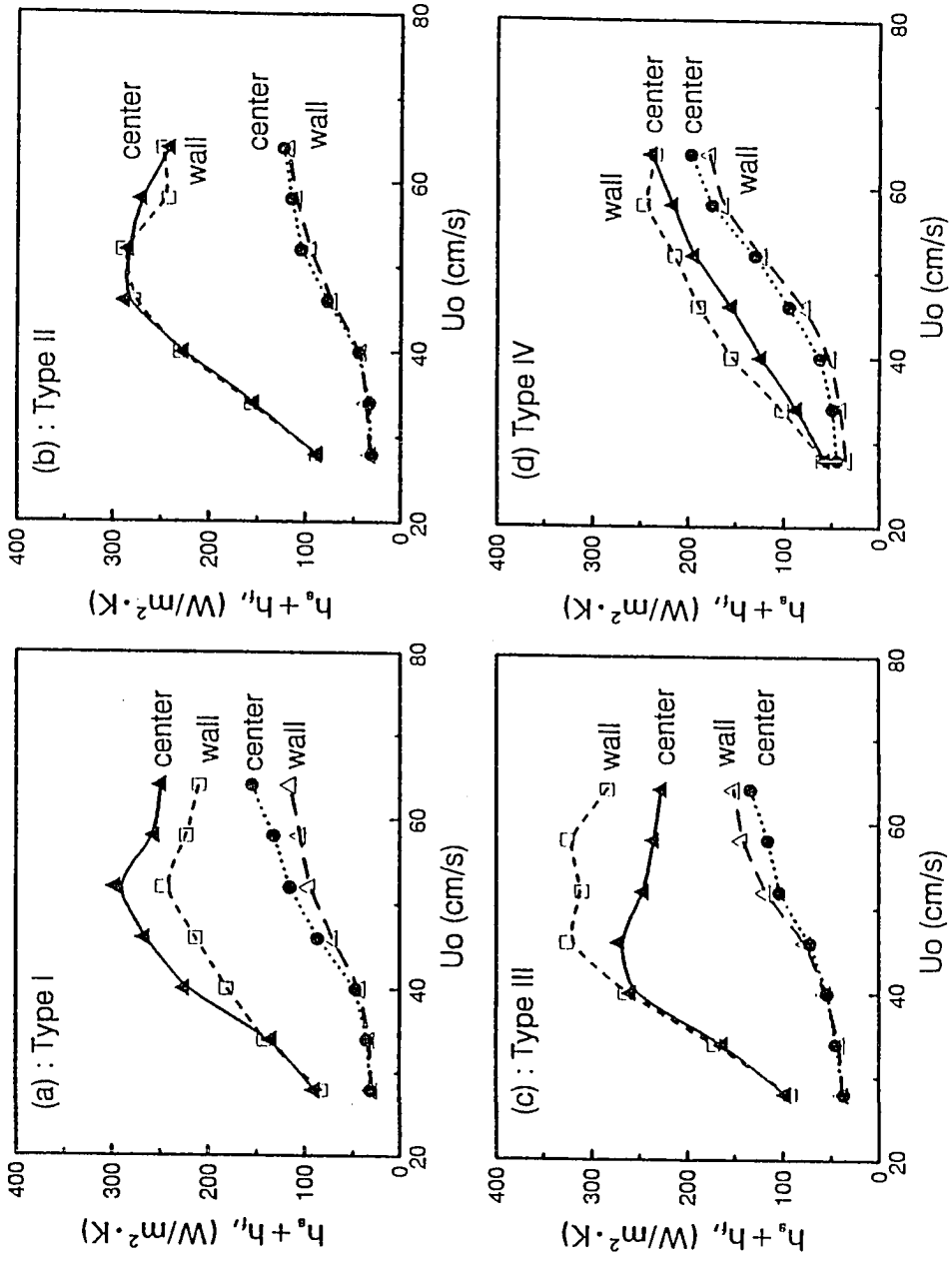

Figure 7.3 Heat transfer coefficients at the column center and in the vicinity of the wall. H-H_0=16 cm: center(▲), wall (□); H-H_0=66 cm: center(●), wall (△).

For Type IV plate, (h_s+h_f) is significantly larger at the wall than at the center for $H-H_0$ = 16 cm (or Z = 0.533). The phenomenon of higher solids concentration near the wall in the lower part of the freeboard explains the observation at this plate elevation.

7.3 Axial Variation of Heat Transfer Coefficients

Variations of average heat transfer coefficients along the freeboard height are shown in Figures 7.4 (a) and 7.4 (b) for plate Types I and IV respectively. The variation of heat transfer rate with elevation in the freeboard is as much as an order of magnitude, decreasing to gas convection with increasing elevation. This is similar to that observed for heat transfer around a horizontal tube in the freeboard region of glass beads (d_p = 275 and 840 μm) and silica sand (d_p= 285 and 465 μm) fluidized beds as shown in Figure 7.4 (c) (Biyikli et al., 1983).

Figure 7.5 compares the present data with those of Kiang et al. (1976) for FCC catalyst particles (d_p: 53 μm) in the freeboard of a 10.2 cm i.d. fluidized bed. Heat transfer coefficients for plate orientation Type I of the present study agree with Kiang's data for the small heat transfer probe (1.91 cm o.d. x 5.72 cm). Those for Type IV are higher for the reason that upward-moving particles bombarded normally to the downward-facing exposed surface of the plate.

Figure 7.6 shows comparison of the present data (Type I) with those given by George and Grace (1982) for 102 μm sand at 112-152 °C in the freeboard of a rectangular bed (43 cm x 25 cm). George's data show steeper variation with elevation of the freeboard. This may be caused by larger and denser particles (used in George and Grace's work) which cause a steeper decrease in solids concentration with increasing elevation (Kunii and Levenspiel, 1990).

7.4 Angular Symmetry of Heat Transfer Coefficients and Reproducibility of the Experimental Data

Angular variation of the heat transfer coefficients was obtained by measuring the coefficients with plates located at the same radial and axial, but different angular locations.

Figure 7.7 shows locations of plates (Type III) and the measured heat transfer coefficients at the column center (r = 0) and the wall vicinity (r = 14 cm). The results indicated that there was angular symmetry of the measured heat transfer coefficients in the freeboard except at lower elevations (e.g., H-Ho = 0.16 m) and higher gas velocities (e.g., U_0 > 0.55 m/s). This phenomenon may be caused by uneven angular distribution and/or time fluctuation in solids concentration at the lower freeboard heights.

Reproducibility of the experimental data can be checked by comparing the heat transfer coefficients ($h_s + h_f$) for plate

Types I and II located at r = 0 and H = 0.45 m (Figure 7.8). As shown in Fig 5.1, at the column center, plate Types I and II should give the same value of heat transfer coefficient if the experimental data are reproducible. Consistency in the data shown in Figure 7.8 indicates the good reproducibility.

7.5 Contour Lines of Heat Transfer Coefficients

Contour lines of heat transfer coefficients in the freeboard are shown in Figures 7.9(a)-(d) for the four plate Types at U_0 = 0.52 m/s. Shirai (1962) has measured the heat transfer coefficients at a small heater immersed in the bed, some of his data are shown in Figure 7.9 (e). The contour patterns shown in Figure 7.9 illustrate different features of the surface-to-suspension heat transfer rate in the bed and the freeboard. Compared with Shirai's result, the magnitude of heat transfer coefficients in the present study are fairly accurate.

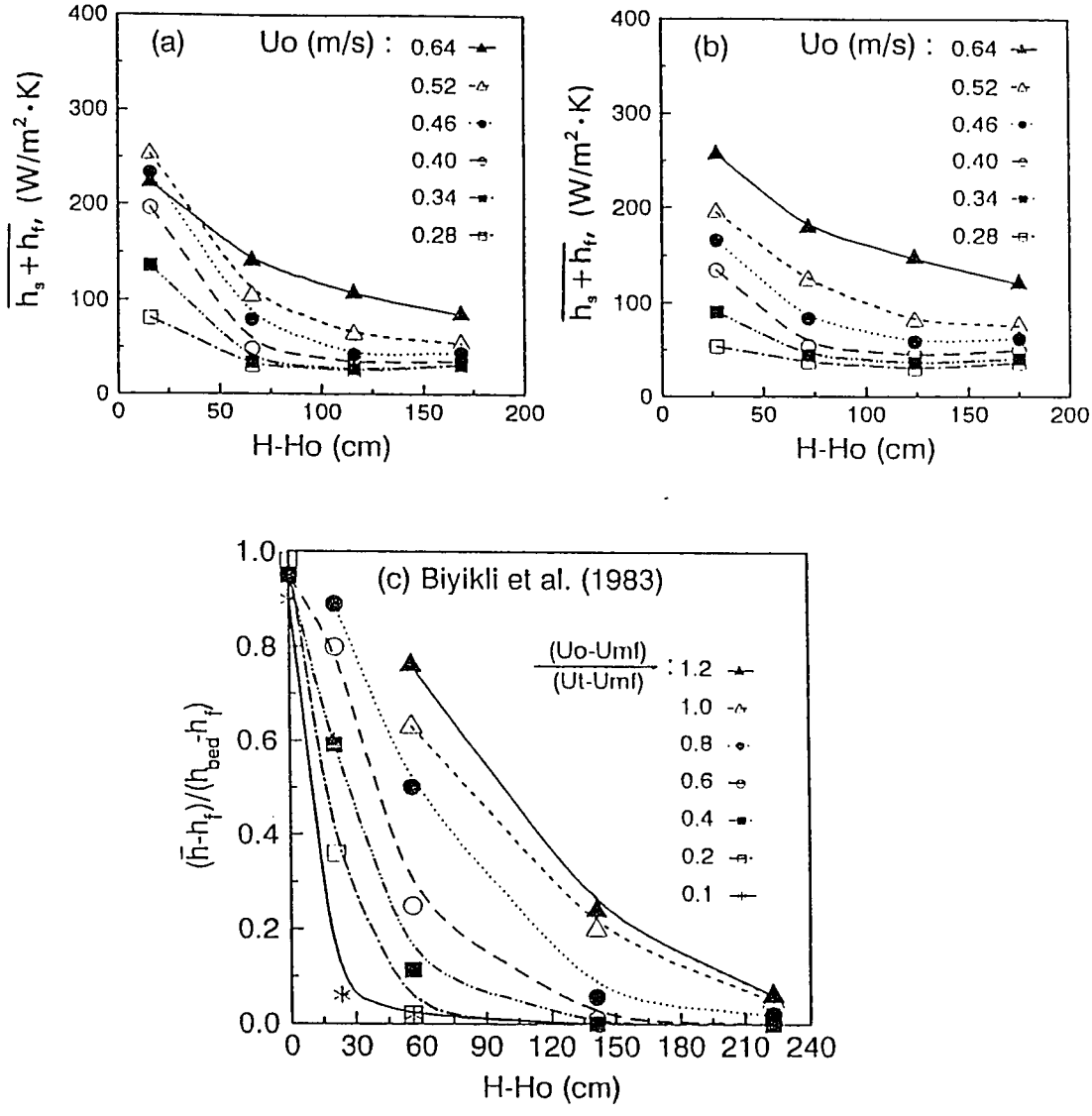

Figure 7.4 Variation of cross-sectionally averaged heat transfer coefficients with freeboard height. (a): Plate Type I; (b): Plate Type IV; (c): Biyikli's data, where h_{bed} is the in-bed heat transfer coefficient.

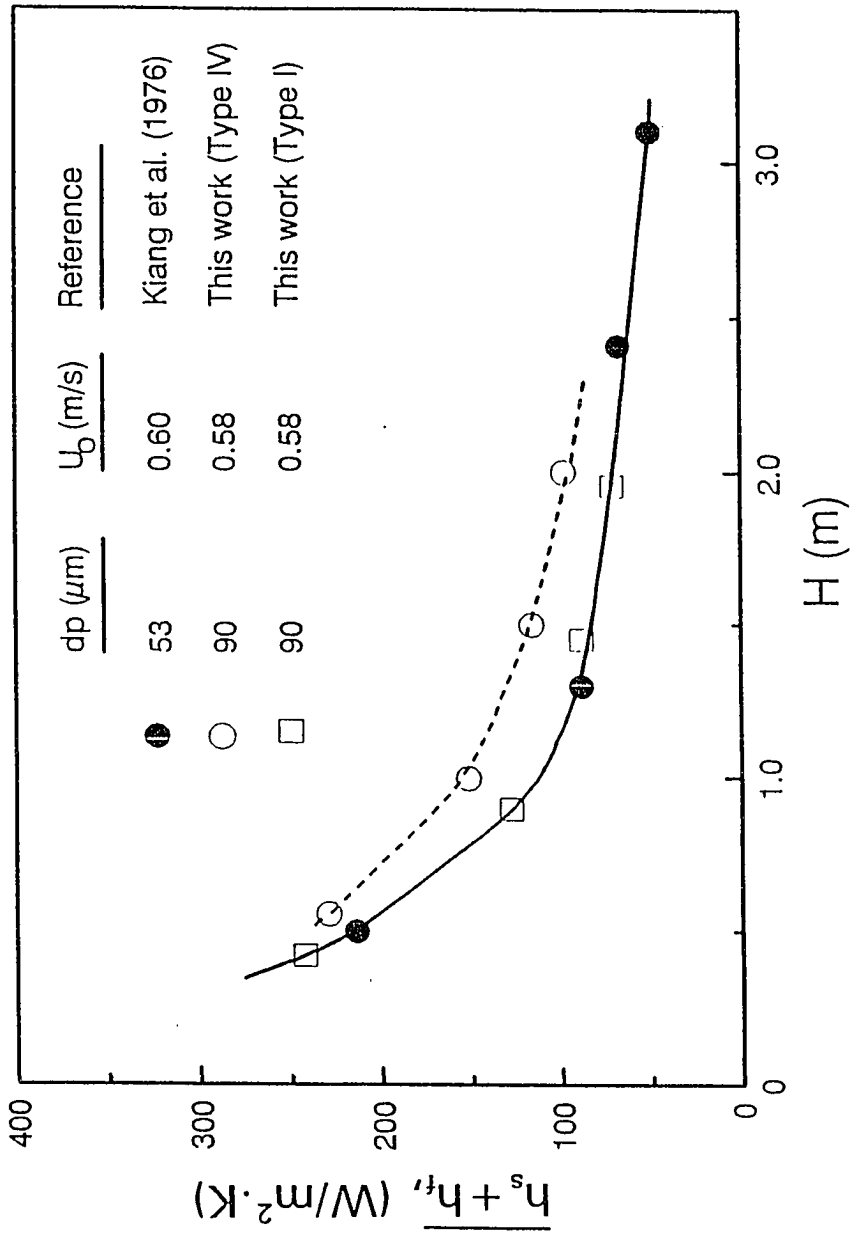

Figure 7.5 Comparison of axial variations of heat transfer coefficient of the present data with those of Kiang et al. (1976).

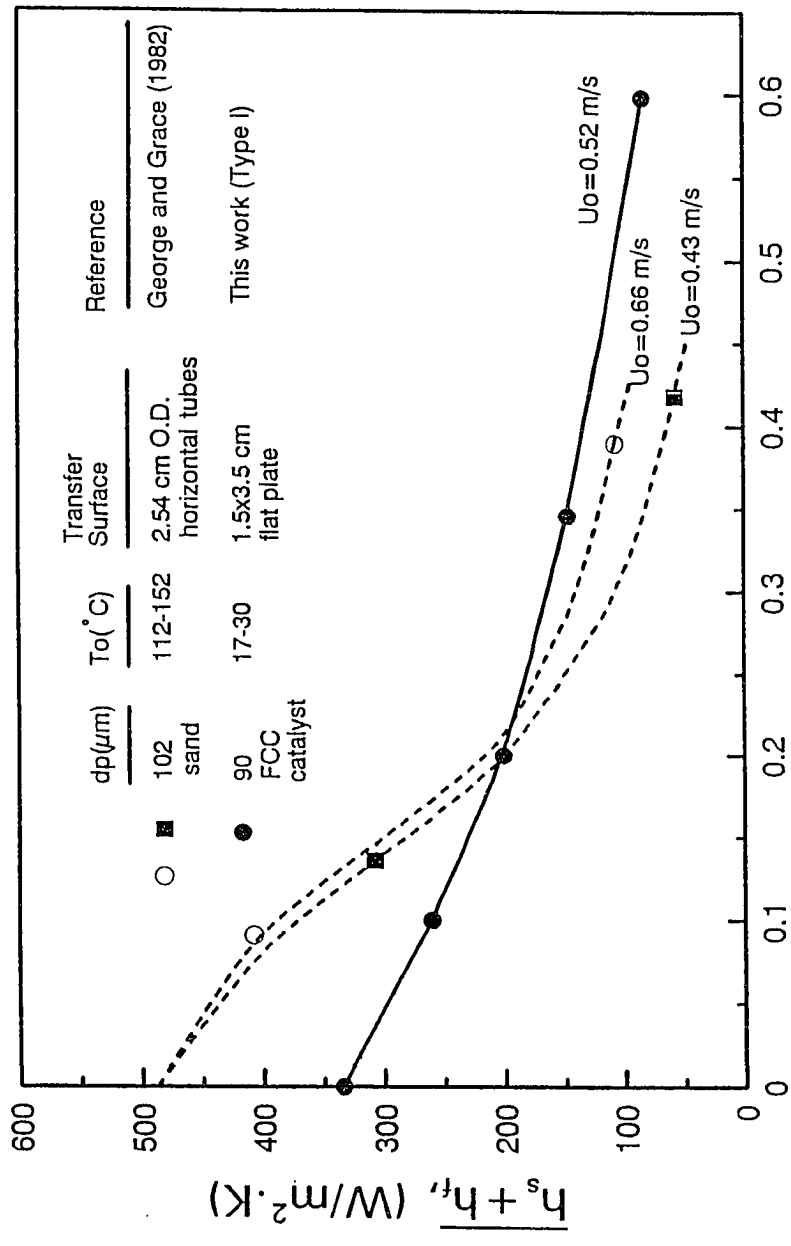

Figure 7.6 Comparison of axial variations of heat transfer coefficient of the present data with those of George and Grace (1982).

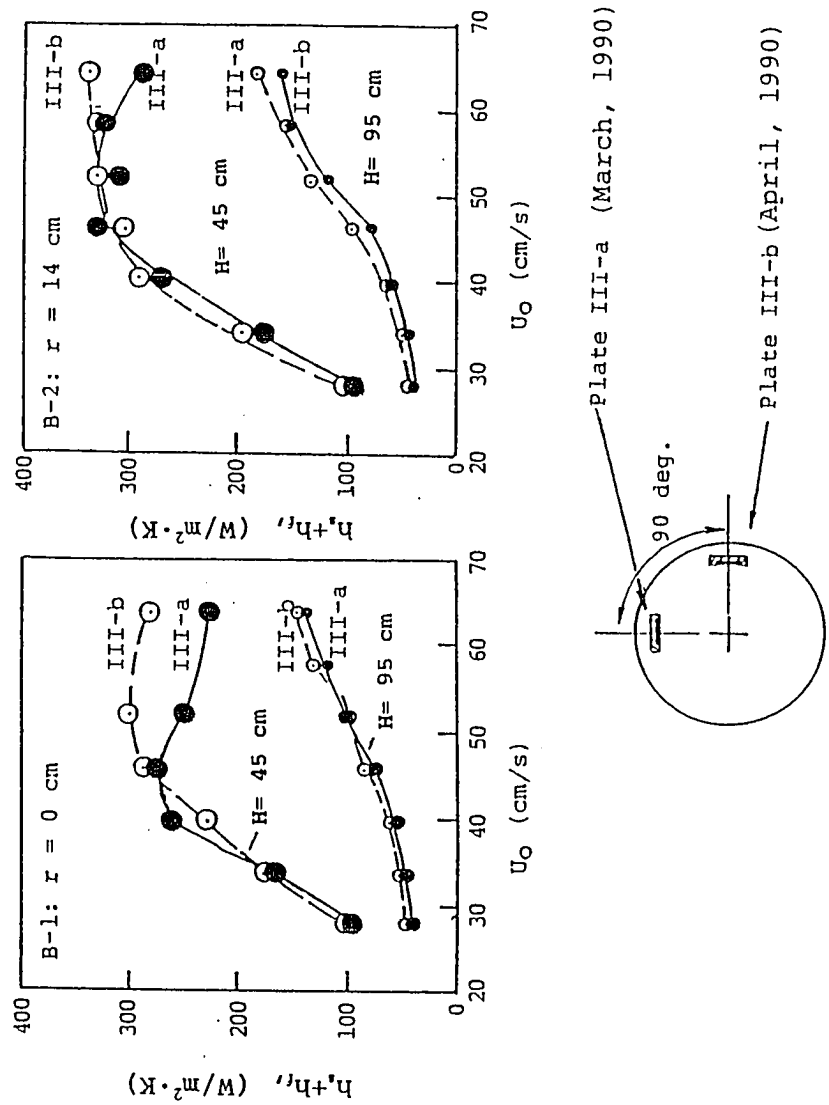

Figure 7.7 Angular symmetry of the measured heat transfer coefficient data.

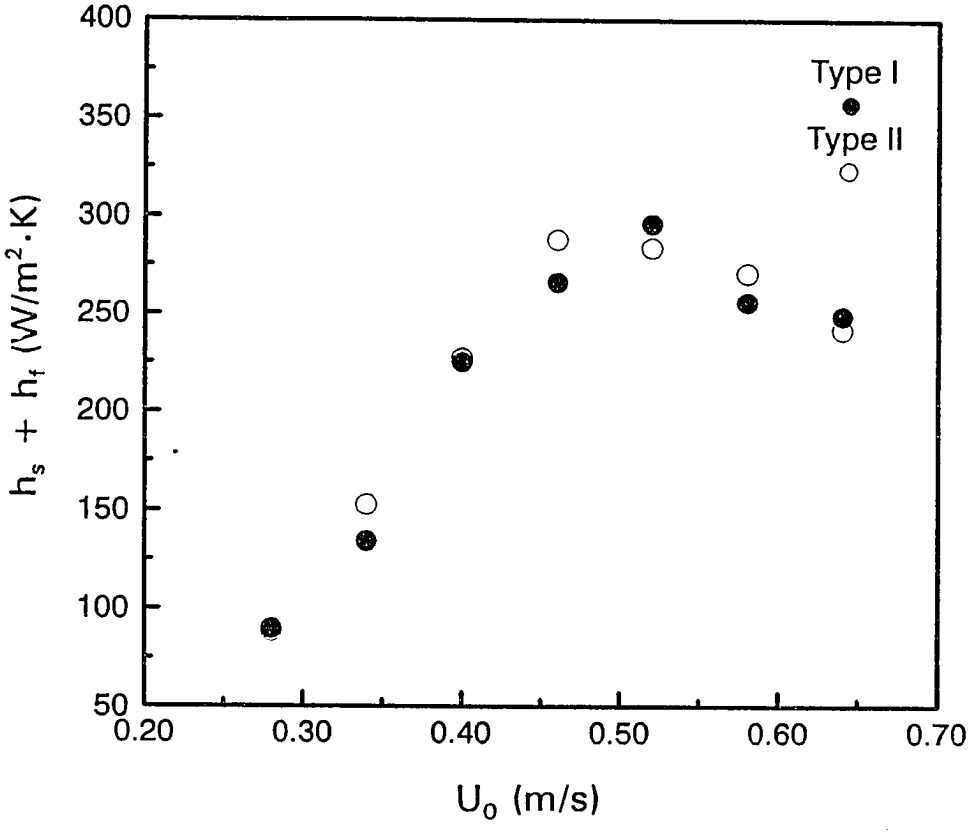

Figure 7.8 Comparison of heat transfer coefficient ($h_s + h_f$) for plate I and II located at r=0 and H=0.45 m.

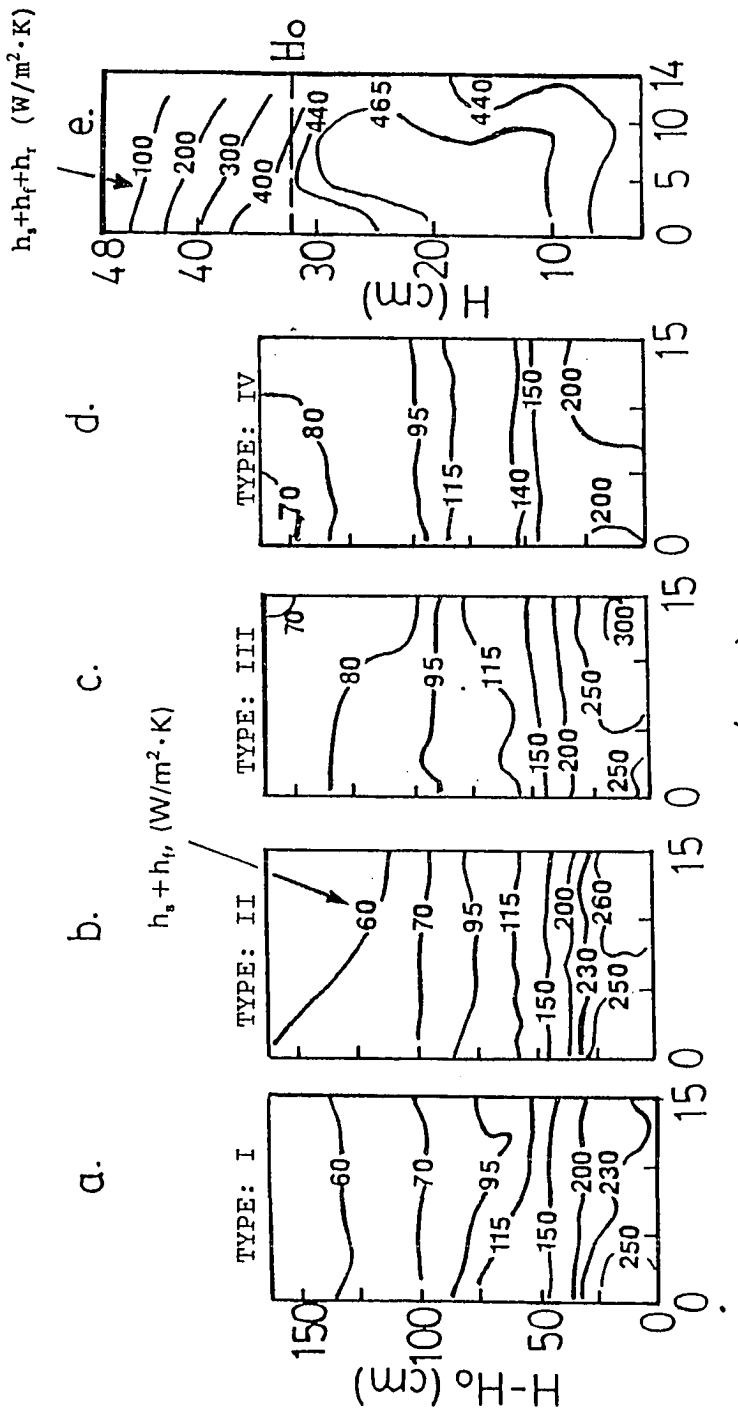

Figure 7.9 Contour lines of heat transfer coefficients in the freeboard [(a)-(d): this work] and in dense bed and freeboard [(e): Alumina catalyst, d_p = 160 μm, Shirai (1962)].

7.6 Correlation of Freeboard Heat Transfer Coefficient

The rate of heat transfer between a fluidized bed and submerged surfaces depends upon a number of factors, including the properties of the bed material, the fluid, solids holdup, bed and surface geometries, and the fluidization state (Kunii and Levenspiel, 1969, Botterill, 1975). Effects of these factors have been discussed in Chapter 2. A number of correlations and models have been reported for heat transfer studies in dense beds and circulating fluidized beds (e.g., Mickley and Fairbanks, 1955; Fraley et al., 1983; Subbarao and Basu, 1986; Martin, 1981; Zabrodsky, 1966; Botterill, 1975; Ziegler et al., 1964b). However, the correlations are rather limited for dilute phases such as those in the freeboard (Hashimoto et al., 1990; Biyikli et al., 1983 and 1987b) and in solids-gas transfer lines (Wen and Miller, 1961).

In the present study, the apparent variables affecting the surface-to-suspension heat transfer coefficients are static bed height, plate location, and gas flow rate. The effect of static bed height on the average heat transfer coefficient was not considered in the present study. Therefore (h_s+h_f) can be correlated with only two parameters, U_0 and $H-H_0$.

The regression results of the experimental data by using the least square method are shown in Table 7.1. In these

correlations, the heat transfer coefficient contributed from free stream air current (h_f) was subtracted from the coefficient calculated by Equation 3.1. h_f's for subtraction were read from Figure 3.4.

Figures 7.10 (a)-(d) illustrate that these correlations are rather good for $U_0 < 0.52$ m/s as compared with the experimental data.

Table 7.1: Correlation of heat transfer coefficients

Plate Orientation	Dimensional Correlation
Type I	$h_s = 0.00912 \cdot U_0^{3.538} \cdot (H-H_0)^{-1.214}$
Type II	$h_s = 0.0115 \cdot U_0^{3.657} \cdot (H-H_0)^{-1.357}$
Type III	$h_s = 0.0876 \cdot U_0^{2.790} \cdot (H-H_0)^{-0.973}$
Type IV	$h_s = 0.0181 \cdot U_0^{3.126} \cdot (H-H_0)^{-0.895}$
Plate Orientation	**Dimensionless Correlation**
Type I	$Nu_L = 1.48 \cdot 10^{-8} \cdot Re_L^{3.538} \cdot y^{-1.214}$
Type II	$Nu_L = 0.84 \cdot 10^{-8} \cdot Re_L^{3.657} \cdot y^{-1.357}$
Type III	$Nu_L = 2.14 \cdot 10^{-8} \cdot Re_L^{2.790} \cdot y^{-0.973}$
Type IV	$Nu_L = 2.45 \cdot 10^{-7} \cdot Re_L^{3.126} \cdot y^{-0.895}$

$Nu_L = (h_s \cdot L/k)$, Nusselt number
$Re_L = [(U_0 \cdot \rho \cdot L)/\mu]$, Reynold number
$y = (H-H_0)/D$, dimensionless bed height measured from the surface of the static bed.
L = Characteristic length of the heating plate (m),
= 4 x (cross-sectional area)/(wetted perimeter)
= 2ab/(a+b)
= 2x1.49x3.5/(1.49+3.5)
= 2.09 cm = 0.029 m

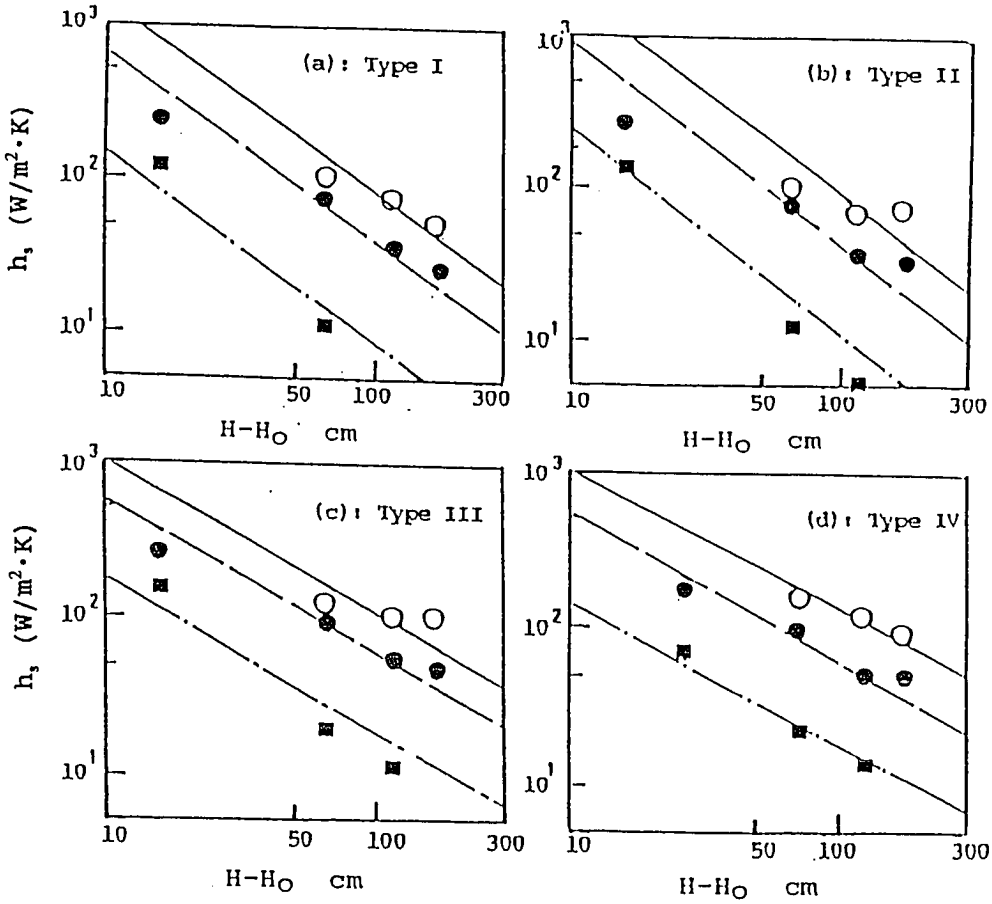

Figure 7.10 Comparison between experimental data and the correlated equations.
U_0 = 34 cm/s: (▣), correlation (-·-);
U_0 = 52 cm/s: (●), correlation (---);
U_0 = 64 cm/s: (○), correlation (——).

7.7 Summary

The heat transfer coefficient varies with the axial and radial position of the plate, plate orientation, and with the gas velocity.

Variations of heat transfer coefficients with radial position are more significant at lower freeboard heights than at higher ones for all the gas velocities examined (Figures 7.1 and 7.2). For plates with the exposed surface parallel both to the axial and radial directions of the column, heat transfer coefficients are higher at the center than at wall (Figure 7.3 a). For plates with the exposed surface parallel to the axial and perpendicular to the radial directions, the heat transfer coefficient is nearly the same as that at the center and the wall (Figure 7.3 b). At low heights of freeboard, center-facing surfaces exhibit higher heat transfer rate than wall-facing ones (Figures 7.3 c and d). The phenomena of higher solids concentration and center to wall movement of particles account for this observation.

Variations of heat transfer coefficients with elevation in the freeboard are as much as an order of magnitude, decreasing to gas convection with increasing elevation (Figure 7.4). These variations are relatively insensitive to plate orientations.

CHAPTER 8

DEVELOPMENT OF GAS-SOLID SUSPENSION-TO-SURFACE HEAT TRANSFER MODEL

As mentioned in Chapter 2, the mechanism of heat transfer between particles and heat exchange surfaces is believed to involve heat absorption and release by moving particles. Although many heat transfer models for dense and lean phases have been developed (see Chapter 2), they can not be directly applied to predict or describe the heat transfer phenomena in the freeboard region. To elucidate the mechanism of suspension-to-surface heat transfer in lean phase systems and extend the applicability of the present results to other operating conditions and system parameters, a mechanistic model is essential.

In this chapter, such a model will be developed. Some applications of the model will also be discussed. The following are major stages for the development of the model:

(1). Development of equations concerning "particle-surface heat transfer for single particles" based on the transient heating (or cooling) of single and discrete particles by the surrounding gas film that has been heated (or cooled) by the neighboring heat transfer surface.

(2). Development of equations concerning "particle-

surface heat transfer for cluster of particles" with surface coverage calculated based on the dynamic equilibrium between attaching and detaching particles.

(3). Estimation of model parameters by incorporating the experimental heat transfer and solids dynamics data into the model.

(4). Testing of the model by comparing the experimental and calculated data.

8.1 Development of Model

8.1.1 Particle-Surface Heat Transfer for A Single Particle

The following assumptions are made for deriving a model for heat transfer between a particle and the heating (or cooling) surface (Figure 8.1):

1. The particle is spherical with diameter d_p.
2. The physical and thermal properties of the solid and the gas are constant.
3. The bulk of the gas consists of a gas-solid suspension.
4. The particles in the suspension are at the same temperature as the gas, i.e., T_0.
5. Particles will move from the bulk to the surface. These particles stay in contact with (or slip past) the surface for a period of time.
6. The particles from the bulk of the suspension arrives at

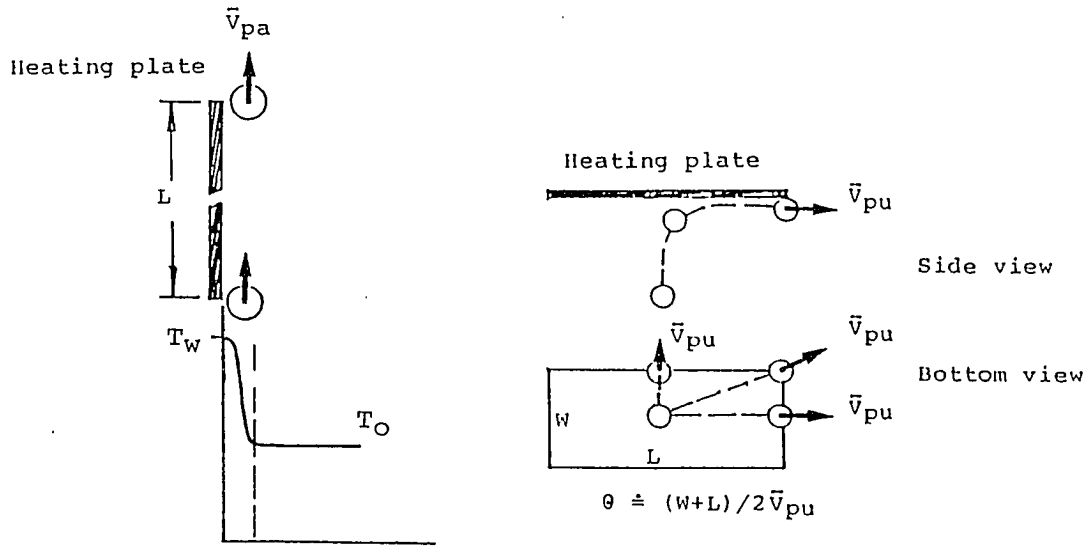

(a) Slipping of a single particle over a vertical heating plate
(Plate orientation type I, II, III)

(b) Collision and slipping of a single particle to and over a horizontal heating plate (Plate orientation type IV)

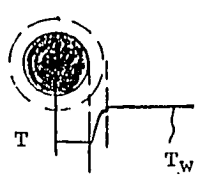

(c) Temperature profile of a heating particle

Figure 8.1: Particle-surface heat transfer mode for single particle.

the heating surface at the bulk temperature, T_0. During the time that the particle contacts at (or slips over) the surface it receives heat by convection from the fluid adjacent to the surface. This fluid is assumed to be at the surface temperature, T_w. After that time, the particle leaves the surface and returns to the bulk suspension. The process is repeated by other particles.

7. Heat transfer by surface-gas convection and thermal radiation are excluded.
8. Conduction at the point of contact of the particle and surface is extremely small and neglected.
9. For the particle near the surface, the Nusselt number (Nu) for fluid to particle convection takes its limiting value of 2. This is reasonable since the surrounding fluid velocity near the surface is small and the particle diameter is also small.
10. Thermal gradients within the particle are negligible.

The above assumptions are similar to those made by Ziegler et al.(1964 b) in deriving a particle-surface heat transfer model in dense beds. In this study, the focus will be on the particle-surface interactions in the lean phase of a freeboard region.

Based on the previous assumptions, the differential equation and initial condition for describing the heat absorbed by the particle when it is adjacent to or slipping

over the surface, may be written as (cf. Figure 8.1):

$$\rho_s C_s[(\pi/6)d_p^3]\frac{dT}{dt} = h_c[\pi d_p^2](T_w-T) \qquad (8.1)$$

$$T = T_0 \text{ , when } t = 0 \qquad (8.2)$$

$$Nu = \frac{h_c d_p}{k_f} \approx 2 \qquad (8.3)$$

In Equation 8.1, ρ_s and C_s are apparent density and heat capacity of the particle respectively. h_c in Equation 8.3 is the convective particle-fluid heat transfer coefficient.

Time variation of the particle temperature can then be expressed as

$$\frac{T_w-T}{T_w-T_0} = \exp\left[-\frac{12k_f}{\rho_s C_s d_p^2}t\right] \qquad (8.4)$$

The instantaneous rate of heat absorption by the particle at the surface as a function of contact time is:

$$\begin{aligned} Q_p(t) &= h_c[\pi d_p^2](T_w-T) \\ &= 2\pi d_p k_f \Delta T \cdot \exp\left[-\frac{12k_f}{\rho_s C_s d_p^2}t\right] \end{aligned} \qquad (8.5)$$

where $\Delta T=(T_w-T_0)$. Average rate of heat absorption by the particle from the time of first contact (t=0) to that of detachment ($t=\theta$) can be expressed as:

$$\bar{Q}_p(\theta) = \frac{[\int_0^{\theta} Q_p(t)\,dt]}{\theta}$$

$$= \frac{2\pi d_p k_f \Delta T\{1-\exp[-\frac{12k_f}{\rho_s C_s d_p^2}\theta]\}}{\frac{12k_f}{\rho_s C_s d_p^2}\theta}$$

$$\bar{Q}_p(\theta) = \frac{[(\pi/6)d_p^3]\rho_s C_s \Delta T}{\theta}\{1-\exp[\frac{12k_f}{\rho_s C_s d_p^2}\theta]\} \qquad (8.6)$$

In case of particle size distribution, the $\bar{Q}_p$ is based on the surface mean particle size, i.e., d_p is replaced by $\bar{d}_p$.

8.1.2 Particle-Surface Heat Transfer for Particles in Suspension

To obtain the unit area heat transfer rate at the heating surface, it is necessary to estimate the maximum number of particles per unit area of heat transfer surface. As described by Ziegler et al. (1964 b), it can be assumed that the heat transfer surface is covered with k layers of particles in hexagonal packing (k may be fractional; k is assumed to be unity in Ziegler et al.'s study (1964b)). Under this assumption,

$$N_{p,max} = \frac{k}{d_p^2(\sqrt{3}/2)} \qquad (8.7)$$

As an example, $N_{p,max}$ = 14260 1/cm^2 for d_p = 90 μm and k = 1.

The product of $Q_p(\theta)$ and $N_{p,max}$ gives the maximum heat transfer rate per unit area when all particles contact at the surface for a residence time of θ. As shown in Figure 8.1, θ is approximately given by L/V_{ps} for short heating surfaces (e.g., L=0.015 m for plate orientation Types I to III in this study). For longer heating surfaces (e.g., outer-surface of vertical tubes in fluidized beds), θ may depends on several variables such as particle velocity, particle geometry, solids rigidity, turbulence, and inner geometry of the system.

To account for the effect of solids hold-up of bulk phase on the cluster-surface heat transfer rate, the chemical collision theory (Lewis, 1918; Polanyi, 1920) and Langmuir treatment of surface adsorption of reacting molecules on the catalyst surface are applied. Consider the interaction of a group of moving particles and its neighboring surface as illustrated in Figure 8.2. The attachment and detachment of particles to and from the immersed surface can be expressed by the following reversible equationn:

$$(n-n_s) + N_{p,max}\frac{S}{V}(1-\sigma) \rightleftharpoons n_s \qquad (8.8)$$

where n : total number of particles per unit volume,

n_s : number of attached particles per unit volume,

$n-n_s$: number of particles in the bulk phase per unit volume,

$N_{p,max}$: maximum allowable number of particles on the heat transfer surface per unit surface area,

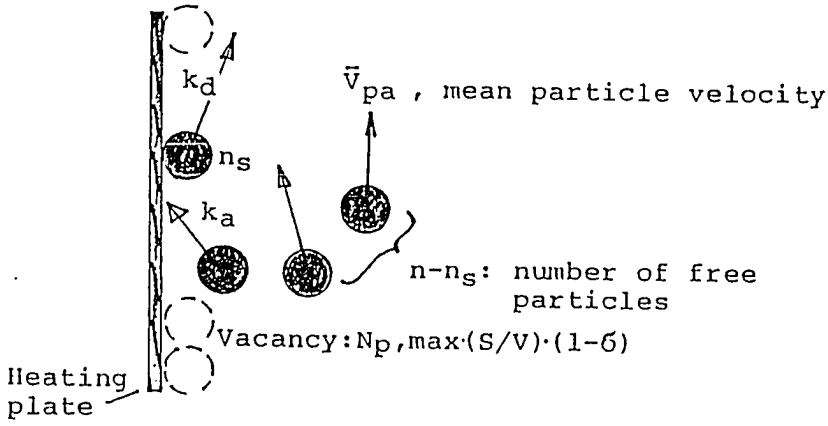

Slipping of a cluster of particles over a heating plate

Figure 8.2: Particle-surface interaction mode for particles in a cluster.

(S/V): surface area for heat transfer per unit freeboard volume,

σ : fraction of allowable site occupied,

k_a : attachment rate constant (s^{-1}),

k_d : detachment rate constant ($1/s \cdot m^3$).

By assuming that the attachment and detachment of particles are in dynamic equilibrium at any time, we have:

$$k_a(n-n_s)N_{p,max}\frac{S}{V}(1-\sigma) = k_d n_s \qquad (8.9)$$

Also,

$$n_s = N_{p,max}\frac{S}{V}\sigma \qquad (8.10)$$

and

$$n \gg n_s \qquad (8.11)$$

for most fluidized bed systems with small S/V. Combining Equations 8.9 to 8.11 yields:

$$\sigma = \frac{n}{n+\frac{k_d}{k_a}} \qquad (8.12)$$

The relation between n and C, the concentration of solids with average diameter d_p, is given by:

$$C = n[(\pi/6)\overline{d_p^3}]\rho_s \qquad (8.13)$$

Substitution of Equation 8.13 into Equation 8.12 gives:

$$\sigma = \frac{C}{C+(k_d/k_a)\,[(\pi/6)\rho_s]\bar{d}_p^3} \tag{8.14}$$

Substituting Equation 8.14 into 8.10, the number of attached particles per unit area of heat transfer surface is obtained:

$$n_s \frac{V}{S} = N_{p,max} \frac{C}{C+(k_d/k_a)\,[(\pi/6)\rho_s]\bar{d}_p^3} \tag{8.15}$$

The heat transfer coefficient contributed from solid (h_s) can be expressed as:

$$h_s = \frac{\bar{Q}_p(\theta)\,[n_s \frac{V}{S}]}{\Delta T} \tag{8.16}$$

Substitutions of Equations 8.15, 8.7 and Equation 8.6 into Equation 8.16, a mechanistic model for surface-to-suspension heat transfer in the freeboard is obtained:

$$h_s = \frac{[(\pi/6)\bar{d}_p^3]\rho_s C_s}{\theta}\{1-\exp[-\frac{12k_f}{\rho_s C_s \bar{d}_p^2}\theta]\}\frac{k}{\bar{d}_p^2(\sqrt{3}/2)}\frac{C}{\{C+(k_d/k_a)\,[(\pi/6)\rho_s]\bar{d}_p^3\}} \tag{8.17}$$

In the above equation, the first group accounts for the effect of thermal flux over the surface, the second group for the effect of degree of thermal equilibrium when the solids slip over the surface, and the last group for the effects of solids concentration and particle size.

Equation (8.17) can be simplified as:

$$h_s = \frac{\bar{d}_p \rho_s C_s}{\theta}\{1-\exp[-\frac{12k_f}{\rho_s C_s \bar{d}_p^2}\theta]\}\frac{KC}{C+K_s\rho_s\bar{d}_p^3} \qquad (8.18)$$

by substituting $K = k(\pi/6)/(3^{1/2}/2)$, where k has been defined in Equation 8.7 as the number of layers of particles on the heat transfer surface, and $K_s = (k_d/k_s)(\pi/6)$ into Equation 8.17. Rearranging, we have:

$$\frac{\frac{(\bar{d}_p/2)\rho_s C_s}{\theta}\{1-\exp[-\frac{12k_f}{\rho_s C_s \bar{d}_p^2}\theta]\}}{h_s} = \frac{C+K_s\rho_s\bar{d}_p^3}{2KC} \qquad (8.19)$$

If Y is defined as:

$$Y = \frac{\frac{(\bar{d}_p/2)\rho_s C_s}{\theta}\{1-\exp[-\frac{12k_f}{\rho_s C_s \bar{d}_p^2}\theta]\}}{h_s}$$

then:

$$Y = \frac{1}{2K} + \frac{K_s\rho_s}{2K}(2\times10^{-5})^3 \cdot \{\frac{[(\bar{d}_p/2)\times10^5]^3}{C}\} \qquad (8.20)$$
$$= \frac{1}{2K} + \frac{K_s\rho_s}{2K}(2\times10^{-5})^3 \cdot X$$

where $X=[(d_p/2)x10^5]^3/C$. In Equation 8.20, Y is dimensionless, and X has the unit of m^6/kg.

According to Equation 8.20 a plot of experimentally obtainable parameters Y versus X should give a straight line with the intercept of (1/2K) and the slope of $(K_s \cdot \rho_s/2K) \cdot (2x10^{-5})^3$.

8.2 Test of the Heat Transfer Model

Steps for test of the model are listed as follows:

1. From the experimental data C, $\bar{d}_p$, h_s and the estimated θ, the parameters X and Y can be calculated (Equation 8.20).

   θ can be estimated by referring to Figure 8.1 and data from Tables A.3.1 and A.3.2 (Appendix 4):

   $$\theta \text{ (plate orientation type I, II, III)} = \frac{L}{\bar{V}_{pa}} \qquad (8.21)$$

   $$\theta \text{ (plate orientation type IV)} = \frac{[(L+W)/2]}{\bar{V}_{pu}} \qquad (8.22)$$

   where L and W are length and width of the heating plate respectively (in this study, L=0.015 m, W=0.030 m). $\bar{V}_{pa}$ is the average particle velocity over the vertical plate. $\bar{V}_{pu}$ is the average upward particle velocity. $\bar{V}_{pa}$ and $\bar{V}_{pu}$ can be calculated from Equation 6.15 and Equation 6.13 respectively.

   Other parameters necessary for the calculation of X and Y are ρ_s=1554 kg/m^3, C_s = 774 J/kg·K, and k_f (air at 25 °C) = 0.0265 W/m·K.

2. Plot Y versus X. The model predicts that this plot should yield a straight line (Equation 8.20).

3. If the model is valid, the parameters K and K_s can be obtained from the slope and intercept of the above Y vs. X plot. Substituting known values of K, K_s, C, $\bar{d}_p$, θ, ρ_s, C_s, and k_f into Equation 8.18, the

surface-cluster heat transfer coefficient, h_s, can be calculated.

4. Compare the calculated h_s with the experimental one for each U_0 and H.

Table 8.1 lists the calculated Y (Y1, Y2, Y3, Y4 for plate orientation Types I, II, III, and IV, respectively) and X in this study. Plots of Y vs. X are shown in Figures 8.3 (a)-(d) for the four plate types. As predicted from the model, all the plots yield straight lines, which is a good indication of the validity of the model. Linear regression formula of the straight lines shown in Figure 8.3 and the calculated K, K_s, and k values are listed in Table 8.1.

Table 8.1. Regression formula of the straight lines shown in Fig. 8.3 and the calculated K, k, K_s values

Plate	Formula	K	$K_s, 10^{10}$ m^{-3}	k
I	Y1 = 6.087 + 0.0824 X	0.0821	0.109	0.136
II	Y2 = 5.290 + 0.1112 X	0.0945	0.169	0.156
III	Y3 = 5.404 + 0.0663 X	0.0925	0.099	0.153
IV	Y4 = 6.790 + 0.0714 X	0.0736	0.085	0.122

$K = k(\pi/6)/(3^{1/2}/2)$; $K_s=(k_d/k_a)(\pi/6)$; k: number of layers of particles (see Equation 8.7)

Data of calculated and experimental h_s are shown in Table A.3.4 of Appendix 3. Comparison between calculated and experimental h_s are shown in Figures 8.4 - 8.7 for h_s versus H, and Figure 8.8 for h_s versus U_0.

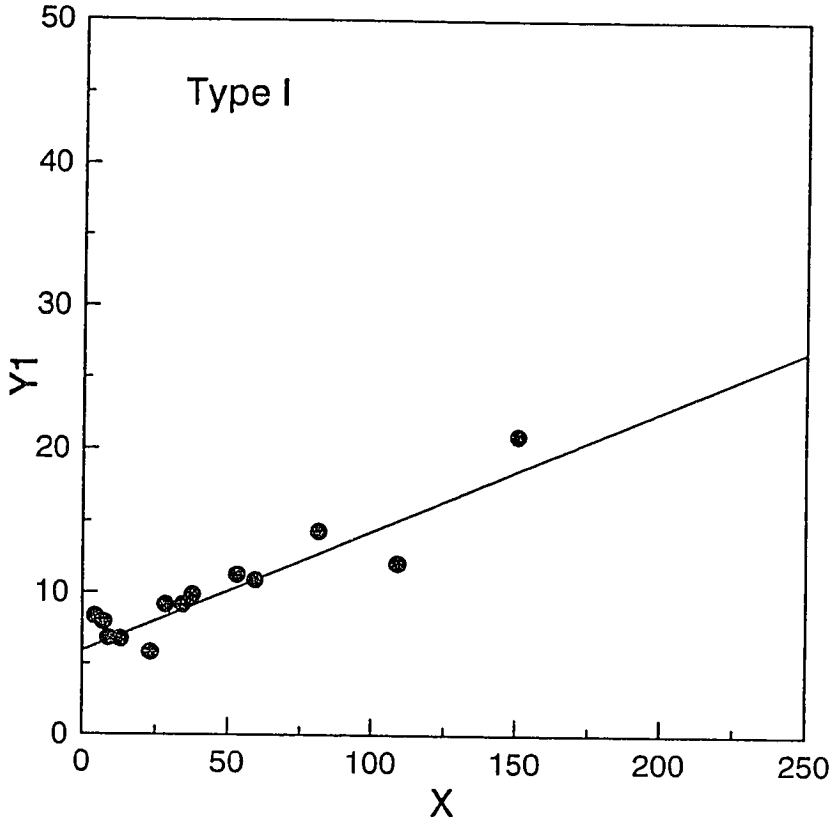

Figure 8.3a: Plot of Y1 vs. X (see Equation 8.20) for Plate Type I.

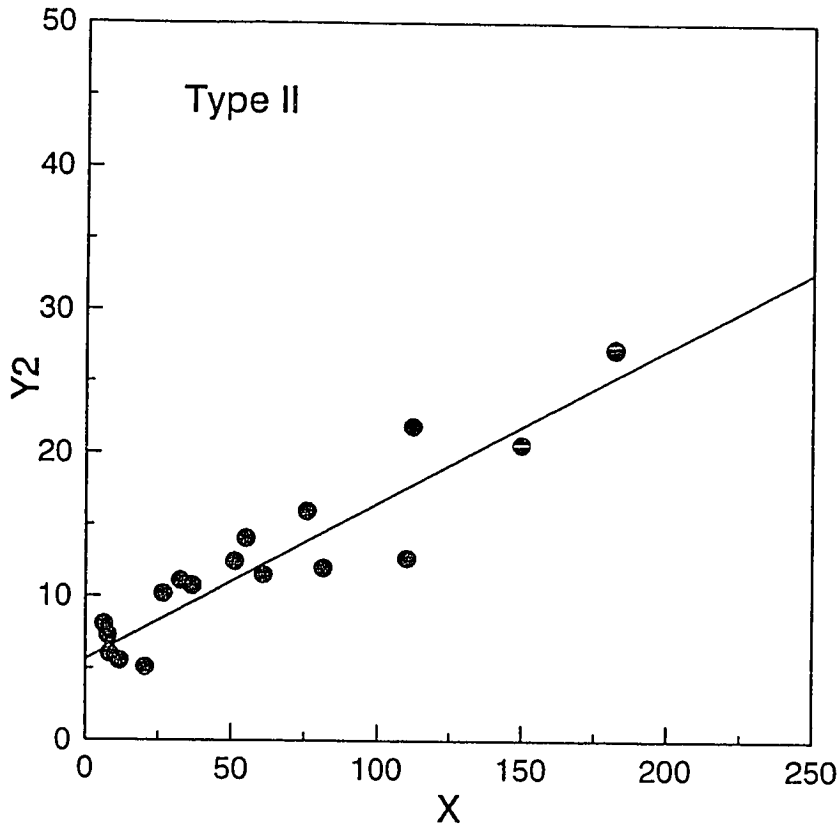

Figure 8.3b: Plot of Y2 vs. X (see Equation 8.20) for Plate Type II.

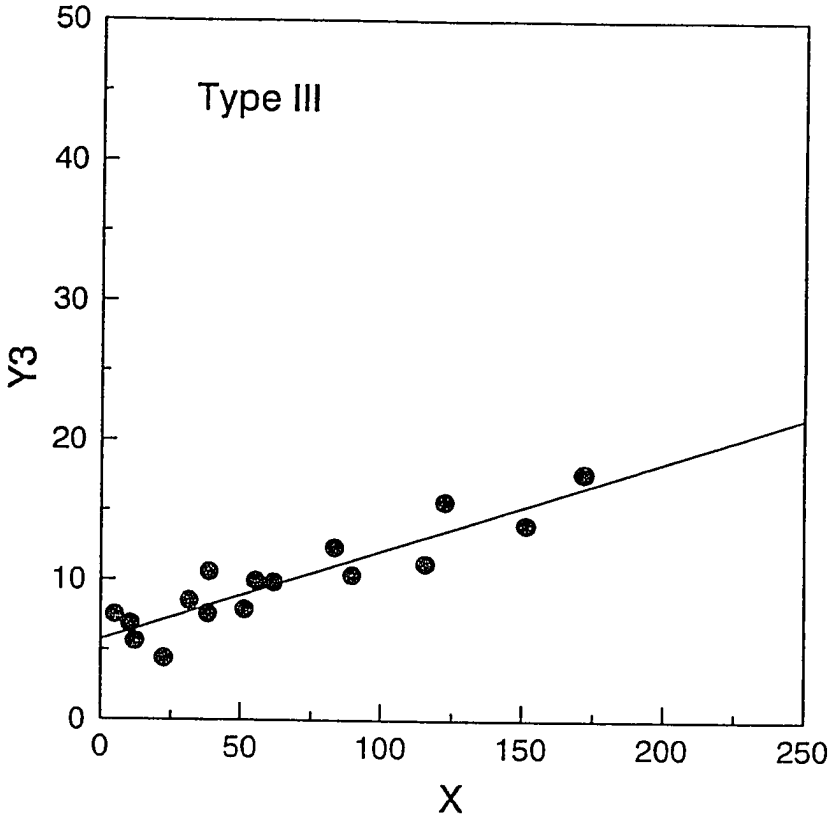

Figure 8.3c: Plot of Y3 vs. X (see Equation 8.20) for Plate Type III.

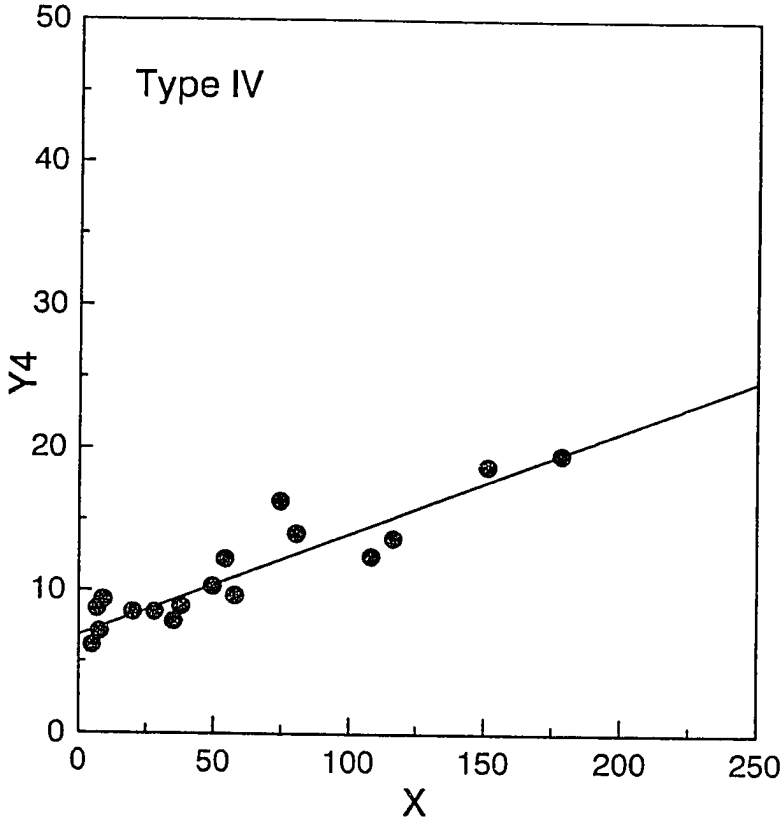

Figure 8.3d: Plot of Y4 vs. X (see Equation 8.20) for Plate Type IV.

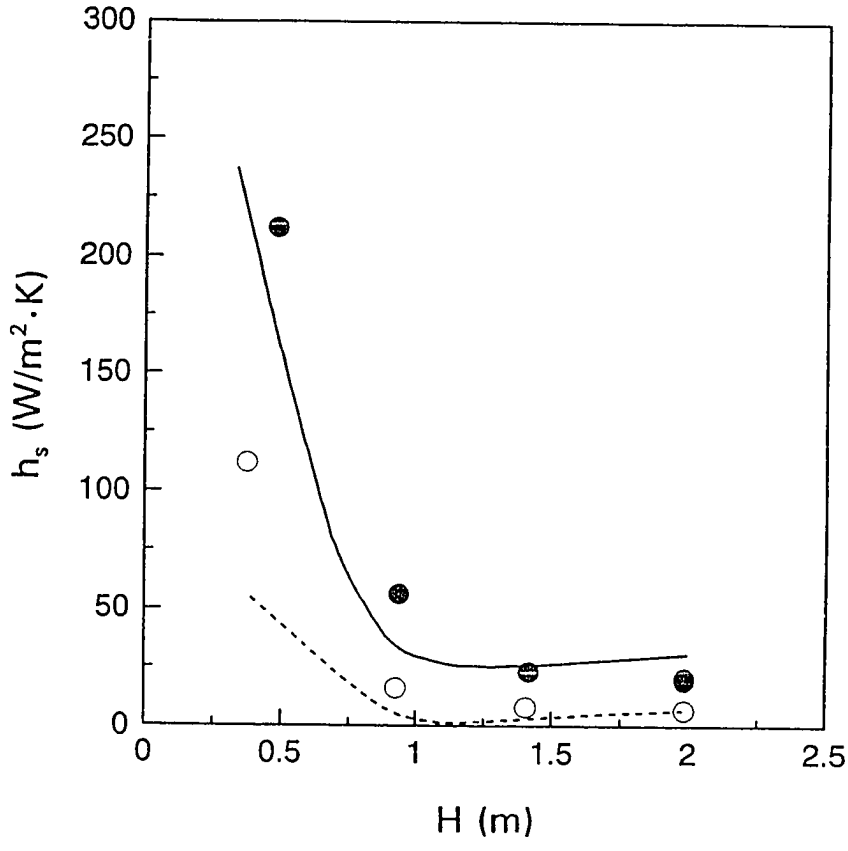

Figure 8.4a Comparison between experimental and calculated particle convective heat transfer coefficients
Plate type I
U_0= 0.46 m/s: (•) experimental, (---) calculated
U_0= 0.34 m/s: (○) experimental, (---) calculated

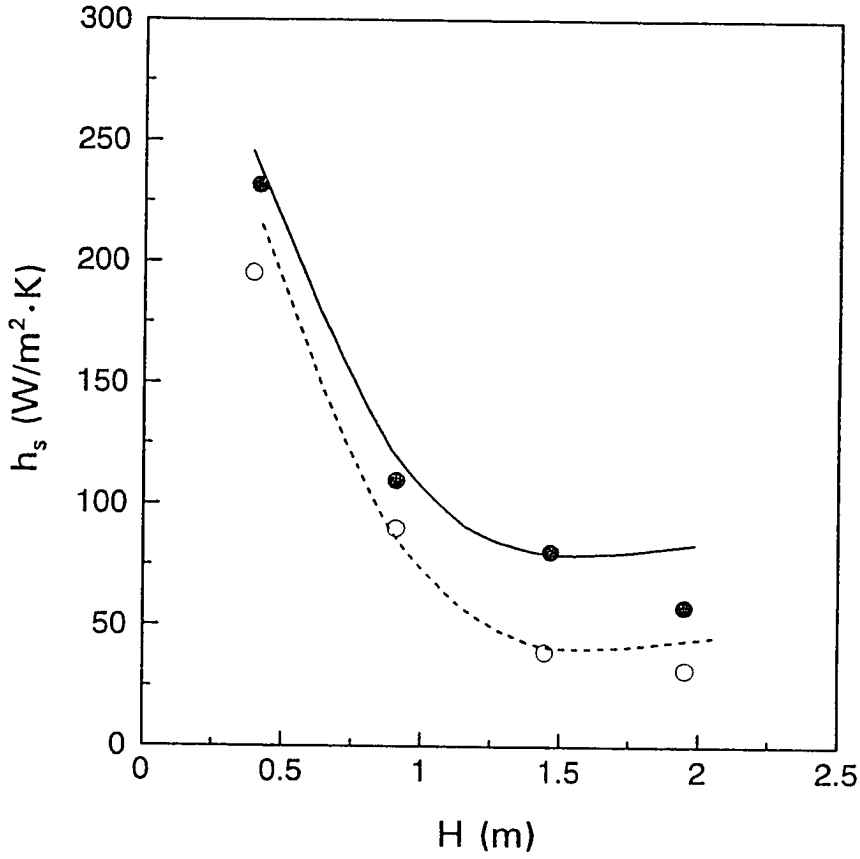

Figure 8.4b Comparison between experimental and calculated particle convective heat transfer coefficients
Plate type I
U_0= 0.64 m/s: (•) experimental, (---) calculated
U_0= 0.52 m/s: (○) experimental, (---) calculated

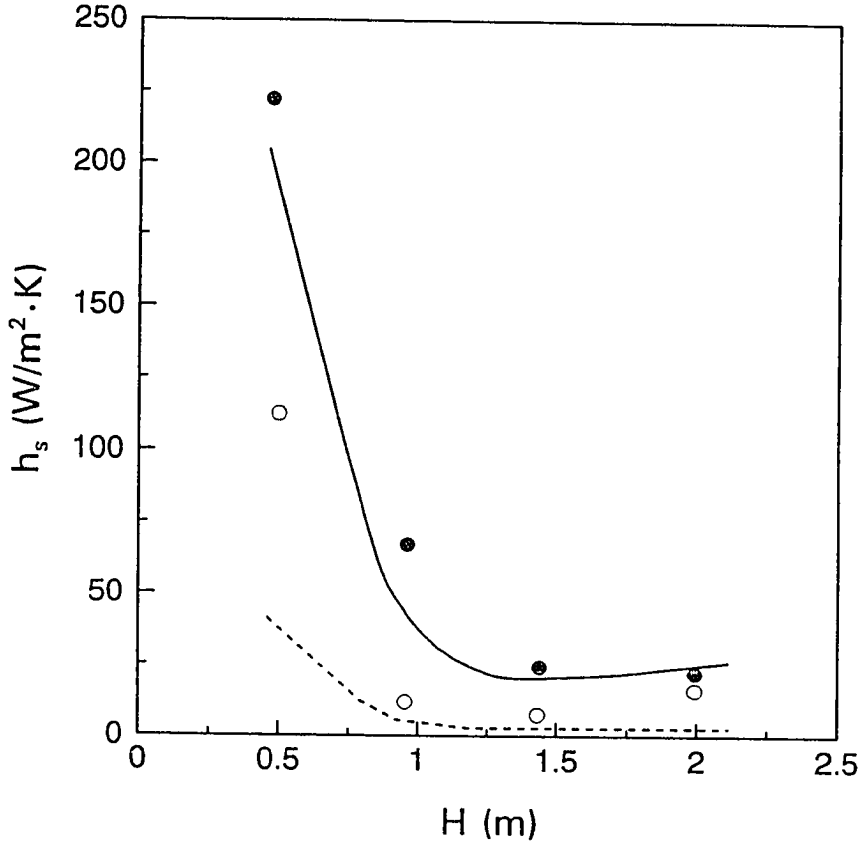

Figure 8.5a Comparison between experimental and calculated particle convective heat transfer coefficients
Plate type II
U_0= 0.46 m/s: (•) experimental, (---) calculated
U_0= 0.34 m/s: (○) experimental, (---) calculated

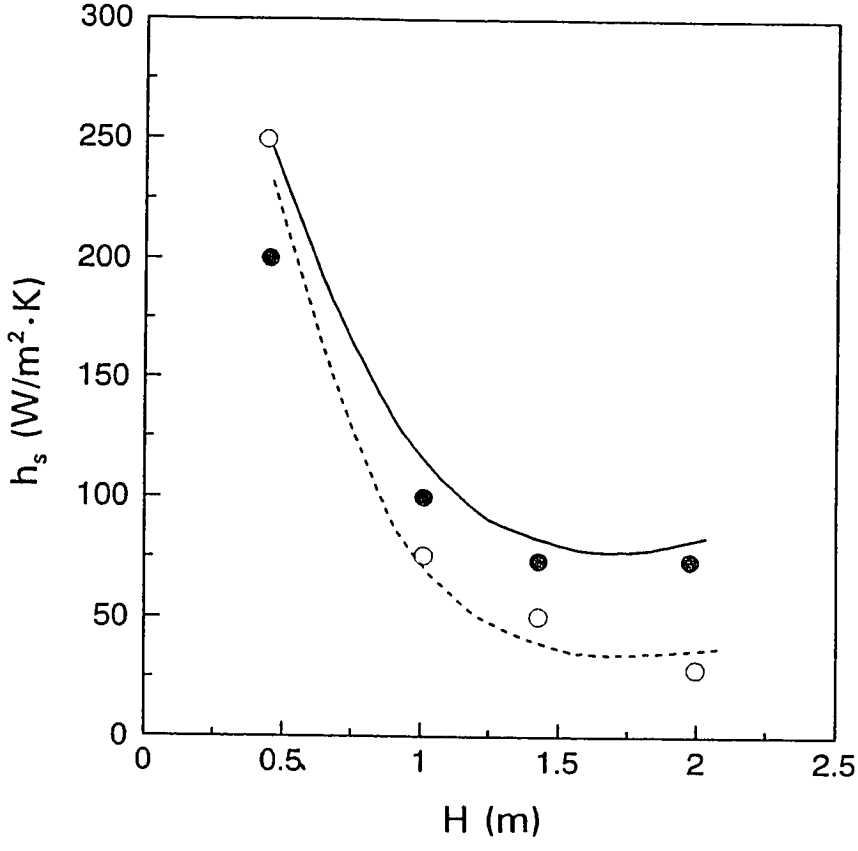

Figure 8.5b Comparison between experimental and calculated particle convective heat transfer coefficients
Plate type II
U_0= 0.64 m/s: (•) experimental, (---) calculated
U_0= 0.52 m/s: (○) experimental, (---) calculated

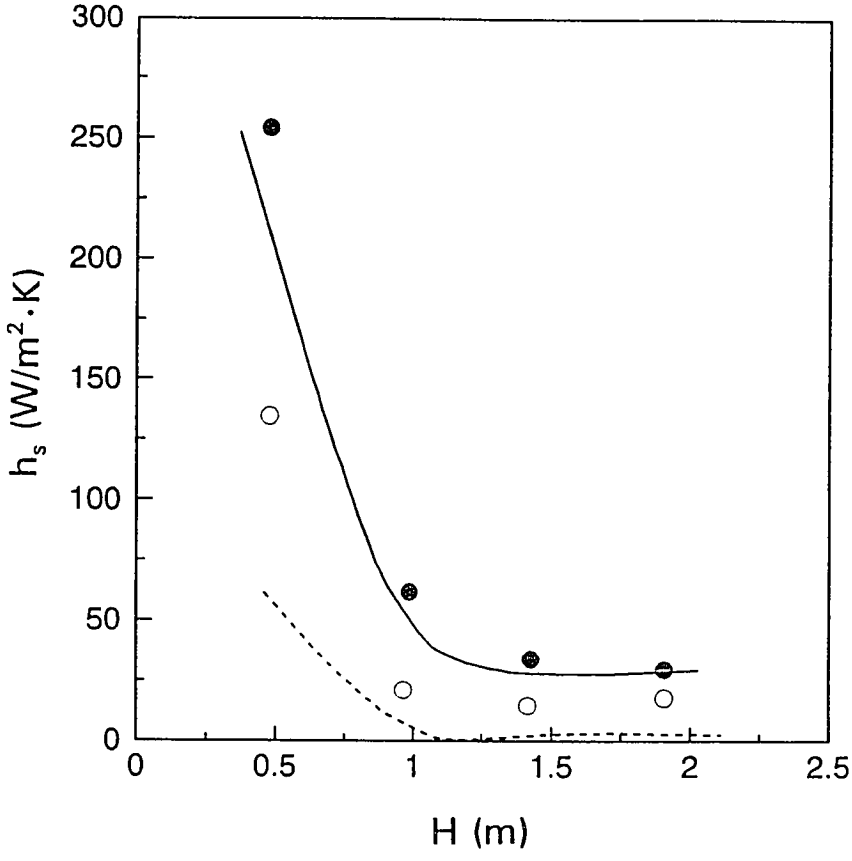

Figure 8.6a Comparison between experimental and calculated particle convective heat transfer coefficients
Plate type III
U_0= 0.46 m/s: (•) experimental, (---) calculated
U_0= 0.34 m/s: (○) experimental, (---) calculated

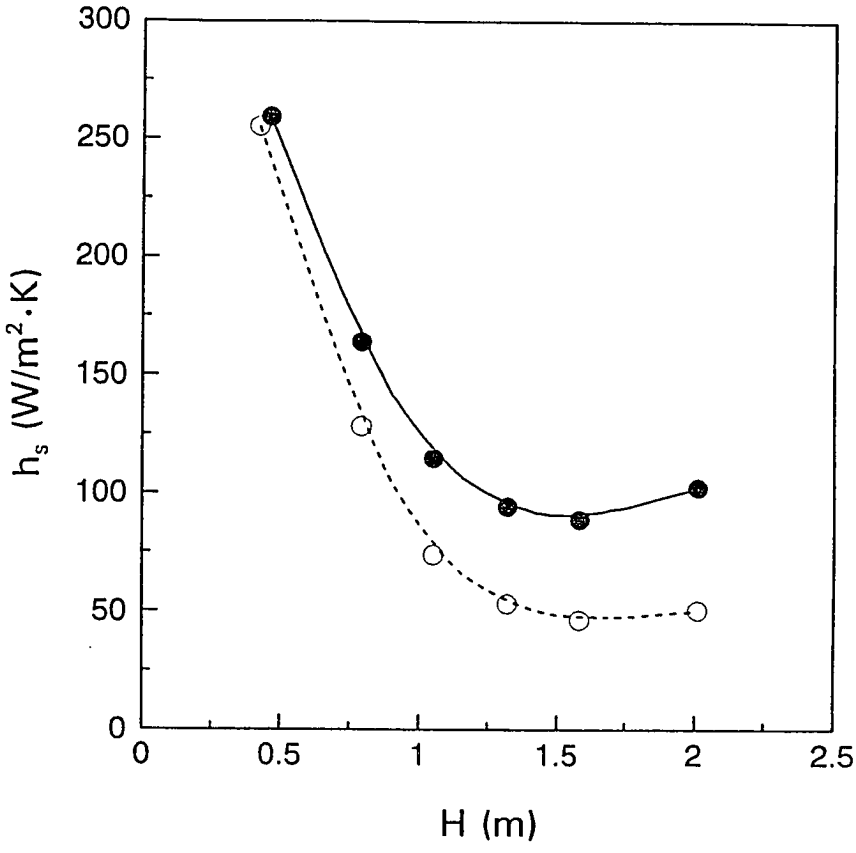

Figure 8.6b Comparison between experimental and calculated particle convective heat transfer coefficients
Plate type III
U_0= 0.64 m/s: (•) experimental, (---) calculated
U_0= 0.52 m/s: (○) experimental, (---) calculated

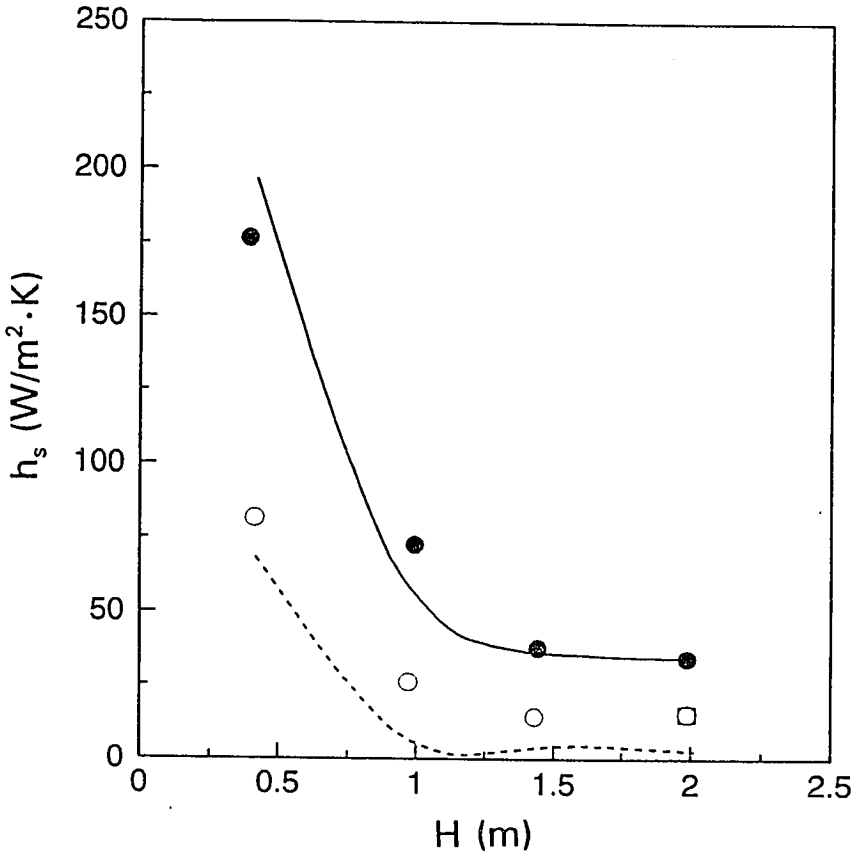

Figure 8.7a Comparison between experimental and calculated particle convective heat transfer coefficients
Plate type IV
U_0= 0.46 m/s: (•) experimental, (---) calculated
U_0= 0.34 m/s: (○) experimental, (---) calculated

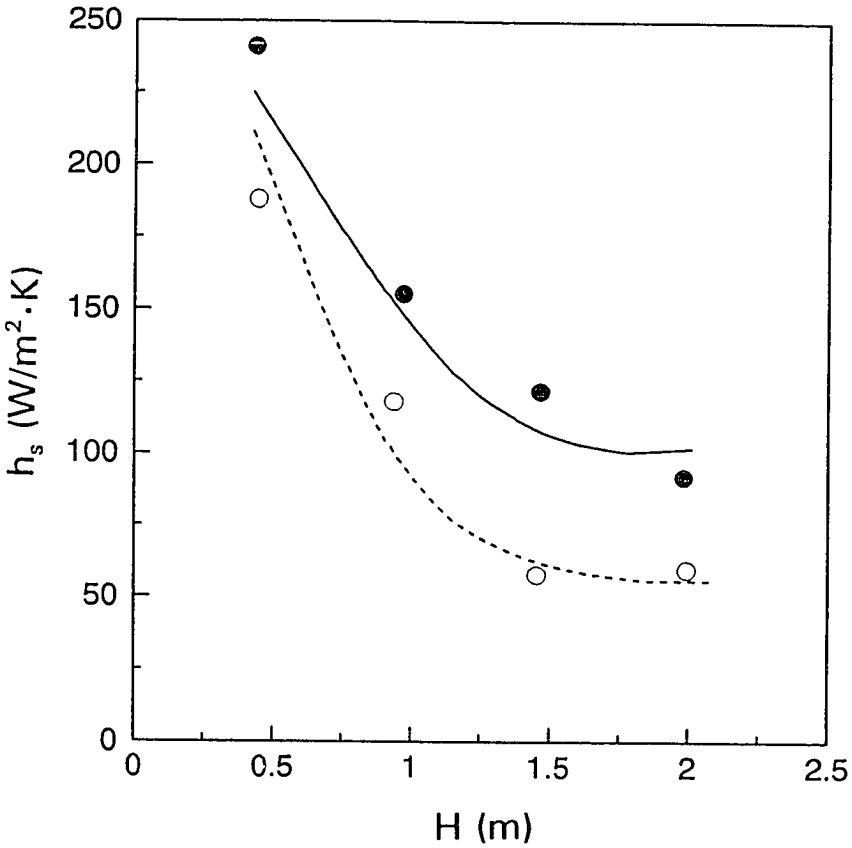

Figure 8.7b Comparison between experimental and calculated particle convective heat transfer coefficients
Plate type IV
U_0= 0.64 m/s: (•) experimental, (---) calculated
U_0= 0.52 m/s: (○) experimental, (---) calculated

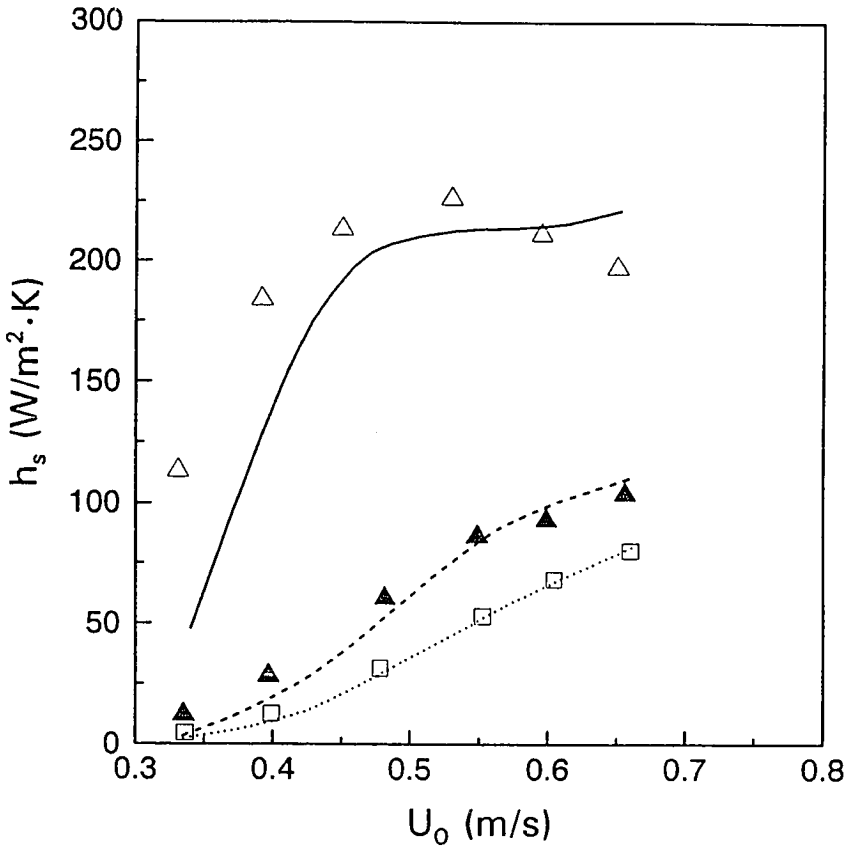

Figure 8.8a Comparison between experimental and calculated particle convective heat transfer coefficients
Plate type I.
Experimental: (△): H= 0.45 m, (▲): H= 0.95 m
(□): H= 1.45 m
Calculated: lines.

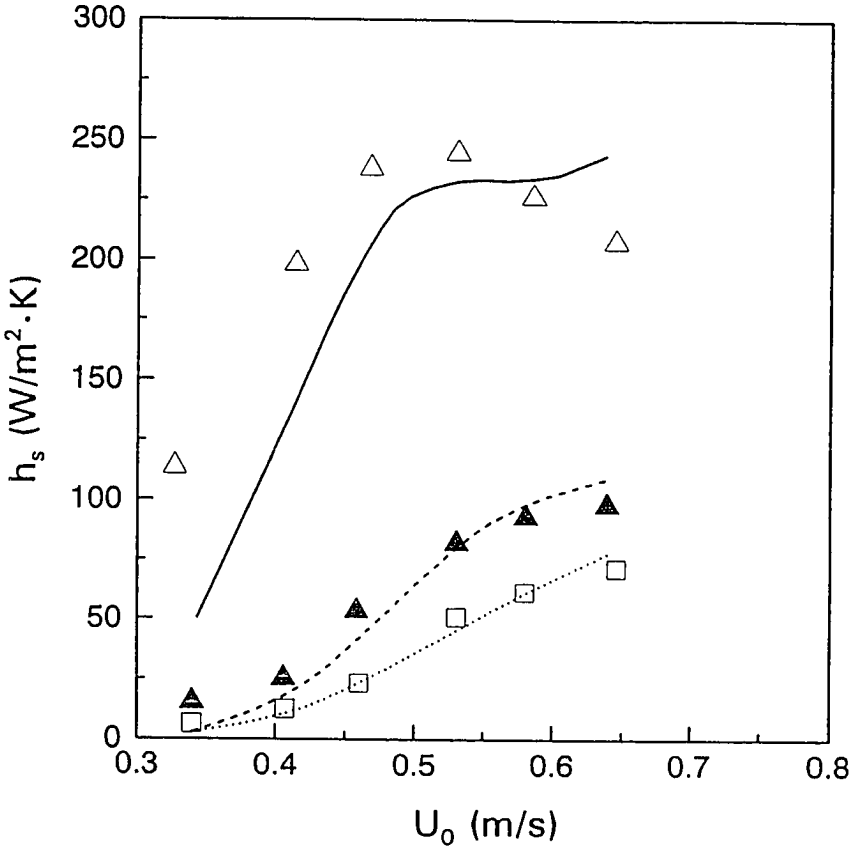

Figure 8.8b Comparison between experimental and calculated particle convective heat transfer coefficients Plate type II.
Experimental: (△): H= 0.45 m, (▲): H= 0.95 m
(□): H= 1.45 m
Calculated: lines.

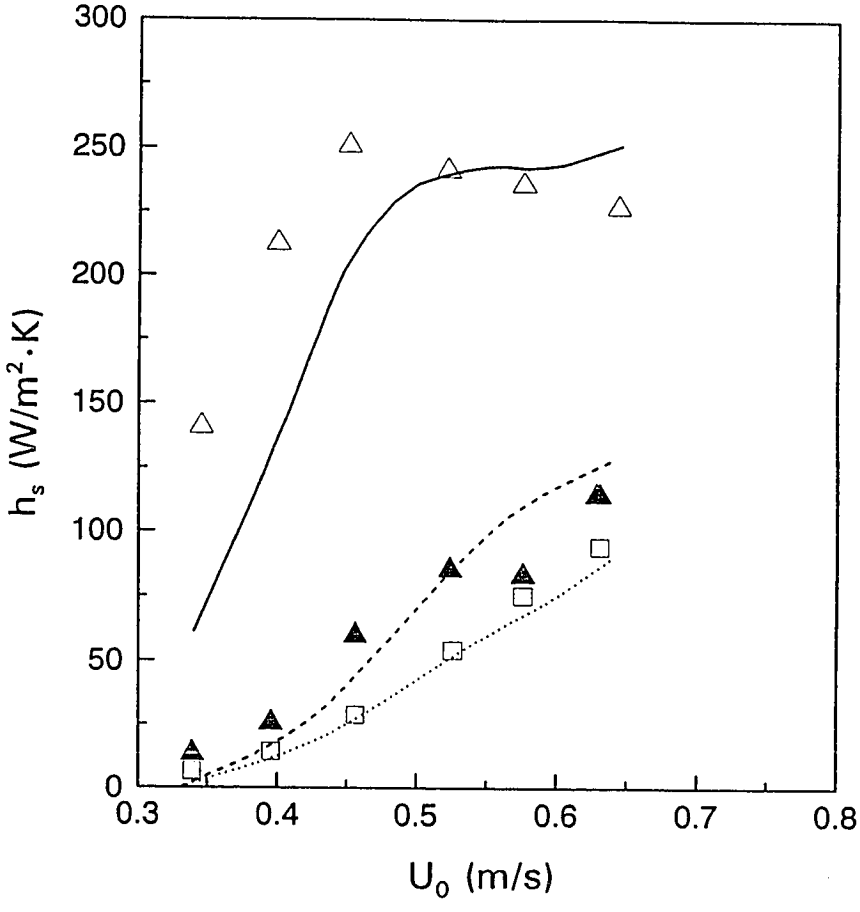

Figure 8.8c Comparison between experimental and calculated particle convective heat transfer coefficients Plate type III.
Experimental: (△): H= 0.45 m, (▲): H= 0.95 m
(□): H= 1.45 m
Calculated: lines.

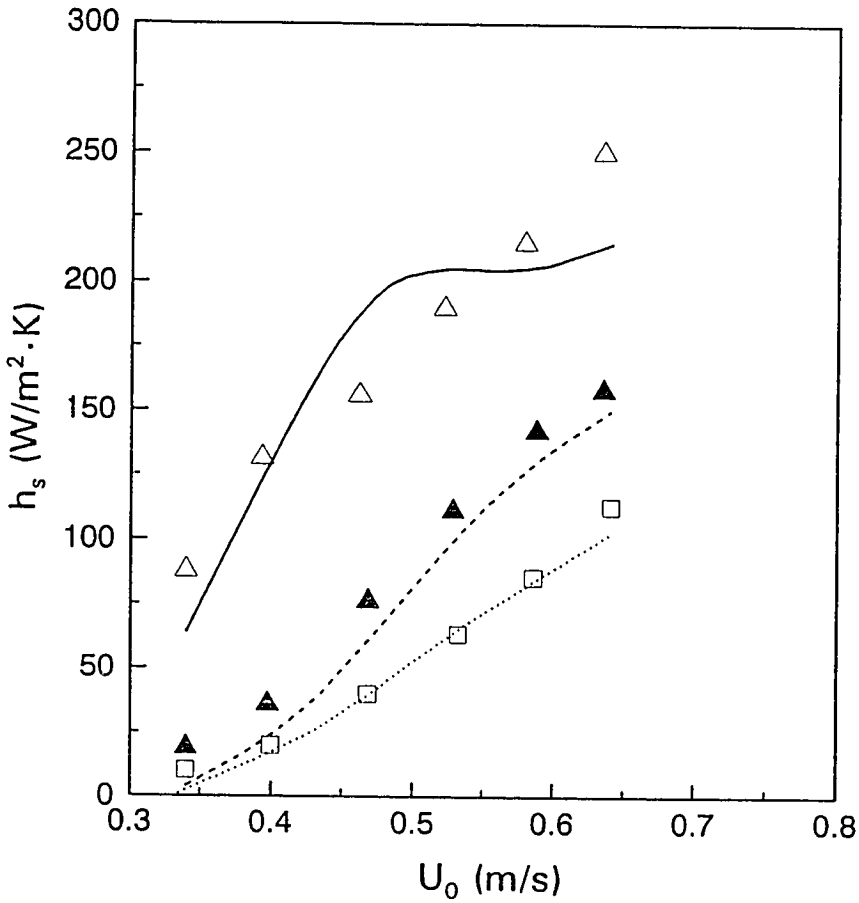

Figure 8.8d Comparison between experimental and calculated particle convective heat transfer coefficients Plate type IV.
Experimental: (△): H= 0.45 m, (▲): H= 0.95 m
(□): H= 1.45 m
Calculated: lines.

Calculated results from model match the experimental data quite well for U_0= 0.46-0.64 m/s and H= 0.45-1.98 m. Relative deviations of experimental and calculated values are within ±15% as shown in Figure 8.9.

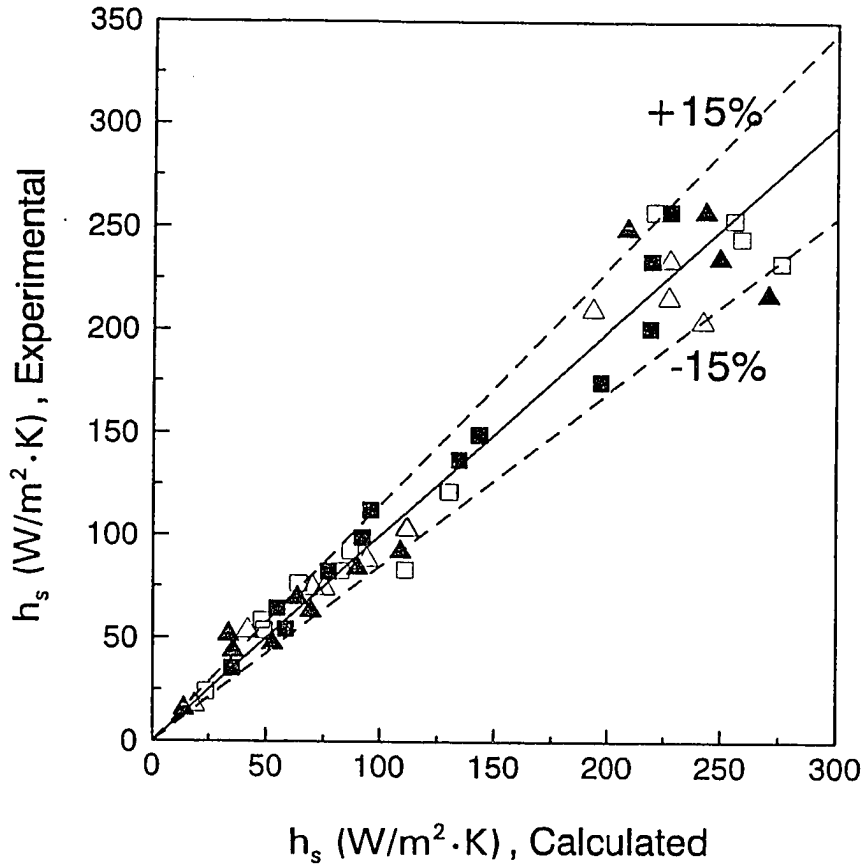

Figire 8.9 Comparison between experimental and calculated h_s for all four plate types at U_0= 0.46-0.64 m/s and H= 0.45-1.45 m.
Plate Type I(△), II(▲), III(□), IV(■).

8.3 Applications of the Heat Transfer Model

The heat transfer model (Equation 8.18) derived in Section 8.1. has been tested by predicting the result of Y versus X plot and by comparing the calculated and the experimental data for h_s. From the above discussion (Section 8.2), the model is considered to be applicable in the freeboard region at least for particle properties and operating conditions for the present study as shown in Table 8.2.

Table 8.2 Particle properties and operating conditions for application of the freeboard heat transfer model

d_p	(μm)	:	40 - 170
ρ_s	(kg/m^3)	:	1554[1]
C_s	(J/kg·K)	:	774
U_0	(m/s)	:	0.34 - 0.64
C	(kg/m^3)	:	0.05 - 12.5
θ	(s)	:	0.015 - 0.15[2]

(1). Al_2O_3-SiO_2
(2). Small heat transfer probe with short residence time.

For more general applications of the model, the effects of particle size (d_p), solids concentration (C), heat capacity of solid material (C_s), and solids residence time (θ) on the calculated surface-to-suspension heat transfer coefficient (h_s) are discussed.

8.3.1 Effect of Particle Size

In general, heat transfer coefficient decreases with increasing particle size both in dense phase and in dilute phase such as the raiser of a circulating fluidized bed (Mickley and Trilling, 1949; Bak et al.,1989; Feugier et al., 1987; Kobro and Brereton, 1986; Subbarao and Basu, 1986).

As shown in Figure 8.10, h_s calculated from the present model (Equation 8.17) increases with increasing particle size for d_p < 40-100 μm, and decreases with increasing particle size for d_p > 40-120 μm. This result is similar to those calculated from the kinetic theory (Martin, 1981) and from packet renewal model (Phillips, 1990) for dense beds as shown in Figure 8.11. The controlling factors of this effect are solids residence time (θ) and solids concentration (C) as shown in Figure 8.10. The decreasing tendency of h_s with increasing d_p for d_p > 100 μm is consistent with most reported experimental data cited above.

8.3.2 Effect of Solids Concentration

Experimental data (Mickley and Trilling, 1949; Kiang et al., 1976; Fraley et al., 1983; Subbarao and Basu, 1986; Feugier et al., 1987; Kobro and Brereton, 1986; Furhci et al., 1988; Wu et al., 1987) on heat transfer in dense and circulating fluidized beds with particle size in the size range of

37-451 μm have shown a dominant effect of bed density or solids concentration on the bed to wall heat transfer. Effects of solids concentration (C) and (C_s/θ) can be approximately expressed as:

$$h_s = \text{Constant} \cdot C^{\alpha} \cdot \left[\frac{C_s}{\theta}\right]^{\beta} \qquad (8.23)$$

Incorporation of the model (Equation 8.18) into Equation 8.23, the exponent α can be obtained:

$$\alpha = \frac{d\ \ln(h_s)}{d\ \ln C} = \frac{K_s \rho_s d_p^3}{C + K_s \rho_s d_p^3} \qquad (8.24)$$

The exponent α depends on C and particle size as shown above. The straight lines in Figure 8.12 exhibit that at low solids concentration ($C < 15$ kg/m^3), Equation (8.23) holds. Figure 8.13 indicates that the exponent "α" increases with d_p. This is consistent with data reported by Mickley and Trilling (1949), Feugier et al. (1987), Wu et al. (1987) as shown in Table 8.3 for comparison. From Equation 8.24, it is clear that the limiting value of α is 1, when $K_s \rho_s d_p^3 >> C$. As can be seen from Table 8.3, α from Mickley & Trilling, Wu et al. are smaller than 1. However, α values from Feugier et al.'s study are greater than 1. The reason is not clear.

Table 8.3 Effect of particle size on exponent α

Reference	d_p (μm)	α	C (kg/m^3)	h (W/m^2·K)
Mickley & Trilling (1949)	41	0.34	60-1400	290-600
	102	0.46	60-1400	140-600
	155	0.49	60-1400	100-490
	284	0.55	80-1400	70-350
	452	0.55	100-1600	60-230
Feugier et al. (1987)	95	1.05	4-40	20-200
	215	1.03	10-60	20-100
	625	1.68	20-50	5-30
Wu et al. (1987)	188	0.37	10-50	35-70
	356	0.82	15-150	25-200
Present model*	90	0.96	0.05	
		0.57	1	
		0.12	10	
	200	0.94	1	
		0.59	10	
	400	0.99	1	
		0.92	10	

* α calculated from Equation 8.24 with $K_s = 0.116 \times 10^{10}$ m^{-3} (average value of Types I-IV, see Table 8.1), $\rho_s = 1554$ kg/m^3

8.3.3 Effects of Solid Heat Capacity And Residence Time

Figure 8.14 gives an example for the effect of C_s/θ on the cluster-surface heat transfer coefficient calculated from the model. The results follow the relationship of h_s and C_s/θ as indicated in Equation 8.23.

Variation of the exponent β (Equation 8.21) with d_p is shown in Figure 8.15. As can be seen from Equation 8.17, β depends only on d_p for solids of known particle density in an air current. Ziegler et al. (1964) measured heat transfer coefficients from a sphere and a cylinder to a gas-fluidized bed of solids of the same density, but with different heat capacity. The heat transfer coefficient was found to increase with solid heat capacity in a fashion similar to Equation 8.23. The exponent β is 0.5 for solids with d_p= 136 μm, this coincides with that calculated from the present model as shown in Figure 8.10. Figure 8.10 also shows that h_s increases with decreasing θ.

The residence time (θ) for a cluster sliding over the surface of a heat transfer probe is approximately proportional to the heater length (L). Data of Wen and Jakob (1951) and Van Heerden et al. (1953) indicate that an exponent of -0.65 for L as cited by Mickley and Fairbanks (1955). This is equivalent to a value of 0.65 for β. Wu et al. (1987) reported a range of exponent of -0.27 to -0.57 for L from heat

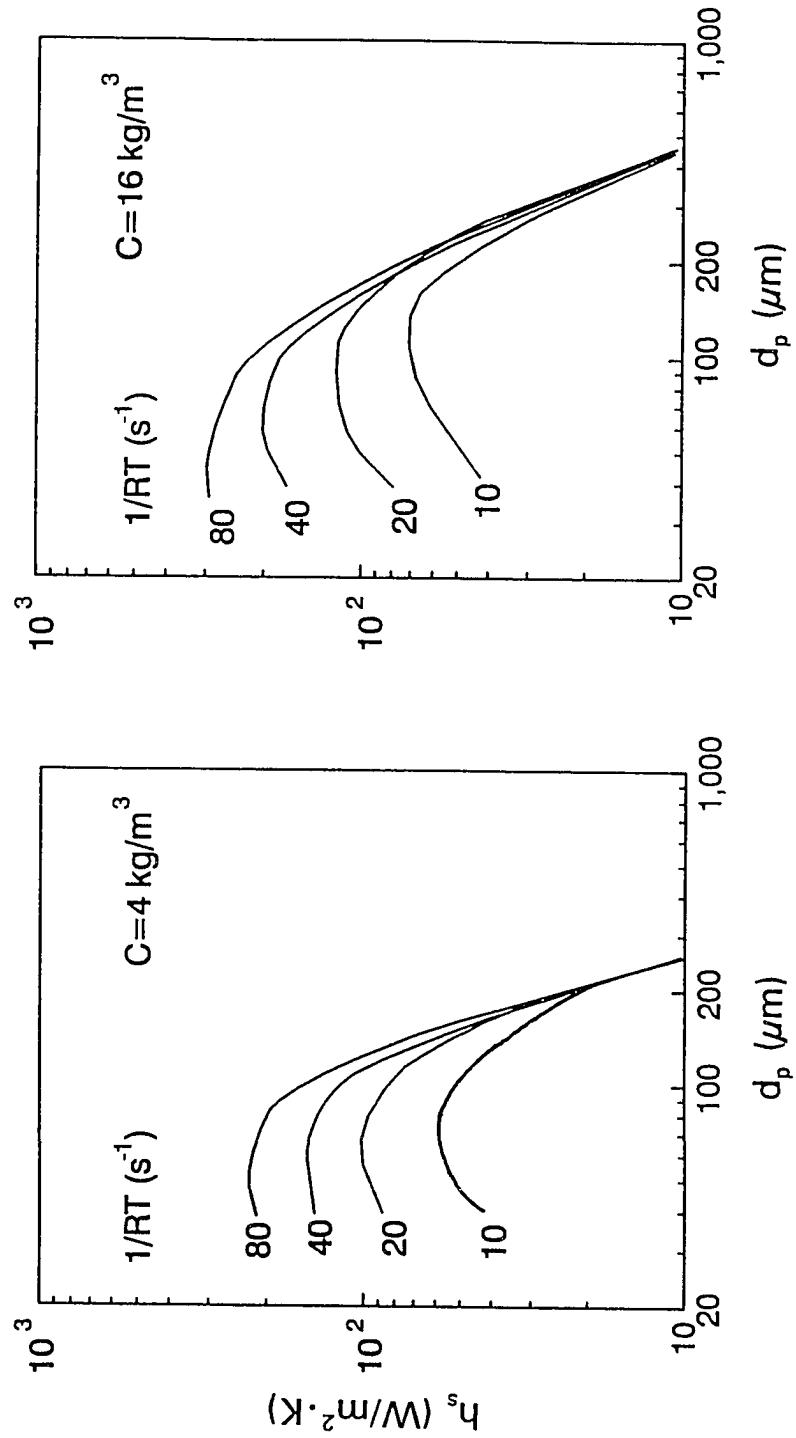

Figure 8.10 Variation of h_s with particle size (d_p). Data calculated from Model (Equation 8.18; $1/RT=1/\theta$, K_s= 0.109 x 10^{10} 1/m^3, C_s = 774 J/kg, ρ_s = 1554 kg/m^3, k_f = 0.0265 W/m·K).

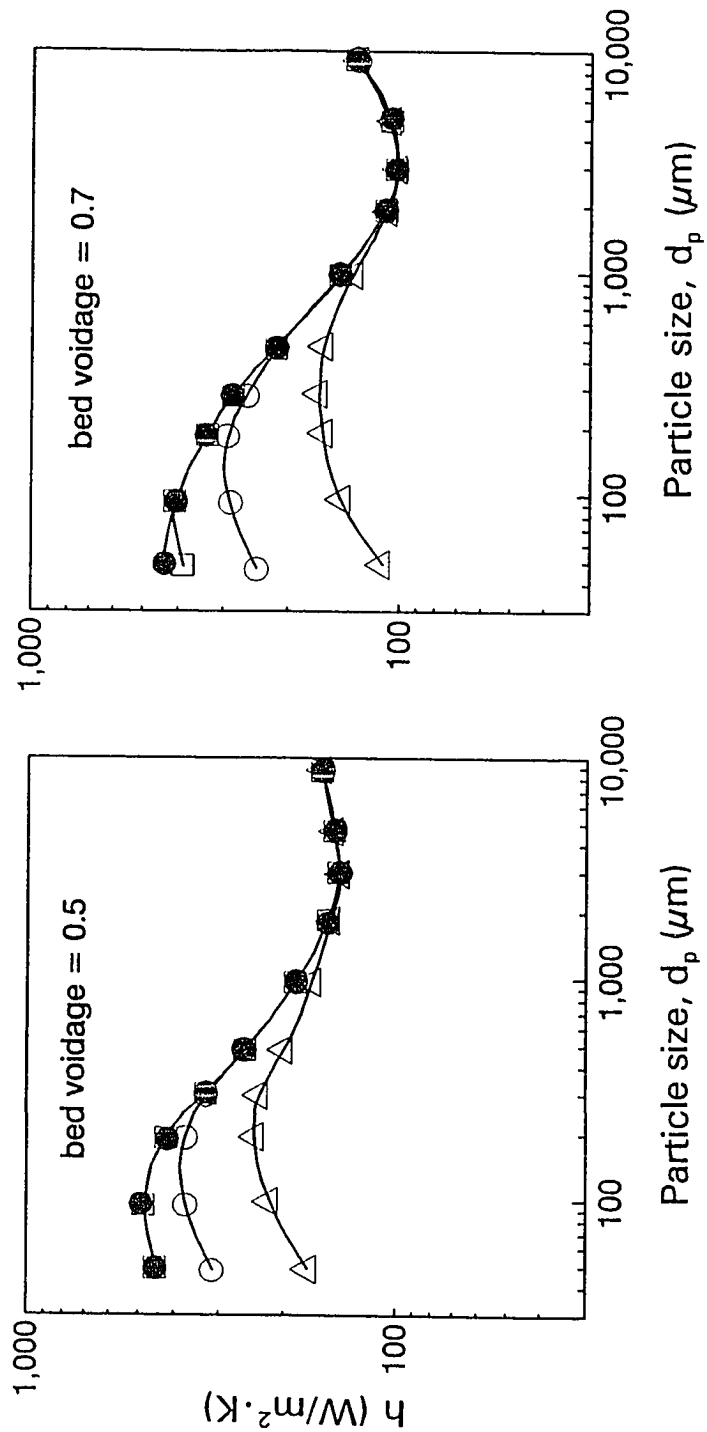

Figure 8.11 Variation of h_s with particle size (d_p) in dense beds (from Phillips, 1990).
Kinetic Theory (Martin, 1981): (•);
Packet Renewal Model (Phillips, 1990): 1/RT (1/s)= 75(□), 15(○), 3(△)

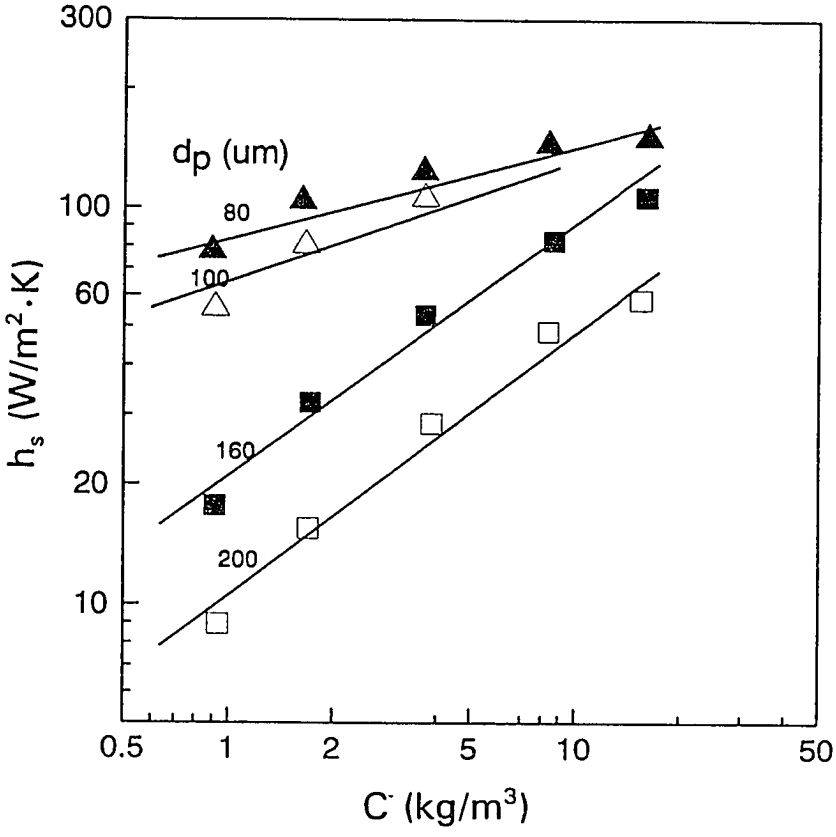

Figure 8.15: Variation of exponent β (in $h_s \propto [C_s/RT]^{\beta}$) with particle size ($d_p$). Data taken from slopes of straight lines shown in Figure 8.14.

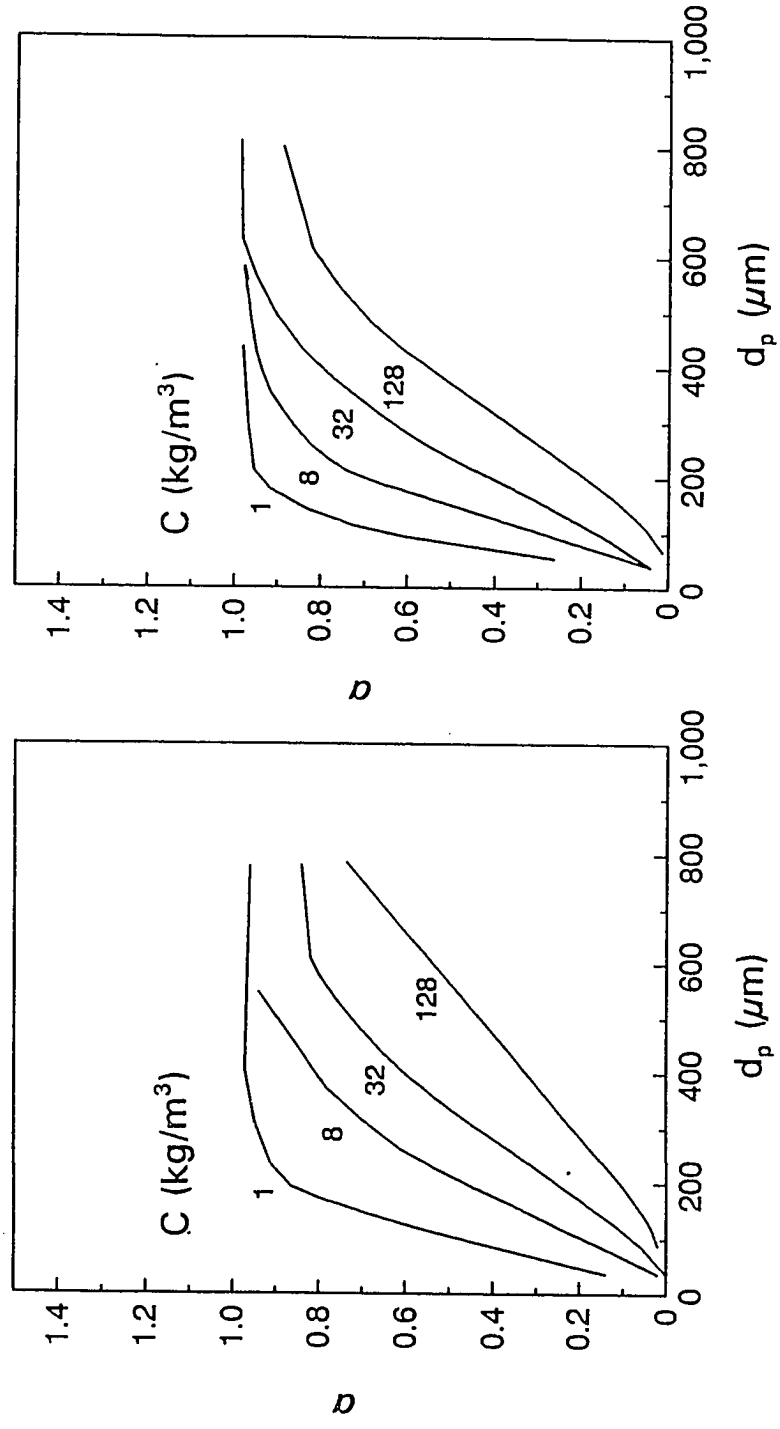

Figure 8.13: Variation of exponent α (in $h_s \propto C^{\alpha}$) with particle size (d_p). Data calculated from Equation 8.4.

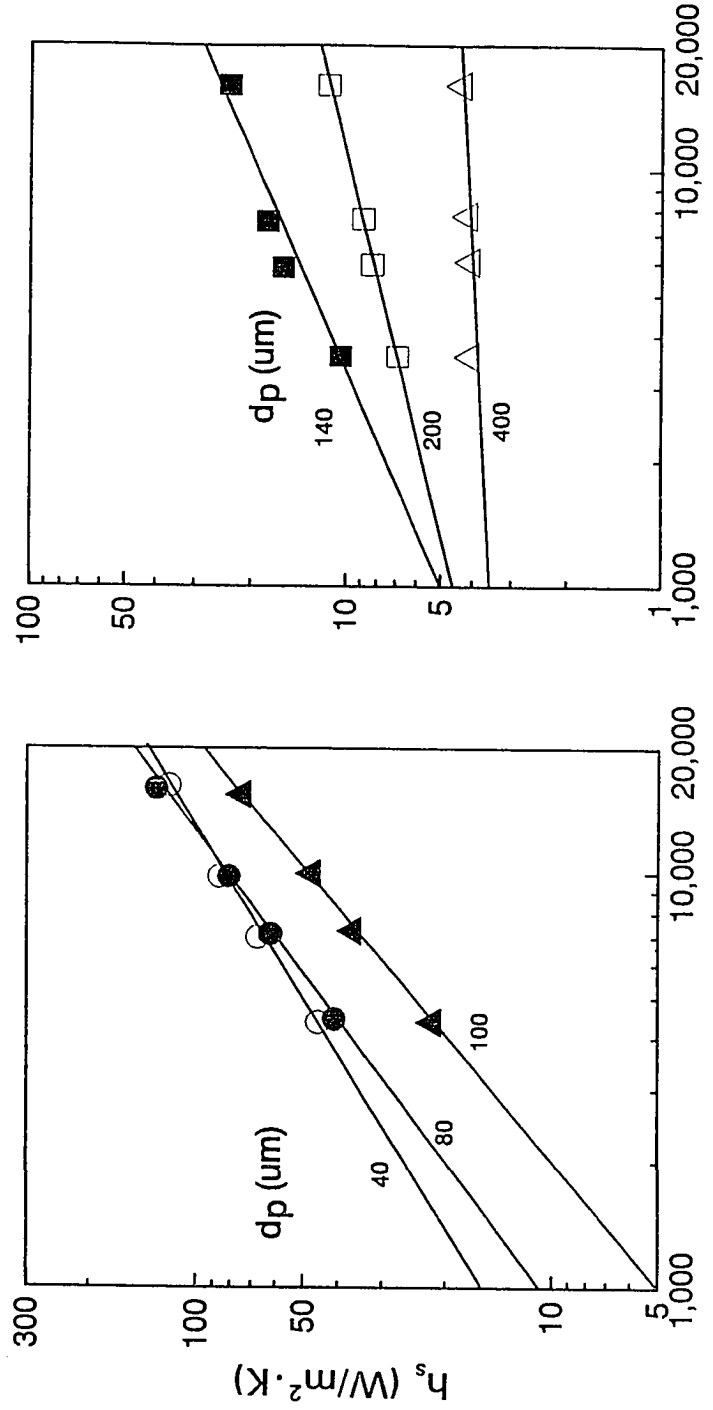

Figure 8.14: Variation of h_s with C_s/RT. Data calculated from the model (Equation 8.18) with $\theta=RT$, K_s= 0.109, ρ_s= 1554 kg/m^3, k= 0.0265 W/m·K, and C= 8 kg/m^3.

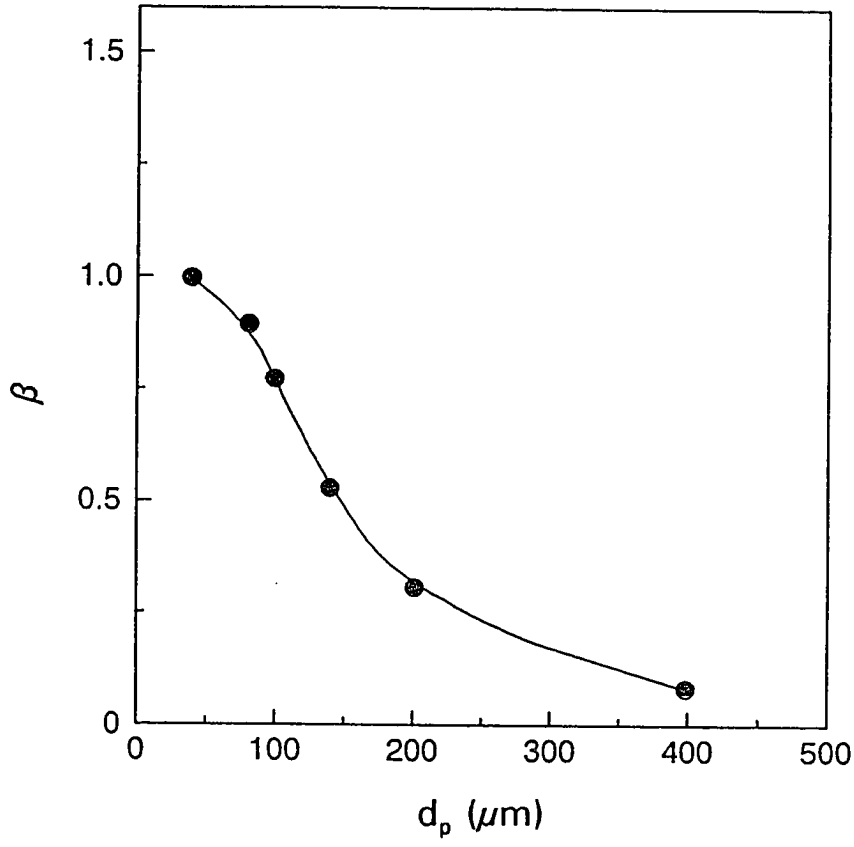

Figure 8.12 Variation of h_s with solids concentration(C). Data calculated from the model (Equation 8.18; θ= 0.05 s, K_s = 0.109 x 10^{10} 1/m^3, C_s= 774 J/kg, ρ_s= 1554 kg/m^3, k_f= 0.0265 W/m·K).

transfer rate measurement over the vertical surface in a circulating fluidized bed. This indicates that the exponent β calculated from the model is reasonable.

As can be seen from Eq. (8.17), if

$$\frac{12k_f}{\rho_s \cdot C_s \cdot d_p^2}\theta < 0.2 \qquad (8.25)$$

then,

$$1-\exp[-\frac{12k_f}{\rho_s \cdot C_s \cdot d_p^2}\theta] \approx \frac{12k_f}{\rho_s \cdot C_s \cdot d_p^2}\theta \qquad (8.26)$$

Under this condition, the model (Eq. 8.17) can be simplified as:

$$h_s \approx \frac{12k_f}{d_p} \cdot \frac{KC}{C+K_s \cdot \rho_s \cdot d_p^3} \qquad (8.27)$$

which shows that on condition that $(12\ k_f\theta)/(\rho_s \cdot C_s \cdot d_p^2) < 0.2$, h_s is independent of θ. Values of θ for the above condition to be valid are shown in Table 8.4. The results show that there is little effect of residence time (θ) on the calculated h_s for larger particles and smaller heat transfer surfaces.

Table 8.4 Maximum θ for $(12\ k_f\theta)/(\rho_s \cdot C_s \cdot d_p^2) < 0.2$

d_p (μm)	θ (s)
100	0.00756
200	0.03024
500	0.189
1000	0.756

k_f = 0.0265 W/m·K, ρ_s =1554 kg/m^3, C_s = 774 J/kg·K

Table 8.5 lists limiting values of h_s as θ approaches zero and $C >> K_s\rho_s d_p^3$. For the case of k = 1 (heat transfer surface covered completely by a single layer of particles), h_s = 2130 W/m^2·K, which is the maximum heat transfer coefficient for 90 μm particles.

Table 8.5 Limiting values of h_s ($\theta \approx 0$, $C >> K_s\rho_s d_p^3$)

Plate	k	K	h_s (W/m^2°K)	Note
I	0.136	0.0821	290	see Table 8.1
II	0.156	0.0945	334	"
III	0.153	0.0925	327	"
IV	0.122	0.0736	260	"
	1	0.603	2130	heat transfer surface covered completely by a single layer of particles

$h_s = (12k_f/d_p)\cdot K$; k_f = 0.0265 W/m·K; d_p = 90 μm.

8.3.4 Application to High Temperature Conditions and to Pipe Surfaces

The model was derived and verified under low temperature conditions and on the interaction between particle clusters and a plate surface.

For application of the model equations to high temperatures, h_f and h_r obtained from pertinent correlations (e.g., Equations 2.2 and 2.3 for h_f and Equation 2.4 for h_r) should be added to h_s calculated from the model (Equation 8.20) to get the total heat transfer coefficient ($h= h_s+h_f+h_r$, Equation 2.1).

For application of the model equations to calculate the heat transfer coefficient to a pipe in the freeboard, model parameters K and K_s should be obtained separately for tube bottom, sides, and top for horizontal tube. Surface-area weighted average parameters are then used. Time required for particles to travel a distance equal to a semi-circle of the pipe can be taken as θ for substituting into the model (Equation 8.20). Further studies are necessary to test the applicability of this model to the pipe surface.

8.4 Summary of the Heat Transfer Model

A model has been developed in this chapter for describing the mechanism of surface-to-suspension heat transfer in the lean phase such as the freeboard of a fluidized bed.

Interactions between single particles and the heat transfer surface were first considered in developing such a model. Single particles receive heat by convection from the fluid adjacent to the surface as they contact at (or slip over) the surface. Particle residence time on the heat transfer surface and the heat capacity of single particles play important roles on this type of heat transfer.

For heat transfer between particle clusters and the surface, dynamic equilibrium between the number of free particles, non-occupied surface sites, and the number of attached particles has been assumed to account for the effect of solids concentration on the cluster-surface heat transfer rate.

The model was then developed by combining the above two effects of single-particle heat absorption and particle concentration. The model is summarized as follows:

1. The model:

$$h_s = \frac{\bar{d}_p \rho_s C_s}{\theta}\{1-\exp[-\frac{12k_f}{\rho_s C_s \bar{d}_p^2}\theta]\}\frac{KC}{C+K_s\rho_s\bar{d}_p^3}$$

where h_s : particle convective suspension-surface heat transfer coefficient ($W/m^2 \cdot K$)

$\bar{d}_p$: particle diameter (m)

ρ_s : particle apparent density (kg/m^3)

C_s : heat capacity of solid particle ($J/kg \cdot K$)

θ : residence time of particles on the heat transfer

k_f : fluid thermal conductivity ($W/m \cdot K$)

K : $k(\pi/6)/(3^{1/2}/2)$, where k = layers of particles which are surrounded by fluid of $T=T_w$.

K_s : $(k_d/k_a)(\pi/6)$, where k_d/k_a = detachment-attachment equilibrium constant ($1/m^3$).

C : solids concentration (kg/m^3)

2. Model parameters: K and K_s

3. Operation variables: C and θ.

4. Applicable range : Listed in Table 8.2.

5. Parameters K and K_s can be found from the intercept and slope of Y versus X plot. Relative deviations of experimental and calculated h_s's are within ±15%. Predicted effects of $\bar{d}_p$, $\rho_s \cdot C_s$, θ, k_f and C on h_s by the model are similar to those reported in the literature.

CHAPTER 9

CONCLUSIONS

A miniature heat transfer probe has been developed in this work to measure the heat transfer coefficients in a specified location and direction in the freeboard region. Surface-to-suspension heat transfer phenomena in the freeboard of a gas fluidized bed (30 cm i.d.) of fine fluidized cracking catalyst particles (d_p = 40-170 μm) has been investigated.

Four types of plate orientations were employed to study the effects of the direction of surface on the heat transfer rate. The heat transfer coefficients and solids concentrations in radial and axial positions of the freeboard has been measured.

From the experimental data, solids dynamics, and the heat transfer model developed in the present study the following conclusions can be drawn:

(1). Surface-to-suspension heat transfer rate in the freeboard drops sharply in the splash zone (Z < 0.5-0.6 m in the present study). This drop is closely related to the sharp decreases in solids concentration and velocity. The splash zone and higher freeboard can be characterized by their individual solids flux (or concentration) decay con-

stants.

(2). In the splash zone, the downward-facing surface exhibits higher heat transfer rate than the wall- or center facing surface in the range of superficial gas velocities investigated. For all tested plate orientations, no significant variation in heat transfer rate in the column core ($r/R < 0.5$) has been observed. The maximum heat transfer rate was observed at $r/R = 0.8$ where the highest solids concentration was also observed. In the wall vicinity ($r/R \approx 0.9$), heat transfer rates are similar to those in the core region. Within the splash zone, the center-facing surface may give as high as two times the heat transfer rate of the wall-facing surface in the annular region ($r/R > 0.8$).

(3). In the freeboard region other than splash zone, significant center-to-wall solids movement at higher gas velocities causes a higher heat transfer rate for the center-facing surface in the annular region than in the core one. Except for the center-facing surface, radial variations of heat transfer coefficients are relatively unimportant in the higher freeboard region for other orientations.

(4). The results predicted from the developed model agree quite well with the experimental data. The surface-to-suspension heat transfer model derived in the present study can well explain the dependence of the measured heat transfer coefficient on solids concentration, solids heat capacity, solid particle size, and solids velocity in the freeboard. Heat transfer data for both dense and circulating fluidized beds cited from literatures can also be explained to some extent by the model.

CHAPTER 10

RECOMMENDATIONS

The present study has provided a newly designed probe for measuring surface-suspension heat transfer coefficients in lean phases of gas-solids suspension such as the freeboard of a fluidized bed and the riser or down-comer of a circulating fluidized bed. However, the probe is restricted to low-temperature ($T < 120$ °C) environments. Probes for high temperature environments such as in the fluidized bed combustors might possibly be developed for more general applications.

The present study has provided an alternative method for detecting directional effect of suspension-surface heat transfer coefficient in the freeboard. However, heat transfer from upward facing surface has not been measured in the present study due to solids accumulation on the plate surface. Characteristics of the solids accumulation effect on heat transfer are worthy of investigation.

The present study has provided the information that proper in-freeboard heat transfer surface can be located in the wall vicinity (e.g., $r/R= 0.8$) for getting a high value of heat transfer rate. However, the conclusion is restricted to the bench-scale bed and fine solid particles used in the present study. More detail studies using large-scale bed and

coarser particles could be made to elucidate this conclusion.

The present study has provided an approach for estimating solids flux and velocity in the freeboard of a fluidized bed of fine solids from measured values of solids concentration along the freeboard height. The extension of this approach to coarser particles could also be examined.

The present study has provided a clear picture of the interactions between particles and the heat transfer surface. The study has also proposed and verified a suspension-surface heat transfer model that clearly interrelated the solids convective heat transfer coefficients with the operating parameters of the bed. However, the model is restricted to beds of fine solids. In addition, radiative heat transfer contribution was not considered in the model. High-temperature beds with wider ranges of particle size could be used for further studies.

The present study has revealed that suspension-surface heat transfer rate is closely related to solids concentration in the freeboard. It seems feasible that the probe or its modifications may be used for measurement of solids concentration in lean gas-solids phases.

REFERENCES

Adibhatla, S. and M. Boggs, Dense Bed, Splash Zone, and Freeboard Heat Transfer in A Fluidized Bed Combustor, AIChE Symp. Series, No. 245, Vol. 81, 55-61, 1985.

Andeen B.R. and L.R. Glicksman, Heat Transfer to Horizontal Tubes in Shallow Fluidized Beds, ASME Paper No. 76-HT-67, ASME-AIChE Heat Transfer Conference, St. Louis, Mo., 1976.

Anderson, B. A., F. Johnson, and B. Leckner, Heat Flow Measurements in Fluidized Bed Boilers, Proc. Int. Conf. Fluidized Bed Combustors, Finland, 1987.

Bachovchin, D. M., J. M. Beer, and A. F. Sarofim, An Investigation into the Steady-State Elutriation of Fines from a Fluidized Bed, AIChE 72nd Meeting, San Francisco, 1979.

Bader, R., J. Findlay, and T. Knowlton, Circulating Fluidized Bed Technology II (Edited by P. Basu and P. Large), pp. 155-164, Pergamon Press, Oxford, 1988.

Bak, T. C., J. E. Son, and S. D. Kim, Heat Transfer Characteristics of A Vertical Tube in A Fluidized-Bed Combuster, Intl. Chem. Eng., 29(1), 166, 1989.

Baron, T., C. L. Briens, P. Galtier, and M. A. Bergougnou, Effect of Bed Height on Particles Entrainment from Gas-Fluidized Beds, Powder Technology, 63, 149- 156, 1990.

Baskakov, A. P. et al. , Heat Transfer to Objects Immersed in Fluidized Beds, Powder Technol., 8, pp. 273-282, 1973.

Baskakov, A. P., O. K. Vitt, V. A. Kirakosyan, V. K. Maskaev, and N. F. Filippovsky, Investigation of Heat Transfer Coefficient Pulsations and of the Mechanism of Heat Transfer from A Surface Immersed in A Fluidized Bed, in La Fluidisation et ses Applications, Societe Chimie Industrielle, Toulouse, pp.293-302, 1974.

Basu, P., Heat Transfer in High Temperature Fast Fluidized Beds, Chem. Eng. Sci., 45(10), 3123-3136, 1990.

Basu, P. and P. K. Nag, An Investigation into Heat Transfer in Circulating Fluidized Beds, Int.J. Heat Mass Transfer, 30, 2300-2409, 1987.

Berg, B. V. and A.P. Baskakov, Investigation of Local Heat Transfer Between A Fixed Horizontal Cylinder and A Fluidized Bed, Intl. Chem. Eng., 14(3), 440, 1974.

Bi, H., J. Yong, Y. Zhiqing, and B. Dingorn, The Radial Distribution of Heat Transfer Coefficient in a Fast Fluidized Bed, Fluidization IV, J. R. Grace, L. W. Shemilt, M. A. Bergougnou (eds.), Engineering Foundation, pp. 701-708, 1989.

Biyikli, S. and J. C. Chen,Effect of Mixed Particle Sizes on Local Heat Transfer Coefficients Around A Horizontal Tube in Fluidized Beds, Proc. 7th Intl. Heat Transfer Conf., Munich, Vol. 6, pp 39-45, 1982.

Biyilki, S., K. Tuzla, and J. C. Chen, Heat Transfer Around A Horizontal Tube in Freeboard Region of Fluidized Beds, AIChE J., 29, 712, 1983.

Biyikli, S., K. Tuzla, and J. C. Chen, Particle Contact Dynamics on Tubesin the Freeboard Region of Fluidized Beds, AICHE J., 33, 1225, 1987a.

Biyikli, S., K. Tuzla, and J.C. Chen, Freeboard Heat Transfer in High Temperature Fluidized Beds, Powder Technology, 53, 187, 1987b.

Botterill, J.S.M. , K. A. Redish, D. K. Ross, and J. R. Williams, Proc, Symp. Interaction between Fluids and Particles, London, 1966.

Botterill, J. S. M. et al.,The Effect of Gas and Solids Thermal Properties on the Rate of Heat Transfer to Gas-Fluidized Beds, in Proc. Intl. Symp. on Fluidization, A.A.H. Drinkenburg (ed.), Amsterdam: Netherlands Univ. Press, pp. 442-453, 1967.

Botterill, J.S.M., Fluid-Bed Heat Transfer, Academic Press, New York, 1975.

Byam, J., K. K. Pillai, and A. G. Roberts, Heat Transfer to Cooling Coils in the "Splash" Zone of a Pressurized Fluidized Bed Combustor, AIChE Symp. Ser., No. 208, Vol. 77, 351-358, 1981.

Chandran, R., J. C. Chen, and F. M. Staub, Local Heat Transfer Coefficients Around Horizontal Tubes in Fluidized Beds, Trans. ASME, 102, 152, 1980.

Chakoraborty, R. K. and M. A. Vickers, Heat Transfer Characteristics of Cooling Tubes in the Expanded and Splash Regions of a Fluidized Bed Combustor, Inst. Energy Conf., "Fluidized Combustion: Is It Achieving Its Promise?" London, 16-17th. October, 1984.

Decker, N. A. and L. R. Glicksman, Conduction Heat Transfer at the Surface of Bodies Immersed in Gas Fluidized Beds of Spherical Particles, AIChE Symp. Ser., 77(208), 341-349, 1981.

Denloye, A. E. and J. S. M. Botterill, Bed to Surface Heat Transfer in A Fluidized Bed of Large Particles, Powder Technology, 19, 197-203, 1977.

Do, H. T., J. R. Grace, R. Clift, Particle Ejection and Entrainment from Fluidized Beds, Powder Technol., 6, 195-220, 1972.

Dow, W. M. and M. Jacob, Heat Transfer between A Vertical Tube and A Fluidized Air-Solid Mixture, Chem. Eng. Prog., 47, 537, 1951.

Eichhorn, J. and R. R. White, Chem. Eng. Prog. Symp. Ser., 48, 11-19, 1952.

Farag, I.H., K. Y. Tsai, Simulation of Fluid Catalytic Cracking Operation, Mathematical Modeling, Vol. 8, pp 311-316, 1987.

Farag, I. H., R. Breault, S. B. R. Karri, and K. Y. Tsai, Heat Transfer,Mass Transfer and Reaction Conversion in Fluidized Beds Using Bubbling-Bed Model, Heat and Technology, Vol. 5, No. 1-2, pp 1-18, 1987.

Farag, I. H., M. J. Believeau, K. A. Woodside, A. Ray, C.M. Mohr, J. H. Porter, and J. N. Cannon, Staged Cascaded Fluidized Bed Combustor (SCFBC) Evaluation, Chem. Eng. Comm., Vol.60, No.1-6, pp 325-341, 1987.

Farag, I. H., R. W. Breault, R. K. Mongeon and A. W. Hall, Multi Solid Fluidized Bed (MSFB) Combustor: Modeling and Analysis, 10th Intl. Conf. on Fluidized Bed Combustion, 4/30 - 5/3 /1989, San Francisco, CA.

Feugier A.,C. Gaulier, and G. Martin, Some Aspects of Hydrodynamics,Heat Transfer and Gas Combustion in Circulating Fluidized Beds, Proc. Intl. Conf. on Fluidized Bed Combustion, 1987.

Fournol, A. B., M. A. Bergougnou, and C.G.J. Baker, Can. J. Chem. Eng., 51, 401, 1973.

Fraley, L. D., Y. Y. Lin, K. H. Hsiao, and A. Solbakken,Heat Transfer Coefficient in Circulating Bed Reactor, ASME Report 83-HT-92, 1983.

Froessling, N., Gerlands Beitr. Geophys., 52, 170, 1938.

Furchi, J. C. L., L. Goldstein, G. Lombardi, and M. Mosheni, Experimental Local Heat Transfer in A Circulating Fluidized Bed, Circulating Fluidized Bed Technology - II, P. Basu and P.

Large (eds.), pp. 263-270, Pergamon Press, Oxford, 1988.

Gabor, J. D., Wall-to-Bed Heat Transfer in Fluidized and Packed Bed, Chem. Eng. Prog. Symp. Ser., 66(105), 76, 1970.

Gabor, J. D., Wall-to-Bed Heat Transfer in Fluidized Beds, AIChE J., 18, 249, 1972.

Geldart, D., Types of Gas Fluidization, Powder Technol., 7, 285-292, 1973.

Geldart, D. EPRI CS 2094, Electric Power Research Institute, Palo Alto, CA, 1981.

Gel'perin, N. I., V. G. Einstein, K. A. Korotjanskaja, and J. P. Perevozchikova, Teoreticheskie Osnovy Khimicheskoi Tekhnologii, 2, 430, 1968.

Gel'perin, N. I. and V. G. Einshtein, Heat Transfer in Fluidized Beds, in Fluidization, J. F. Davidson and D. Harrison (eds.), Academic Press, New York, pp. 517-540, 1971.

George, S. E. and J. R. Grace, Heat Transfer to Horizontal Tubes in Freeboard Region of a Gas Fluidized Bed, AIChE Meeting, San Francisco, No. 7E, 1979.

George, S. E. and J. R. Grace, Heat Transfer to Horizontal Tubes in the Freeboard Region of a Gas Fluidized Bed, AIChE J., 28 (5), 759, 1982.

Glicksman, L. R., Circulating Fluidized Bed Heat Transfer, in Circulating Fluidized Bed Technology II, P. Basu and J.F. Large (eds.), Proc. 2nd Conf. on Circulating Fluidized Beds, pp. 13-29, Compiegne, France, 1988.

Grace, J. R., Fluidization, Handbook of Multiphase Systems, Hetsroni, G. (ed.), Vol. 8, p.2, 1982.

Grace, J. R., Heat Transfer in Circulating Fluidized Beds, Circulating Fluidized Bed Technology, P. Basu (ed.), p. 63, Pergamon, Toronto, 1986.

Grewal, N. S. and E. S. Sorenson, Heat Transfer between Horizontal Tubes and Freeboard Region of a Low-Rank Coal Fluidized Bed Combustor, Chem. Eng. Comm., 60, 311-324, 1987.
Griswold, C. R. and R. P. Van Driesen, Commercial Experience with H-Oil, Hydrocarbon Processing, 45(5), 153-158, 1966.

Grootenhuis, R. C., A. Mackworth, and O. A. Saunder, Proc. Inst. Mech. Eng., 363-370, 1951.

Guigon, P. et al. Proc. Second Intern. Conf. Circulating Fluidized Beds, Compiegne, p. 65, 1988.

Hamdullahpur, F., Two Phase Flow Behavior in the Freeboard of a Gas Fluidized Bed, Technical University of Nova Scotla Library Press, April, 1985.

Harakas, N. K. and K. O. Beatty, Jr., Moving Bed Heat Transfer: 1. Effect of Interstitial Gas with Fine Particles, Chem.Eng. Prog. Symp. Ser., 59(41), 122, 1963.

Hashimoto, O., S. Mori, S. Hiraoka, I.Yamada, T. Kojima, and K. Tsuji, Heat Transfer to the Surface of Vertical Tubes in the
Freeboard of a Turbulent Fluidized Bed, Intl. Chem. Eng., 30(2), 254, 1990.

Heertjes, P. M. and S. W. Mckibbons, The Partial Coefficients of Heat Transfer in a Drying Fluidized Bed, Chem. Eng. Sci., 5,
161-167, 1956.

Hellwig, K. C., E. S. Johanson, C. A. Johnson, S. C. Schuman, and H. H. Stotler, Make Liquid Fuels from Coal, Hydrocarbon Processing, 45(5), 165-169, 1966.

Hill, F. B.and R. H. Wilhelm, Radiative and Conductive Heat Transfer in a Quiescent Gas-Solid Bed of Particles, AIChE J., 5, 486-496, 1959.

Hoggen, B., T. Lendstad, and T. A. Engh, in K. úpstergaard and A. Sorensen (eds.), Fluidization V, p. 297, Engineering Foundation, New York, 1986.

Horio, M., A. Taki, Y. S. Hsieh, and I. Muchi, Elutriation and Particle Transport through the Freeboard of a Gas-Fluidized Bed, 3rd International Conference on Fluidization, Henniker, New Hampshire, 1980.

Horio, M., T. Shibata, S. Muchi, Design Criteria for the Fluidized Bed Freeboard, Proc. 4th Intl. Conf. on Fluidization, Japan, 1983.

Horio, M., K. Morishita, O. Tachibana, and N. Murata, Circulating Fluidized Bed Technology II (Edited by P. Basu and P. Large), pp. 147-154, Pergamon Press, Oxford, 1988.

Ismail, S. and J. C. Chen, Volume Fraction of Solids in the Freeboard Region of Fluidized Beds, AIChE Symp. Ser., 80, 114-118, 1984.

Jolley, L. T. and J. E. Stantan, Fluidization in Beds of Coal and Coke Particles: Some Effect of Size of Particles and Viscosity, Density and Velocity of Gas, J. Appl. Chem., 2, Supplementary Issue, No. 1, 562, 1952.

Kale, S. R.and J. K. Eaton, An Experimental Investigation of

Gas-Particle Flows through Diffusers in the Freeboard Region of Fluidized Beds, Int. J. Multiphase Flow, 11(5), 659-674, 1985.

Kays, W. M. and M. E. Crawford, Convective Heat and Mass Transfer, p.151, 2nd ed., McGraw-Hill Book Co., 1980.

Kettenring, K. N., E. L. Manderfield, and J. M. Smith, Heat and Mass Transfer in Fluidized Systems, Chem. Eng. Prog., 46, 139-145, 1950.

Kiang, K. D., K. T. Liu, H. Nack, and J. H. Oxley, Heat Transfer in Fast Fluidized Beds, in Fluidization Technology, Ed. D. L. Keairus, Hemisphere, Washington, 2, 471, 1976.

Knudsen, J. C. and D. L. Katz, Fluid Dynamics and Heat Transfer, McGraw-Hill Book Company, New York, 1985.

Kobro, H. and C. Brereton, Control and Fuel Flexibility of Circulating Fluidized Beds, P. Basu (ed.), Proc. First Int. Conf. on Circulating Fluidized Beds, pp. 263-272, Pergamon Press, 1986.

Kortleven, A., J. Bast, and J. Meulink, Heat Transfer to Horizontal Tubes in a Splash Zone of a 0.6 x 0.6 m AFBC Research Facility, in "Heat and Mass Transfer in Fixed and Fluidized Beds,"

Van Swaaij, W. P. M. and N. H. Afgan (eds.), Hemisphere Publishing Corp., New York, pp. 181-196, 1986.

Krell, L., H.-J. Kunne, and L. Morl, Floww Regimes and Heat and Mass Transfer in Gas-Fluidized Beds of Solids, Intl. Chem. Eng., 30(1), 45, 1990.

Kunii, D. and O. Levenspiel, Fluidization Engineering, Wiley, New York, pp. 265-301, 1969.

Kunii, D. and O. Levenspiel, Entrainment of Solids from Fluidized Beds: I. Hold-Up of Solids in the Freeboard, II.Operation of Fast Fluidized Beds, Powder Technology, 61, 193-206, 1990.

Kunii, D. and O. Levenspiel, Powder Technol., 61, 193, 1990.
Kunii, D. and O. Levenspiel, A General Equation for the Heat Transfer Coefficient at Wall Surfaces of Gas/Solid Contactors, Ind. Eng. Chem. Res., 30, 136-141, 1991.

Kunii, D. and J. M. Smith, Heat Transfer Characteristics of Porous Rocks, International Powder Bulk Solids Handling and Processing Conference, May, 1976.

Large, J. F., Y. Martinie,and M. A. Bergougnou,Interpretive Thermal Conductivity of Unconsolidated Particles with Flowing Fluids, AIChE J., 7, 29-34, 1961.

Leva, M., Fluidization, New York: McGraw-Hill, pp. 183-186, 1959.

Leva, M. and C. Y. Wen, Elutriation, in Fluidization, eds., J. F. Davidson and D. C. Harrison, p. 627, Academic, New York,1971.

Levenspiel, O. and J. S. Walton, Wall Bed Heat Transfer in Fluidized Systems, Chem. Eng. Prog. Symp. Ser., 50(9), pp.1-13, 1954.

Lewis, W. K., E. R. Gillil and, and P. M. Lang, Chem. Eng. Prog. Symp. Ser., 38, 59, 1962.

Lewis, W. K., E. R. Gillil and H. Girouard, Heat Transfer- and Solids Mixing in Beds of Fluidized Solids, Chem. Eng. Prog. Symp. Ser. 38, Vol. 58, pp. 87-97, 1962.

Lewis, W. C. McC., J. Chem. Soc. (London), 113, 471, 1918.
Logan, T.J., R. M. Felder, and J. K. Ferrell, AIChE Symp. Series No. 137, Vol. 70, 310, 1974.

Lop, C. O. G. and R. W. Hawley, Unsteady-State Heat Transfer between Air and Loose Solids, Ind. Eng. Chem., 40, 1061-1070, 1948.

Martin, H., Fluid-Bed Heat Exchangers -- A New Model for Particle Convective Energy Transfer, Chem. Eng. Commun., 13, 1-16, 1981.

Mickley, H. S. and C. A. Trilling, Heat Transfer Characteristics of Fluidized Beds, Ind. Eng. Chem., 41, 1135, 1949.

Mickley, H. S. and D. F. Fairbanks, Mechanism of Heat Transfer to Fluidized Beds, AIChE J., 374, Sep. 1955.

Morooka, S., K. Kawazuishi, and Y. Kato, Holdup and Flow Pattern of Solid Particles in Freeboard of Gas-Solid Fluidized Bed with Fine Particles, Powder Technology, 26, 75, 1980.

Nazemi, A.,M. A. Bergougnou, and G. G. J. Baker, Dilute Phase Hold-up in a Large Gas Fluidized Bed, AIChE Symp. Series, 70, No. 141, 98, 1974.

Noack, R., Chem. Ing. Tech., 42, 371-376, 1970.

Pemberton, S. T. and J. F. Davidson, Chem. Eng. Sci., 39, 829, 1984

Pemberton, S. T. and J. F. Davidson, Elutriation from Fluidized Beds - II. Disengagement of Particles from Gas in the Freeboard, Chem. Eng. Sci., 41(2), 253-262, 1986.

Perry, R. H. and C. L. Chilton, Chemical Engineers' Handbook, p. 3-220, 5th ed., McGraw-Hill Book Co., 1973.

Phillips, M. C., A Parametric Sensitivity Study on the Relative Importance of Packet Formation and Single-Particle Motion in Fluidized Bed Heat Transfer, Chem. Eng. Sci., 45(8), 21952202,
1990.

Polanyi, Z., Elektrochem., 26, 48, 1920.

Ranz, W. E.and W. R. Marshall, Jr., Chem. Eng. Prog., 48, 141, 1952.

Rhodes, M. and G. Geldart, Circulating Fluidized Bed Technology II (Edited by P. Basu and P. Large),pp. 155-164, Pergamon Press, Oxford, 1988.

Saxena, S. C., N. S. Grewal, and J. D. Gabor, Heat Transfer Between A Gas Fluidized Bed and Immersed Tubes, Advances in Heat Transfer, Vol. 14, pp. 149-247, 1978.

Saxena, S. C. and J. D. Garbor, Mechanisms of Heat Transfer Between a Surface and a Gas-Fluidized Bed for Combustor Application, Prog. Energy Combust. Sci., 7, 73-102, 1981.

Sekthira, A., Y. Y. Lee, and W. E. Genetti, Heat Transfer in a Circulating Fluidized Bed, 25th National Heat Transfer Conf., Houston, July, 1989.

Selzer, V. W. and W. J. Thomson, Fluidized Bed Heat Transfer-The Packet Theory Revisited, AIChE Symp. Ser., 73(161), 29-37, 1977.

Shah, V., Handbook of Plastics Testing Technology, p. 104, John Wiley & Sons, Inc., 1984.

Shirai, T., Kagaku Kogaku (Chem. Eng. Japan), 26, 637, 1962.

Stenhouse, J. I. T. and P. J. Lloyd, AIChE Symp. Ser. 137(70), 310, 1974.

Subbarao, D. and P. Basu, A Model for Heat Transfer in Circulating Fluidized Beds, Intl. J. Heat and Mass Transfer, 29, p.487, 1986.

Tabatabaie-Farashahi, M., S. N. Upadhyay, and S. C. Saxena, Fluidized Bed and Freeboard Heat Transfer Studies with Vertical Tube Bundles, Letters, Heat and Mass Transfer, 8, 91, 1981.

Toomey, R. D. and H. F. Johnstone, Gaseous Fluidization of Solid Particles, Chem. Eng. Progr., 48(5), 220, 1952.

Tremblay, D. A., M. D. Beliveau, and I. H. Farag, Cold Flow Study of A Circulating Fluidized Bed Combustor, Symposium on Multiphase Flow, 21st Annual Meeting of the Five Particle Society, San Diego, CA, Aug. 21-25, 1990.

Tung, Y., J. Li, M. Kwauk, Radial Voidage Profile in a Fast Fluidized Bed, Fluidization'88, M. Kwauk and D. Kunii (eds.), Science Press, Beijing, pp. 139-145, 1988.

Tweddle, T. A., C. E. Capes, and G. L. Osberg, Effect of Screen Packing on Entrainment from Fluidized Beds, I & EC Process Des. Dev., 6(1), 85, 1970.

Van Heerden, C. P. Nobel, and D.W. Van Krevelen, Ind. Eng. Chem., 45, 1237, 1953.

Vreedenberg, H. A.,Heat Transfer between a Fluidized Bed and a Horizontal Tube, Chem. Eng. Sci., 9, 52, 1958.

Vreedenberg, H. A.,Heat Transfer between a Fluidized Bed and a Vertical Tube, Chem. Eng. Sci., 11, 274-285, 1960.

Wasan, D. T. and Ahluwalia, M. S.,Consecutive Film and Surface Renewal Mechanism for Heat and Mass Transfer from a Wall, Chem. Eng. Sci., 24, 1535, 1969.

Wen, C. Y. and R. F. Hashinger, Elutriation of Solid Particles from a Dense Phase Fluidized Bed, AIChE J., 6, 220-226, 1960.

Wen, C. Y. and E. N. Miller, Heat Transfer in Solids-Gas Transport Lines, Ind. Eng. Chem., 53(1), 51-53, 1961.

Wen, C. Y. and T. M. Chang, Particle-to-Particle Heat Transfer in Air-Fluidized Beds, Proc. Int.Symp. Fluidization, A. A. H. Drinkenburg (ed.), pp. 491-506, Netherlands Univ. Press, Amsterdam, 1967.

Wen, C. Y. and M. Leva, AIChE J., 2, 482, 1956.

Wen, C. Y. and Y. H. Yu, Mechanics of Fluidization, Chem. Eng. Prog Symp. Ser., 62(62), 100-111, 1966a.

Wen, C. Y. and Y. H. Yu, A Generalized Method for Predicting the Minimum Fluidization Velocity, AIChE J., 12, 610-612, 1966b.

Wender, L. and G. T. Cooper, AIChE J., 4, 15, 1958.

Wicke, E. and F. Fitting, Chem. Ing. Tech., 26, 301, 1954.

Wood, R. T., M. Kuwata, and F. W. Staub, Heat Transfer to Horizontal Tube Banks in the Splash Zone of a Fluidized Bed of Large Particles, in Fluidization, Grace, J. R. and J. M. Matsen (eds.), Plenum, New York, pp. 235-242, 1980.

Wu, R. L., C. J. Lim, J. Chaouki, and J. R. Grace,Heat Transfer from A Circulating Fluidized Bed to Membrane Water-wall Surfaces, AIChE J., 33(11), 1988, 1987.

Wu, R. L., C. J. Lim, and J. R. Grace, The Measurement of Instantaneous Local Heat Transfer Coefficients in a Circulating Fluidized Bed, Can. J. Chem. Eng. 67, 301, 1989.

Wu, R. L., J. R. Grace, C. J. Lim, A Model for Heat Transfer in Circulating Fluidized Beds, Chem. Eng. Sci., 45(12), 3389, 1990.

Xavier, A. M. and J. A. Davidson,Heat Transfer to Surfaces Immersed in Fluidized Beds,Particularly Tube Arrays, in Fluidization, J. F. Davidson and D. L. Keairns (eds.), Cambridge Univ. Press, Cambridge, England, pp. 333-338, 1978.

Xavier, A. M. andJ. F. Davidson, Heat Transfer to Surfaces Immersed in Fluidized Beds and in the Freeboard Region, AIChE Symp. Series, No. 208, Vol. 77, 368-373, 1981.

Yates, J. G. and P. N. Rowe, A Model for Chemical Reaction in the Freeboard Region above a Fluidized Bed, Trans. Inst. Chem. Eng., 55, 137-142, 1977.

Yoshida, K., T. Ueno, and D. Kunii, Mechanism of Bed-Wall Heat Transfer in A Fluidized Bed at High Temperatures, Chem. Eng. Sci., 29, 77-82, 1974.

Zabrodsky, S. S.,Hydrodynamics and Heat Transfer in Fluidized Beds, Cambridge, The M.I.T. Press, pp. 226-299, 1966.

Zenz, F. A.and D. F. Othmer, Fluidization and Fluid-Particle Systems, Reinhold, New York, 1960.

Zenz, F. A. and N. A. Weil, AIChE J., 4, 472, 1958.

Zenz, F. A., State of the Art Review and Report on Critical Aspects and Scale-Up Considerations in the Design of Fluidized Bed Reactors, US Government Report No. DOE/MC/14141-1304, US National Technical Information No. DE83003632, 1983.

Ziegler, E. N. and W. T. Brazelton, Mechanism of Heat Transfer to Fixed Surfaces in Fluidized Bed, I & EC Fundamentals, 3, 94, 1964a.

Ziegler, E. N., L. B. Koppel, and W. T. Brazelton, Effects of Solid Thermal Properties on Heat Transfer to Gas Fluidized Beds, I & EC Fundamentals, 3(4), 324, 1964b.

APPENDIXES

Appendix 1

Experiemntal Data for Heat Transfer Coefficient Measurement

Table A.1.1-A.1.30. Original experimental data for heat transfer coefficient measurement

Table	Exp. No.	Plate orientation type	Plate radial location r (cm)	Plate axial location H (cm)	Uo (m/s)
A.1.1-A.1.6	4001-4006	I	0, 3, 6, 9, 9, 12, 13.2	45, 95, 145, 198	0.28, 0.34, 0.40 0.46, o.52, 0.64
A.1.7-A.1.12	4007-4012	II	0, 3, 6, 9, 9, 12, 14	45, 95, 145, 198	0.28, 0.34, 0.40, 0.46, o.52, 0.64
A.1.13-A.1.18	4013-4018	III	0, 3, 6, 9, 9, 12, 14	45, 95, 145, 198	0.28, 0.34, 0.40, 0.46, o.52, 0.64
A.1.19-A.1.24	4019-4024	IV	0, 3, 6, 9, 9, 12, 13.5	56, 101, 153, 204	0.28, 0.34, 0.40, 0.46, o.52, 0.64
A.1.25-A.1.30	4025-4030	III	0, 3, 6, 9, 9, 12, 13.5	56, 101, 153, 204	0.28, 0.34, 0.40, 0.46, o.52, 0.64
	Test for angular symmetry (See: Section 7.4 and Figure 7.7)				

Table A.1.1

1. Exp. No. : 4001
2. Date : 900303
3. Static Bed Hei. (cm) : 29.00
4. Plate Rad. Loc. (cm) : 0.00

Uo(m/s)	Ht.(cm)	To(C)	Tj(C)	Tw(C)	Q(w)	Qr(w)	h_c+h_r(W/m²·K)
0.279	45	19.500	49.400	47.575	2.738	0.115	89.576
	95	19.500	101.500	99.499	3.002	0.424	30.898
	145	19.500	57.000	56.269	1.097	0.158	24.499
	198	19.500	56.000	55.140	1.290	0.152	30.603
0.339	45	20.000	41.400	39.530	2.806	0.077	133.946
	95	20.000	95.500	93.479	3.031	0.379	34.602
	145	20.000	55.000	54.269	1.097	0.146	26.618
	198	20.000	55.000	54.148	1.278	0.145	31.792
0.399	45	19.000	32.400	30.565	2.753	0.043	224.596
	95	19.000	77.500	75.480	3.030	0.266	46.916
	145	19.000	52.000	51.252	1.122	0.135	29.342
	198	19.000	53.000	52.149	1.277	0.139	32.912
0.459	45	19.000	30.400	28.600	2.700	0.036	266.103
	95	19.000	52.500	50.511	2.984	0.131	86.797
	145	19.000	41.000	40.261	1.109	0.084	46.210
	198	19.000	46.000	45.157	1.265	0.106	42.495
0.519	45	19.000	29.400	27.606	2.691	0.032	296.196
	95	19.000	45.500	43.476	3.036	0.098	115.070
	145	19.000	36.000	35.260	1.111	0.063	61.796
	198	19.000	42.000	41.153	1.270	0.088	51.165
0.579	45	19.500	31.400	29.581	2.729	0.038	255.922
	95	19.500	42.500	40.517	2.975	0.083	131.898
	145	19.500	32.000	31.237	1.144	0.044	89.842
	198	19.500	37.000	36.128	1.309	0.064	71.737
0.639	45	20.000	32.400	30.546	2.781	0.040	249.248
	95	20.000	40.500	38.468	3.049	0.073	154.523
	145	20.000	30.000	29.206	1.190	0.035	120.372
	198	20.000	34.000	33.111	1.333	0.050	93.836

Table A.1.2

1. Exp. No. : 4002
2. Date : 900303
3. Static Bed Hei. (cm) : 29.00
4. Plate Rad. Loc. (cm) : 3.00

Uo(m/s)	Ht.(cm)	To(C)	Tj(C)	Tw(C)	Q(w)	Qr(w)	h_c+h_r(W/m^2·K)
0.279	45	20.000	56.400	54.546	2.781	0.147	73.108
	95	20.000	97.500	95.485	3.023	0.393	33.394
	145	20.000	57.000	56.240	1.140	0.156	26.036
	198	20.000	57.000	56.132	1.303	0.155	30.448
0.339	45	19.500	39.400	37.499	2.852	0.070	148.198
	95	19.500	101.500	99.461	3.059	0.424	31.590
	145	19.500	58.000	57.230	1.155	0.163	25.232
	198	19.500	56.000	55.115	1.328	0.152	31.657
0.399	45	19.500	33.900	31.959	2.912	0.047	220.456
	95	19.500	69.500	67.346	3.231	0.217	60.396
	145	19.500	50.000	49.171	1.244	0.123	36.225
	198	19.500	53.500	52.585	1.373	0.139	35.745
0.459	45	19.500	32.400	30.536	2.796	0.042	239.283
	95	19.500	54.500	52.472	3.042	0.139	84.419
	145	19.500	43.000	42.231	1.154	0.091	44.858
	198	19.500	48.000	47.127	1.309	0.113	41.497
0.519	45	20.000	31.400	29.556	2.767	0.036	274.017
	95	20.000	46.500	44.492	3.012	0.099	114.037
	145	20.000	37.000	36.231	1.154	0.063	64.462
	198	20.000	43.000	42.145	1.283	0.089	51.718
0.579	45	20.000	33.400	31.556	2.767	0.044	225.931
	95	20.000	43.500	41.528	2.958	0.086	127.901
	145	20.000	33.000	32.231	1.154	0.047	86.837
	198	20.000	39.000	38.149	1.277	0.071	63.689
0.639	45	20.500	34.400	32.562	2.757	0.046	215.495
	95	20.500	40.500	38.506	2.991	0.071	155.476
	145	20.500	31.000	30.233	1.150	0.037	109.670
	198	20.500	35.000	34.157	1.264	0.053	85.042

Table A.1.3

1. Exp. No. : 4003
2. Date : 900303
3. Static Bed Hei. (cm) : 29.00
4. Plate Rad. Loc. (cm) : 6.00

Uo(m/s)	Ht.(cm)	To(C)	Tj(C)	Tw(C)	Q(w)	Qr(w)	h_c+h_r(W/m^2·K)
0.279	45	19.500	52.900	51.065	2.753	0.132	79.604
	95	19.500	98.500	96.498	3.003	0.402	32.384
	145	19.500	57.500	56.744	1.134	0.160	25.066
	198	19.500	57.000	56.136	1.296	0.157	29.812
0.339	45	20.000	40.900	39.072	2.743	0.075	134.120
	95	20.000	89.500	87.498	3.003	0.338	37.852
	145	20.000	54.500	53.755	1.118	0.143	27.693
	198	20.000	55.000	54.144	1.284	0.145	31.970
0.399	45	20.000	35.400	33.565	2.753	0.052	190.878
	95	20.000	70.500	68.504	2.994	0.222	54.803
	145	20.000	49.000	48.243	1.136	0.117	34.616
	198	20.000	53.000	52.127	1.309	0.135	35.025
0.459	45	20.500	33.400	31.584	2.724	0.042	231.961
	95	20.500	55.500	53.535	2.948	0.140	81.498
	145	20.500	43.000	42.243	1.136	0.087	46.256
	198	20.500	47.000	46.144	1.284	0.105	44.070
0.519	45	20.500	33.400	31.584	2.724	0.042	231.961
	95	20.500	47.500	45.518	2.973	0.102	110.017
	145	20.500	37.000	36.237	1.144	0.061	65.974
	198	20.500	42.000	41.136	1.296	0.082	56.392
0.579	45	21.000	33.400	31.568	2.748	0.040	245.599
	95	21.000	44.500	42.480	3.030	0.087	131.361
	145	21.000	34.000	33.218	1.174	0.047	88.431
	198	21.000	39.000	38.161	1.258	0.068	66.502
0.639	45	21.000	34.400	32.568	2.748	0.044	224.035
	95	21.000	44.500	42.510	2.986	0.087	129.217
	145	21.000	32.000	31.218	1.174	0.039	106.499
	198	21.000	36.000	35.132	1.303	0.055	84.654

Table A.1.4

1. Exp. No. : 4004
2. Date : 900303
3. Static Bed Hei. (cm) : 29.00
4. Plate Rad. Loc. (cm) : 9.00

Uo(m/s)	Ht.(cm)	To(C)	Tj(C)	Tw(C)	Q(w)	Qr(w)	h_s+h_f(W/m^2·K)
0.279	45	19.500	54.400	52.578	2.733	0.139	75.194
	95	19.500	105.500	103.524	2.964	0.454	28.637
	145	19.500	58.000	57.260	1.109	0.163	24.037
	198	19.500	57.000	56.136	1.296	0.157	29.817
0.339	45	20.500	42.400	40.578	2.733	0.080	126.711
	95	20.500	96.500	94.505	2.993	0.385	33.789
	145	20.500	55.000	54.260	1.109	0.144	27.417
	198	20.500	55.000	54.186	1.221	0.144	30.670
0.399	45	20.300	36.400	34.581	2.728	0.055	179.455
	95	20.300	81.500	79.560	2.910	0.286	42.452
	145	20.300	49.000	48.247	1.130	0.116	34.812
	198	20.300	51.000	50.153	1.271	0.125	36.829
0.459	45	20.500	33.400	31.562	2.757	0.042	235.326
	95	20.500	59.500	57.493	3.010	0.160	73.862
	145	20.500	42.000	41.235	1.148	0.083	49.267
	198	20.500	47.000	46.127	1.309	0.105	45.043
0.519	45	20.500	33.400	31.546	2.781	0.042	237.732
	95	20.500	51.500	49.492	3.012	0.121	95.611
	145	20.500	38.000	37.231	1.154	0.065	62.396
	198	20.500	43.000	42.123	1.315	0.087	54.468
0.579	45	21.000	33.400	31.553	2.771	0.040	248.124
	95	21.000	48.500	46.492	3.012	0.105	109.336
	145	21.000	34.000	33.218	1.174	0.047	88.431
	198	21.000	40.000	39.119	1.321	0.072	66.128
0.639	45	21.000	35.400	33.546	2.781	0.048	208.827
	95	21.000	47.500	45.490	3.015	0.100	114.121
	145	21.000	32.000	31.237	1.144	0.039	103.510
	198	21.000	37.000	36.128	1.309	0.059	79.192

Table A.1.5

1. Exp. No. : 4005
2. Date : 900303
3. Static Bed Hei. (cm) : 29.00
4. Plate Rad. Loc. (cm) : 12.00

Uo(m/s)	Ht.(cm)	To(C)	Tj(C)	Tw(C)	Q(w)	Qr(w)	h_c+h_f(W/m²·K)
0.279	45	20.500	53.400	51.462	2.908	0.130	86.016
	95	20.500	108.500	106.410	3.136	0.473	29.718
	145	20.500	59.000	58.205	1.193	0.164	26.154
	198	20.500	58.500	57.581	1.379	0.161	31.505
0.339	45	20.500	43.400	41.462	2.908	0.084	129.172
	95	20.500	102.500	100.385	3.173	0.427	32.955
	145	20.500	57.000	56.230	1.155	0.154	26.863
	198	20.500	57.000	56.085	1.373	0.153	32.860
0.399	45	20.500	36.400	34.581	2.728	0.054	182.053
	95	20.500	83.500	81.521	2.969	0.298	41.971
	145	20.500	50.000	49.241	1.138	0.120	33.984
	198	20.500	52.000	51.136	1.296	0.129	36.544
0.459	45	20.500	34.400	32.603	2.695	0.046	209.823
	95	20.500	58.500	56.568	2.899	0.156	72.926
	145	20.500	44.000	43.249	1.126	0.092	43.604
	198	20.500	47.000	46.144	1.284	0.105	44.070
0.519	45	20.500	33.400	31.594	2.709	0.042	230.450
	95	20.500	51.500	49.548	2.929	0.121	92.680
	145	20.500	38.000	37.233	1.150	0.066	62.146
	198	20.500	43.000	42.140	1.290	0.087	53.303
0.579	45	21.000	34.400	32.546	2.781	0.044	227.252
	95	21.000	49.500	47.477	3.035	0.109	105.937
	145	21.000	35.000	34.228	1.158	0.051	80.237
	198	21.000	40.000	39.107	1.340	0.072	67.177
0.639	45	21.000	34.400	32.530	2.805	0.044	229.546
	95	21.000	46.500	44.462	3.057	0.095	121.016
	145	21.000	33.000	32.237	1.144	0.043	93.955
	198	21.000	37.000	36.103	1.346	0.059	81.690

Table A.1.6

1. Exp. No. : 4006
2. Date : 900303
3. Static Bed Hei. (cm) : 29.00
4. Plate Rad. Loc. (cm) : 13.20

Uo(m/s)	Ht.(cm)	To(C)	Tj(C)	Tw(C)	Q(w)	Qr(w)	h_s+h_f(W/m^2·K)
0.279	45	20.500	52.400	50.581	2.728	0.126	82.940
	95	20.500	104.500	102.531	2.954	0.443	29.350
	145	20.500	58.000	57.251	1.124	0.159	25.180
	198	20.500	57.000	56.132	1.303	0.153	30.923
0.339	45	20.500	40.400	38.581	2.728	0.071	140.884
	95	20.500	97.500	95.550	2.926	0.392	32.366
	145	20.500	54.000	53.255	1.118	0.139	28.664
	198	20.500	54.000	53.144	1.284	0.138	33.638
0.399	45	20.500	36.400	34.588	2.719	0.054	181.309
	95	20.500	83.500	81.506	2.991	0.298	42.326
	145	20.500	48.000	47.255	1.118	0.110	36.125
	198	20.500	51.000	50.136	1.296	0.124	37.927
0.459	45	20.500	34.400	32.581	2.728	0.046	212.841
	95	20.500	60.500	58.497	3.005	0.166	71.658
	145	20.500	42.000	41.243	1.136	0.083	48.691
	198	20.500	46.000	45.128	1.309	0.100	47.036
0.519	45	21.000	33.400	31.559	2.761	0.040	247.083
	95	21.000	51.500	49.531	2.954	0.119	95.278
	145	21.000	37.000	36.233	1.150	0.059	68.645
	198	21.000	43.000	42.128	1.309	0.085	55.525
0.579	45	21.000	34.400	32.581	2.728	0.044	222.179
	95	21.000	49.500	47.495	3.008	0.109	104.891
	145	21.000	34.000	33.237	1.144	0.047	85.959
	198	21.000	40.000	39.157	1.265	0.072	63.006
0.639	45	21.300	35.400	33.581	2.728	0.047	209.282
	95	21.300	47.500	45.501	2.998	0.099	114.853
	145	21.300	32.000	31.229	1.157	0.038	108.103
	198	21.300	37.000	36.128	1.309	0.058	80.864

Table A.1.7

1. Exp. No. : 4007
2. Date : 900304
3. Static Bed Hei. (cm) : 29.00
4. Plate Rad. Loc. (cm) : 0.00

Uo(m/s)	Ht.(cm)	To(C)	Tj(C)	Tw(C)	Q(W)	Qr(W)	h_s+h_r(W/m²·K)
0.279	45	19.000	50.600	48.695	2.858	0.122	88.333
	95	19.000	103.500	101.438	3.094	0.440	30.863
	145	19.000	58.000	57.232	1.152	0.164	24.769
	198	19.000	56.000	55.123	1.315	0.154	30.827
0.339	45	19.000	38.100	36.228	2.808	0.067	152.587
	95	19.000	97.000	94.984	3.025	0.393	33.207
	145	19.000	56.000	55.240	1.140	0.154	26.076
	198	19.000	54.000	53.132	1.303	0.144	32.553
0.399	45	19.500	33.100	31.224	2.814	0.044	226.522
	95	19.500	79.000	77.035	2.948	0.273	44.564
	145	19.500	51.000	50.239	1.142	0.128	31.641
	198	19.500	50.000	49.115	1.328	0.123	39.023
0.459	45	19.500	31.100	29.146	2.931	0.036	287.730
	95	19.500	55.500	53.560	2.910	0.144	77.860
	145	19.500	42.500	41.719	1.172	0.089	46.768
	198	19.500	45.000	44.123	1.315	0.099	47.343
0.519	45	19.600	30.600	28.765	2.752	0.034	284.323
	95	19.600	48.500	46.462	3.057	0.110	105.191
	145	19.600	37.000	36.227	1.160	0.064	63.192
	198	19.600	39.500	38.661	1.259	0.075	59.561
0.579	45	19.800	31.100	29.290	2.716	0.036	270.758
	95	19.800	46.000	44.001	2.998	0.098	114.911
	145	19.800	33.000	32.252	1.122	0.047	82.763
	198	19.800	35.500	34.645	1.283	0.057	79.185
0.639	45	19.900	32.600	30.751	2.774	0.041	241.510
	95	19.900	44.000	42.045	2.933	0.089	123.142
	145	19.900	31.000	30.225	1.163	0.039	104.402
	198	19.900	32.500	31.648	1.277	0.045	100.612

Table A.1.8

1. Exp. No. : 4008
2. Date : 900304
3. Static Bed Hei. (cm) : 29.00
4. Plate Rad. Loc. (cm) : 3.00

Uo(m/s)	Ht.(cm)	To(C)	Tj(C)	Tw(C)	Q(w)	Qr(w)	h_c+h_r(W/m^2·K)
0.279	45	19.500	51.600	49.688	2.868	0.125	87.097
	95	19.500	102.000	99.959	3.062	0.428	31.390
	145	19.500	57.000	56.240	1.140	0.158	25.635
	198	19.500	56.000	55.123	1.315	0.152	31.310
0.339	45	19.500	38.600	36.732	2.802	0.067	152.188
	95	19.500	95.500	93.497	3.005	0.381	34.002
	145	19.500	54.000	53.244	1.134	0.143	28.164
	198	19.500	53.500	52.636	1.296	0.140	33.466
0.399	45	19.600	33.100	31.236	2.796	0.044	226.728
	95	19.600	80.500	78.501	2.998	0.282	44.213
	145	19.600	49.000	48.239	1.142	0.118	34.291
	198	19.600	50.000	49.136	1.296	0.122	38.106
0.459	45	20.000	31.100	29.258	2.764	0.035	282.606
	95	20.000	57.000	55.000	3.001	0.149	78.102
	145	20.000	42.500	41.733	1.150	0.087	46.908
	198	20.000	44.000	43.140	1.290	0.093	49.588
0.519	45	20.000	30.600	28.775	2.738	0.033	295.602
	95	20.000	49.500	47.524	2.964	0.113	99.301
	145	20.000	37.000	36.218	1.174	0.063	65.672
	198	20.000	39.500	38.624	1.315	0.073	63.914
0.579	45	20.000	31.600	29.746	2.782	0.037	270.059
	95	20.000	46.500	44.499	3.002	0.099	113.613
	145	20.000	33.000	32.229	1.156	0.047	86.983
	198	20.000	34.000	33.124	1.315	0.050	92.384
0.639	45	20.000	34.100	32.247	2.780	0.047	213.963
	95	20.000	44.500	42.511	2.983	0.090	123.207
	145	20.000	31.000	30.264	1.105	0.039	99.582
	198	20.000	32.000	31.148	1.278	0.042	106.238

Table A.1.9

1. Exp. No. : 4009
2. Date : 900304
3. Static Bed Hei. (cm) : 29.00
4. Plate Rad. Loc. (cm) : 6.00

Uo(m/s)	Ht.(cm)	To(C)	Tj(C)	Tw(C)	Q(w)	Qr(w)	h_s+h_f(W/m²·K)
0.279	45	18.400	55.100	53.060	3.061	0.145	80.639
	95	18.400	105.500	103.363	3.207	0.457	31.028
	145	18.400	60.000	59.153	1.270	0.176	25.729
	198	18.400	58.000	57.068	1.399	0.166	30.573
0.339	45	18.600	39.600	37.642	2.938	0.074	144.198
	95	18.600	95.500	93.408	3.139	0.384	35.310
	145	18.600	56.000	55.192	1.212	0.155	27.687
	198	18.600	55.000	54.085	1.372	0.150	33.031
0.399	45	18.600	33.600	31.654	2.919	0.049	210.759
	95	18.600	80.500	78.424	3.114	0.285	45.332
	145	18.600	50.000	49.190	1.215	0.126	34.128
	198	18.600	51.000	50.089	1.366	0.130	37.631
0.459	45	18.800	31.600	29.653	2.922	0.041	254.520
	95	18.800	57.000	54.935	3.097	0.153	78.111
	145	18.800	42.500	41.712	1.183	0.091	45.676
	198	18.800	45.000	44.094	1.360	0.102	47.690
0.519	45	19.000	32.100	30.224	2.814	0.042	236.802
	95	19.000	49.000	46.916	3.126	0.114	103.462
	145	19.000	37.000	36.193	1.211	0.066	63.831
	198	19.000	40.000	39.085	1.373	0.079	61.759
0.579	45	19.100	31.600	29.673	2.891	0.040	258.609
	95	19.100	45.500	43.441	3.089	0.098	117.811
	145	19.100	33.000	32.200	1.201	0.050	84.255
	198	19.100	35.000	34.094	1.360	0.057	83.284
0.639	45	19.100	32.600	30.668	2.899	0.044	236.676
	95	19.100	44.500	42.437	3.095	0.093	123.339
	145	19.100	31.000	30.190	1.214	0.042	101.390
	198	19.100	32.000	31.081	1.379	0.045	106.738

Table A.1.10

1. Exp. No. : 4010
2. Date : 900304
3. Static Bed Hei. (cm) : 29.00
4. Plate Rad. Loc. (cm) : 9.00

Uo(m/s)	Ht.(cm)	To(C)	Tj(C)	Tw(C)	Q(w)	Qr(w)	h_c+h_r(W/m^2·K)
0.279	45	19.000	50.600	48.667	2.900	0.122	89.771
	95	19.000	100.000	97.931	3.104	0.415	32.668
	145	19.000	56.500	55.712	1.183	0.157	26.793
	198	19.000	56.000	55.106	1.341	0.154	31.522
0.339	45	19.000	39.100	37.161	2.908	0.071	149.802
	95	19.000	97.000	94.938	3.094	0.393	34.102
	145	19.000	54.500	53.706	1.190	0.147	28.835
	198	19.000	54.000	53.098	1.353	0.144	34.019
0.399	45	19.100	33.600	31.727	2.810	0.048	209.763
	95	19.100	79.500	77.499	3.002	0.278	44.731
	145	19.100	48.000	47.215	1.178	0.115	36.264
	198	19.100	50.000	49.102	1.347	0.124	39.088
0.459	45	19.000	31.600	29.714	2.829	0.040	249.563
	95	19.000	57.500	55.455	3.068	0.155	76.613
	145	19.000	42.000	41.204	1.195	0.088	47.787
	198	19.000	46.000	45.106	1.341	0.106	45.358
0.519	45	19.100	30.600	28.679	2.882	0.036	284.864
	95	19.100	48.500	46.460	3.061	0.111	103.345
	145	19.100	37.000	36.216	1.176	0.066	62.191
	198	19.100	41.500	40.607	1.340	0.085	55.962
0.579	45	19.100	32.600	30.649	2.927	0.043	239.343
	95	19.100	45.500	43.447	3.080	0.098	117.423
	145	19.100	33.000	32.216	1.176	0.050	82.364
	198	19.100	35.000	34.107	1.340	0.057	81.967
0.639	45	19.400	33.600	31.692	2.862	0.047	219.583
	95	19.400	43.500	41.456	3.067	0.088	129.494
	145	19.400	31.000	30.216	1.176	0.041	100.683
	198	19.400	32.000	31.123	1.315	0.044	103.942

Table A.1.11

1. Exp. No. : 4011
2. Date : 900304
3. Static Bed Hei. (cm) : 29.00
4. Plate Rad. Loc. (cm) : 12.00

Uo(m/s)	Ht.(cm)	To(C)	Tj(C)	Tw(C)	Q(w)	Qr(w)	h_s+h_f(W/m^2·K)
0.279	45	19.000	52.600	50.653	2.922	0.132	84.506
	95	19.000	101.500	99.451	3.074	0.426	31.566
	145	19.000	57.000	56.234	1.149	0.159	25.494
	198	19.000	55.000	54.107	1.340	0.149	32.526
0.339	45	19.000	39.100	37.220	2.821	0.071	144.720
	95	19.000	93.500	91.469	3.047	0.369	35.434
	145	19.000	54.000	53.240	1.140	0.144	27.878
	198	19.000	42.000	41.115	1.327	0.088	53.736
0.399	45	19.300	33.100	31.232	2.802	0.045	221.564
	95	19.300	79.500	77.474	3.039	0.277	45.528
	145	19.300	49.000	48.236	1.146	0.119	34.025
	198	19.300	49.000	48.124	1.315	0.119	39.790
0.459	45	19.200	31.600	29.668	2.899	0.039	261.943
	95	19.200	56.500	54.441	3.089	0.150	79.961
	145	19.200	43.000	42.228	1.158	0.092	44.394
	198	19.200	45.000	44.107	1.340	0.100	47.735
0.519	45	19.500	31.600	29.697	2.855	0.038	264.882
	95	19.500	48.500	46.453	3.070	0.110	105.296
	145	19.500	38.000	37.227	1.160	0.069	59.023
	198	19.500	41.000	40.102	1.347	0.081	58.880
0.579	45	19.800	32.600	30.715	2.827	0.041	244.711
	95	19.800	45.000	42.903	3.146	0.093	126.714
	145	19.800	34.000	33.211	1.184	0.051	81.010
	198	19.800	36.000	35.111	1.333	0.059	79.792
0.639	45	19.800	33.600	31.649	2.927	0.045	233.224
	95	19.800	43.500	41.441	3.089	0.086	133.015
	145	19.800	32.000	31.236	1.146	0.043	92.445
	198	19.800	33.000	32.095	1.358	0.047	102.268

Table A.1.12

1. Exp. No. : 4012
2. Date : 900304
3. Static Bed Hei. (cm) : 29.00
4. Plate Rad. Loc. (cm) : 14.00

Uo(m/s)	Ht.(cm)	To(C)	Tj(C)	Tw(C)	Q(w)	Qr(w)	h_s+h_f(W/m²·K)
0.279	45	19.500	50.600	48.716	2.826	0.121	88.767
	95	19.500	99.500	97.491	3.014	0.410	32.014
	145	19.500	56.000	55.248	1.128	0.152	26.154
	198	19.500	55.000	54.132	1.302	0.147	31.988
0.339	45	19.700	38.600	36.709	2.837	0.066	156.207
	95	19.700	92.500	90.479	3.032	0.360	36.207
	145	19.700	53.000	52.244	1.134	0.137	29.369
	198	19.700	52.000	51.136	1.296	0.131	35.515
0.399	45	19.700	33.100	31.226	2.811	0.044	230.222
	95	19.700	80.500	78.585	2.872	0.282	42.172
	145	19.700	48.000	47.247	1.130	0.113	35.406
	198	19.700	49.000	48.148	1.277	0.117	39.102
0.459	45	20.000	31.600	29.697	2.855	0.036	278.717
	95	20.000	59.500	57.474	3.039	0.162	73.614
	145	20.000	43.000	42.239	1.142	0.089	45.407
	198	20.000	45.500	44.632	1.302	0.100	46.805
0.519	45	20.000	31.100	29.220	2.820	0.035	289.657
	95	20.000	51.000	48.992	3.012	0.120	95.630
	145	20.000	38.000	37.235	1.148	0.067	60.136
	198	20.000	42.000	41.140	1.290	0.084	54.666
0.579	45	19.800	32.600	30.726	2.811	0.041	243.071
	95	19.800	47.500	45.456	3.067	0.104	110.703
	145	19.800	35.000	34.263	1.106	0.056	69.649
	198	19.800	37.000	36.136	1.296	0.063	72.340
0.639	45	20.000	32.600	30.720	2.820	0.041	248.579
	95	20.000	45.500	43.505	2.993	0.095	118.208
	145	20.000	33.000	32.267	1.100	0.047	82.341
	198	20.000	34.000	33.136	1.296	0.050	90.921

Table A.1.13

1. Exp. No. : 4013
2. Date : 900309
3. Static Bed Hei. (cm) : 29.00
4. Plate Rad. Loc. (cm) : 0.00

Uo(m/s)	Ht.(cm)	To(C)	Tj(C)	Tw(C)	Q(w)	Qr(w)	h_c+h_f(W/m²·K)
0.279	45	20.900	69.000	63.390	2.248	0.095	97.040
	95	20.900	109.000	103.592	1.815	0.226	36.833
	145	20.900	62.000	59.655	0.768	0.085	33.766
	198	20.900	63.000	60.531	0.815	0.088	35.176
0.339	45	21.100	54.000	48.483	2.381	0.057	162.574
	95	21.100	105.000	99.085	2.065	0.208	45.619
	145	21.100	60.000	57.676	0.771	0.080	36.215
	198	21.100	61.000	58.565	0.813	0.082	37.368
0.399	45	21.200	45.000	39.467	2.507	0.036	259.090
	95	21.200	96.000	90.076	2.140	0.176	54.615
	145	21.200	56.000	53.709	0.782	0.070	41.986
	198	21.200	57.000	54.552	0.845	0.072	44.418
0.459	45	21.400	44.000	38.578	2.467	0.034	271.288
	95	21.400	81.000	75.323	2.160	0.128	72.179
	145	21.400	50.000	47.650	0.857	0.055	58.561
	198	21.400	53.000	50.565	0.871	0.061	53.189
0.519	45	21.600	46.000	40.527	2.468	0.038	245.967
	95	21.600	69.000	63.199	2.350	0.093	103.937
	145	21.600	43.000	40.756	0.876	0.038	83.740
	198	21.600	48.000	45.612	0.895	0.049	67.479
0.579	45	22.000	47.000	41.560	2.444	0.040	235.474
	95	22.000	65.000	59.308	2.346	0.082	116.242
	145	22.000	40.000	37.756	0.913	0.031	107.226
	198	22.000	43.000	40.612	0.951	0.037	93.991
0.639	45	22.500	48.000	42.592	2.421	0.041	226.887
	95	22.500	63.000	57.066	2.498	0.076	134.232
	145	22.500	38.000	35.820	0.910	0.026	127.141
	198	22.500	39.000	36.612	1.002	0.028	132.289

Table A.1.14

1. Exp. No. : 4014
2. Date : 900309
3. Static Bed Hei. (cm) : 29.00
4. Plate Rad. Loc. (cm) : 3.00

Uo(m/s)	Ht.(cm)	To(C)	Tj(C)	Tw(C)	Q(w)	Qr(w)	h_s+h_f(W/m²·K)
0.279	45	22.800	72.000	66.673	2.096	0.101	87.120
	95	22.800	108.000	102.245	1.985	0.217	42.640
	145	22.800	63.000	60.740	0.738	0.085	32.984
	198	22.800	61.000	58.532	0.838	0.079	40.702
0.339	45	22.900	55.000	49.446	2.410	0.056	169.856
	95	22.900	108.000	102.049	2.074	0.216	44.965
	145	22.900	62.000	59.603	0.801	0.081	37.578
	198	22.900	60.000	57.457	0.879	0.076	44.498
0.399	45	23.200	50.000	44.501	2.450	0.044	216.373
	95	23.200	94.000	88.018	2.202	0.166	60.182
	145	23.200	57.000	54.615	0.831	0.068	46.546
	198	23.200	57.000	54.420	0.921	0.068	52.349
0.459	45	23.300	47.000	41.520	2.482	0.037	257.027
	95	23.300	78.000	72.187	2.276	0.116	84.674
	145	23.300	51.000	48.558	0.909	0.053	64.899
	198	23.300	54.000	51.433	0.941	0.060	60.015
0.519	45	23.500	48.000	42.520	2.471	0.039	244.951
	95	23.500	69.000	62.996	2.473	0.089	115.620
	145	23.500	45.000	42.531	0.985	0.039	95.272
	198	23.500	50.000	47.495	0.951	0.050	71.922
0.579	45	23.600	49.000	43.520	2.459	0.041	232.534
	95	23.600	65.000	59.214	2.412	0.079	125.503
	145	23.600	41.000	38.542	1.027	0.030	127.823
	198	23.600	46.000	43.482	1.000	0.041	92.387
0.639	45	23.800	50.000	44.501	2.458	0.043	223.479
	95	23.800	63.000	57.195	2.448	0.074	136.222
	145	23.800	39.000	36.536	1.057	0.025	155.188
	198	23.800	41.000	38.470	1.066	0.029	135.331

Table A.1.15

1. Exp. No. : 4015
2. Date : 900309
3. Static Bed Hei. (cm) : 29.00
4. Plate Rad. Loc. (cm) : 6.00

Uo(m/s)	Ht.(cm)	To(C)	Tj(C)	Tw(C)	Q(w)	Qr(w)	h_c+h_r(W/m^2·K)
0.279	45	23.800	77.000	71.532	2.123	0.113	80.680
	95	23.800	111.000	105.035	2.066	0.226	43.387
	145	23.800	65.000	62.720	0.742	0.088	32.163
	198	23.800	64.000	61.470	0.853	0.085	39.056
0.339	45	23.800	58.000	52.557	2.327	0.062	150.907
	95	23.800	103.000	97.144	2.074	0.196	49.045
	145	23.800	63.000	60.700	0.760	0.083	35.157
	198	23.800	62.000	59.433	0.882	0.079	43.159
0.399	45	24.200	51.000	45.520	2.440	0.044	215.296
	95	24.200	89.000	83.112	2.212	0.148	67.128
	145	24.200	59.000	56.664	0.802	0.071	43.116
	198	24.200	59.000	56.433	0.907	0.071	49.702
0.459	45	24.300	48.000	42.557	2.463	0.037	254.474
	95	24.300	81.000	75.069	2.314	0.122	82.682
	145	24.300	53.000	50.672	0.846	0.056	57.346
	198	24.300	55.000	52.420	0.947	0.061	60.407
0.519	45	24.500	48.000	42.520	2.484	0.037	260.167
	95	24.500	71.000	65.126	2.397	0.093	108.624
	145	24.500	47.000	44.684	0.899	0.042	81.391
	198	24.500	51.000	48.470	0.963	0.051	72.923
0.579	45	24.800	50.000	44.501	2.471	0.041	236.292
	95	24.800	67.000	61.107	2.457	0.082	125.299
	145	24.800	43.000	40.709	0.934	0.032	108.582
	198	24.800	46.000	43.445	1.031	0.039	102.018
0.639	45	25.000	52.000	46.483	2.457	0.045	215.046
	95	25.000	64.000	58.034	2.532	0.073	142.581
	145	25.000	41.000	38.712	0.959	0.028	130.049
	198	25.000	42.000	39.383	1.112	0.029	144.222

Table A.1.16

1. Exp. No. : 4016
2. Date : 900309
3. Static Bed Hei. (cm) : 29.00
4. Plate Rad. Loc. (cm) : 9.00

Uo(m/s)	Ht.(cm)	To(C)	Tj(C)	Tw(C)	Q(w)	Qr(w)	h_c+h_r(W/m²·K)
0.279	45	24.100	75.000	69.520	2.153	0.106	86.335
	95	24.100	115.000	109.130	2.000	0.241	39.629
	145	24.100	66.000	63.688	0.752	0.090	32.014
	198	24.100	65.000	62.470	0.849	0.087	38.029
0.339	45	24.000	57.000	51.612	2.314	0.059	156.434
	95	24.000	110.000	103.920	2.125	0.221	45.649
	145	24.000	63.000	60.720	0.752	0.082	34.947
	198	24.000	62.000	59.470	0.867	0.079	42.551
0.399	45	24.000	50.000	44.538	2.441	0.043	223.765
	95	24.000	94.000	87.916	2.257	0.164	62.754
	145	24.000	58.000	55.697	0.793	0.069	43.730
	198	24.000	58.000	55.433	0.913	0.069	51.484
0.459	45	24.100	47.000	41.594	2.454	0.036	264.872
	95	24.100	80.000	74.029	2.341	0.120	85.247
	145	24.100	52.000	49.649	0.864	0.054	60.696
	198	24.100	55.000	52.395	0.957	0.061	60.686
0.519	45	24.300	47.000	41.557	2.476	0.035	270.961
	95	24.300	70.000	64.048	2.445	0.091	113.467
	145	24.300	47.000	44.593	0.942	0.042	84.969
	198	24.300	51.000	48.445	0.973	0.051	73.165
0.579	45	24.500	49.000	43.470	2.496	0.039	248.107
	95	24.500	65.000	59.031	2.515	0.077	135.267
	145	24.500	43.000	40.695	0.938	0.033	107.001
	198	24.500	46.000	43.309	1.096	0.039	107.675
0.639	45	25.000	49.000	43.470	2.503	0.038	255.615
	95	25.000	62.000	56.088	2.529	0.068	151.642
	145	25.000	42.000	39.604	1.001	0.030	127.381
	198	25.000	43.000	40.433	1.075	0.031	129.520

Table A.1.17

1. Exp. No. : 4017
2. Date : 900310
3. Static Bed Hei. (cm) : 29.00
4. Plate Rad. Loc. (cm) : 12.00

Uo(m/s)	Ht.(cm)	To(C)	Tj(C)	Tw(C)	Q(w)	Qr(w)	h_c+h_f(W/m²·K)
0.279	45	24.500	76.000	70.427	2.193	0.108	86.937
	95	24.500	107.000	101.096	2.071	0.209	46.561
	145	24.500	65.000	62.700	0.753	0.087	33.434
	198	24.500	64.000	61.333	0.918	0.083	43.402
0.339	45	22.000	54.000	48.270	2.500	0.055	178.304
	95	22.000	110.000	103.688	2.216	0.224	46.711
	145	22.000	63.000	60.620	0.784	0.086	34.616
	198	22.000	62.000	59.334	0.914	0.082	42.648
0.399	45	22.400	47.500	41.789	2.581	0.039	251.091
	95	22.400	95.500	89.326	2.273	0.171	60.143
	145	22.400	59.000	56.664	0.790	0.075	39.988
	198	22.400	58.000	55.371	0.929	0.072	49.823
0.459	45	22.700	44.000	38.377	2.587	0.031	312.316
	95	22.700	76.000	69.770	2.497	0.110	97.173
	145	22.700	55.000	52.708	0.800	0.064	46.974
	198	22.700	55.000	52.408	0.939	0.064	56.445
0.519	45	22.800	44.000	38.483	2.534	0.031	305.751
	95	22.800	63.000	56.996	2.536	0.075	137.885
	145	22.800	47.000	44.739	0.855	0.045	70.731
	198	22.800	49.000	46.472	0.965	0.049	74.116
0.579	45	22.800	44.000	38.501	2.525	0.031	304.230
	95	22.800	59.000	53.054	2.556	0.065	157.756
	145	22.800	43.000	40.727	0.902	0.036	92.569
	198	22.800	45.000	42.497	0.994	0.040	92.799
0.639	45	22.900	44.000	38.532	2.510	0.031	303.794
	95	22.900	56.000	49.952	2.648	0.057	183.434
	145	22.900	41.000	38.747	0.916	0.032	106.914
	198	22.900	42.000	39.470	1.043	0.033	116.720

Table A.1.18

1. Exp. No. : 4018
2. Date : 900310
3. Static Bed Hei. (cm) : 29.00
4. Plate Rad. Loc. (cm) : 14.00

Uo(m/s)	Ht.(cm)	To(C)	Tj(C)	Tw(C)	Q(w)	Qr(w)	h_a+h_f(W/m^2·K)
0.279	45	22.300	71.000	65.509	2.182	0.099	92.375
	95	22.300	118.000	112.029	2.015	0.256	37.561
	145	22.300	64.000	61.735	0.733	0.088	31.326
	198	22.300	62.000	59.485	0.849	0.082	39.507
0.339	45	22.400	54.000	48.496	2.391	0.055	171.485
	95	22.400	110.000	104.162	2.006	0.225	41.734
	145	22.400	61.000	58.756	0.739	0.080	34.736
	198	22.400	60.000	57.508	0.852	0.077	42.315
0.399	45	22.600	46.000	40.477	2.507	0.036	264.809
	95	22.600	97.000	90.957	2.199	0.177	56.682
	145	22.600	57.000	54.723	0.778	0.070	42.269
	198	22.600	56.000	53.495	0.889	0.066	51.008
0.459	45	22.600	43.000	37.459	2.557	0.030	325.911
	95	22.600	83.000	77.018	2.300	0.131	76.352
	145	22.600	54.000	51.697	0.812	0.062	49.378
	198	22.600	54.000	51.483	0.912	0.062	56.379
0.519	45	22.700	44.000	38.404	2.573	0.031	310.084
	95	22.700	67.000	61.047	2.462	0.086	118.698
	145	22.700	47.000	44.765	0.842	0.045	69.175
	198	22.700	49.000	46.231	1.082	0.049	84.073
0.579	45	22.700	43.000	37.491	2.542	0.029	325.463
	95	22.700	62.000	55.980	2.556	0.073	142.946
	145	22.700	42.000	39.639	0.957	0.034	104.336
	198	22.700	45.000	42.445	1.019	0.040	94.984
0.639	45	23.000	45.000	39.557	2.486	0.033	283.740
	95	23.000	60.000	54.105	2.521	0.067	151.122
	145	23.000	40.000	37.695	0.955	0.029	120.649
	198	23.000	42.000	39.483	1.038	0.033	116.785

Table A.1.19

1. Exp. No. : 4019
2. Date : 900307
3. Static Bed Hei. (cm) : 29.00
4. Plate Rad. Loc. (cm) : 0.00

Uo(m/s)	Ht.(cm)	To(C)	Tj(C)	Tw(C)	Q(w)	Qr(w)	h_s+h_f(W/m²·K)
0.279	56	18.000	92.000	85.945	2.208	0.168	57.507
	101	18.000	111.000	104.543	2.245	0.234	44.507
	153	18.000	64.000	61.518	0.802	0.095	31.091
	204	18.000	64.000	61.164	0.950	0.094	37.960
0.339	56	18.000	73.000	67.095	2.319	0.111	86.156
	101	18.000	104.000	97.634	2.255	0.209	49.219
	153	18.000	61.000	58.589	0.786	0.088	32.979
	204	18.000	62.000	59.255	0.922	0.089	38.684
0.399	56	18.100	60.000	54.199	2.414	0.076	124.041
	101	18.100	89.000	82.847	2.282	0.158	62.839
	153	18.100	55.000	52.620	0.807	0.072	40.770
	204	18.100	56.000	53.306	0.941	0.074	47.157
0.459	56	18.200	54.000	48.200	2.487	0.062	154.910
	101	18.200	72.000	65.856	2.449	0.107	94.169
	153	18.200	49.000	46.562	0.879	0.058	55.504
	204	18.200	51.000	48.242	1.013	0.062	60.643
0.519	56	18.400	49.000	43.182	2.563	0.050	194.267
	101	18.400	60.000	54.036	2.500	0.075	130.323
	153	18.400	45.000	42.550	0.923	0.048	69.430
	204	18.400	47.000	44.331	1.009	0.052	70.700
0.579	56	18.600	47.000	41.182	2.591	0.045	216.035
	101	18.600	54.000	47.741	2.725	0.060	175.228
	153	18.600	41.000	38.534	0.974	0.039	89.873
	204	18.600	44.000	41.434	0.992	0.045	79.397
0.639	56	18.800	45.000	39.253	2.584	0.040	238.260
	101	18.800	51.000	44.813	2.730	0.053	197.150
	153	18.800	37.000	34.522	1.028	0.030	121.531
	204	18.800	41.000	38.332	1.076	0.038	101.820

Table A.1.20

1. Exp. No. : 4020
2. Date : 900307
3. Static Bed Hei. (cm) : 29.00
4. Plate Rad. Loc. (cm) : 3.00

Uo(m/s)	Ht.(cm)	To(C)	Tj(C)	Tw(C)	Q(w)	Qr(w)	h_s+h_f(W/m²·K)
0.279	56	18.500	94.000	88.467	1.953	0.176	48.665
	101	18.500	116.000	109.946	2.039	0.255	37.390
	153	18.500	64.000	61.672	0.743	0.095	28.748
	204	18.500	63.000	60.373	0.869	0.091	35.577
0.339	56	18.700	73.000	67.360	2.196	0.110	82.113
	101	18.700	107.000	100.811	2.158	0.219	45.230
	153	18.700	58.000	55.604	0.800	0.079	37.421
	204	18.700	59.000	56.371	0.895	0.081	41.413
0.399	56	18.800	58.000	52.289	2.401	0.070	133.319
	101	18.800	93.000	87.117	2.126	0.171	54.823
	153	18.800	53.000	50.626	0.823	0.066	45.546
	204	18.800	54.000	51.397	0.920	0.068	50.062
0.459	56	19.000	53.000	47.551	2.333	0.059	152.585
	101	19.000	75.000	69.088	2.311	0.115	84.025
	153	19.000	47.000	44.638	0.868	0.052	60.990
	204	19.000	49.000	46.409	0.959	0.056	63.096
0.519	56	19.200	51.000	45.551	2.360	0.054	167.691
	101	19.200	63.000	57.140	2.421	0.082	118.114
	153	19.200	42.000	39.638	0.919	0.040	82.333
	204	19.200	46.000	43.433	0.978	0.049	73.468
0.579	56	19.300	48.000	42.501	2.425	0.047	196.394
	101	19.300	57.000	51.140	2.494	0.067	146.063
	153	19.300	39.000	36.606	0.968	0.034	103.479
	204	19.300	43.000	40.433	1.010	0.042	87.767
0.639	56	19.600	45.000	39.514	2.462	0.039	233.031
	101	19.600	54.000	48.175	2.518	0.059	164.836
	153	19.600	36.000	33.593	1.014	0.027	135.096
	204	19.600	39.000	36.348	1.101	0.033	122.158

Table A.1.21

1. Exp. No. : 4021
2. Date : 900308
3. Static Bed Hei. (cm) : 29.00
4. Plate Rad. Loc. (cm) : 6.00

Uo(m/s)	Ht.(cm)	To(C)	Tj(C)	Tw(C)	Q(w)	Qr(w)	h_c+h_r(W/m^2·K)
0.279	56	18.100	94.000	88.353	2.002	0.176	49.803
	101	18.100	115.000	108.881	2.071	0.251	38.406
	153	18.100	62.000	59.640	0.761	0.090	30.948
	204	18.100	62.000	59.420	0.852	0.090	35.353
0.339	56	18.600	75.000	69.396	2.157	0.116	76.966
	101	18.600	102.000	95.694	2.247	0.200	50.862
	153	18.600	58.000	55.667	0.772	0.079	35.801
	204	18.600	58.000	55.395	0.890	0.078	42.270
0.399	56	19.000	63.000	57.464	2.257	0.083	108.268
	101	19.000	91.000	85.095	2.154	0.164	57.706
	153	19.000	53.000	50.688	0.797	0.066	44.167
	204	19.000	54.000	51.408	0.917	0.068	50.175
0.459	56	19.100	55.000	49.501	2.334	0.063	143.117
	101	19.100	74.000	68.018	2.357	0.111	87.958
	153	19.100	47.000	44.709	0.835	0.052	58.620
	204	19.100	49.000	46.470	0.931	0.056	61.236
0.519	56	19.300	49.000	43.587	2.368	0.049	182.944
	101	19.300	60.000	54.069	2.494	0.074	133.335
	153	19.300	42.000	39.638	0.920	0.040	82.854
	204	19.300	45.000	42.482	0.965	0.046	75.908
0.579	56	19.700	47.000	41.520	2.434	0.044	209.857
	101	19.700	54.000	48.118	2.548	0.059	167.787
	153	19.700	37.000	34.583	1.007	0.029	125.985
	204	19.700	42.000	39.507	0.989	0.039	91.818
0.639	56	19.800	45.000	39.520	2.462	0.039	235.338
	101	19.800	52.000	46.078	2.595	0.054	185.262
	153	19.800	35.000	32.597	1.026	0.024	149.919
	204	19.800	40.000	37.433	1.049	0.035	110.214

Table A.1.22

1. Exp. No. : 4022
2. Date : 900308
3. Static Bed Hei. (cm) : 29.00
4. Plate Rad. Loc. (cm) : 9.00

Uo(m/s)	Ht.(cm)	To(C)	Tj(C)	Tw(C)	Q(w)	Qr(w)	h_s+h_f(W/m²·K)
0.279	56	19.700	93.000	87.637	1.892	0.171	48.550
	101	19.700	119.000	113.048	1.987	0.265	35.338
	153	19.700	62.000	59.806	0.702	0.088	29.335
	204	19.700	62.000	59.507	0.824	0.087	35.476
0.339	56	19.600	72.000	66.569	2.113	0.106	81.855
	101	19.600	112.000	106.105	2.001	0.238	39.049
	153	19.600	58.000	55.783	0.729	0.078	34.468
	204	19.600	59.000	56.507	0.841	0.079	39.528
0.399	56	19.800	58.000	52.574	2.270	0.069	128.608
	101	19.800	100.000	94.122	2.076	0.193	48.533
	153	19.800	53.000	50.783	0.760	0.065	42.971
	204	19.800	54.000	51.507	0.877	0.067	48.981
0.459	56	20.000	52.000	46.459	2.404	0.054	170.141
	101	20.000	81.000	74.701	2.449	0.129	81.246
	153	20.000	49.000	46.739	0.812	0.055	54.213
	204	20.000	50.000	47.458	0.936	0.057	61.329
0.519	56	20.300	49.000	43.477	2.437	0.047	197.566
	101	20.300	63.000	56.983	2.513	0.079	127.076
	153	20.300	44.000	41.747	0.856	0.043	72.652
	204	20.300	46.000	43.482	0.965	0.047	75.872
0.579	56	20.600	47.000	41.427	2.493	0.042	225.453
	101	20.600	57.000	50.993	2.585	0.064	158.875
	153	20.600	40.000	37.703	0.923	0.034	99.634
	204	20.600	44.000	41.434	1.013	0.042	89.286
0.639	56	20.900	43.000	37.361	2.584	0.032	296.943
	101	20.900	52.000	46.350	2.471	0.052	182.059
	153	20.900	35.000	32.759	0.958	0.023	151.037
	204	20.900	40.000	37.459	1.048	0.033	117.519

Table A.1.23

1. Exp. No. : 4023
2. Date : 900308
3. Static Bed Hei. (cm) : 29.00
4. Plate Rad. Loc. (cm) : 12.00

Uo(m/s)	Ht.(cm)	To(C)	Tj(C)	Tw(C)	Q(w)	Qr(w)	h_c+h_f(W/m²·K)
0.279	56	21.000	87.000	81.448	2.040	0.148	59.970
	101	21.000	123.000	117.034	1.980	0.279	33.932
	153	21.000	63.000	60.709	0.742	0.088	31.573
	204	21.000	64.000	61.495	0.826	0.090	34.798
0.339	56	21.200	65.000	59.400	2.291	0.084	110.678
	101	21.200	112.000	105.899	2.101	0.234	42.239
	153	21.200	59.000	56.697	0.768	0.077	37.312
	204	21.200	60.000	57.483	0.856	0.079	40.996
0.399	56	21.300	55.000	49.432	2.397	0.059	159.194
	101	21.300	101.000	95.215	2.037	0.194	47.769
	153	21.300	53.000	50.685	0.815	0.062	49.092
	204	21.300	56.000	53.495	0.879	0.069	48.199
0.459	56	21.900	52.000	46.564	2.375	0.051	180.516
	101	21.900	82.000	76.195	2.217	0.130	73.639
	153	21.900	48.000	45.695	0.858	0.049	65.146
	204	21.900	51.000	48.483	0.932	0.056	63.169
0.519	56	22.000	49.000	43.546	2.425	0.044	211.663
	101	22.000	68.000	62.038	2.447	0.090	112.785
	153	22.000	43.000	40.661	0.927	0.038	91.288
	204	22.000	47.000	44.409	1.008	0.046	82.233
0.579	56	22.200	45.000	39.484	2.512	0.035	274.601
	101	22.200	62.000	56.154	2.462	0.074	134.733
	153	22.200	40.000	37.747	0.920	0.031	109.506
	204	22.200	43.000	40.448	1.034	0.037	104.750
0.639	56	22.600	44.000	38.522	2.512	0.032	298.375
	101	22.600	57.000	51.164	2.523	0.061	165.159
	153	22.600	36.000	33.747	0.973	0.022	163.402
	204	22.600	39.000	36.544	1.038	0.028	138.816

Table A.1.24

1. Exp. No. : 4024
2. Date : 900308
3. Static Bed Hei. (cm) : 29.00
4. Plate Rad. Loc. (cm) : 13.50

Uo(m/s)	Ht.(cm)	To(C)	Tj(C)	Tw(C)	Q(w)	Qr(w)	h_s+h_f(W/m²·K)
0.279	56	22.200	89.000	83.455	2.030	0.152	58.735
	101	22.200	123.000	117.051	1.979	0.277	34.380
	153	22.200	64.000	61.747	0.728	0.088	30.975
	204	22.200	64.000	61.383	0.881	0.087	38.774
0.339	56	22.200	68.000	62.473	2.232	0.090	101.877
	101	22.200	114.000	107.992	2.054	0.240	40.511
	153	22.200	59.000	56.662	0.790	0.075	39.724
	204	22.200	60.000	57.532	0.841	0.077	41.381
0.399	56	22.100	56.000	50.514	2.352	0.060	154.556
	101	22.100	101.000	94.917	2.181	0.191	52.332
	153	22.100	54.000	51.763	0.778	0.063	46.182
	204	22.100	56.000	53.408	0.926	0.067	52.531
0.459	56	22.200	52.000	46.422	2.451	0.050	189.872
	101	22.200	82.000	75.955	2.337	0.129	78.699
	153	22.200	50.000	47.691	0.845	0.053	59.482
	204	22.200	52.000	49.445	0.944	0.057	62.319
0.519	56	22.700	50.000	44.441	2.474	0.045	214.070
	101	22.700	66.000	60.010	2.492	0.083	123.695
	153	22.700	44.000	41.723	0.893	0.039	86.002
	204	22.700	48.000	45.445	0.987	0.047	79.195
0.579	56	23.300	48.000	42.441	2.509	0.039	247.157
	101	23.300	59.000	52.974	2.603	0.064	163.940
	153	23.300	40.000	37.779	0.916	0.029	117.435
	204	23.300	44.000	41.557	0.982	0.037	99.106
0.639	56	23.300	49.000	43.422	2.505	0.041	234.513
	101	23.300	57.000	50.976	2.627	0.059	177.786
	153	23.300	37.000	34.709	0.988	0.022	162.172
	204	23.300	41.000	38.407	1.091	0.030	134.525

Table A.1.25

1. Exp. No. : 4025
2. Date : 900429
3. Static Bed Hei. (cm) : 29.00
4. Plate Rad. Loc. (cm) : 0.00

Type III, 90 deg. apart from Exp.No. 4013

Uo(m/s)	Ht.(cm)	To(C)	Tj(C)	Tw(C)	Q(w)	Qr(w)	h_c+h_f(W/m²·K)
0.279	45	29.000	80.000	73.730	2.543	0.109	104.236
	95	29.000	119.000	112.442	2.315	0.245	47.517
	145	29.000	68.000	65.442	0.873	0.086	41.399
	198	29.000	67.000	64.217	0.982	0.082	48.933
0.339	45	29.000	64.000	57.735	2.733	0.065	177.873
	95	29.000	115.000	108.309	2.407	0.229	52.617
	145	29.000	67.000	64.361	0.916	0.083	45.148
	198	29.000	66.000	63.166	1.013	0.079	52.364
0.399	45	29.400	59.000	52.660	2.842	0.051	229.813
	95	29.400	109.000	102.261	2.483	0.204	59.914
	145	29.400	64.000	61.407	0.921	0.074	50.683
	198	29.400	67.000	64.105	1.036	0.081	52.725
0.459	45	29.600	55.000	48.642	2.907	0.041	288.293
	95	29.600	92.000	85.281	2.641	0.144	85.884
	145	29.600	59.000	56.229	1.051	0.060	71.297
	198	29.600	60.000	57.098	1.105	0.062	72.650
0.519	45	29.200	50.000	44.607	2.476	0.033	303.836
	95	29.200	77.000	71.285	2.303	0.102	100.213
	145	29.200	49.000	46.649	0.946	0.037	99.714
	198	29.200	54.000	51.495	0.968	0.049	78.958
0.579	45	29.400	50.000	43.998	2.791	0.031	362.184
	95	29.400	73.000	66.694	2.648	0.088	131.470
	145	29.400	46.000	43.558	1.028	0.030	135.094
	198	29.400	50.000	47.307	1.107	0.039	114.335
0.639	45	29.400	54.000	47.935	2.768	0.040	281.951
	95	29.400	71.000	64.515	2.762	0.082	146.193
	145	29.400	44.000	41.569	1.048	0.025	160.957
	198	29.400	47.000	44.244	1.175	0.031	147.561

Table A.1.26

1. Exp. No. : 4026
2. Date : 900429
3. Static Bed Hei. (cm) : 29.00
4. Plate Rad. Loc. (cm) : 3.00

Type III, 90 deg. apart from Exp.No. 4014

Uo(m/s)	Ht.(cm)	To(C)	Tj(C)	Tw(C)	Q(w)	Qr(w)	h_c+h_f(W/m^2·K)
0.279	45	29.200	83.000	77.307	2.227	0.120	83.922
	95	29.200	131.000	124.931	2.028	0.298	34.610
	145	29.200	74.000	71.623	0.767	0.103	29.993
	198	29.200	71.000	68.384	0.881	0.093	38.501
0.339	45	29.300	64.000	57.688	2.761	0.064	181.987
	95	29.300	124.000	117.301	2.345	0.265	45.279
	145	29.300	71.000	68.391	0.879	0.093	38.487
	198	29.300	69.000	66.112	1.017	0.087	48.385
0.399	45	29.200	54.000	47.671	2.901	0.040	296.701
	95	29.200	109.000	102.260	2.482	0.205	59.707
	145	29.200	65.000	62.391	0.919	0.077	48.580
	198	29.200	64.000	61.168	1.030	0.074	57.338
0.459	45	29.400	50.000	43.576	3.007	0.030	402.284
	95	29.400	89.500	82.740	2.685	0.136	91.543
	145	29.400	57.500	54.870	0.996	0.057	70.629
	198	29.400	60.000	57.110	1.097	0.063	71.512
0.519	45	29.400	50.000	43.637	2.976	0.030	396.377
	95	29.400	77.000	70.220	2.838	0.098	128.560
	145	29.400	51.000	48.358	1.070	0.041	103.996
	198	29.400	55.000	52.122	1.143	0.050	92.111
0.579	45	29.500	50.000	43.666	2.963	0.030	396.589
	95	29.500	73.000	66.300	2.847	0.087	143.704
	145	29.500	47.000	44.396	1.099	0.032	137.320
	198	29.500	51.000	48.068	1.216	0.040	121.368
0.639	45	29.600	50.000	43.632	2.981	0.030	402.955
	95	29.600	71.000	64.300	2.873	0.081	154.148
	145	29.600	45.000	42.361	1.143	0.027	167.538
	198	29.600	48.000	45.085	1.245	0.033	149.942

Table A.1.27

1. Exp. No. : 4027
2. Date : 900430
3. Static Bed Hei. (cm) : 29.00
4. Plate Rad. Loc. (cm) : 6.00

Type III, 90 deg. apart from Exp.No. 4015

Uo(m/s)	Ht.(cm)	To(C)	Tj(C)	Tw(C)	Q(w)	Qr(w)	h_s+h_f(W/m^2·K)
0.279	45	28.400	78.000	72.154	2.348	0.106	98.177
	95	28.400	124.000	117.689	2.166	0.268	40.711
	145	28.400	70.000	67.475	0.843	0.092	36.790
	198	28.400	68.000	65.307	0.929	0.086	43.745
0.339	45	27.600	58.000	51.800	2.760	0.053	214.268
	95	27.600	117.000	110.263	2.401	0.239	50.097
	145	27.600	67.000	64.384	0.896	0.085	42.207
	198	27.600	65.000	62.147	1.018	0.079	52.070
0.399	45	28.500	54.000	47.706	2.873	0.041	282.488
	95	28.500	104.000	97.302	2.501	0.188	64.396
	145	28.500	62.000	59.350	0.956	0.070	55.030
	198	28.500	62.000	59.172	1.040	0.070	60.604
0.459	45	28.750	51.000	44.783	2.878	0.034	339.869
	95	28.750	83.000	76.379	2.681	0.118	103.090
	145	28.750	56.000	53.365	1.006	0.054	74.087
	198	28.750	58.000	55.172	1.080	0.059	74.051
0.519	45	29.000	51.000	44.765	2.891	0.033	347.209
	95	29.000	73.000	66.320	2.831	0.088	140.809
	145	29.000	49.000	46.348	1.094	0.037	116.653
	198	29.000	53.000	50.184	1.130	0.046	97.966
0.579	45	28.950	52.000	45.741	2.889	0.036	325.482
	95	28.950	70.000	63.320	2.867	0.080	155.376
	145	28.950	45.000	42.303	1.164	0.028	162.968
	198	28.950	48.000	45.197	1.181	0.035	135.154
0.639	45	29.100	51.000	44.812	2.868	0.033	345.649
	95	29.100	66.000	59.398	2.880	0.069	177.741
	145	29.100	43.000	40.393	1.146	0.023	190.409
	198	29.100	45.000	42.209	1.214	0.027	173.329

Table A.1.28

1. Exp. No. : 4028
2. Date : 900430
3. Static Bed Hei. (cm) : 29.00
4. Plate Rad. Loc. (cm) : 9.00

Type III, 90 deg. apart from Exp.No. 4016

Uo(m/s)	Ht.(cm)	To(C)	Tj(C)	Tw(C)	Q(w)	Qr(w)	h_s+h_f(W/m^2·K)
0.279	45	29.000	78.000	71.958	2.452	0.104	104.725
	95	29.000	120.000	113.535	2.265	0.250	45.677
	145	29.000	69.000	66.445	0.865	0.088	39.753
	198	29.000	67.000	64.271	0.957	0.082	47.491
0.339	45	29.100	61.000	54.900	2.689	0.058	195.408
	95	29.100	115.000	108.339	2.394	0.228	52.345
	145	29.100	67.000	64.388	0.905	0.082	44.630
	198	29.100	66.000	63.271	0.965	0.079	49.656
0.399	45	29.200	54.000	47.918	2.774	0.040	279.806
	95	29.200	102.000	95.339	2.508	0.179	67.452
	145	29.200	63.000	60.382	0.939	0.072	53.291
	198	29.200	63.000	60.222	1.014	0.071	58.225
0.459	45	29.500	52.000	45.789	2.872	0.035	333.621
	95	29.500	84.000	77.339	2.698	0.119	103.267
	145	29.500	57.000	54.331	1.020	0.055	74.456
	198	29.500	59.000	56.209	1.060	0.060	71.703
0.519	45	29.900	53.000	46.789	2.863	0.036	320.661
	95	29.900	76.000	69.339	2.796	0.095	131.202
	145	29.900	51.000	48.396	1.057	0.040	105.330
	198	29.900	55.000	52.160	1.130	0.049	92.990
0.579	45	30.000	53.000	46.753	2.883	0.036	325.537
	95	30.000	71.000	64.280	2.888	0.080	156.918
	145	30.000	48.000	45.343	1.120	0.033	135.756
	198	30.000	50.000	47.143	1.196	0.037	129.563
0.639	45	30.250	54.000	47.695	2.903	0.038	314.597
	95	30.250	69.000	62.220	2.947	0.074	172.119
	145	30.250	46.000	43.359	1.139	0.028	162.441
	198	30.250	48.000	45.143	1.224	0.032	153.331

Table A.1.29

1. Exp. No. : 4029
2. Date : 900430
3. Static Bed Hei. (cm) : 29.00
4. Plate Rad. Loc. (cm) : 12.00

Type III, 90 deg. apart from Exp.No. 4017

Uo(m/s)	Ht.(cm)	To(C)	Tj(C)	Tw(C)	Q(w)	Qr(w)	h_s+h_f(W/m^2·K)
0.279	45	30.500	79.000	72.923	2.476	0.104	107.098
	95	30.500	123.000	116.499	2.271	0.259	44.829
	145	30.500	72.000	69.399	0.876	0.094	38.548
	198	30.500	69.000	66.287	0.946	0.085	46.095
0.339	45	30.800	60.000	53.975	2.686	0.052	217.765
	95	30.800	113.000	106.518	2.341	0.218	53.708
	145	30.800	68.000	65.371	0.918	0.082	46.320
	198	30.800	66.000	63.234	0.996	0.076	54.356
0.399	45	30.750	55.000	49.080	2.699	0.040	277.851
	95	30.750	100.000	93.690	2.373	0.171	67.042
	145	30.750	64.000	61.427	0.922	0.071	53.150
	198	30.750	63.000	60.311	0.985	0.068	59.427
0.459	45	31.000	53.000	46.935	2.803	0.035	332.872
	95	31.000	84.000	77.573	2.599	0.117	102.076
	145	31.000	60.000	57.438	0.955	0.060	64.815
	198	31.000	61.000	58.238	1.041	0.062	68.838
0.519	45	31.200	54.000	47.882	2.820	0.036	319.616
	95	31.200	75.000	68.418	2.784	0.090	138.690
	145	31.200	55.000	52.303	1.073	0.047	93.127
	198	31.200	57.000	54.222	1.092	0.052	86.534
0.579	45	31.300	53.000	47.010	2.769	0.034	333.533
	95	31.300	70.000	63.535	2.788	0.076	161.183
	145	31.300	50.000	47.388	1.089	0.035	125.512
	198	31.300	52.000	49.299	1.110	0.039	113.924
0.639	45	31.300	54.000	48.010	2.756	0.036	311.732
	95	31.300	67.000	60.554	2.816	0.068	179.980
	145	31.300	48.000	45.388	1.113	0.030	147.257
	198	31.300	50.000	47.299	1.134	0.035	131.562

Table A.1.30

1. Exp. No. : 4030
2. Date : 900430
3. Static Bed Hei. (cm) : 29.00
4. Plate Rad. Loc. (cm) : 14.00

Type III, 90 deg. apart from Exp.No. 4018

Uo(m/s)	Ht.(cm)	To(C)	Tj(C)	Tw(C)	Q(w)	Qr(w)	h_c+h_r(W/m^2·K)
0.279	45	30.700	80.000	73.998	2.429	0.107	102.752
	95	30.700	124.000	117.497	2.267	0.263	44.233
	145	30.700	71.000	68.366	0.898	0.090	41.097
	198	30.700	70.000	67.287	0.940	0.087	44.661
0.339	45	30.800	63.000	56.829	2.721	0.059	195.937
	95	30.800	117.000	110.379	2.373	0.233	51.505
	145	30.800	69.000	66.303	0.941	0.084	46.210
	198	30.800	68.000	65.209	0.992	0.081	50.670
0.399	45	30.000	54.000	47.940	2.774	0.039	292.036
	95	30.000	101.000	94.516	2.440	0.175	67.268
	145	30.000	64.000	61.348	0.953	0.073	53.805
	198	30.000	63.000	60.263	1.002	0.070	59.005
0.459	45	29.000	53.000	46.735	2.878	0.038	306.809
	95	29.000	86.000	79.300	2.690	0.126	97.621
	145	29.000	60.000	57.315	0.995	0.064	62.991
	198	29.000	60.000	57.279	1.012	0.064	64.218
0.519	45	29.700	52.000	45.905	2.815	0.035	328.660
	95	29.700	74.000	67.438	2.768	0.090	135.966
	145	29.700	53.000	50.315	1.073	0.045	95.500
	198	29.700	56.000	53.238	1.078	0.052	83.504
0.579	45	29.500	52.000	45.812	2.860	0.035	331.787
	95	29.500	70.000	63.339	2.864	0.079	157.699
	145	29.500	49.000	46.326	1.111	0.036	122.339
	198	29.500	52.000	49.184	1.146	0.043	107.404
0.639	45	29.800	52.000	45.812	2.864	0.034	338.568
	95	29.800	66.000	59.339	2.919	0.068	184.916
	145	29.800	47.000	44.326	1.138	0.031	146.055
	198	29.800	49.000	46.238	1.158	0.035	130.869

Table A.1.31. Heat transfer coefficient from solids convection (h_s) - Experimental data (Plate I)

Uo	Plate location		h_s ($W/m^2 \cdot K$)						
(cm/s)	H (cm)	r(cm)	0	3	6	9	12	14	Avg.
28	45		68.1	51.6	58.1	53.7	64.5	61.4	59.5
	95		9.4	11.9	10.9	7.1	8.2	7.9	9.2
	145		3.0	4.5	3.6	2.5	4.7	3.7	3.7
	198		9.1	8.9	8.3	8.3	10.0	9.4	9.0
34	45		110.9	125.2	109.6	103.7	106.2	117.9	112.5
	95		11.6	8.6	13.4	10.8	10.0	9.4	10.9
	145		3.6	2.2	3.2	4.4	3.9	5.7	4.1
	198		8.8	8.7	9.0	7.7	9.9	10.6	9.1
40	45		200.1	196.0	166.4	155.0	157.6	156.8	172.0
	95		22.4	35.9	30.3	18.0	7.5	17.8	23.6
	145		4.8	11.7	10.1	10.3	9.5	11.6	9.7
	198		8.4	11.2	10.5	12.3	12.0	13.4	11.3
46	45		240.1	213.3	206.0	209.3	183.8	186.8	206.6
	95		60.8	58.4	55.5	47.9	46.9	45.7	52.5
	145		20.2	18.9	20.3	23.3	17.8	22.7	20.5
	198		16.5	15.5	18.1	19.0	18.0	21.0	18.0
52	45		269.2	247.0	205.0	210.7	203.5	220.1	225.9
	95		88.1	87.0	83.0	68.6	65.7	68.3	76.8
	145		34.8	37.4	39.0	35.4	35.1	41.6	37.2
	198		24.1	24.7	29.4	27.5	26.3	28.5	26.8
58	45		227.4	197.4	217.1	219.6	198.8	193.7	209.1
	95		103.4	99.4	102.9	80.8	77.4	76.4	90.1
	145		61.3	58.3	59.9	59.9	51.7	57.5	58.1
	198		43.2	35.2	38.0	37.6	38.7	34.5	37.9
64	45		219.5	185.8	194.3	179.1	199.8	179.6	193.0
	95		124.8	125.8	98.5	84.4	91.3	85.1	101.8
	145		90.7	80.0	76.8	73.8	64.3	78.4	77.3
	198		64.1	55.3	55.0	49.5	52.0	51.2	54.5

Table A.1.32. Heat transfer coefficient from solids convection (h_s) - Experimental data (Plate II)

Uo	Plate location		h_s (W/m²·K)						
(cm/s)	H (cm)	r(cm)	0	3	6	9	12	14	Avg.
28	45		66.8	65.6	59.1	68.3	63.0	67.3	65.0
	95		9.4	9.9	9.5	11.2	10.1	10.5	10.1
	145		3.3	4.1	4.2	5.3	4.0	4.7	4.3
	198		9.3	9.8	9.1	10.0	11.1	10.5	10.0
34	45		129.6	129.2	121.2	126.8	121.7	133.2	127.0
	95		10.2	11.0	12.3	11.1	12.4	13.2	11.8
	145		3.1	5.2	4.7	5.8	4.9	6.4	5.0
	198		9.6	10.5	10.0	11.0	30.7	12.5	14.1
40	45		202.0	202.2	186.3	185.2	197.1	205.7	196.4
	95		20.1	19.7	20.8	20.2	21.0	17.6	19.9
	145		7.1	9.8	9.6	11.8	9.5	10.9	9.8
	198		14.5	13.6	13.1	14.6	15.2	14.6	14.3
46	45		261.7	256.6	228.5	223.6	235.9	252.7	243.2
	95		51.9	52.1	52.1	50.6	54.0	47.6	51.4
	145		20.8	20.9	19.7	21.7	18.4	19.4	20.2
	198		21.3	23.6	21.7	19.3	21.7	20.8	21.4
52	45		257.3	268.6	209.8	257.9	237.9	262.7	249.0
	95		87.2	72.3	76.5	76.3	78.3	68.6	75.0
	145		36.2	38.7	36.8	35.2	32.0	33.1	35.3
	198		32.6	36.9	34.8	29.0	31.9	27.7	32.1
58	45		242.3	241.6	230.1	210.8	216.2	214.6	225.8
	95		86.4	85.1	89.3	88.9	98.2	82.2	88.4
	145		54.3	58.5	55.8	53.9	52.5	41.1	52.7
	198		50.7	63.8	54.8	53.5	51.3	43.8	53.0
64	45		211.8	184.3	107.0	189.9	203.5	218.9	202.6
	95		93.4	93.5	93.6	99.8	103.3	88.5	95.4
	145		74.7	69.9	71.7	71.0	62.7	52.6	67.1
	198		70.9	76.5	77.0	74.3	72.6	61.2	72.1

Table A.1.33. Heat transfer coefficient from solids convection (h_s) - Experimental data (Plate III)

Uo	Plate location		h_s ($W/m^2 \cdot K$)						
(cm/s)	H (cm)	r(cm)	0	3	6	9	12	14	Avg.
28	45		75.5	65.6	59.2	64.8	65.4	70.9	66.9
	95		15.3	21.1	21.9	18.1	25.1	16.1	19.4
	145		12.3	11.5	10.7	10.5	11.9	9.8	11.1
	198		13.7	19.2	17.6	16.5	21.9	18.0	17.8
34	45		139.6	146.9	127.9	133.4	155.3	148.8	142.0
	95		22.6	22.0	26.0	22.6	23.7	18.7	22.3
	145		13.2	14.6	12.2	11.9	11.6	11.7	12.5
	198		14.4	21.5	20.2	19.6	19.6	19.3	19.1
40	45		234.6	191.8	190.8	199.3	226.6	240.3	213.9
	95		30.1	35.7	42.6	38.3	35.6	32.2	35.8
	145		17.5	22.0	18.6	19.2	15.5	17.8	18.4
	198		19.9	27.8	25.2	27.0	25.3	26.5	25.3
46	45		245.3	231.0	228.5	238.9	286.3	299.9	255.0
	95		46.2	58.7	56.7	59.2	71.2	50.4	57.1
	145		32.6	38.9	31.3	34.7	21.0	21.4	30.3
	198		27.2	34.0	34.4	34.7	30.4	30.4	31.9
52	45		219.0	218.0	233.2	244.0	278.8	283.1	246.0
	95		76.9	88.6	81.6	86.5	110.9	91.7	89.0
	145		56.7	68.3	54.4	58.0	43.7	42.2	53.9
	198		40.5	44.9	45.9	46.2	47.1	57.0	46.9
58	45		207.0	204.0	207.8	219.6	275.7	297.0	235.2
	95		87.7	97.0	96.8	106.8	129.3	114.4	84.5
	145		78.7	99.3	80.1	78.5	64.3	75.8	79.5
	198		65.5	63.9	73.5	79.1	64.3	66.5	69.0
64	45		197.2	193.8	185.3	225.9	274.1	254.0	221.7
	95		104.5	106.5	112.9	121.9	153.7	121.4	120.3
	145		97.4	125.5	100.3	97.7	77.2	90.9	98.3
	198		103.0	105.6	114.5	99.8	87.0	87.1	99.4

Table A.1.34. Heat transfer coefficient from solids convection (h_s) - Experimental data (Plate IV)

Uo (cm/s)	Plate location H (cm)	r(cm)	h_s (W/m²·K) 0	3	6	9	12	13.5	Avg.
28	56		36.0	27.2	28.3	27.1	38.5	37.2	32.4
	101		23.0	15.9	16.9	13.8	12.4	12.9	15.8
	153		9.6	7.2	9.4	7.8	10.1	9.5	8.9
	204		16.5	14.1	13.9	14.0	13.3	17.3	14.8
34	56		63.2	59.1	54.0	58.9	87.7	78.9	66.9
	101		26.2	22.2	27.9	16.0	19.2	17.5	21.5
	153		10.0	14.4	12.8	11.4	14.3	16.7	13.3
	204		15.7	18.4	19.3	16.5	18.0	18.4	17.7
40	56		99.5	108.8	83.8	104.1	137.4	130.1	110.2
	101		38.3	30.3	33.2	24.0	23.3	27.8	29.5
	153		16.3	21.0	19.7	18.5	24.5	21.7	20.3
	204		22.7	25.5	26.5	24.5	23.7	28.0	25.0
46	56		128.9	126.6	117.0	144.1	154.5	163.9	139.2
	101		68.2	58.5	62.0	55.2	47.6	52.7	57.3
	153		29.5	35.0	32.6	28.2	39.1	33.5	33.0
	204		34.6	37.0	35.2	35.3	37.1	36.3	36.0
52	56		167.3	140.7	155.9	170.6	184.7	187.1	167.7
	101		103.3	91.1	106.3	100.1	85.8	96.7	97.2
	153		42.4	55.3	55.9	45.7	64.3	59.0	53.8
	204		43.7	46.4	48.9	48.9	55.2	52.2	59.2
58	56		187.5	167.9	181.4	197.0	246.1	218.7	199.8
	101		146.7	117.6	139.3	130.4	106.2	135.4	129.3
	153		61.4	75.0	97.5	71.1	81.0	88.9	79.2
	204		50.9	59.3	63.3	60.8	76.3	70.6	63.5
64	56		208.6	203.3	205.6	267.2	268.7	204.8	226.4
	101		167.5	135.1	155.6	152.4	135.5	148.1	149.0
	153		91.8	105.4	120.2	121.3	133.7	132.5	117.8
	204		72.1	92.5	80.5	87.8	109.1	10.8	91.1

Appendix 2

Experimental Data for Solids Concentration and Particle Size Distributuin Measurements

Table A.2.1. Solids concentration in the freeboard (Uo: 0.34 m/s)

Uo (m/s)	Sampling point H (cm)	Run	Solids concentration (kg/m3) r(cm) 0	6	9	12	13.5	Avg.*
0.34	52	1	0.249	0.210	0.297	0.343	0.384	
		2	0.285	0.281	0.266	0.441	0.400	
		3	0.272	0.408	0.224	0.315	0.414	
		4	0.305	0.357	0.318	0.339	0.421	
		avg.	0.278	0.314	0.277	0.360	0.405	0.360
0.34	104	avg.						
0.34	152	1	0.0157	0.0133	0.0157	0.0153	0.0144	
		2	0.0121	0.0127	0.0136	0.0137	0.0143	
		avg.	0.0139	0.0130	0.0147	0.0145	0.0144	0.0144
0.34	194	1	0.0098	0.0117	0.0115	0.0124	0.0123	
		2	0.0090	0.0105	0.0102	0.0122	0.0093	
		avg.	0.0094	0.0111	0.0109	0.0123	0.0108	0.0113

* Radially averaged $\bar{C} = \Sigma (C \cdot r^2)/(\Sigma r^2)$

Table A.2.2. Solids concentration in the freeboard (Uo: 0.40 m/s)

Uo (m/s)	Sampling point H (cm)	Run	Solids concentration (kg/m3) r(cm) 0	6	9	12	13.5	Avg.
0.40	52	1	2.970	2.470	1.703	1.870	1.550	
		2	4.300	1.990	1.902	1.660	1.608	
		3	2.400	2.320	2.001	2.062	2.516	
		4	3.990	2.590	2.781	2.424	1.681	
		avg.	3.420	2.340	2.097	2.004	1.839	1.980
0.40	104	avg.	0.075	0.086		0.092	0.092	0.091
0.40	152	1	0.0524	0.0496	0.0667	0.0644	0.0712	
		2	0.0462	0.0548	0.0572	0.0664	0.0675	
		avg.	0.0493	0.0522	0.0620	0.0654	0.0694	0.0653
0.40	194	1	0.0432	0.0451	0.0477	0.0580	0.0507	
		2		0.0488	0.0506	0.0553	0.0505	
		avg.	0.0432	0.0470	0.0492	0.0567	0.0506	0.0520

Table A.2.3. Solids concentration in the freeboard (Uo: 0.46 m/s)

Uo (m/s)	Sampling point H (cm)	Run	Solids concentration (kg/m3) r(cm) 0	6	9	12	13.5	Avg.
0.46	52	1	3.170	3.400	2.970	3.540	4.480	
		2	4.440	3.580	3.120	4.240	4.830	
		3	4.590	3.020	3.280	4.970	3.900	
		4	5.840	3.600	2.620	4.820	4.230	
		avg.	4.510	3.400	3.000	4.390	4.360	4.040
0.46	104	avg.	0.231	0.245	0.280	0.311	0.258	0.279
0.46	152	1	0.140	0.170	0.171	0.192	0.181	
		2	0.150	0.127	0.172	0.186	0.172	
		avg.	0.145	0.149	0.172	0.189	0.177	0.177
0.46	194	1	0.093	0.116	0.132	0.144	0.169	
		2	0.100	0.109	0.120	0.140	0.155	
		avg.	0.096	0.112	0.126	0.142	0.162	0.145

Table A.2.4. Solids concentration in the freeboard (Uo: 0.52 m/s)

Uo (m/s)	Sampling point H (cm)	Run	Solids concentration (kg/m3) r(cm) 0	6	9	12	13.5	Avg.
0.52	52	1	4.791	6.505	4.465	4.407	5.978	
		2	5.170	4.918	5.297	6.244	4.482	
		3	7.017	5.423	5.020	4.862	4.820	
		4	6.882	4.660	6.641	5.052	6.154	
		5			6.347	6.680		
		avg.	5.965	5.377	5.554	5.449	5.359	5.425
0.52	104	avg.	0.456	0.489	0.529	0.630	0.530	0.559
0.52	152	1	0.272	0.300	0.354	0.419	0.364	
		2	0.289	0.343	0.346	0.412	0.408	
		avg.	0.281	0.322	0.350	0.416	0.386	0.393
0.52	194	1	0.138	0.189	0.224	0.277	0.298	
		2	0.135	0.196	0.234	0.275	0.299	
		avg.	0.136	0.192	0.229	0.276	0.298	0.270

Table A.2.5. Solids concentration in the freeboard (Uo: 0.58 m/s)

Uo (m/s)	Sampling point H (cm)	Run	Solids concentration (kg/m3) r(cm) 0	6	9	12	13.5	Avg.
0.58	52	1	3.550	4.580	4.960	7.310	7.010	
		2	3.260	3.510	4.520	7.560	5.450	
		3	4.560	3.440	5.150	6.680	5.270	
		4	4.580	5.280	6.830	5.910	5.530	
		5		3.880				
		avg.	3.990	4.140	5.370	6.870	5.820	5.940
0.58	104	avg.	0.935	1.017	1.165	1.274	1.068	1.151
0.58	152	1	0.618	0.593	0.676	0.839	0.679	
		2	0.527	0.588	0.672	0.885	0.758	
		avg.	0.573	0.591	0.674	0.862	0.719	0.747
0.58	194	1	0.233	0.328	0.397	0.477	0.513	
		2	0.296	0.345	0.373	0.499	0.527	
		avg.	0.265	0.336	0.385	0.488	0.520	0.483

Table A.2.6. Solids concentration in the freeboard (Uo: 0.64 m/s)

Uo (m/s)	Sampling point H (cm)	Run	Solids concentration (kg/m3) r(cm) 0	6	9	12	13.5	Avg.
0.64	52	1	8.090	7.230	7.500	8.470	8.220	
		2	5.450	8.230	8.360	10.570	10.210	
		3	6.220	8.030	9.700	7.590	9.260	
		4	8.170	8.070	8.040	9.480	10.520	
		avg.	6.980	7.890	8.400	9.030	9.550	9.040
0.64	104	avg.	1.531	1.590	1.862	2.082	1.590	1.803
0.64	152	1	0.888	0.996	1.182	1.462	1.226	
		2	0.857	0.991	1.311	1.421	1.260	
		3	0.923	0.972	1.241	1.460	1.243	
		4	0.811	0.981	1.242	1.448	1.231	
		avg.	0.870	0.985	1.249	1.448	1.240	1.289
0.64	194	1	0.450	0.510	0.624	0.848	0.911	
		2	0.433	0.529	0.647	0.880	0.911	
		avg.	0.441	0.520	0.636	0.864	0.911	0.832

Table A.2.7. Particle size distribution of the sample solids in the column

Uo (m/s)	H (cm)	r (cm)	% Volume fraction								$\bar{d}_{p,mean}$ (μm)	Radially averaged $\bar{d}_p$ (μm)
			dp(μm) 150	106	75	53	38	27	19	14		
0.34	52	0	12.8	30.6	32.6	18.0	4.5	0.0	0.7	0.4	75.07	71.6
		9	10.3	29.7	32.2	20.1	7.4	0.0	0.0	0.0	73.96	
		12	8.3	24.8	36.7	22.9	6.0	0.5	0.5	0.0	70.75	
		13.5	5.4	23.1	36.4	25.2	8.1	0.3	0.7	0.4	66.47	
	104	0	0.0	6.5	28.8	43.0	21.5	0.0	0.0	0.0	54.87	55.6
		9	0.0	5.7	31.5	43.3	19.3	0.0	0.0	0.0	55.60	
		12	0.0	7.5	31.0	42.0	17.8	0.0	1.2	0.2	54.87	
		13.5	0.0	7.7	33.3	42.7	16.2	0.0	0.0	0.0	57.19	
	152	12	0.0	6.8	31.2	43.7	18.1	0.0	0.0	0.0	56.15	56.0
		13.5	0.0	6.2	31.3	43.9	18.5	0.0	0.0	0.0	55.84	
	194	0	0.0	3.7	24.9	45.1	26.1	0.0	0.0	0.0	52.50	52.0
0.46	52	0	15.5	33.6	34.5	13.2	1.4	1.0	0.2	0.2	81.43	80.0
		9	14.9	34.0	33.8	13.8	1.8	1.5	0.0	0.0	81.03	
		12	15.6	32.5	36.0	12.9	0.8	1.1	0.2	0.6	80.05	
		13.5	11.4	32.2	37.0	15.6	2.4	0.3	0.9	0.0	77.57	
	104	0	0.8	13.9	37.8	36.2	11.2	0.0	0.0	0.0	61.80	62.4
		9	0.0	14.4	40.3	35.1	9.9	0.0	0.0	0.0	62.66	
		12	0.0	14.8	39.7	35.1	10.2	0.0	0.0	0.0	62.51	
		13.5	1.5	15.6	37.1	34.6	10.9	0.0	0.0	0.0	62.83	
	152	0	0.0	11.9	36.1	38.8	13.1	0.0	0.0	0.0	59.87	60.4
		9	0.5	13.2	34.8	38.2	13.0	0.0	0.0	0.0	60.43	
		12	0.0	13.1	37.5	36.4	12.9	0.0	0.0	0.0	60.61	
		13.5	0.1	12.7	36.9	37.7	12.3	0.0	0.0	0.0	60.70	
	194	0	0.0	9.7	34.7	39.8	15.6	0.0	0.0	0.0	58.29	59.0
		9	0.0	10.5	35.1	39.7	14.6	0.0	0.0	0.0	58.81	
		12	0.0	11.6	35.3	39.4	13.6	0.0	0.0	0.0	59.47	
		13.5	0.0	11.9	34.8	38.6	14.5	0.0	0.0	0.0	59.31	
0.58	52	0	17.5	37.5	32.9	8.8	2.2	0.9	0.0	0.0	85.74	84.3
		9	16.1	35.6	32.9	11.3	2.0	1.7	0.1	0.1	81.76	
		12	17.1	36.4	32.9	10.2	1.8	0.9	0.4	0.0	84.01	
		13.5	14.7	34.4	38.9	11.9	0.0	0.0	0.0	0.0	85.78	
	104	0	6.2	25.8	39.2	23.4	3.9	0.6	0.6	0.0	71.16	71.9
		9	4.9	23.1	40.8	26.2	4.8	0.0	0.0	0.0	70.66	
		12	7.4	27.5	40.5	19.9	3.5	0.4	0.5	0.0	73.67	
		13.5	5.2	24.7	40.5	25.8	3.6	0.0	0.0	0.0	71.98	
	152	0	3.0	19.7	40.9	28.9	5.7	0.2	1.2	0.0	65.92	68.1
		9	3.5	22.0	41.8	26.1	5.1	0.5	0.6	0.0	68.26	
		12	3.5	22.5	41.0	28.2	4.5	0.0	0.0	0.0	69.80	
		13.5	3.3	20.4	41.4	29.2	5.5	0.0	0.0	0.0	68.39	
	194	0	2.9	19.8	38.1	31.0	8.1	0.0	0.0	0.0	66.13	66.6
		9	3.3	20.2	37.8	31.1	7.4	0.0	0.0	0.0	66.75	
		12	3.0	20.7	39.4	28.2	6.9	0.1	1.0	0.3	65.27	
		13.5	3.6	20.7	40.1	29.2	6.2	0.0	0.0	0.0	68.12	

Appendix 3

Data for Verification of the Heat Transfer Model

Table A.3.1. Calculation of solids flux and particle velocity in the lower freeboard

Uo m/s	Guo kg/m2.s	a 1/m		Port#1	Z=0.25	Z=0.35	Z=0.50
0.34	0.2952	3.3500	Z (m)	0.200	0.250	0.350	0.500
			$\bar{G}u$ (kg/m2.s)	0.1061	0.0899	0.0646	0.0395
			$\bar{G}d$ (kg/m2.s)	0.1043	0.0881	0.0629	0.0378
			$\bar{C}$ (kg/m3)	0.3680	0.3590	0.2880	0.2520
			$\bar{V}pu$(m/s)	0.2882	0.2503	0.2243	0.1567
			$\bar{V}pd$(m/s)	0.2835	0.2455	0.2183	0.1499
			$\bar{V}pa$(m/s)	0.2859	0.2480	0.2213	0.1534
0.40	1.4128	3.6940	Z (m)	0.180	0.250	0.350	0.500
			$\bar{G}u$ (kg/m2.s)	0.7333	0.5678	0.3945	0.2295
			$\bar{G}d$ (kg/m2.s)	0.7240	0.5584	0.3851	0.2202
			$\bar{C}$ (kg/m3)	1.9800	1.6550	1.2260	0.6270
			$\bar{V}pu$(m/s)	0.3704	0.3431	0.3218	0.3661
			$\bar{V}pd$(m/s)	0.3656	0.3374	0.3141	0.3511
			$\bar{V}pa$(m/s)	0.3680	0.3403	0.3180	0.3588
0.46	4.9305	3.7650	Z (m)	0.140	0.250	0.350	0.500
			$\bar{G}u$ (kg/m2.s)	2.9348	1.9479	1.3444	0.7748
			$\bar{G}d$ (kg/m2.s)	2.9010	1.9141	1.3105	0.7409
			$\bar{C}$ (kg/m3)	4.0400	3.0600	2.2370	1.1190
			$\bar{V}pu$(m/s)	0.7264	0.6366	0.6010	0.6924
			$\bar{V}pd$(m/s)	0.7181	0.6255	0.5859	0.6621
			$\bar{V}pa$(m/s)	0.7223	0.6311	0.5935	0.6776
0.52	7.8578	3.6360	Z (m)	0.120	0.250	0.350	0.500
			$\bar{G}u$ (kg/m2.s)	5.1293	3.2161	2.2509	1.3256
			$\bar{G}d$ (kg/m2.s)	5.0592	3.1459	2.1808	1.2555
			$\bar{C}$ (kg/m3)	5.4250	3.8820	2.8110	1.4880
			$\bar{V}pu$(m/s)	0.9455	0.8285	0.8008	0.8909
			$\bar{V}pd$(m/s)	0.9326	0.8104	0.7758	0.8438
			$\bar{V}pa$(m/s)	0.9391	0.8195	0.7885	0.8680
0.58	6.7180	3.0120	Z (m)	0.120	0.250	0.350	0.500
			$\bar{G}u$ (kg/m2.s)	4.7745	3.2582	2.4353	1.5843
			$\bar{G}d$ (kg/m2.s)	4.6322	3.1158	2.2929	1.4419
			$\bar{C}$ (kg/m3)	5.9400	4.4810	3.4100	2.0880
			$\bar{V}pu$(m/s)	0.8038	0.7271	0.7142	0.7588
			$\bar{V}pd$(m/s)	0.7798	0.6953	0.6724	0.6906
			$\bar{V}pa$(m/s)	0.7920	0.7116	0.6939	0.7263
0.64	14.0042	2.9310	Z (m)	0.130	0.250	0.350	0.500
			$\bar{G}u$ (kg/m2.s)	9.7328	6.8960	5.1861	3.4002
			$\bar{G}d$ (kg/m2.s)	9.4559	6.6190	4.9092	3.1233
			$\bar{C}$ (kg/m3)	9.0400	7.0360	5.4290	3.3570
			$\bar{V}pu$(m/s)	1.0766	0.9801	0.9553	1.0123
			$\bar{V}pd$(m/s)	1.0460	0.9407	0.9043	0.9304
			$\bar{V}pa$(m/s)	1.0615	0.9608	0.9305	0.9734

Table A.3.2. Calculation of solids flux and particle velocity in the higher freeboard

Uo m/s	Guo kg/m2.s	a 1/m		Port#2	Port#3	Port#4	Zf
0.34	0.0053	1.2270	Z (m)	0.72	1.20	1.62	1.72
			$\bar{G}u$ (kg/m2.s)	0.0033	0.0023	0.0018	0.0017
			$\bar{G}d$ (kg/m2.s)	0.0016	0.0006	0.0001	0.0000
			$\bar{C}$ (kg/m3)	0.0300	0.0144	0.0113	0.0106
			$\bar{V}pu$(m/s)	0.1091	0.1593	0.1594	0.1620
			$\bar{V}pd$(m/s)	0.0519	0.0400	0.0075	0.0000
			$\bar{V}pa$(m/s)	0.0907	0.1353	0.1526	0.1620
0.40	0.0206	1.2060	Z (m)	0.70	1.18	1.60	1.70
			$\bar{G}u$ (kg/m2.s)	0.0156	0.0117	0.0097	0.0094
			$\bar{G}d$ (kg/m2.s)	0.0062	0.0023	0.0003	0.0000
			$\bar{C}$ (kg/m3)	0.0910	0.0653	0.0520	0.0448
			$\bar{V}pu$(m/s)	0.1710	0.1787	0.1866	0.2090
			$\bar{V}pd$(m/s)	0.0681	0.0354	0.0065	0.0000
			$\bar{V}pa$(m/s)	0.1417	0.1551	0.1805	0.2090
0.46	0.1183	1.5180	Z (m)	0.66	1.14	1.56	1.66
			$\bar{G}u$ (kg/m2.s)	0.0678	0.0453	0.0354	0.0338
			$\bar{G}d$ (kg/m2.s)	0.0339	0.0114	0.0016	0.0000
			$\bar{C}$ (kg/m3)	0.2790	0.1770	0.1450	0.1370
			$\bar{V}pu$(m/s)	0.2429	0.2558	0.2441	0.2470
			$\bar{V}pd$(m/s)	0.1216	0.0646	0.0108	0.0000
			$\bar{V}pa$(m/s)	0.2024	0.2173	0.2343	0.2470
0.52	0.2441	1.5190	Z (m)	0.64	1.12	1.54	1.64
			$\bar{G}u$ (kg/m2.s)	0.1422	0.0944	0.0734	0.0701
			$\bar{G}d$ (kg/m2.s)	0.0721	0.0243	0.0033	0.0000
			$\bar{C}$ (kg/m3)	0.5590	0.3930	0.2700	0.2410
			$\bar{V}pu$(m/s)	0.2544	0.2403	0.2720	0.2910
			$\bar{V}pd$(m/s)	0.1290	0.0619	0.0123	0.0000
			$\bar{V}pa$(m/s)	0.2122	0.2038	0.2608	0.2910
0.58	0.6718	1.6080	Z (m)	0.64	1.12	1.54	1.64
			$\bar{G}u$ (kg/m2.s)	0.3344	0.2052	0.1508	0.1424
			$\bar{G}d$ (kg/m2.s)	0.1920	0.0629	0.0084	0.0000
			$\bar{C}$ (kg/m3)	1.1510	0.7470	0.4830	0.4200
			$\bar{V}pu$(m/s)	0.2905	0.2748	0.3121	0.3390
			$\bar{V}pd$(m/s)	0.1668	0.0842	0.0174	0.0000
			$\bar{V}pa$(m/s)	0.2454	0.2301	0.2966	0.3390
0.64	1.0518	1.3620	Z (m)	0.65	1.13	1.55	1.65
			$\bar{G}u$ (kg/m2.s)	0.5997	0.3914	0.2931	0.2769
			$\bar{G}d$ (kg/m2.s)	0.3228	0.1145	0.0162	0.0000
			$\bar{C}$ (kg/m3)	1.8030	1.2890	0.8320	0.7230
			$\bar{V}pu$(m/s)	0.3326	0.3037	0.3523	0.3830
			$\bar{V}pd$(m/s)	0.1790	0.0889	0.0195	0.0000
			$\bar{V}pa$(m/s)	0.2789	0.2551	0.3349	0.3830

Table A.3.3. Data for calculating Y and X (Eq. 5.18) and the calculated results

H1,H2, H3, H4: Experimental h_s for plate type I, II, III, IV.

Uo (m/s)	H (m)	$\bar{V}$,a m/s	$\bar{V}u$ m/s	$\bar{C}$ Kg/m3	$\bar{d}p$ μm	H1	H2	H3	H4 (w/m2.K)	Y1	Y2	Y3	Y4	X
0.34	0.45	0.295	0.305	0.407	73	113	127	142	82	7.0	6.3	5.6	12.2	121.0
0.34	0.95	0.110	0.123	0.022	58	11	12	22	25	23.2	21.3	11.6	15.2	1118.1
0.34	1.45	0.120	0.150	0.015	54	4	5	13	14	65.4	52.4	20.1	31.0	1350.6
0.34	1.98	0.160	0.159	0.011	52	9	14	19	18	36.7	23.7	17.5	24.8	1597.8
Uo (m/s)	H (m)	$\bar{V}$,a m/s	$\bar{V}u$ m/s	$\bar{C}$ Kg/m3	$\bar{d}p$ μm	H1	H2	H3	H4 (w/m2.K)	Y1	Y2	Y3	Y4	X
0.40	0.45	0.395	0.395	2.532	77	172	196	214	137	5.8	5.1	4.6	8.5	22.1
0.40	0.95	0.175	0.215	0.099	62	24	20	36	37	17.9	21.5	12.0	18.5	293.7
0.40	1.45	0.150	0.190	0.068	58	10	10	18	21	34.7	34.7	19.3	27.5	355.7
0.40	1.98	0.210	0.190	0.051	56	11	14	25	25	41.6	32.9	18.6	22.5	430.4
Uo (m/s)	H (m)	$\bar{V}$,a m/s	$\bar{V}u$ m/s	$\bar{C}$ Kg/m3	$\bar{d}p$ μm	H1	H2	H3	H4 (w/m2.K)	Y1	Y2	Y3	Y4	X
0.46	0.45	0.730	0.746	5.600	80	207	243	255	167	6.5	5.5	5.3	8.9	11.3
0.46	0.95	0.250	0.260	0.299	65	53	51	57	66	12.0	12.5	11.2	12.7	114.8
0.46	1.45	0.177	0.213	0.182	61	21	20	30	36	20.4	21.5	14.3	18.7	152.8
0.46	1.98	0.250	0.231	0.142	59	18	21	32	36	32.5	27.3	18.3	19.7	180.8
Uo (m/s)	H (m)	$\bar{V}$,a m/s	$\bar{V}u$ m/s	$\bar{C}$ Kg/m3	$\bar{d}p$ μm	H1	H2	H3	H4 (w/m2.K)	Y1	Y2	Y3	Y4	X
0.52	0.45	1.000	1.000	7.170	81	226	249	246	194	6.5	5.9	6.0	8.1	9.3
0.52	0.95	0.320	0.330	0.722	70	77	75	89	105	10.7	11.0	9.3	9.8	58.4
0.52	1.45	0.204	0.235	0.414	65	37	45	54	57	14.2	11.6	9.7	13.5	81.8
0.52	1.98	0.290	0.272	0.258	63	27	32	47	59	26.5	22.1	15.1	14.4	121.1
Uo (m/s)	H (m)	$\bar{V}$,a m/s	$\bar{V}u$ m/s	$\bar{C}$ Kg/m3	$\bar{d}p$ μm	H1	H2	H3	H4 (w/m2.K)	Y1	Y2	Y3	Y4	X
0.58	0.45	1.065	1.070	7.790	83	209	226	235	227	7.1	6.6	6.3	7.0	9.0
0.58	0.95	0.340	0.440	1.379	74	90	88	85	138	9.9	10.1	10.5	8.9	37.0
0.58	1.45	0.230	0.263	0.791	69	58	53	80	85	10.7	11.7	7.7	10.3	51.5
0.58	1.98	0.333	0.314	0.457	66	38	53	69	64	21.7	15.5	11.9	15.4	78.6
Uo (m/s)	H (m)	$\bar{V}$,a m/s	$\bar{V}u$ m/s	$\bar{C}$ Kg/m3	$\bar{d}p$ μm	H1	H2	H3	H4 (w/m2.K)	Y1	Y2	Y3	Y4	X
0.64	0.45	1.130	1.130	12.400	83	193	203	222	254	7.8	7.4	6.8	6.3	5.8
0.64	0.95	0.360	0.550	2.080	79	102	95	120	157	9.3	9.9	7.9	8.6	29.4
0.64	1.45	0.255	0.290	1.365	73	77	67	98	122	9.2	10.5	7.2	7.9	35.5
0.64	1.98	0.375	0.355	0.788	70	55	72	99	91	17.1	12.9	9.4	11.9	54.4

Table A.3.4. Data for comparison between calculated (Eq. 5.17) and experimental h,s

Uo	H	$\bar{V}$,a	$\bar{V}$u	$\bar{C}$	$\bar{d}$p	D.E	He1	He2	He3	He4	Hc1	Hc2	Hc3	Hc4
m/s	m	m/s	m/s	Kg/m3	μm	-	w/m2.K				w/m2.K			
0.34	0.45	0.295	0.305	0.407	73	0.920	113	127	142	82	49.8	42.8	59.6	65.0
0.34	0.95	0.110	0.123	0.022	58	1.000	11	12	22	25	2.6	2.0	3.2	4.4
0.34	1.45	0.120	0.150	0.015	54	1.000	4	5	13	14	2.3	1.7	2.8	4.3
0.34	1.98	0.160	0.159	0.011	52	1.000	9	14	19	18	2.4	1.8	3.0	3.6
0.40	0.45	0.395	0.395	2.532	77	0.816	172	196	214	137	125.3	127.7	144.3	138.9
0.40	0.95	0.175	0.215	0.099	62	0.997	24	20	36	37	14.0	11.2	17.1	24.4
0.40	1.45	0.150	0.190	0.068	58	1.000	10	10	18	21	9.8	7.7	11.9	17.9
0.40	1.98	0.210	0.190	0.051	56	0.998	11	14	25	25	11.3	8.9	13.9	15.0
0.46	0.45	0.730	0.746	5.600	80	0.572	207	243	255	167	190.6	204.2	217.4	194.2
0.46	0.95	0.250	0.260	0.299	65	0.977	53	51	57	66	40.9	35.2	48.9	56.1
0.46	1.45	0.177	0.213	0.182	61	0.998	21	20	30	36	22.8	19.1	27.4	37.7
0.46	1.98	0.250	0.231	0.142	59	0.989	18	21	32	36	27.9	23.0	33.7	35.9
0.52	0.45	1.000	1.000	7.170	81	0.454	226	249	246	194	215.0	233.1	244.8	211.6
0.52	0.95	0.320	0.330	0.722	70	0.920	77	75	89	105	75.3	69.5	88.5	93.9
0.52	1.45	0.204	0.235	0.414	65	0.990	37	45	54	57	40.7	36.3	48.3	60.8
0.52	1.98	0.290	0.272	0.258	63	0.968	27	32	47	59	44.1	37.8	52.8	55.4
0.58	0.45	1.065	1.070	7.790	83	0.418	209	226	235	227	216.3	234.5	246.1	211.6
0.58	0.95	0.340	0.440	1.379	74	0.881	90	88	85	138	97.5	94.8	113.4	130.8
0.58	1.45	0.230	0.263	0.791	69	0.973	58	53	80	85	59.7	56.0	70.0	83.6
0.58	1.98	0.333	0.314	0.457	66	0.935	38	53	69	64	65.6	58.7	77.6	78.9
0.64	0.45	1.130	1.130	12.400	83	0.399	193	203	222	254	228.7	253.1	259.4	220.9
0.64	0.95	0.360	0.550	2.080	79	0.829	102	95	120	157	110.8	110.1	128.3	150.9
0.64	1.45	0.255	0.290	1.365	73	0.946	77	67	98	122	78.2	76.3	90.9	103.3
0.64	1.98	0.375	0.355	0.788	70	0.884	55	72	99	91	88.1	82.1	103.3	101.7

Note: Hel, He2, He3, He4: Experimentally obtained h,s for Types I, II, III, IV, respectively.
Hcl, Hc2, Hc3, Hc4: Calculated h,s for Types I, II, III, IV, respectively.

Appendix 4

Calculation of Heat Loss from Corkboard Insulation for Plate Type III and IV

Referring to Figure A.4.1, plate heat loss from corkboard can be calculated as follows:

$$Q_i = A_0 \cdot \frac{(T_w - T_0)}{(\frac{A_0}{A_{ln}}) \cdot (\frac{B_i}{k_i}) + (\frac{1}{h})}$$

where

Q_i : insulation heat loss (W),

A_{ln} : logarithmic mean interface area of the corkboard insulation, A,ln = 12.0 cm2 for the plate,

A_0 : outer surface area of the corkboard insulation, A_0 = 16.4 cm^2 for the plate,

k_i : thermal conductivity of the corkboard, k_i = 0.04 W/m.K (ref. Perry, R. H. and D. Green, Perry's Chemical Engineers' Handbook, 6th ed., p.3-262, McGraw-Hill Inc., 1984),

B_i : thickness of the insulation corkboard, B_i = 0.3 cm,

h : suspension-to-surface heat transfer coefficient, calculated by iteration method:

a. First iteration

$$(h)_1 = \frac{(Q - Q_r)}{[A_p \cdot (T_w - T_0)]}$$

$$Q_{i1} = A_0 \cdot \frac{(T_w - T_0)}{(\frac{A_0}{A_{ln}}) \cdot (\frac{B_i}{k_i}) + (\frac{1}{(h)_1})}$$

where A_p is the exposed surface area of the steel plate, A_p = 5.22 cm^2.

b. Second iteration

$$(h)_2 = \frac{(Q - Q_r - Q_{i1})}{[A_p \cdot (T_w - T_0)]}$$

$$Q_{i2} = A_0 \cdot \frac{(T_w - T_0)}{(\frac{A_0}{A_{ln}}) \cdot (\frac{B_i}{k_i}) + (\frac{1}{(h)_2})}$$

c. Third iteration

$$(h)_3 = \frac{(Q - Q_r - Q_{i2})}{[A_p \cdot (T_w - T_0)]}$$

$$Q_{i3} = A_0 \cdot \frac{(T_w - T_0)}{(\frac{A_0}{A_{ln}}) \cdot (\frac{B_i}{k_i}) + (\frac{1}{(h)_3})}$$

Generally, three iterations are enough. h is then calculated as:

$$h = (h)_4 = \frac{(Q - Q_r - Q_{i3})}{[A_p \cdot (T_w - T_0)]}$$

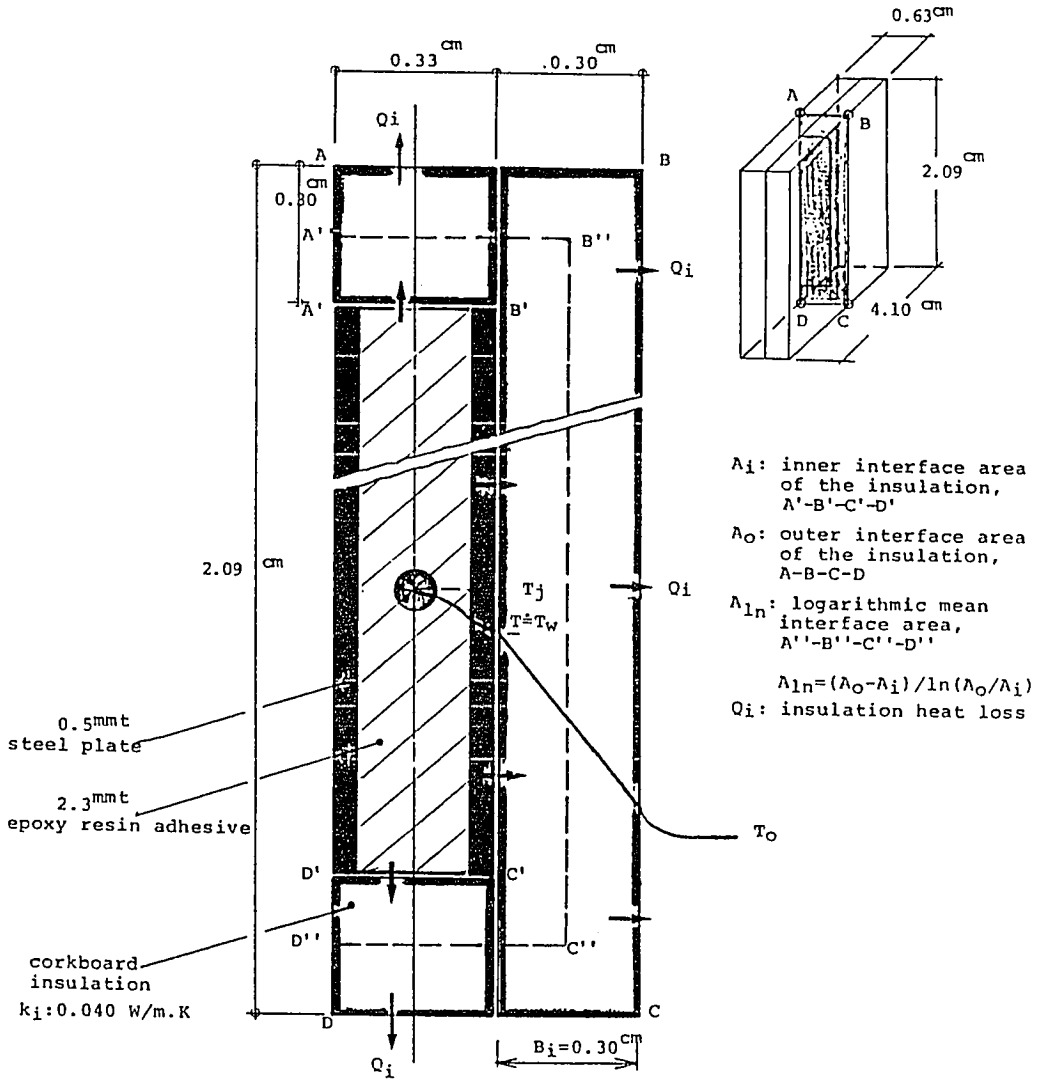

Fig. A.4.1: Cross-sectional view of the one-side insulated heating plate (Types III and IV) for calculation of insulation heat loss.

Appendix 5

Calculation of Radiative Heat Dissipation from Plate Surface

The radiative heat transfer from dispersed phase such as the freeboard of bubbling beds can be found from

$$Q_r = A \cdot \sigma \cdot \epsilon \cdot (T_w^4 - T_0^4) \qquad \textbf{(A.5.1)}$$

where ϵ is the effective emissivity of the plate surface for the dispersed-surface system. ϵ can be found from (e.g., Basu, P., Chem. Eng. Sci., 45(10), 3123, 1990)

$$\epsilon = \frac{1}{\frac{1}{\epsilon_d} + \frac{1}{\epsilon_s} - 1} \qquad \textbf{(A.5.2)}$$

where ϵ_d and ϵ_s are emissivities of the dispersed phase and the heat transfer surface respectively. ϵ_d may be calculated according to Brewster (Brewster, M. Q., Trans. ASME, 108, 710, 1986) from the following equation

$$\epsilon_d = \{ \frac{\epsilon_p}{(1-\epsilon_p) \cdot B} \cdot [\frac{\epsilon_p}{(1-\epsilon_p) \cdot B} + 2] \}^{0.5} - \frac{\epsilon_p}{(1-\epsilon_p) \cdot B} \qquad \textbf{(A.5.3)}$$

where ϵ_p is the emissivity of the particle surface. For iso-tropic scattering B = 0.5 and for diffusely reflecting particles B = 0.667.

In the present study, 60 % area of the surface of the finished heating plate was covered by black shiny lacquer and the residual 40 % was shiny metallic surface due to sand paper polishing.

The effective emissivity (ϵ) for the present study was estimated to be around 0.6 as shown in Table A.5.1 according to Eqs. (A.5.2) and (A.5.3) and emissivity of surfaces listed in the table. As shown in Table A.5.1, the effective emissivity for the present study (ϵ = 0.6) is approximately equal to the emissivity for the plate in the free air stream (ϵ_s = 0.64).

Table A.5.1. Emissivity of surfaces

Surface	Emissivity	Note
Wrought iron, highly polished (100-480 °F)	ϵ_{s1} = 0.28	1
Black shiny lacquer, sprayed on iron	ϵ_{s2} = 0.875	1
Heat transfer surface, present study	ϵ_s = 0.64	2
Refractory material	ϵ_p = 0.65-0.90	1,3
Dispersed phase (B = 0.5)	ϵ_d = 0.89-0.97	4
Dispersed phase (B = 0.667)	ϵ_d = 0.87-0.97	4
Dispersed phase-heat transfer surface, present study	ϵ = 0.58-0.63	5

Notes

1. Perry, R. H. and D. Green, Perry's Chemical Engineers' Handbook, 6th ed., pp. 10-51, 52, McGraw-Hill Inc., 1984.
2. $\epsilon_s = 0.40\ \epsilon_{s1} + 0.60\ \epsilon_{s2}$
3. Particle material of the present study (SiO_2-Al_2O_3) is similar to refractory material.
4. Calculated from Eq. (A.5.3).
5. Calculated from Eq. (A.5.2).

Appendix 6

Specifications of the Experimental Fluidized Bed and the Auxiliary Instruments

1. Fluidized bed

(1)	Bed column :	
	a. Inner diameter	30 cm
	b. Outer diameter	42 cm
	c. Wall thickness	6 cm
	d. Column height	204 cm
	e. Material of construction	Transparent acrylic resin
(2)	Perforated plate for air distribution	
	a. Diameter of perforation region	30 cm
	b. Plate thickness	1 cm
	c. Perforation hole diameter	0.2 cm
	d. Perforation hole pitch	0.85 cm square
	e. Perforation area %	4.35 %
(3)	Cyclone	
	a. Collection efficiency	>98% (+5 μm)
	b. Inner diameter of cylinder	30 cm
	c. Height of cylinder	50 cm
	d. Height of cone	50 cm
	e. Wall thickness of cylinder and cone	0.2 cm
	f. Size of gas exhaust pipe	4" (Sch.# 40)
	g. Size of solids downcomer pipe (transparent acrylic resin)	2" (Sch.# 80)
	h. Angle between solids downcomer pipe and column wall	45°
	i. Material of construction (excluding downcomer pipe)	SUS 304

2. Air supply and delivery system

(1)	Blower	
	a. Supplier	Ta-Hong Machinery Co., Ltd. (Taiwan)
	b. Motor	15 HP, 220 V, 3 Phase
	c. Type	Roots
	d. Discharge rate	8 m3/min (25°C, 1 atm)
	e. Discharge pressure	Max. 5000 mmaq
	f. AC inverter	0.3-60 Hz adjustable
(2)	Piping	3" PE flexible

3. Temperature measurement system	
(1) For heating plate (embedded thermocouple) and bed temperature	0-200°C , Model SDC101-OB, Yamatake-Honeywell, Japan
(2) For surface temperature of heating plate	
a. Temperature indicator and recorder	0-200°C , Model HL-206 and AP-100, Anritsu Meter Co., Japan
b. Surface temperature probe	0-200°C , Model C-355, Anritsu Meter Co., Japan
4. DC power supply and measurements	
(1) Power supply (2) DC current and voltage	6 DCV Digital multimeter, Cole-Parmer 01558-10
5. Thermal anemometer	0-10 m/s, Model 8525, Alnor Co., USA

Appendix 7

Clarification of the Sampling Result: Solids Concentration of Flux ?

Due to the observed microscopically random motion of the solid particles in the freeboard, the measured values using the probe shown in Fig. 4.3 were considered as solids concentrations.

Results from the two preliminary test (see below) runs may be an additional support :

a. The calculated solids concentration is nearly independent of sampler mouth direction and the suction air velocity at the mouth entrance (Ue).

b. The calculated solids flux (into the sampler mouth) is linearly proportional to Ue and the flux is also independent of sampler mouth direction. This indicates that the fine particles in the freeboard may easily be affected by the sampling air current even if Ue is lower than Uo.

Preliminary Test Run No. 1 (Feb. 1, 1990)

1.1. Sampler (Fig. S.1)

a. Location : H = 0.93-0.96 m, r = 0
b. Type : Un enlarged mouth
c. Mouth direction : (1) Downward
(2) Radial & horizontal

1.2. Operation conditions

a. Static bed height : Ho = 0.18 m
b. Superficial velocity : Uo = 0.40 m/s
c. Bed temperature : To = 17-18 Deg. C.

1.3. Data

Mouth direction	F (liter/min)	Ue (m/s)	t (min)	W (g)	C (kg/m3)	G (g/cm2.min)
Downward	0.68	0.40	8.0	0.5669	0.104	0.251
	1.72	1.01	4.0	0.7874	0.115	0.697
	3.24	1.91	2.0	1.0850	0.168	1.921
	4.74	2.80	2.0	1.6116	0.170	2.852
Radial & Horizontal	0.68	0.40	8.0	0.6340	0.117	0.280
	1.91	1.13	3.0	0.9434	0.164	1.111
	2.94	1.73	3.5	1.8066	0.175	1.826
	4.42	2.61	3.5	2.4649	0.159	2.491

F : Suction air flowrate
Ue: Suction air velocity at the sampler mouth, Ue = F/Ae, where Ae is the cross-sectional area of the sampler mouth (Ae = 0.6 cm x 0.6 cm x 0.785).
t : Sampling time
W : Weight of sampled solids
C : Calculated solids concentration, C = W/(F x t)
G : Calculated solids flux at at the sampler mouth, G = W/(t x Ae).

1.4. Discussions

a. Variations of C and G with Ue are shown in Fig. A.7.1.

b. The measured solids concentration (C) is nearly independent of Ue and sampler mouth direction.

c. The measured solids flux (into the sampler) is linearly proportional to Ue for both sampler mouth directions.

Preliminary Test Run No. 2 (July 29-30, 1990)

2.1. Sampler

a. Location : H = 1.02 m, r = 0
b. Type : Enlarged mouth
c. Mouth direction : Downward

2.2. Operation conditions

a. Static bed height : Ho = 0.29 m
b. Superficial velocity : Uo = 0.41 m/s
c. Bed temperature : To = 29-31 Deg. C.

2.3. Data

F (liter/min)	Ue (m/s)	t (min)	W (g)	C (kg/m3)	G (g/cm2.min)
1.13	0.218	32	2.541	0.0703	0.092
1.64	0.316	33	5.069	0.0937	0.177
1.91	0.368	34	7.399	0.114	0.251
2.50	0.481	27	8.008	0.119	0.342
2.78	0.535	27	8.539	0.114	0.365

F : Suction air flowrate
Ue: Suction air velocity at the sampler mouth, Ue = F/Ae, where Ae is the cross-sectional area of the sampler mouth (Ae= 1.05 cm x 1.05 cm x 0.785).
t : Sampling time
W : Weight of sampled solids
C : Calculated solids concentration, C = W/(F x t)
G : Calculated solids flux at at the sampler mouth, G= W/(t x Ae).

2.4. Discussions

a. Variations of C and G are shown in Fig. A.7.2.

b. The measured solids concentration (C) is nearly indenpendent of Ue for Ue > 0.35 m/s.

c. The measured solids flux (into the sampler) is linearly proportional to Ue.

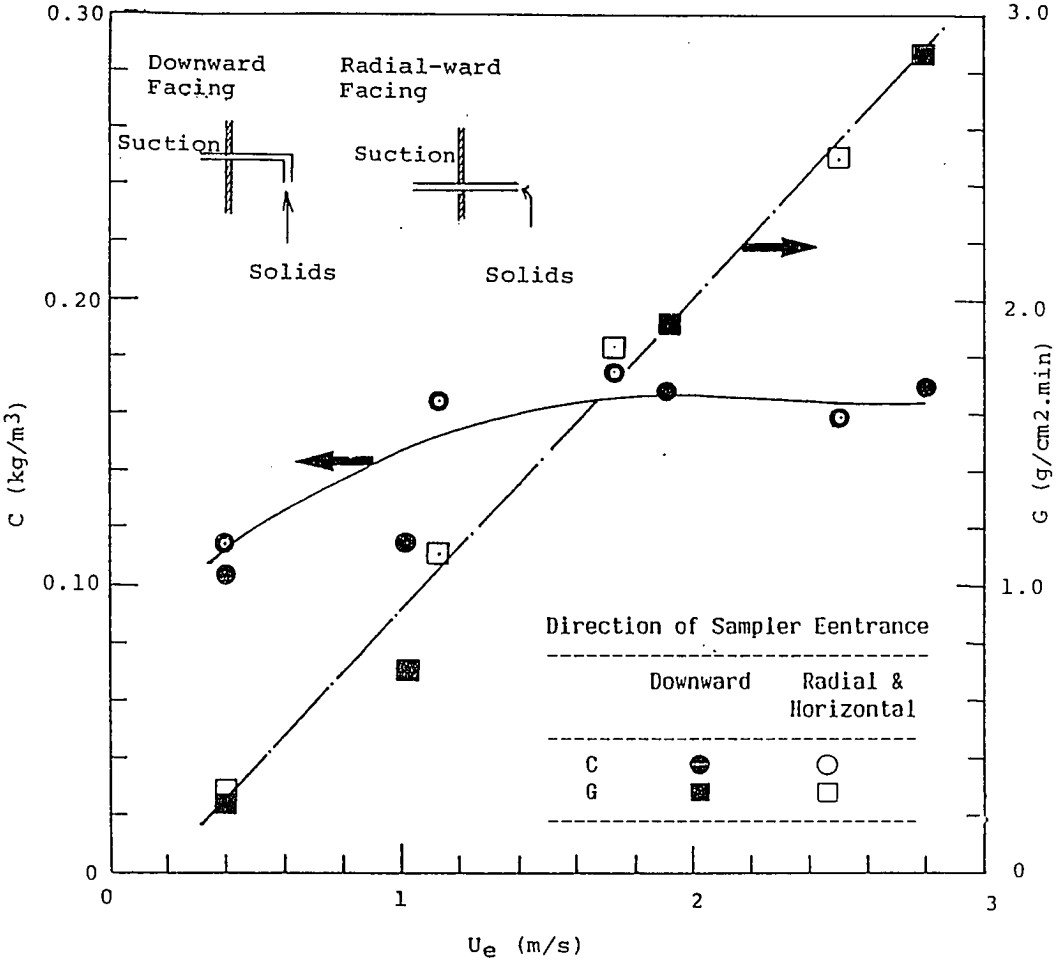

Fig. A.7.1: Variations of calculated solids concentration (C) and flux (G) with the sampler entrance air velocity (U_e) for non-enlarged sampler mouth.

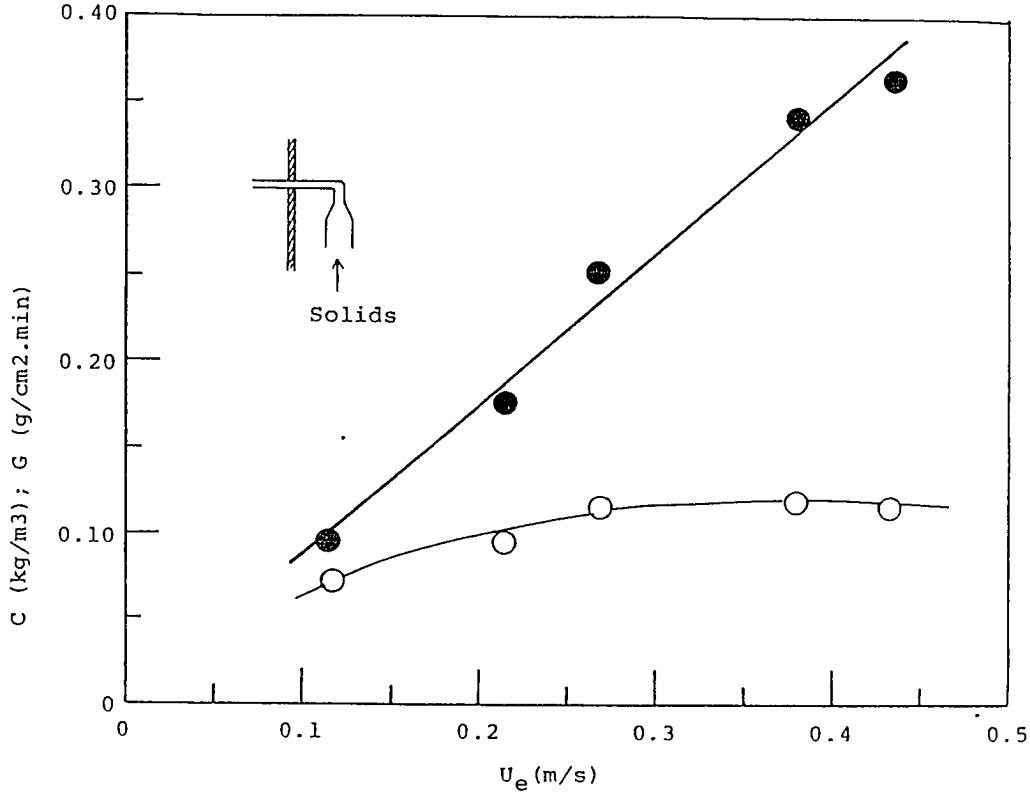

Fig. A.7.2: Variations of calculated solids concentration C (○), and solids flux G (●) with the sampler entrance air velocity (U_e) for enlarged sampler mouth.

Appendix 8

Sample Calculation of Heat Transfer Coefficient from Measured Bed Temperature (T_0), Plate Temperature (T_j), Voltage (V), and Current (A)

1. Exp. No. : 4025
2. Date : 900429
3. Static bed height : H_O = 29 cm
4. Plate radial location: r = 0
5. Plate type : III
6. Measured data (Note)

f (Hz)	H (cm)	T_O(℃)	Tj(℃)	V (volt)	A (ampere)
9.3	45	29.0	80	2.98	1.05
	95		119	3.01	1.09
	145		68	1.85	0.69
	198		67	1.99	0.70
13.3	45	29.4	59	3.02	1.05
	95		109	2.93	1.15
	145		64	1.88	0.69
	198		67	2.10	0.69
17.3	45	29.2	50	2.64	1.02
	95		77	2.53	1.13
	145		49	1.73	0.68
	198		54	0.99	0.69
21.3	45	29.4	54	2.94	1.03
	95		71	2.90	1.12
	145		44	1.76	0.69
	198		47	2.00	0.69

Note: f : frequency of output of the AC inverter, U_O (m/s) = 0.03 • f
H : plate height measured from perforated plate
T_O: bed temperature
T_j: plate temperature
V : voltage drop across heating wire segment embedded in heat transfer plate
A : electrical current in the heating wire.

7. Calculated result: Shown in Table A.8.1.

Aable A.8.1 Heat transfer coefficient calculation from measured T_o,T_j,A,V.

U_o (m/s)	H (cm)	T_o(C)	T_j(C)	T_w(C)	Q(w)	Q_r(w)	Q_i(w)	h_s+h_f (W/m^{2}K)
0.279	45	29.000	80.000	73.730	3.135	0.109	0.592	104.236
	95	29.000	119.000	112.442	3.279	0.245	0.964	47.517
	145	29.000	68.000	65.442	1.279	0.086	0.406	41.399
	198	29.000	67.000	64.217	1.392	0.082	0.410	48.933
0.399	45	29.400	59.000	52.660	3.170	0.051	0.328	229.813
	95	29.400	109.000	102.261	3.369	0.204	0.886	59.914
	145	29.400	64.000	61.407	1.296	0.074	0.376	50.683
	198	29.400	67.000	64.105	1.447	0.081	0.411	52.725
0.519	45	29.200	50.000	44.607	2.697	0.033	0.220	303.836
	95	29.200	77.000	71.285	2.858	0.102	0.554	100.213
	145	29.200	49.000	46.649	1.175	0.037	0.230	99.714
	198	29.200	54.000	51.495	1.252	0.049	0.284	78.958
0.639	45	29.400	54.000	47.935	3.032	0.040	0.264	281.951
	95	29.400	71.000	64.515	3.242	0.082	0.480	146.193
	145	29.400	44.000	41.569	1.216	0.025	0.168	160.957
	198	29.400	47.000	44.244	1.378	0.031	0.203	147.561